Calspan

On November 17, 1972 Cornell Aeronautical Laboratory (CAL) changed its name to Calspan Corporation and converted to for-profit operations. Calspan is dedicated to carrying on CAL's long-standing tradition of advanced research and development from an independent viewpoint. All of CAL's diverse scientific and engineering programs for government and industry are being continued in the aerosciences, electronics and avionics, computer sciences, transportation and vehicle research, and the environmental sciences. Calspan is composed of the same staff, management, and facilities as CAL, which operated since 1946 under federal income tax exemption.

BICYCLE DYNAMICS
RIDER GUIDANCE MODELING AND
DISTURBANCE RESPONSE

Calspan Report No. ZS-5157-K-1

April 1973

Prepared For:

SCHWINN BICYCLE COMPANY
CHICAGO, ILLINOIS 60639

Prepared By: R. Douglas Roland
R. Douglas Roland
Research Engineer
Vehicle Research Department

Approved By: K.D. Bird
K.D. Bird, Head
Vehicle Research Department

R.S. Rice
Roy S. Rice, Head
Vehicle Systems Section
Vehicle Research Department

FOREWORD

The work reported herein was performed in the Vehicle Research Department of Calspan Corporation under Contract No. CC-~~182~~ 220 for the Schwinn Bicycle Company. The period of performance was from 10 May 1972 to 10 April 1973.

TABLE OF CONTENTS

1.0 INTRODUCTION

For the past two years Calspan has been engaged in a research program in bicycle dynamics sponsored by the Schwinn Bicycle Company. Most of the work on this program has been devoted to the development of a realistic computer simulation of the bicycle and rider.

To provide the basic data for computer simulation, full-scale experiments on bicycle stability and control were performed and documented both by motion picture films and by recorded measurements of important rider inputs and resultant bicycle motions. Section 2 discusses the latest series of experimental tests. Measurements from these tests provided the required insight into bicycle and rider behavior needed in the development of the simulation. Comparison of simulation runs with these tests showed that the simulation accurately depicts real-life performance of present designs and therefore will provide a valid representation of the performance of future design modifications without the need for prototype hardware.

Phase II included the formulation and implementation of the roll stabilization-steering control mode of the rider control model. This program included the continued development of the rider model aimed at providing path following performance and rider lean control, discussed in Sections 3 and 4.

As originally planned this general program of research in bicycle dynamics has proceeded in a series of steps. The simulation has already been used to study the effects of present design parameters on the stability of a riderless bicycle (Phase I) and for identifying rider skill requirements in stabilizing a bicycle in a simple turn (Phase II). Phase III was a milestone in this continuing program of research in bicycle dynamics. It was in this step that the computer simulation was first used to study the stability of a bicycle which is controlled by rider steering. Once the rider control model was operational in both the roll stabilization and guidance

modes and a base set of rider model coefficients had been determined, the computer simulation was in a highly advanced state capable of performing path following maneuvers on curved paths in the presence of disturbance inputs. Using the simulation a parameter study was made to determine the effects of various design parameters on bicycle stability in just this type of maneuver. Comparisons of the effects of bicycle design variations on stability as well as the differences in the three basic bicycle configurations are presented in Section 5.

A classical problem in the operation of two wheel vehicles has been the occurrance of a front wheel steering oscillation at high speeds. With the increasing demand for high speed bicycles the probability has significantly increased for reaching operating speeds which might cause this form of instability. Section 6 discusses a preliminary simulation study of this phenomenon, including the effects of certain front fork geometry changes on a Paramount configuration.

As pointed out previously, most of the effort through Phase II had been directed toward the development of a complex rider-bicycle simulation for the study of the influences of rider and bicycle characteristics on system dynamics. An approach of this type was essential for developing a capability for quantitative evaluation of bicycle designs. On the other hand, the required sophistication of the mathematical model of the system inhibits easy identification of specific effects via examination of the equations of motion. That is, the bicycle design parameters do not stand out in these nonlinear, higher-ordered, interacting expressions and it is difficult to achieve a ready understanding of design effects. Section 7 discusses a brief study which was performed to derive simplified expressions for the motions of a bicycle intended for providing insight into the probable effects of design changes.

In several meetings among Schwinn and Calspan personnel the subject of the effects of bicycle weight, tire rolling resistance, and

aerodynamic drag on bicycle performance efficiency was discussed. The literature was found to contain a few simple analyses which showed the power requirements of various resistances versus speed. However, no comprehensive analytical formulation of bicycle speed and power input was found which included the effects of mechanical friction, tire rolling resistance, bicycle weight, aerodynamic drag for different riding positions, road grade, and wind velocity. Section 8 discussed a study which was made to show in proper perspective the quantitative effects of different changes in bicycle configuration and riding conditions.

Appendix A discussed experimental measurements which were made of the aerodynamic drag of spinning bicycle wheels. Appendix B contains abstracts and comments on previous bicycle analyses. Plotted results of the simulation parameter studies are included in Appendices C and D.

Another task of this program was the production of a narrated color motion picture. The movie describes all aspects of this continuing research program including the development of the bicycle simulation and its current and future applications.

2.0 EXPERIMENTAL TESTING OF BICYCLE

Using an instrumented bicycle, experimental tests were performed and rider and bicycle motions were recorded. Several different maneuvers were run and a data bank was created for analyzing the control inputs of an actual rider. The immediate applications of these data were: (1) to provide base data for comparison with computer simulation runs to determine the influences of rider model characteristics in a stabilization task, (2) to analyze rider leaning as a means of stabilizing and controlling the bicycle.

The instrumentation included a potentiometer for measuring rider lean angle, Figure 1 . Rider lean motion (relative to the bicycle frame) was transferred from the rider's back through a long rod to the potentiometer which was mounted on the rear of the bicycle seat. Other measured and recorded data included steer angle, bicycle roll angle and speed. Data were recorded on Brush strip chart recorders for approximately 45 instrumented runs and 16 mm. motion pictures were made of all tests.

Each of the five maneuvers used in the experimental test program is discussed below. Data traces of the most representative test runs have been included in associated figures.

2.1 Low Speed Straight Line Stability

The purpose of this task was to determine to what extent and how the rider used leaning as a means of stabilizing the bicycle. Figures 3 and 4 are records of 4, 8, and 10 mph straight path following runs. It should be noted that for the lean angle and roll angle traces the center of the chart does not necessarily represent a zero angle. Considerable difficulty was experienced in trying to fix the zero because of the type of instrumentation required and the high sensitivities involved. In these

Figure 1 - RIDER LEAN ANGLE SENSOR

Figure 2 - MOUNTING BARREL FOR ROCKET MOTORS

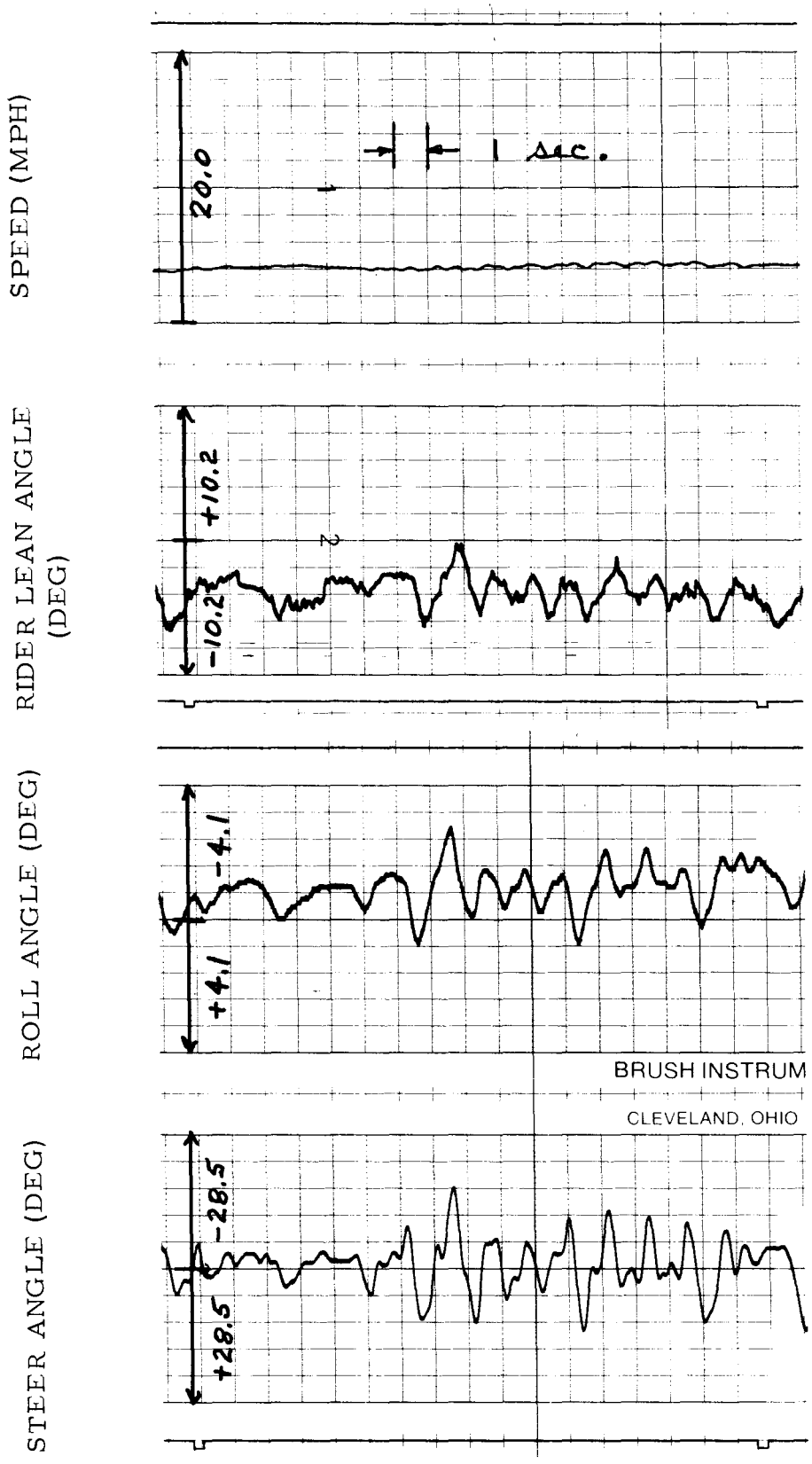

FIGURE 3. 4 MPH STRAIGHT TRAVEL

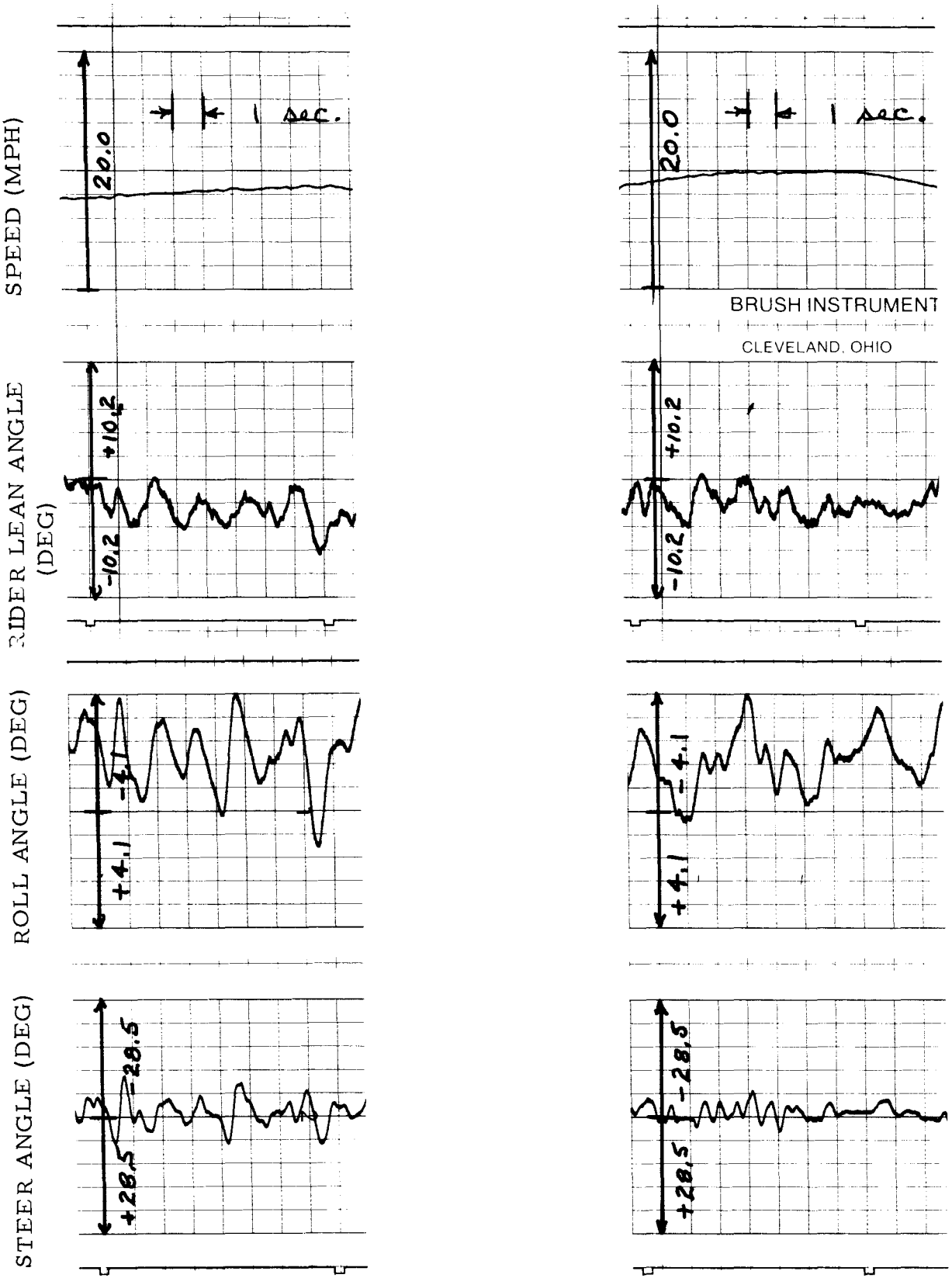

FIGURE 4. 8 MPH AND 10 MPH STRAIGHT TRAVEL

runs the zeros should be inferred from the "steady state" portions of the traces before and after the maneuver. The rider lean angle trace is inverted to aid in comparing it with the roll angle and steer angle traces. The time scale is one horizontal division equals one second, with time proceeding from left to right.

These traces show that the steering oscillations increase from $\pm$ 3 degrees to $\pm$ 15 degrees when speed is decreased from 10 to 4 mph. However, the rider lean angle oscillations remain constant at about $\pm$ 3 degrees. The roll angle oscillations remain relatively constant at about $\pm$ 2 degrees (note scale difference between lean angle and roll angle traces). There is a very strong correlation between roll angle and rider lean angle. This is more apparent when traces are viewed with one trace overlaid on the other. The rider appears to be compensating for the roll angle by leaning in the opposite direction (note scale inversion on lean angle) with a time lag of about 0.2 to 0.3 seconds. Steer angle also has a strong correlation with roll angle. The rider appears to steer in the direction that the bike is rolling with no appreciable time lag. The fact that the rider steer compensation is practically in phase with the roll angle certainly indicates that he is sensing roll angle derivatives (roll velocity and angular acceleration). This is significant since these terms were believed to be important in the early rider control analysis and were included in the rider control model in the Phase II bicycle dynamics program (Reference 1).

2.2 Side Force Disturbance Response

The primary purpose of these runs was to obtain data to be compared with simulation data for a stabilization task that could be reproduced with the bicycle simulation program. The riding situation consisted of straight path following with an artificial side wind distrubance created by a solid propelent rocket (18 lb. -sec. impulse). The rocket was rigidly attached to the frame of the bicycle beneath the seat with the

thrust vector perpendicular to the frame of the bicycle and to the right, Figure 2. The resultant effect was to push the bicycle to the right causing positive (clockwise) rolling motion. The test was performed at speeds of 6 and 10 mph. Figures 5 through 7 and 8 through 10 show the most consistent sets of three runs for each of the two speeds. Approximately six instrumented runs were performed at each speed. As is obvious from these figures, rider control motions were not consistent.

Figure 11 shows an idealized control procedure for this test. Initially the disturbance forces the bicycle to roll to the right. When the rider senses this, he must steer to the right to maintain equilibrium. In order to maintain path as well as equilibrium he causes the bike to roll to the left against the side force and hold this position (center section of curves) as long as the side force is present. When the distrubance force ends, the bicycle dips further to the left but the rider senses this, steers to the left, and brings the bicycle back upright. The last steering pulse to the right is to equalize the roll velocity effect as the roll angle approaches zero. This pulse may be nonexistant if the righting maneuver is done smoothly.

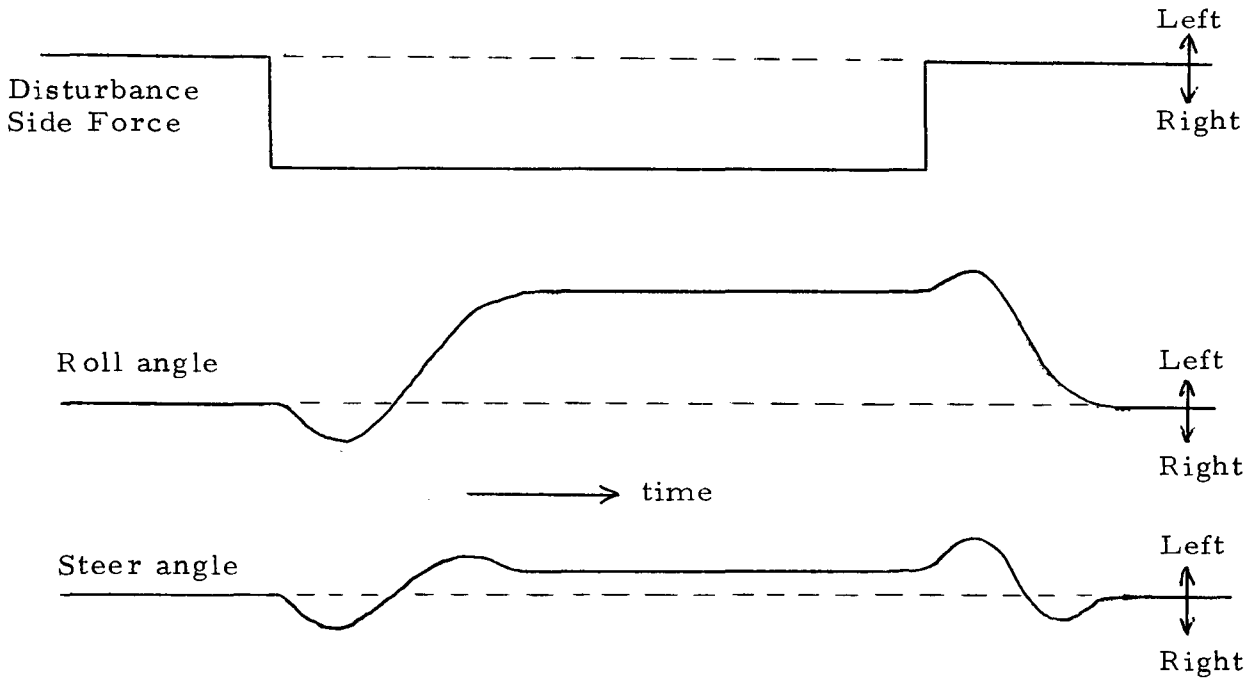

FIGURE 11. IDEALIZED DISTURBANCE RESPONSE CONTROL PROCEDURE

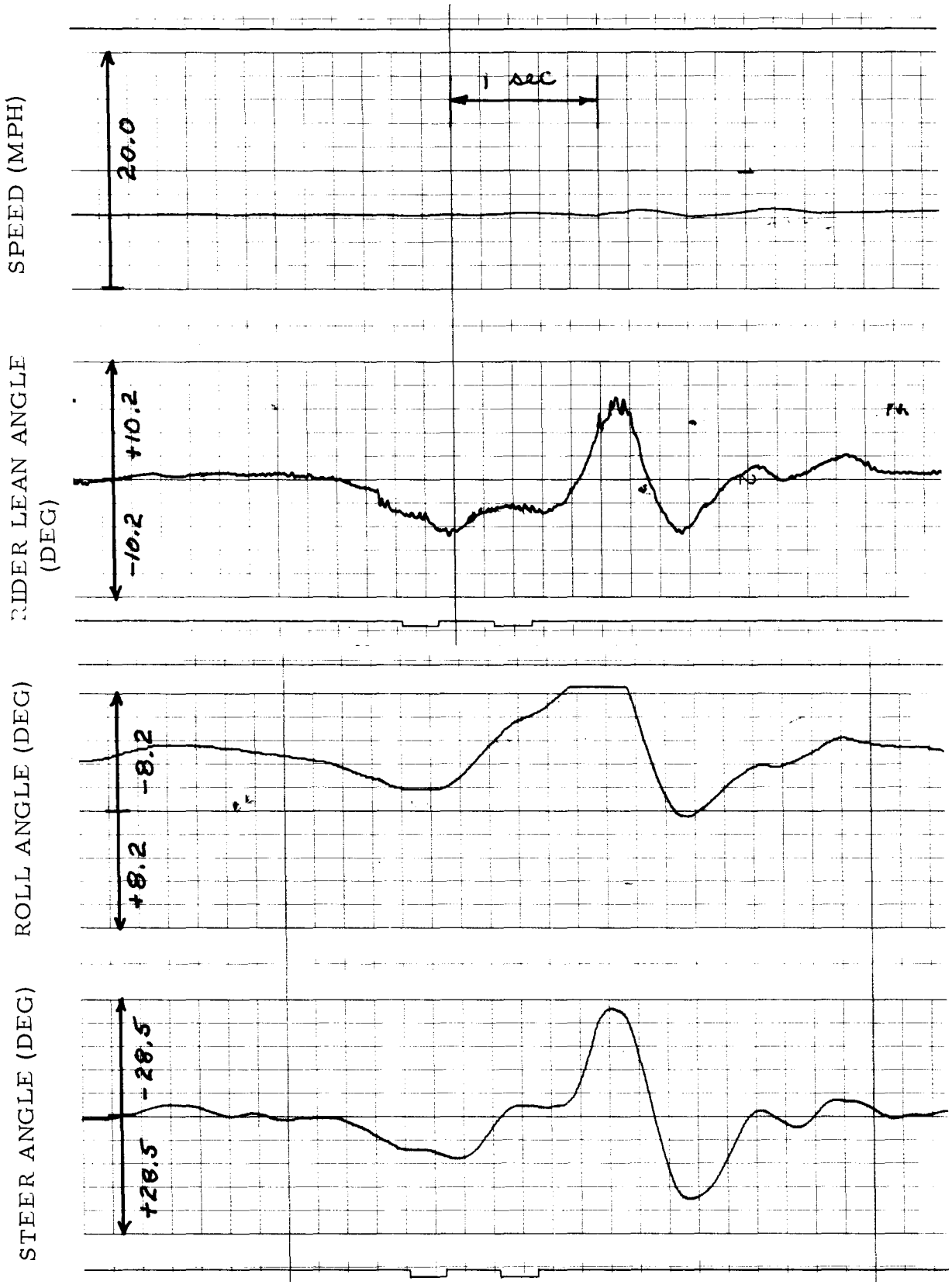

FIGURE 5. 6 MPH SIDE FORCE DISTURBANCE RESPONSE #1.

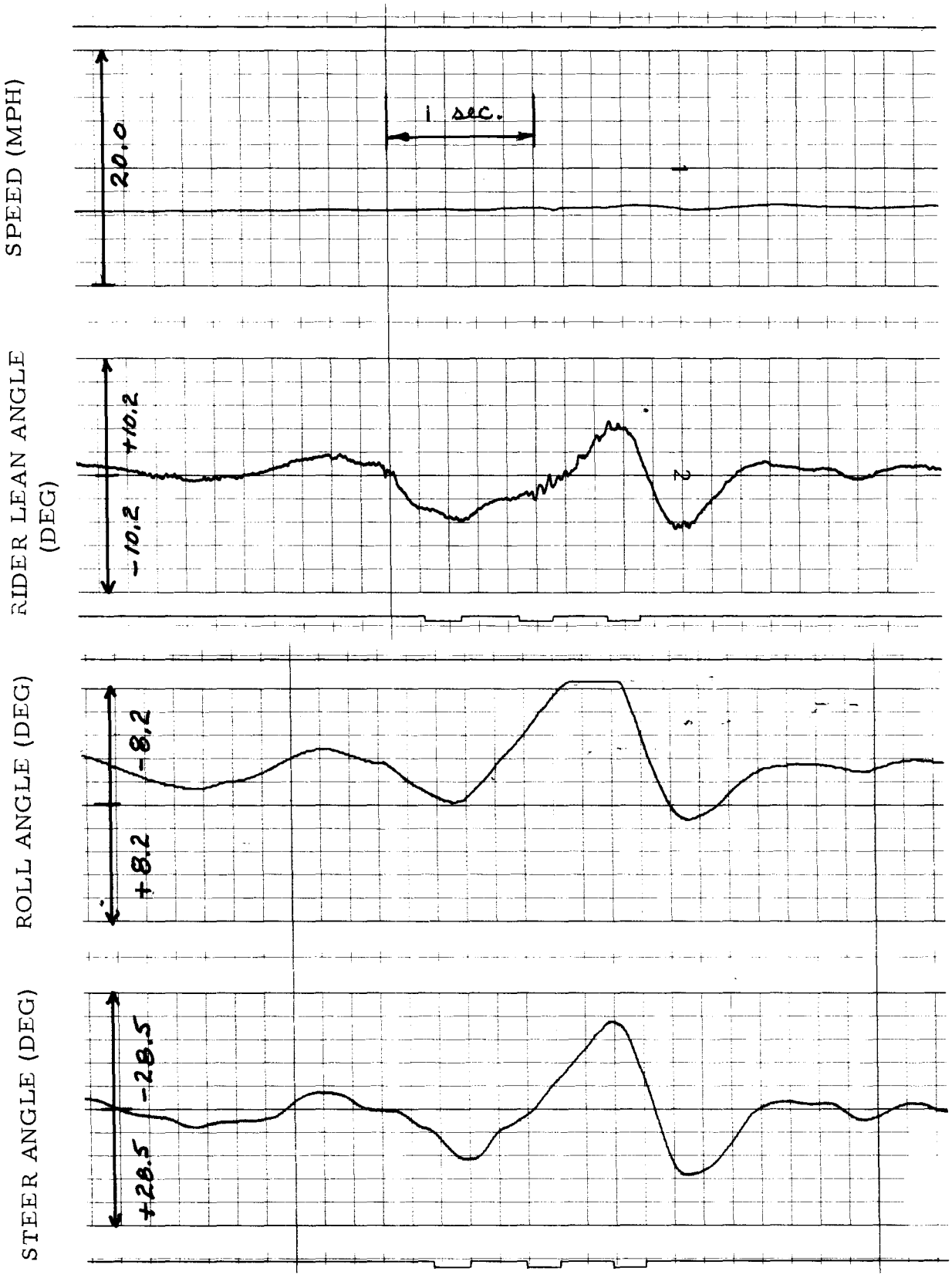

FIGURE 6. 6 MPH SIDE FORCE DISTURBANCE RESPONSE #2.

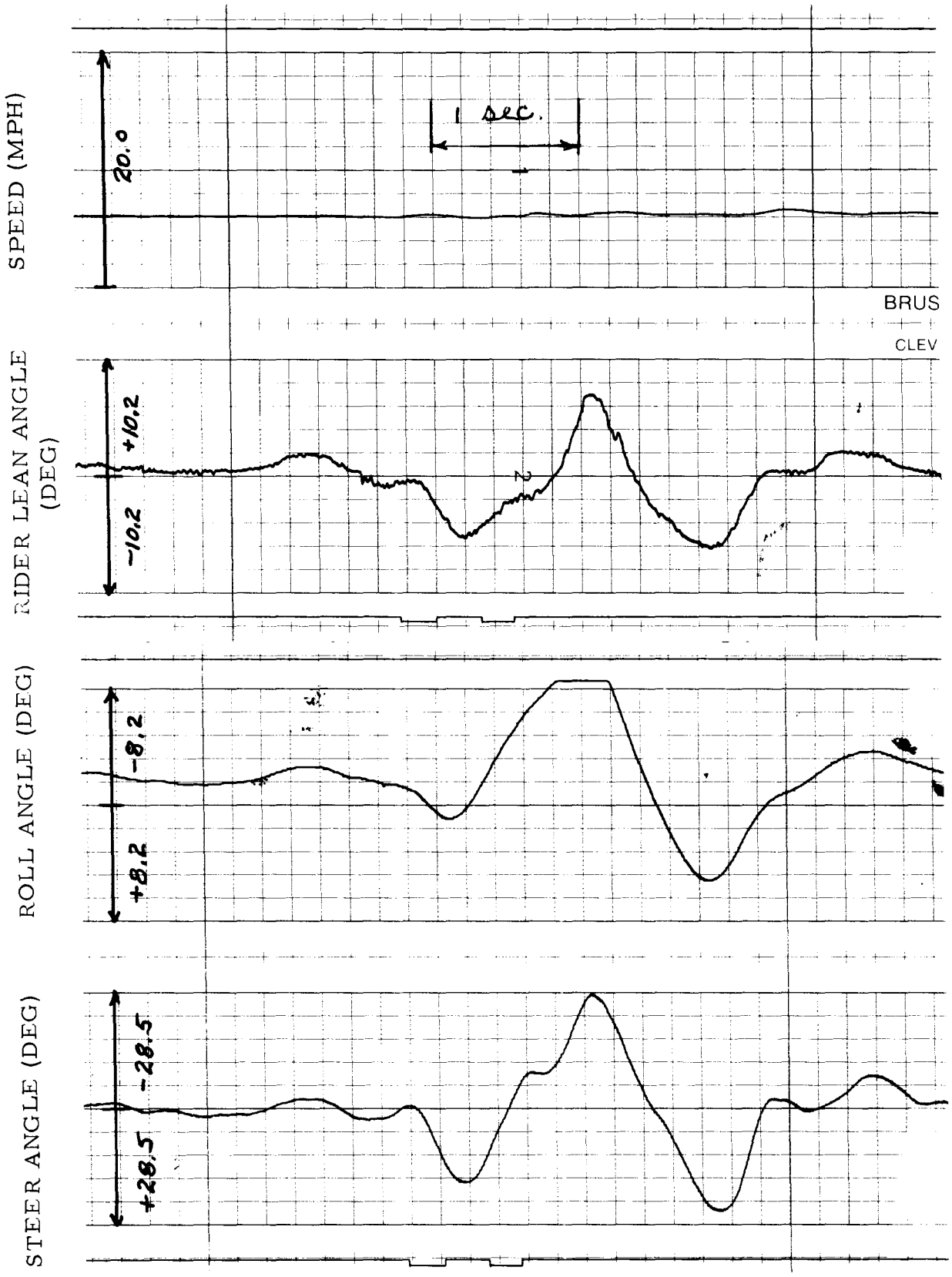

FIGURE 7. 6 MPH SIDE FORCE DISTURBANCE RESPONSE #3.

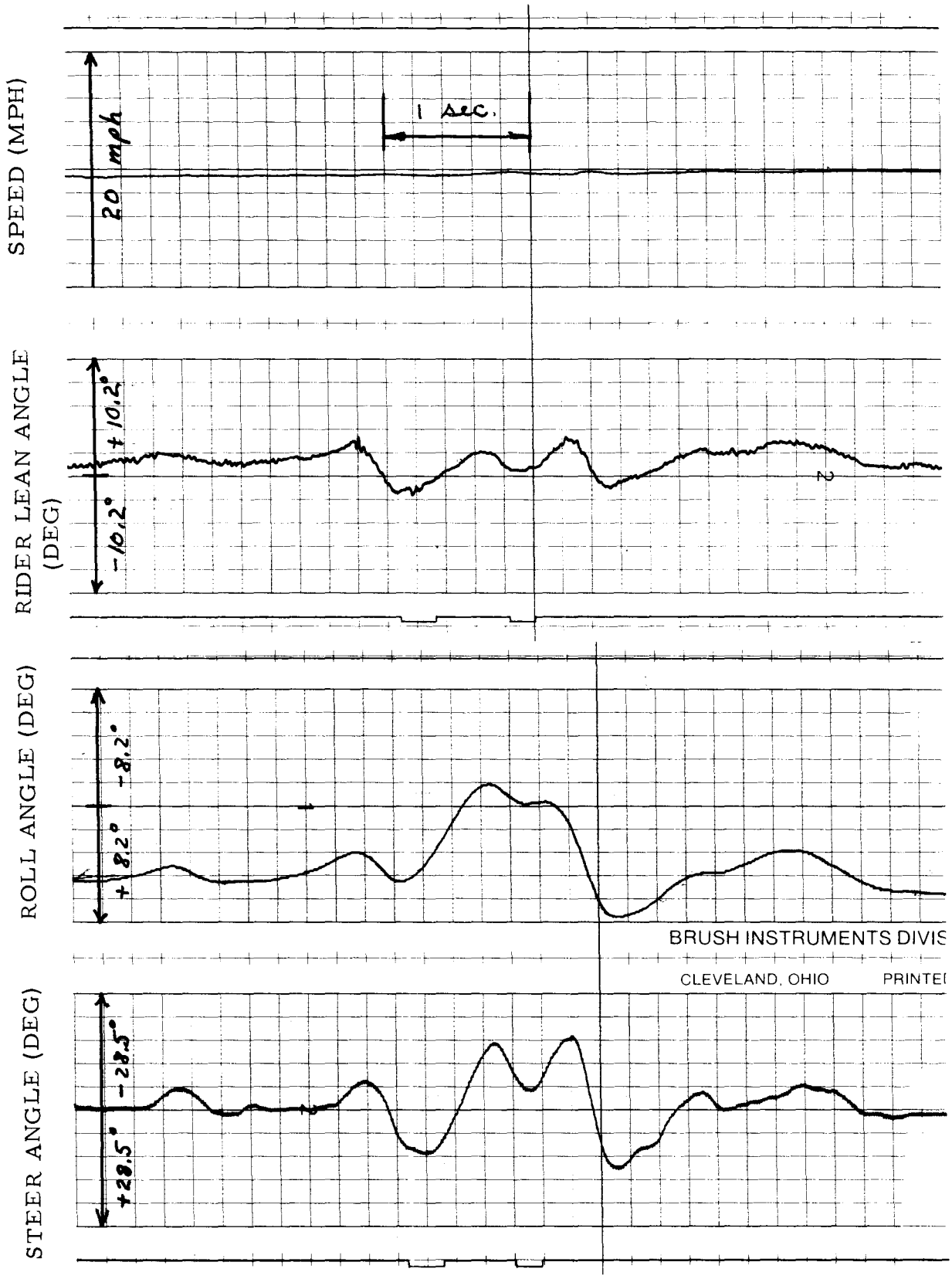

FIGURE 8. 10 MPH SIDE FORCE DISTURBANCE RESPONSE #1.

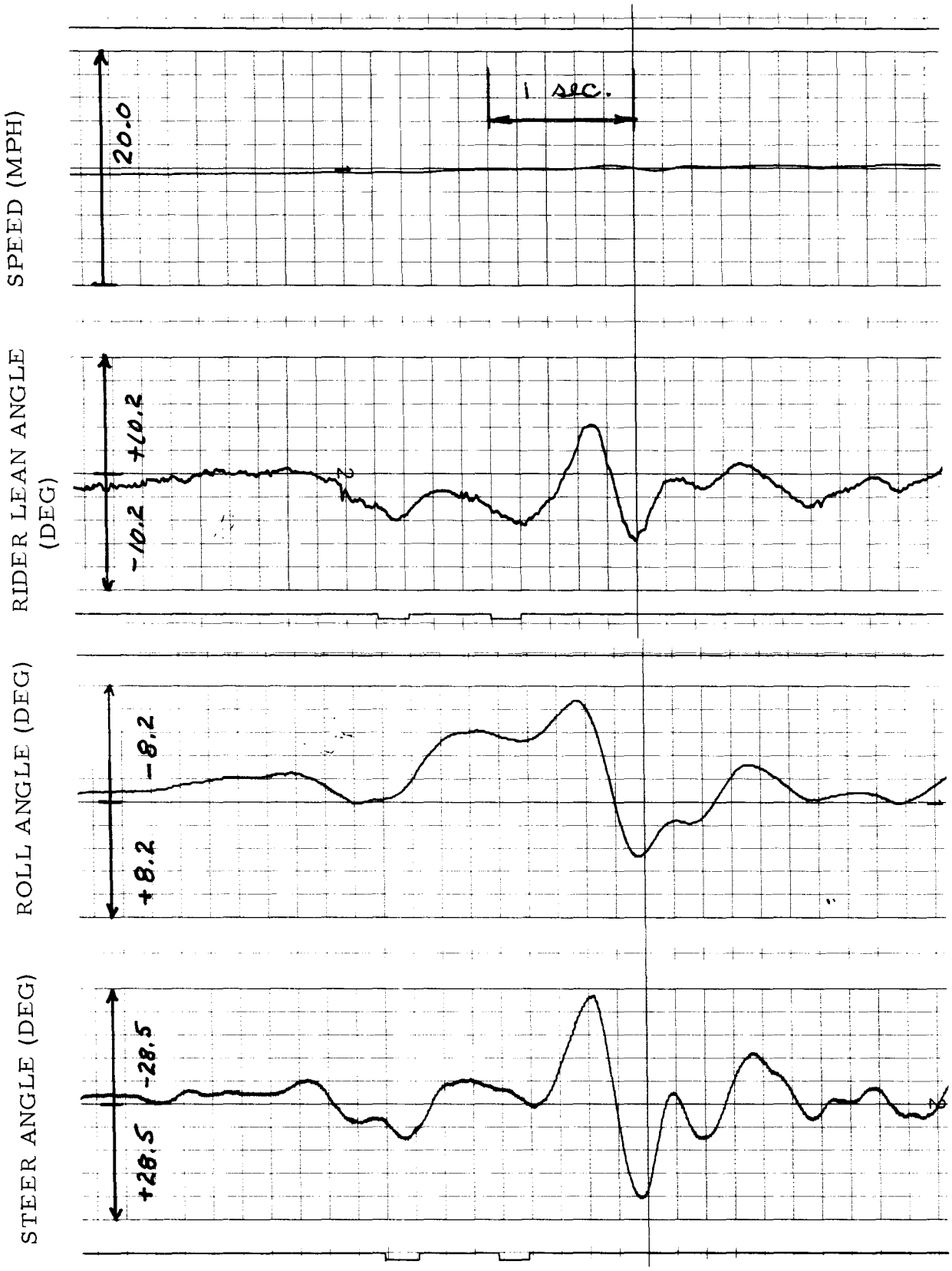

FIGURE 9. 10 MPH SIDE FORCE DISTURBANCE RESPONSE #2.

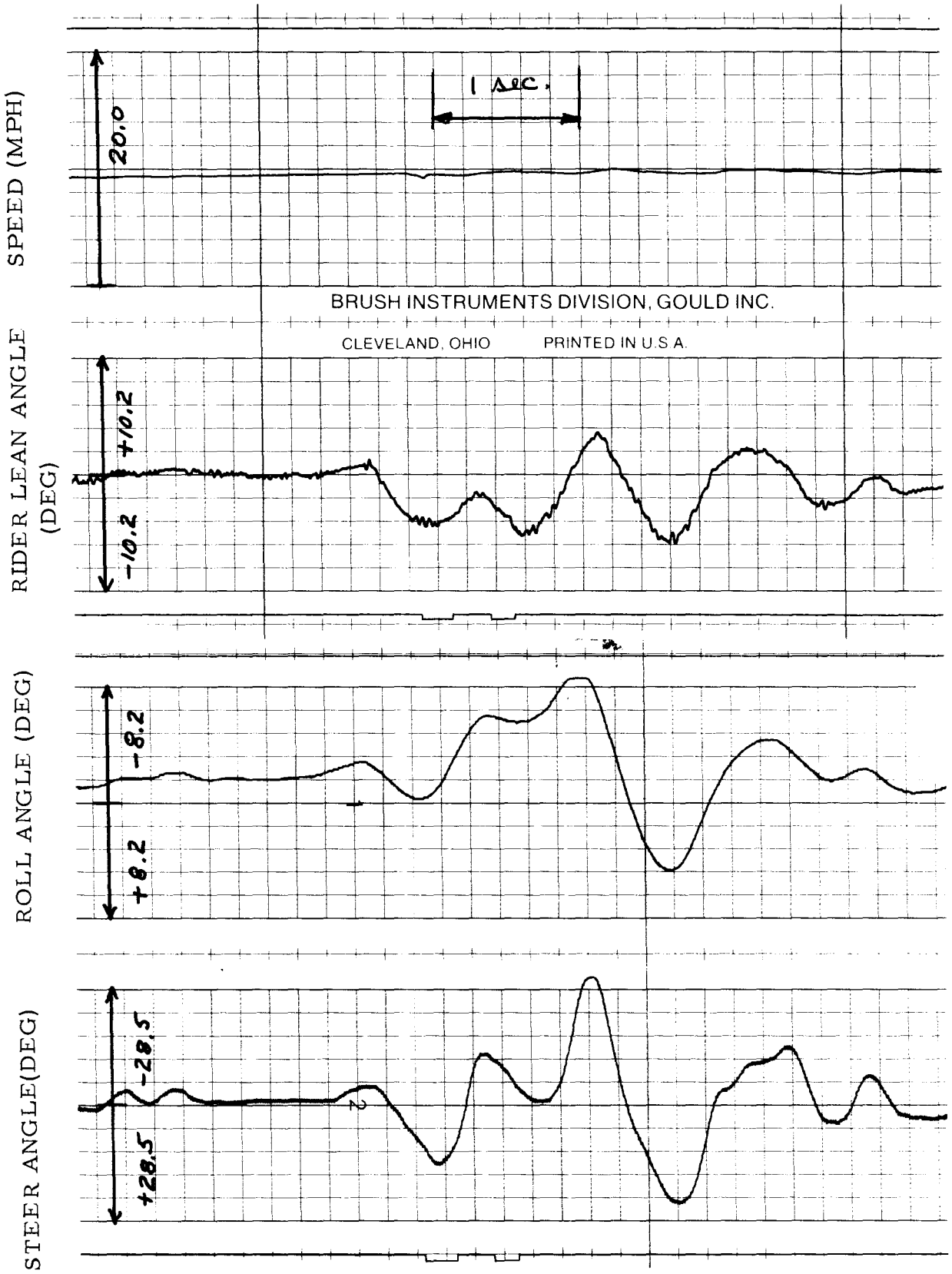

FIGURE 10. 10 MPH SIDE FORCE DISTURBANCE RESPONSE #3.

Most of the disturbance response traces tend to have this characteristic shape to some degree. In the actual traces the two top bumps on the steer trace tend to be very close to each other and the period of the steady state roll angle is short. This is because the duration of the rocket blast is also very short - only 1.2 seconds. Note the time scale for these distrubance response records is five horizontal divisions equal one second. The initiation of the rocket blast is approximately 0.25 seconds before the first tick mark.

The function of rider leaning is not clear in these runs. Initially the rider appears to be leaning to counteract the roll motion. After that the motion is difficult to interpret. However, the characteristic shape of the rider lean angle traces is consistent for all runs.

2.3 Wide Slalom and Avoidance Maneuvers

The purpose of these maneuvers was to study riding technique. The wide slalom maneuver consisted of an eleven pylon course with a longitudinal separation of ten feet and a lateral separation of two feet between successive pylons , Figure 12 . The avoidance maneuver consisted of a one foot wide lane with a two foot wide obstacle placed four feet beyond the end of the lane. The rider's task in this maneuver was to ride through the lane at constant speed then turn sharply to avoid the obstacle. Figures 13 through 19 show responses for these maneuvers.

The control motions in both maneuvers have similar characteristics. Steer angle correlates very strongly with roll angle and they are practically in phase with each other. (The simulated slalom maneuver performed in Phase II showed roll leading steer by about 20 degrees phase angle). The rider appears to lean in the opposite direction from bicycle roll and leads roll angle by about 50 degrees phase angle. One theory for such lean motion is that the rider minimizes the motion of his upper body in space (this is readily apparent in "head on" movies of the slalom maneuver).

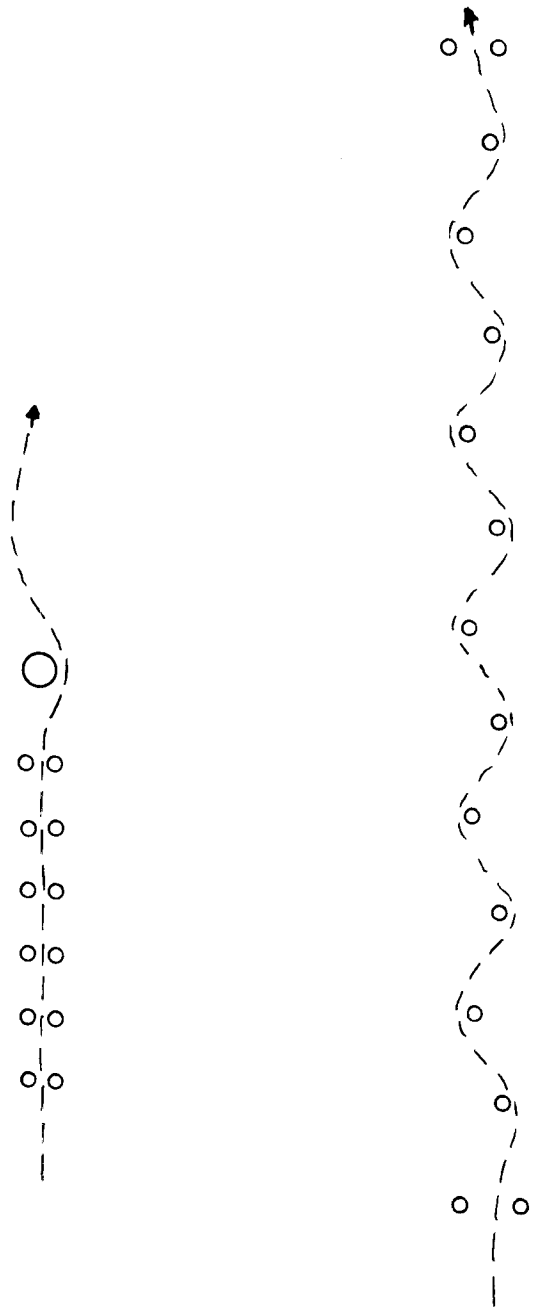

Avoidance Maneuver Slalom Course

FIGURE 12. EXPERIMENT TEST COURSE LAYOUTS

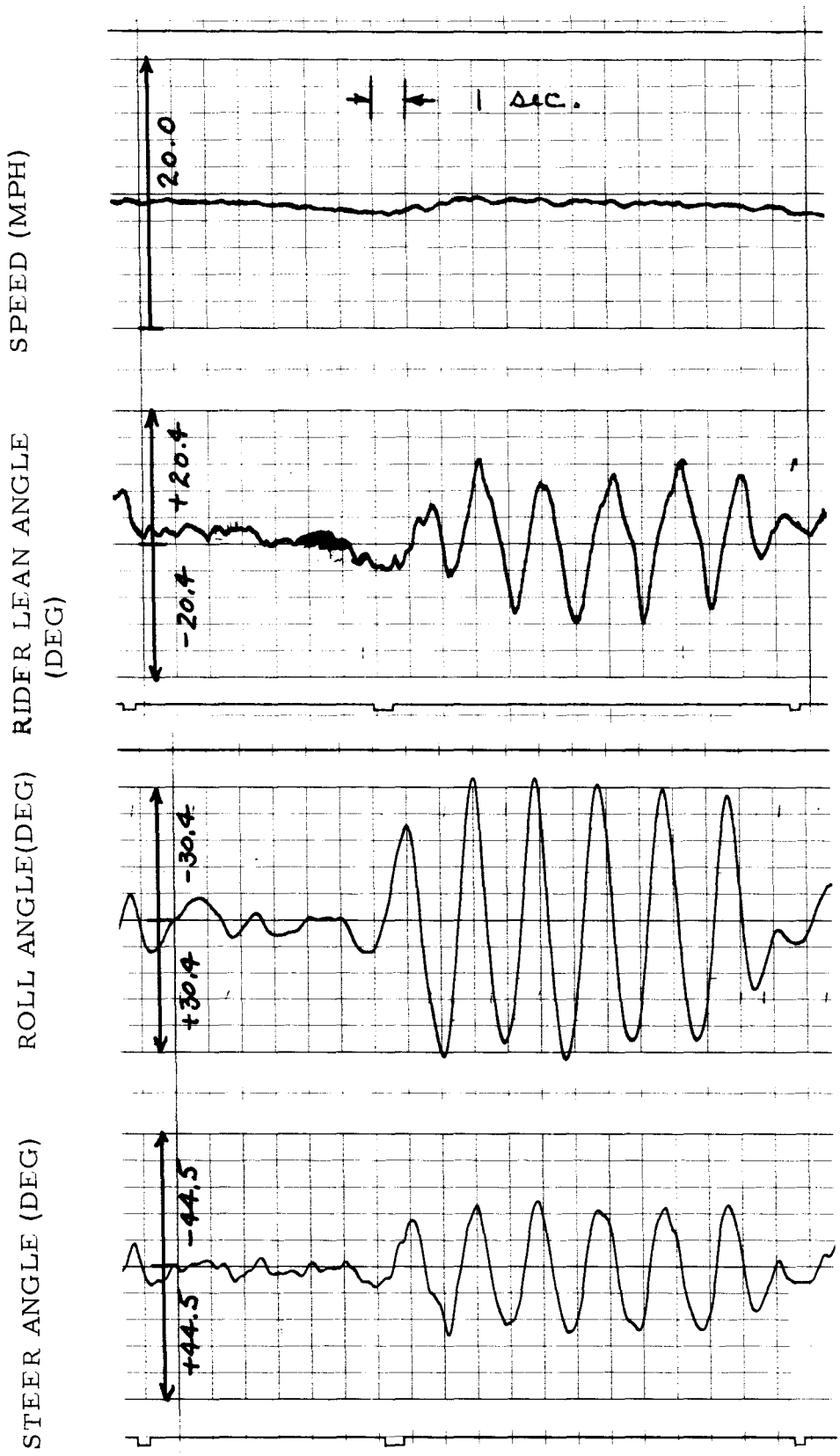

FIGURE 13. WIDE SLALOM MANEUVER #1.

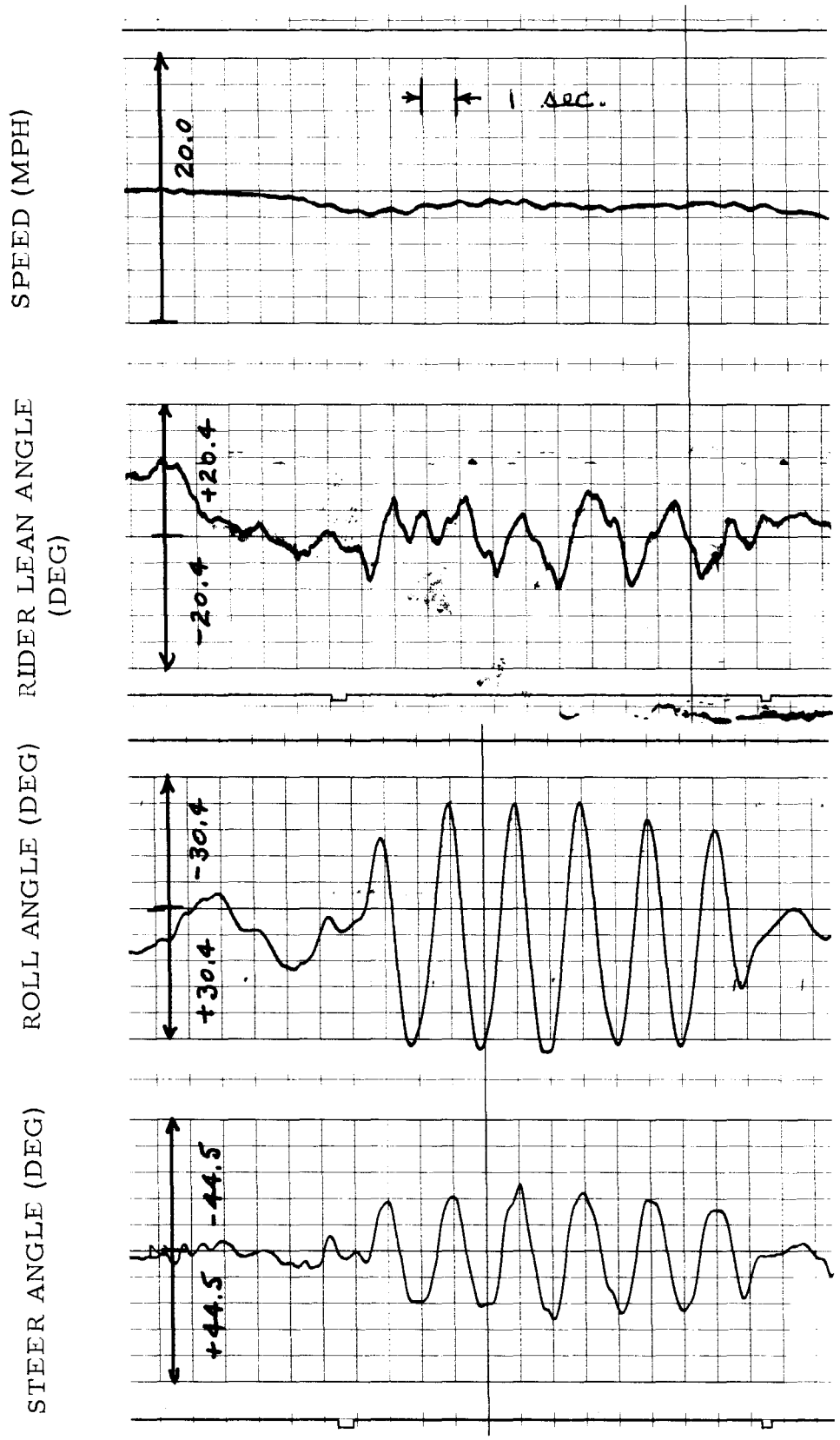

FIGURE 14. WIDE SLALOM MANEUVER #2.

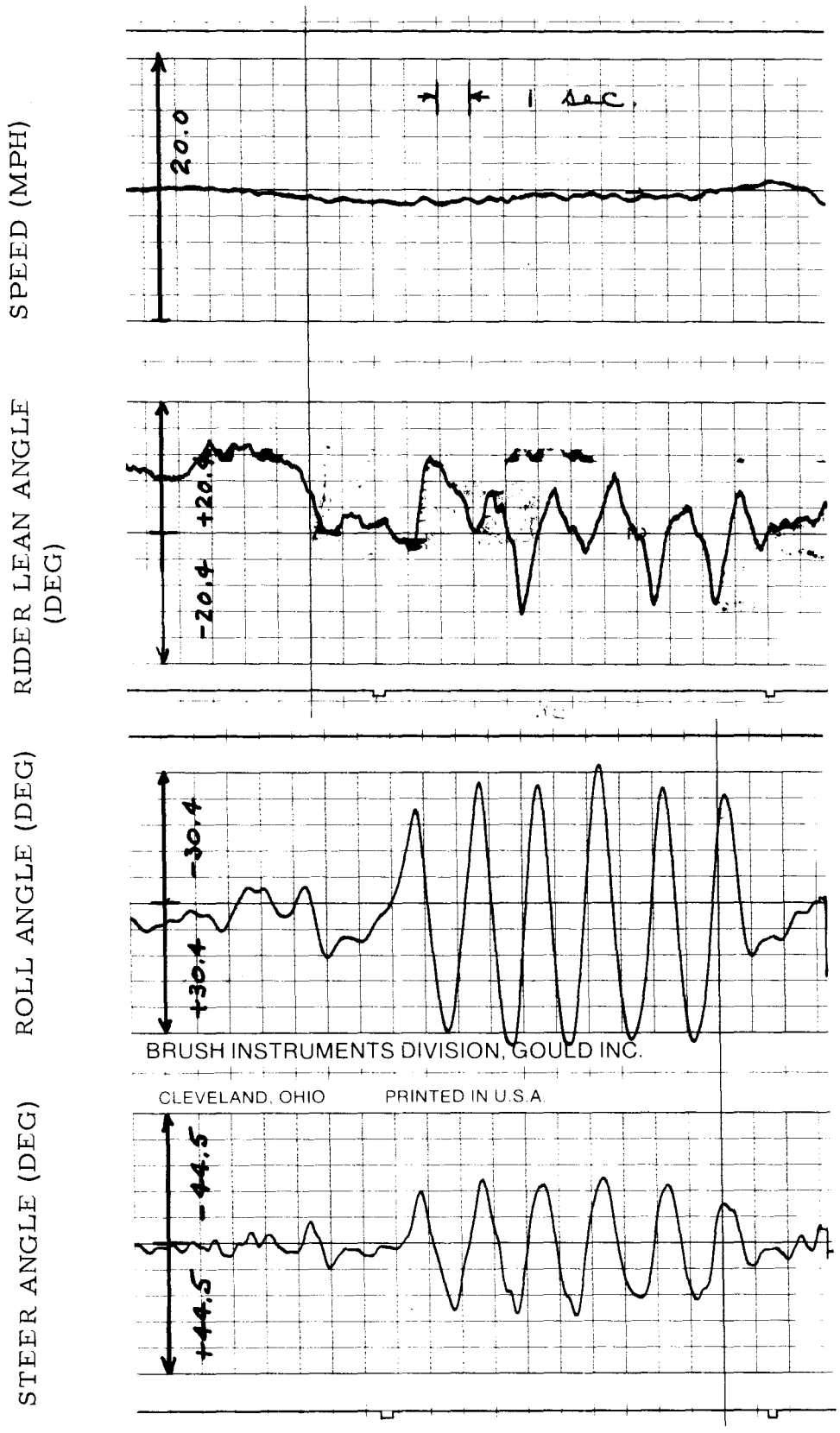

FIGURE 15. WIDE SLALOM MANEUVER #3.

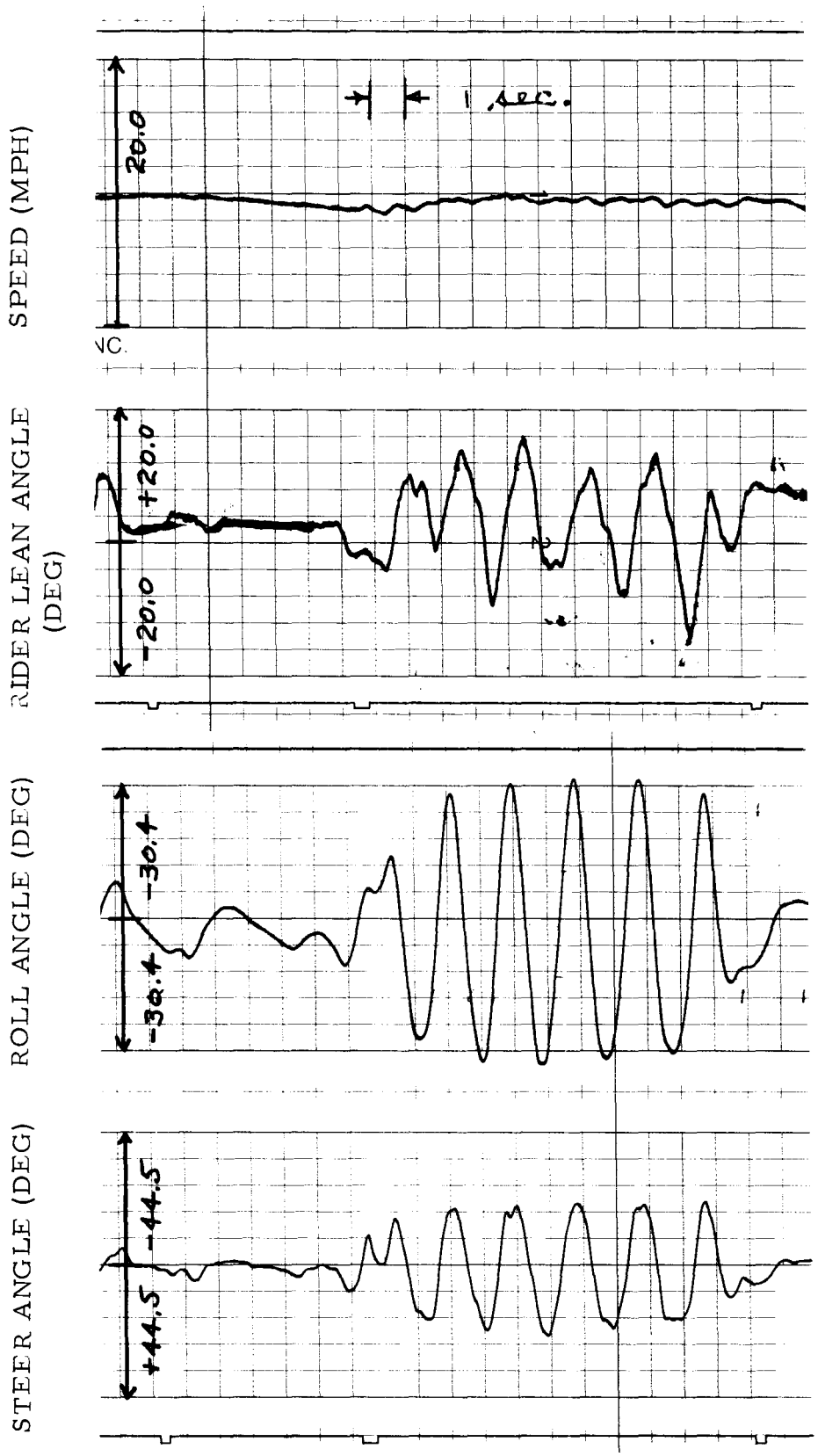

FIGURE 16. WIDE SLALOM MANEUVER #4

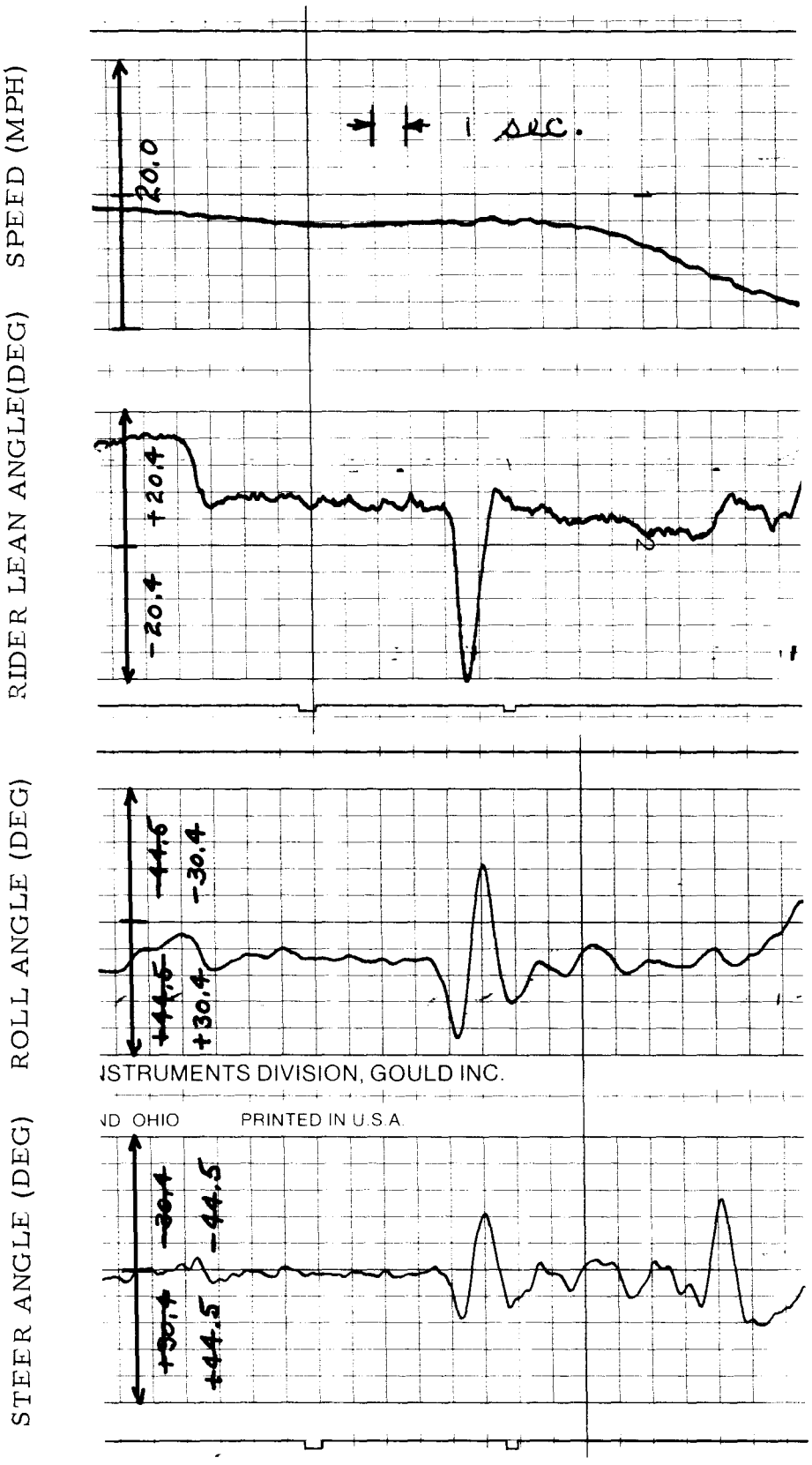

FIGURE 17. AVOIDANCE MANEUVER #1.

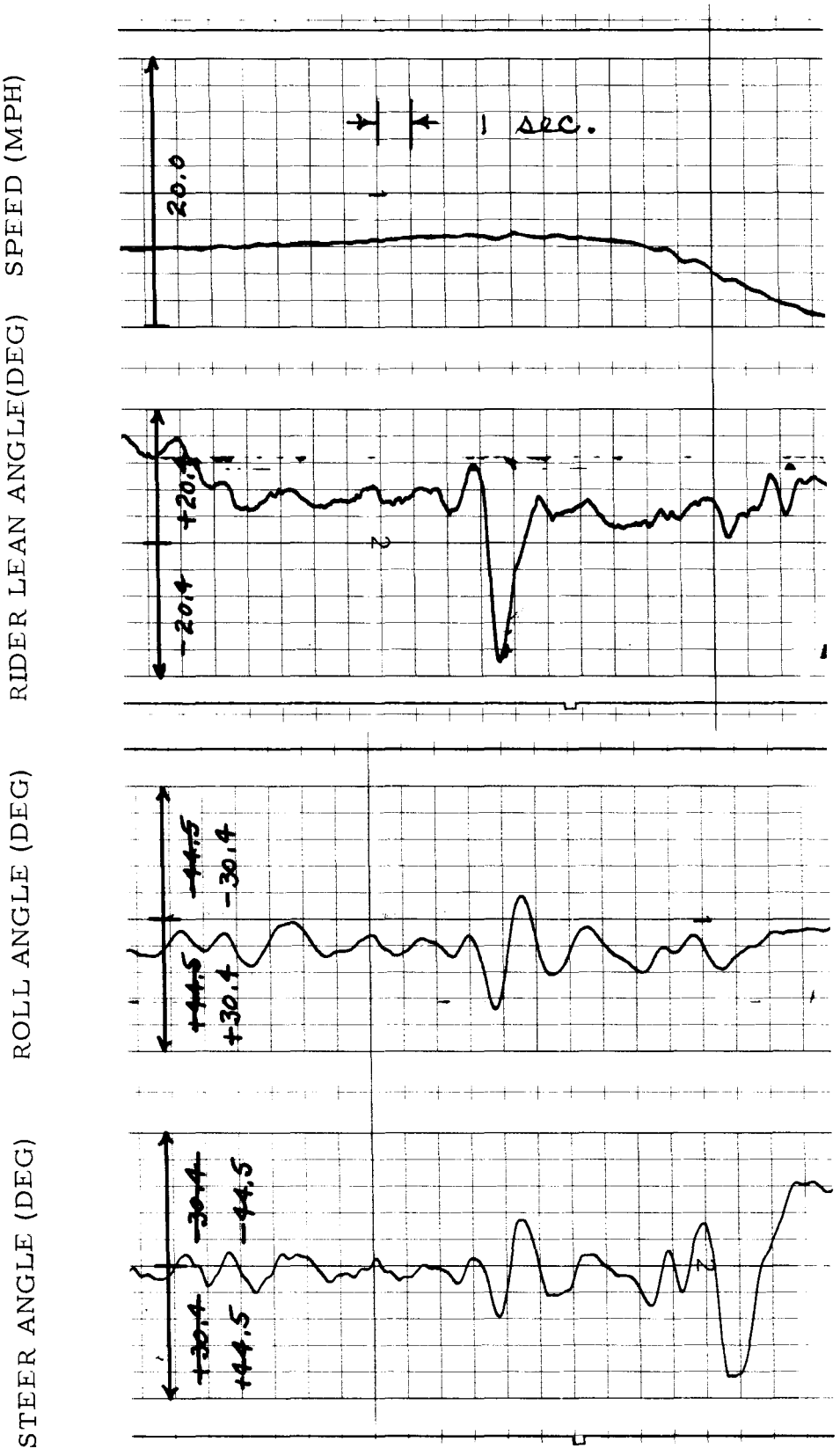

FIGURE 18. AVOIDANCE MANEUVER #2.

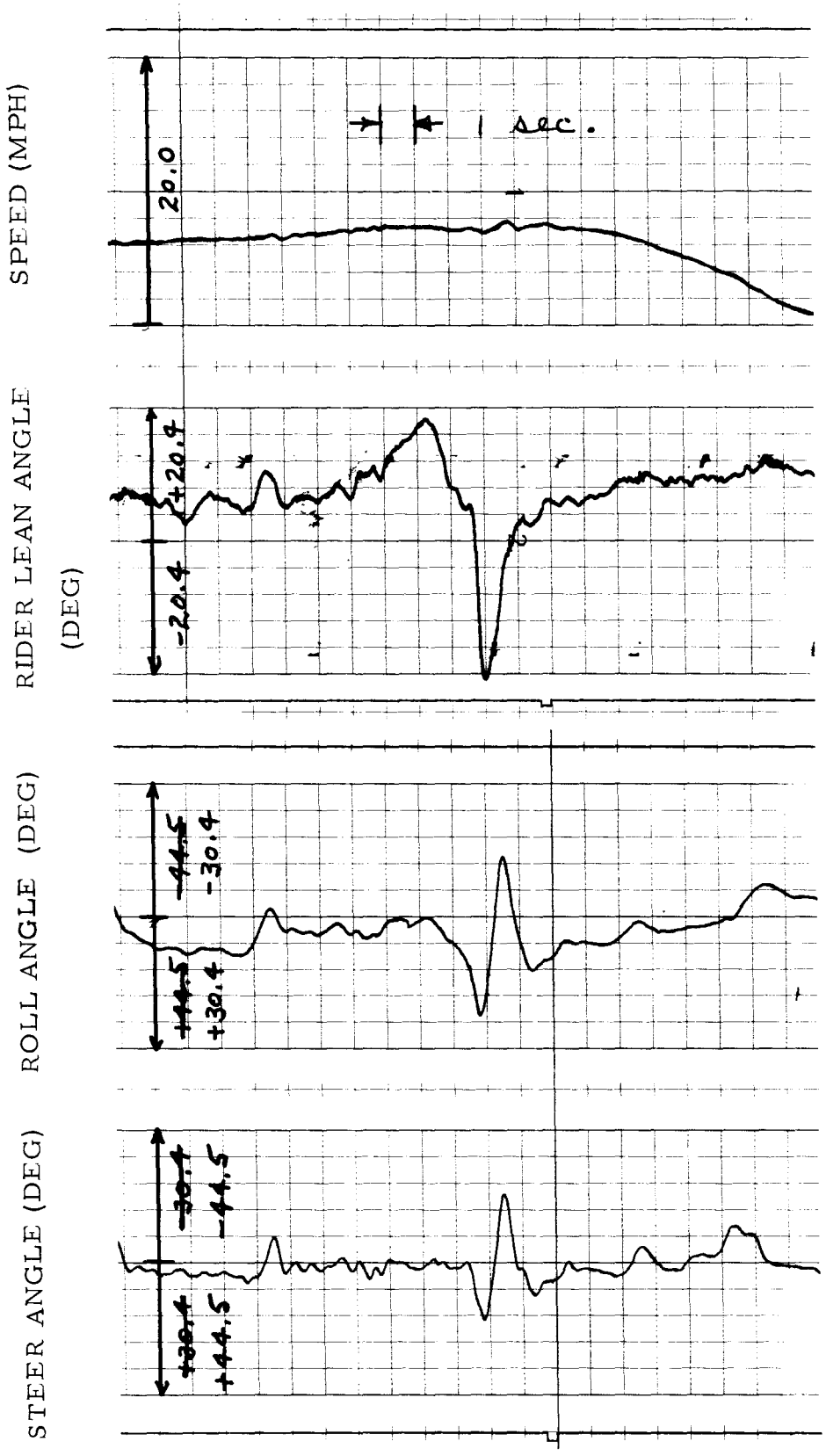

FIGURE 19. AVOIDANCE MANEUVER #3.

The rider's center of mass tends to stay fixed laterally in space while the bicycle moves alternately left and right beneath him to avoid the pylons in the slalom and the obstacle in the avoidance maneuver. Rider lean control behavior appears to be different in the avoidance maneuver. Normally the rider tends to exert lean torques to bring himself back to the in-plane position after entering or leaving a turn. However, in the avoidance maneuver the rider gets so far off balance after avoiding the object that he is forced to steer the bicycle back underneath himself to prevent falling over. This behavior is also evident in the slalom maneuver but it is done in a smooth rythmic motion.

This theory suggest a cross coupling between the lean and steer control modes. This could be a coupling between rider lean angle or lean torque and command roll angle. Thus, if the lean torques get too large the rider will steer the bicycle to develop some lateral acceleration to help move his body upright. However, the existing stabilization function may already include this control procedure, i.e., if the lean torque which the rider uses to pull himself upright are so large that they tend to pull the bicycle over, then the stabilization function will naturally steer to maintain balance.

2.5 Ninety Degree Right Turn

The purpose of this test was to study rider steer and lean control motions involved in negotiating a turn. The task consisted of approaching a corner on a straight path, turning approximately 90 degrees and leaving the corner on a straight path. The speed for this task was approximately 6 mph. This test is very interesting in that rider lean motions play an important part in controlling the bicycle. Figures 20 through 22 (time scale five horizontal divisions equal one second) show the three most consistent runs. Figure 23 shows the idealized control procedure for this maneuver.

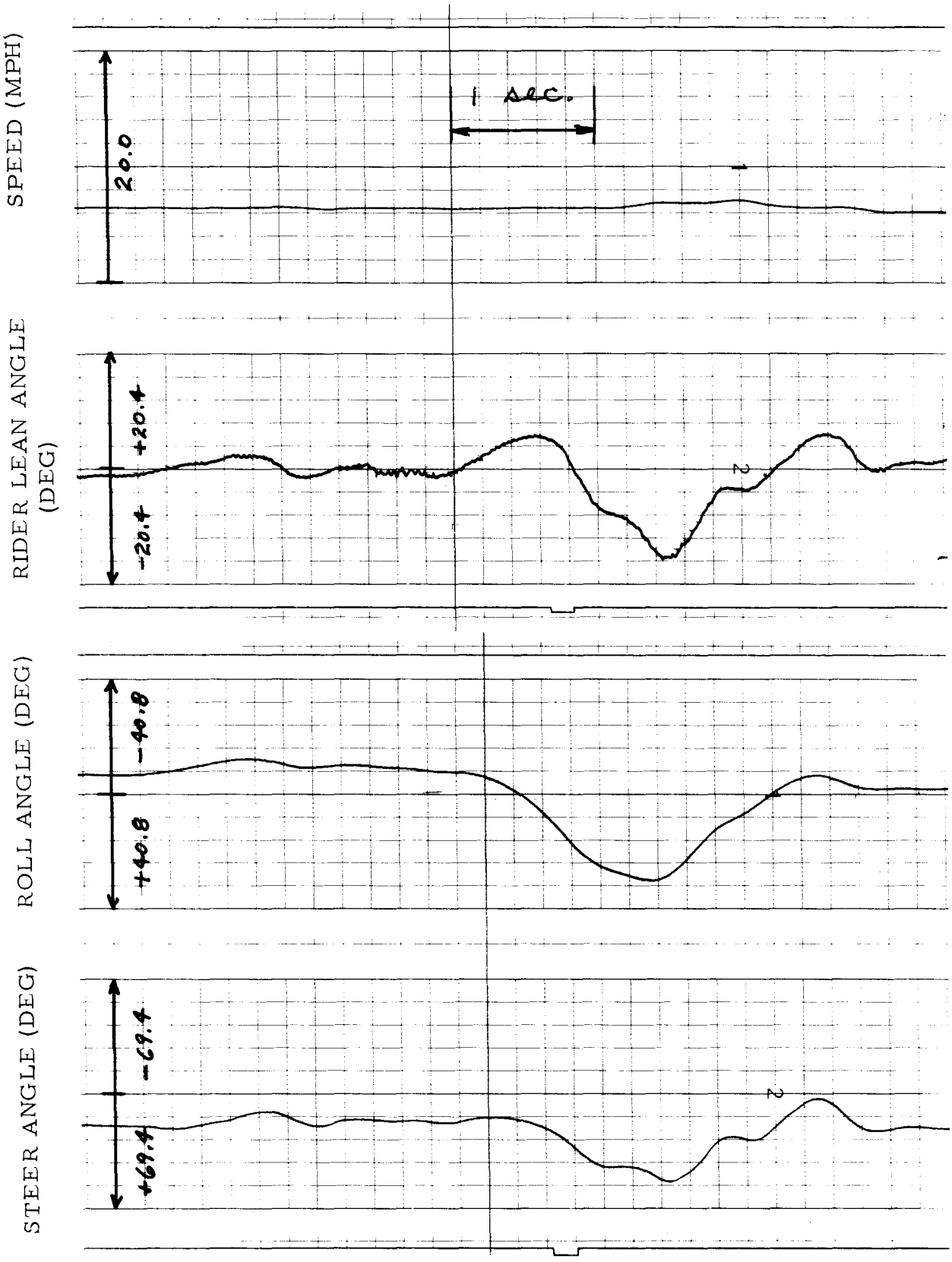

FIGURE 20. 90 DEGREE RIGHT TURN #1.

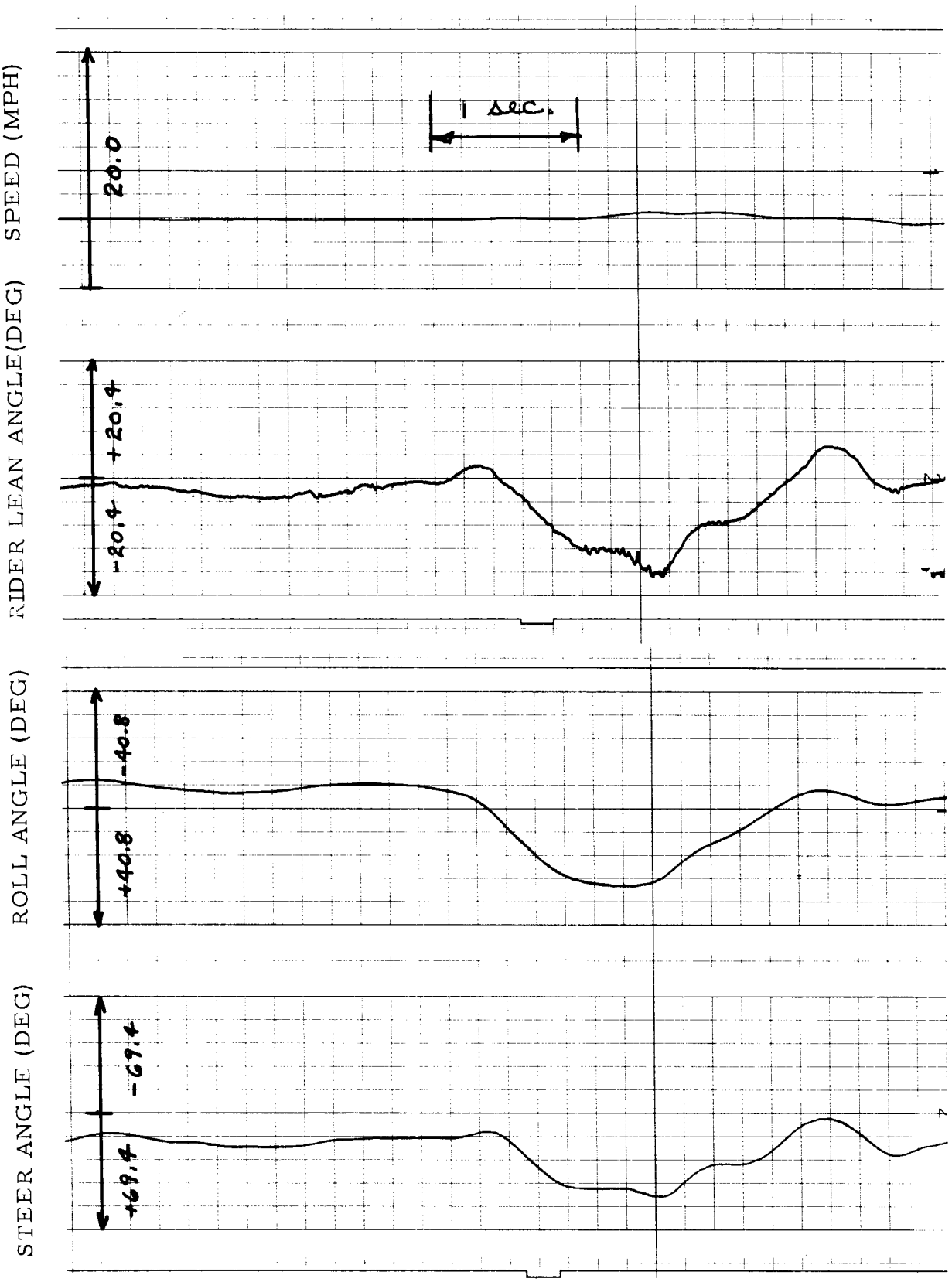

FIGURE 21. 90 DEGREE RIGHT TURN #2.

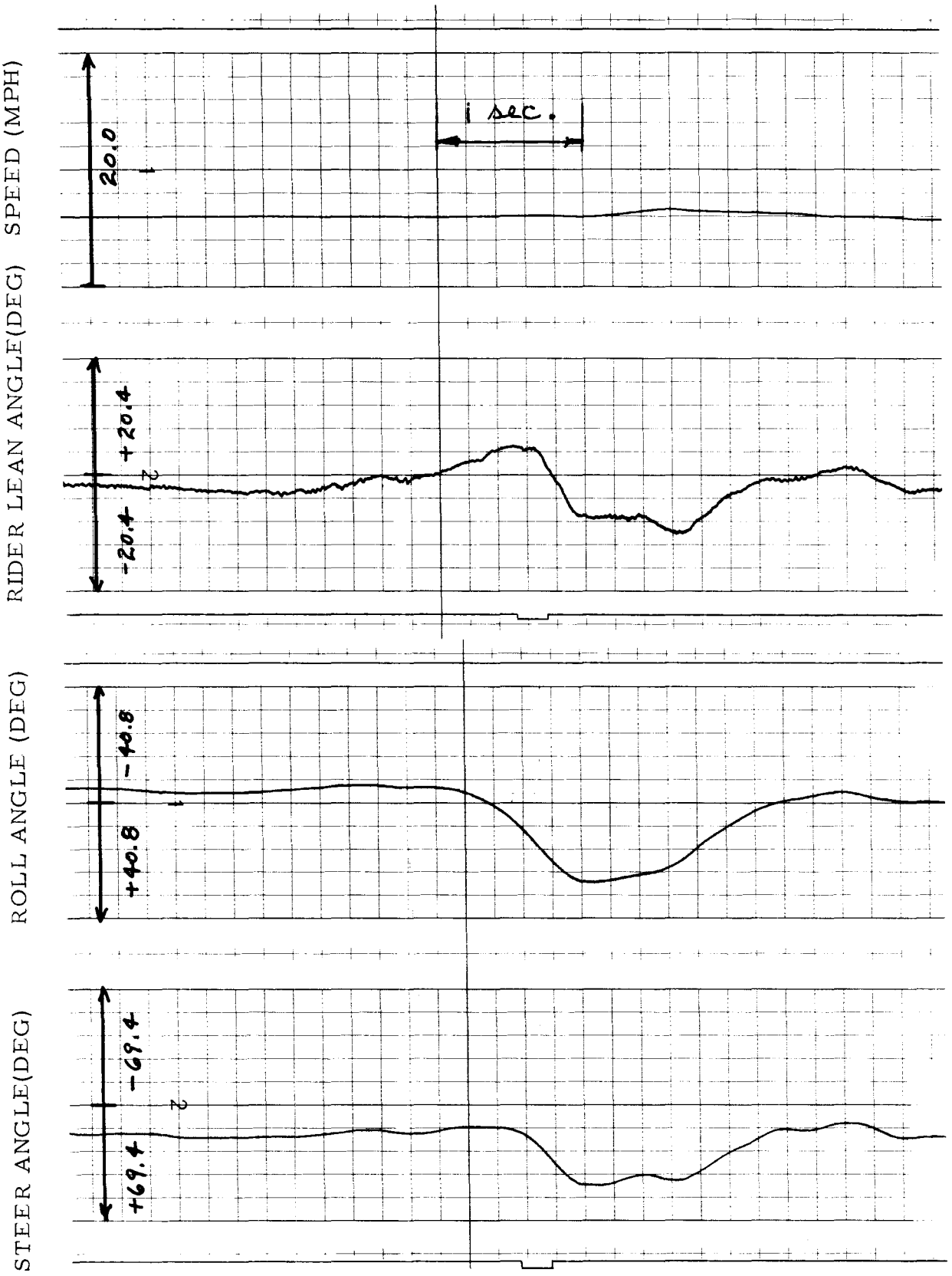

FIGURE 22. 90 DEGREE RIGHT TURN #3.

These curves show that initially the rider leans into the turn (in the direction he wants the bicycle to roll) and steers out of the turn to start the bicycle rolling in the correct direction. Thus lean control motion for initiating a turn is in the opposite direction to the lean motion for stabilizing the bicycle. This makes sense because the rider must deliberately destabilize the bicycle in order to set up for a turn. In this sharp turn the maximum lean angle into the turn was about 5 degrees, peaking at about the same time as the outward steering pulse.

Once the turn has been started the rider tends to lean out of the turn. The length of time taken before leaning out apparently depends on the magnitude of the initial countersteer pulse. With more counter steering the duration of the inward lean became shorter (about 2 seconds). With no obvious countersteer motion the duration of the inward lean was about four seconds. This strengthens the theory that the rider can initiate a turn by merely leaning, without counter steer motion, but the response will be slow. If a quick turn is required then countersteering must be used. The magnitude of the outward rider lean angle was large --- about 15 degrees or approximately half the value of bicycle roll angle at the same point in the turn.

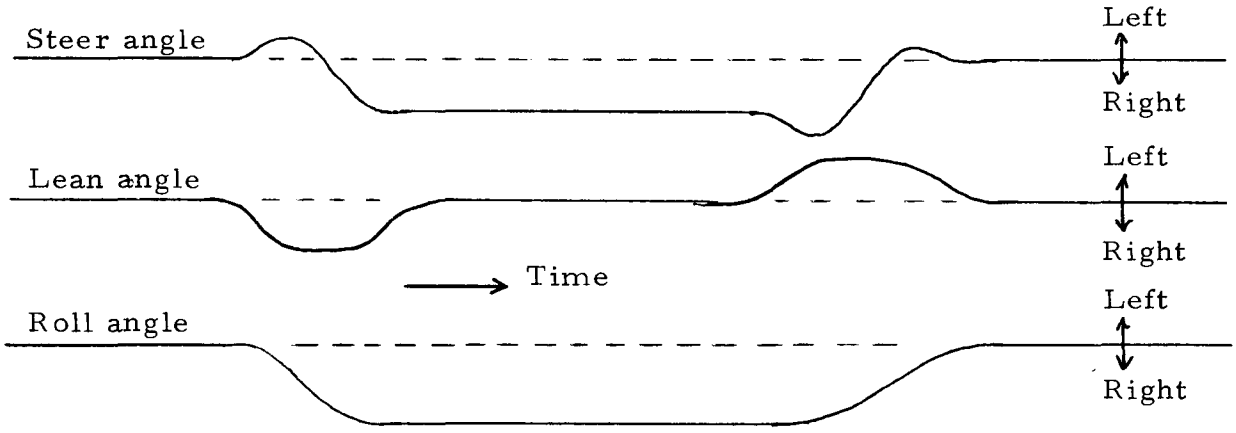

FIGURE 23. IDEALIZED CONTROL PROCEDURE FOR TRANSIENT TURN

It was noted that the peak in the inward lean angle occurred just after the point of maximum curvature in the bicycle roll angle trace (i.e., point of maximum roll acceleration). This suggests a strong roll acceleration to rider lean torque coupling. The basic inward lean could be due to a command roll angle-roll angle error term. The outward lean may be for stabilization. The turn is so quick that it is difficult to determine whether the rider might continue to lean out in a long steady state turn. If this were so, it would be an indication of a direct roll angle feedback, suggesting that the rider prefers to ride upright relative to the world as well as relative to the bicycle.

The steering motions in this maneuver have a similar function: initially steering the "wrong" way to cause rolling motion and, when coming out of the turn, steering further into the turn to roll the bicycle back to the vertical.

3.0 RIDER CONTROL MODEL DEVELOPMENT

Unlike three and four wheeled vehicles which have inherent roll stability, the bicycle must be constantly controlled by the rider to maintain an upright position, as well as to follow the intended path. It is therefore essential that a computer simulation which is designed to study bicycle stability and handling contain a mathematical model of the rider.

Basically, the rider has two means of controlling the bicycle: by steering and by leaning his body relative to the bicycle frame. These two control actions allow the rider to stabilize the bicycle in an upright position in straight running and at a constant roll angle in steady turns and to initiate turns and guide the bicycle along a desired path. Thus, there are two control functions: roll stabilization and guidance, and two control modes: steering and rider leaning, Figure 24.

The steer mode and the stabilization control function were developed and made operational in Phase II effort, see Reference 1 . One task of this Phase III effort was the development and implementation of the rider lean mode of control and the guidance function.

During Phase II a path following rider guidance function was formulated based on a "preview-predictor" model of the automobile driver previously developed by Calspan. This rider model derived control commands based on multiple error samples between the desired path and the predicted path of the bicycle. Initially in Phase III this model was incorporated in the bicycle simulation. An effort of several weeks was spent in attempting to obtain stable path following performance with no success. After having made a detailed study of the results of this guidance function and of the bicycle path following task in general, a new guidance function was developed. By using path heading error in addition to lateral path error in this guidance function, the bicycle-rider simulation was capable of following curved paths with proficiency.

Figure 24 , a revised block diagram of the bicycle rider control model, shows the feedback loops of both guidance and stabilization functions which are now operational with both the steer and lean control modes.

3.1 Guidance Function

The guidance function of the rider control model, although mathematically complex, is conceptually very simple. The concept is based on the ability of a bicycle rider (or human controller of any vehicle) to mentally visualize his future path, to compare it with his desired path, and to initiate control inputs correlated with the predicted deviations.

Thus the basis of the guidance function is an exceedingly simple mathematical model of bicycle dynamics which is hypothesized to exist within the mind of the rider. In order to avoid confusion, this simple model is called the "predictor model" since it is used by the rider to predict the bicycle's future trajectory.

Before discussing the formulation of the predictor model it is appropriate to explain some basic principles of human control theory.

1. Experiments with human operators have shown that they do not monitor control inputs continuously,but do so at discrete intervals in time. This sample time increment varies with the task and operator condition and becomes smaller with increasing task activity. A value of 0.1 second has been used for the "rider sample time increment" of the rider control model. This value which is small relative to the range of estimated sample time intervals from experimental measurements, has been purposely chosen to prevent control difficulties which migh arise from too infrequent sampling.

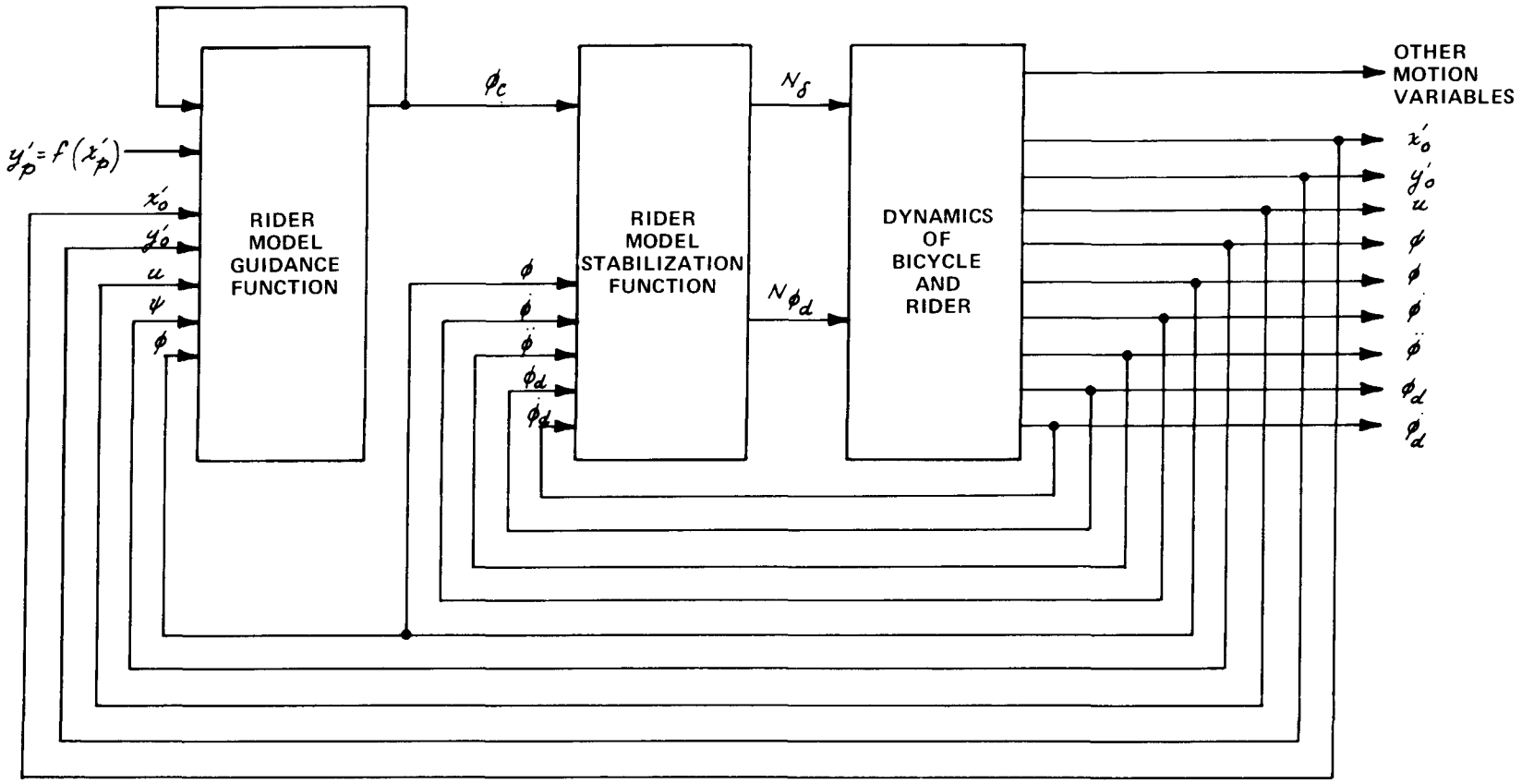

x'_o, y'_o	– BICYCLE COORDINATES	ϕ_d	– RIDER LEAN ANGLE
u	– FORWARD VELOCITY	$\dot{\phi}_d$	– RIDER LEAN ANGULAR VELOCITY
ψ	– YAW ANGLE	ϕ_c	– COMMAND ROLL ANGLE
ϕ	– ROLL ANGLE	N_δ	– STEER TORQUE
$\dot{\phi}$	– ROLL VELOCITY	N_{ϕ_d}	– RIDER LEAN TORQUE
$\ddot{\phi}$	– ROLL ACCELERATION	$y'_p = f(x'_p)$	– DESIRED PATH

FIGURE 24. BLOCK DIAGRAM OF BICYCLE RIDER CONTROL MODEL

2. Another important time-dependent variable associated with human operator control of vehicles is the "preview time increment". Controlling a moving vehicle would be impossible through a curved path by looking only at the path directly beneath the vehicle. Because of response lags in both the vehicle and the human it is necessary to look at the path ahead and make control corrections based on anticipated path errors. The look-ahead distance is largely dependent on vehicle veolocity. It is the look ahead distance divided by velocity or "preview time increment" which is the independent variable used in this study.

Thus the guidance function of the rider control model behaves as follows: At each rider sample time increment, the predicted path of the bicycle is generated by the predictor model. At a distance in front of bicycle determined by its speed and the preview time increment, the deviation between the desired path and the predicted path is computed. Based on path deviation errors the command roll angle is corrected. By means of the rider control model stabilization function, this changes the actual roll angle, which effectively changes lateral acceleration and leads to corrections in the actual path.

The predictor model is a simple one degree-of-freedom mathematical model of bicycle motion. The only independent variable is predicted lateral acceleration (a_{y_p}) which is a function of predicted roll angle (Φ_p). The forward velocity (u) is assumed to remain constant. The predicted motion variables of interest are the coordinates of the predicted path (x'_p , y'_p) the predicted yaw angle (Ψ_p), and the predicted yaw rate (r_p). These variables are functions of t_p and are compared with the desired path when t_p equals the preview time increment (t_s). The equations of motion of the predictor model are shown in Figure 25. This coupled set of equations is integrated from $t_p = 0$ to $t_p = t_s$. The resultant values

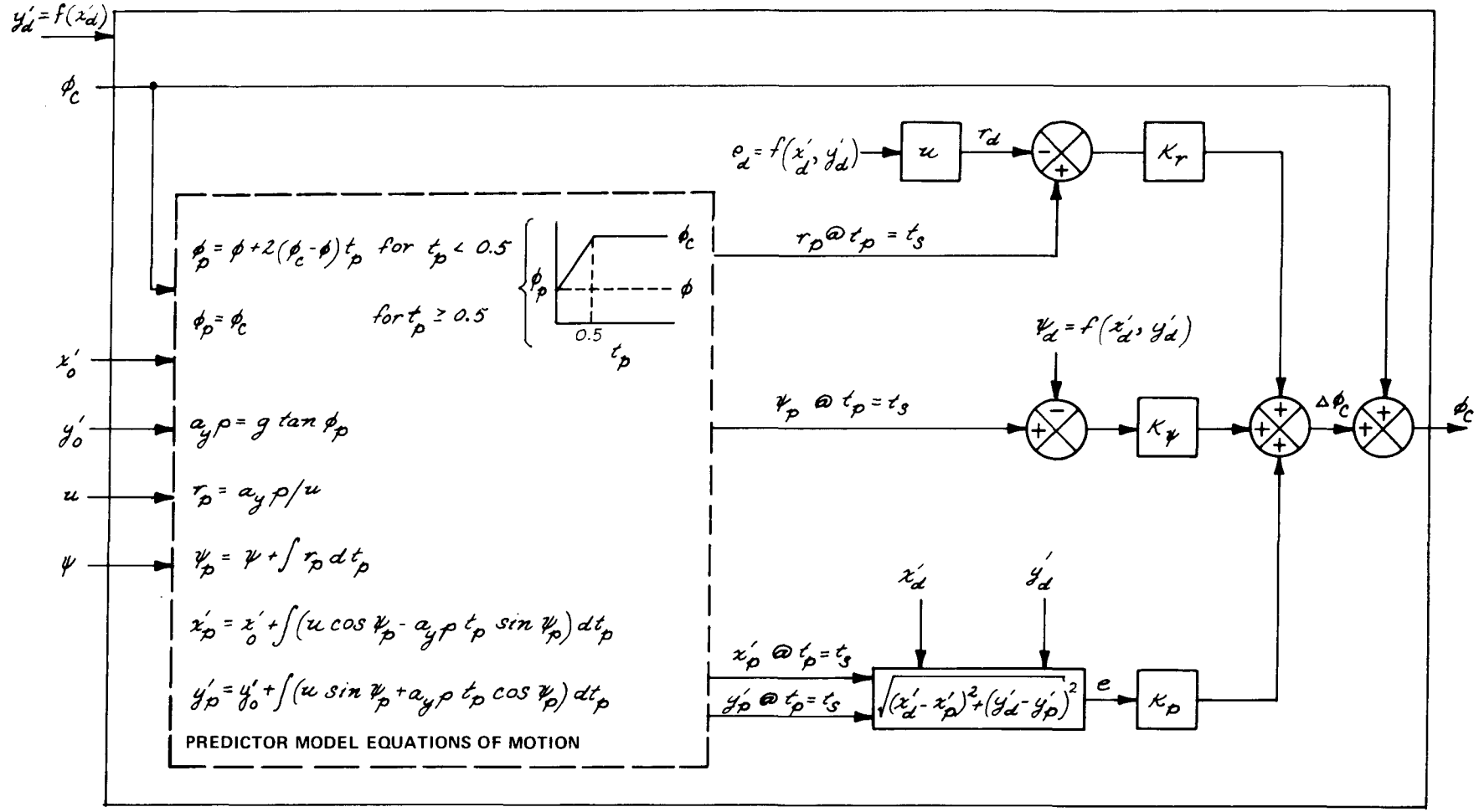

Figure 25. BLOCK DIAGRAM OF GUIDANCE FUNCTION OF RIDER CONTROL MODEL

of r_p, ψ_p, x'_p and y'_p at $t = t_s$ are compared with the appropriate desired path variables as explained later.

The predicted roll angle is initially equal to the actual bicycle roll angle (ϕ). The predicted roll angle changes at constant rate to the command roll angle (ϕ_c), i.e., $\phi_p = \phi_c$ @ $t_p = 0.5$ second as shown in Figure 26 .

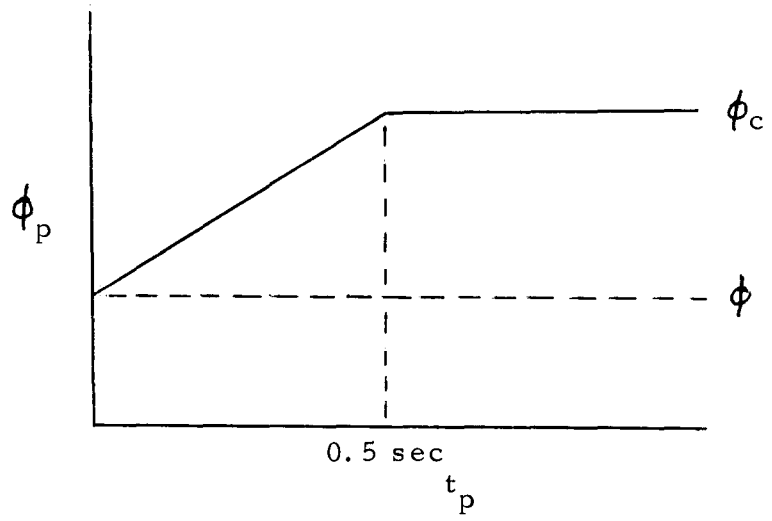

FIGURE 26. PREDICTED ROLL ANGLE VS. PREDICTOR TIME

This function is a simple representation of the lagging response of the actual bicycle roll angle to a command roll angle input as exhibited in several simulation runs.

The eventual output of the guidance function will be the corrected command roll angle. The magnitude of this correction will depend on three error factors relating the predicted path and the desired path. These error factors, which are measured at a point on the predicted

path (u t_s) inches ahead of the bicycle, are (1) lateral path error, (2) path heading error and (3) yaw rate error.

The lateral path error (e) is measured normal to the predicted path at the point (x'_p, y'_p). The desired path, $y'_d = f(x'_d)$ is defined by a series of circular arcs and straight line segments which connect points whose coordinate are specified. The circular arcs are mathematically defined to produce tangency at the junctions. The path error is computed by solving the analytical expressions relating the intersection (x'_d, y'_d) of the error line (the normal to the predicted path) with the appropriate segment of the desired path.

The path heading error is the difference in the predicted heading angle (ψ_p) at (x'_p, y'_p) and the heading angle of the desired path (ψ_d) at the intersection point (x'_d, y'_d). The desired path heading angle (ψ_d) is computed from the equation of the appropriate path segment.

The yaw rate error is the difference between the predicted yaw rate (r_p) at (x'_p, y'_p) and the steady state yaw rate (r_d) on the desired path at the bicycle velocity (u). The desired yaw rate (r_d) is computed by multiplying the curvature (ρ_d) of the respective segment of the desired path by the forward speed (u). The three error terms are then multiplied by their respective gain coefficients (K_p, K_ψ, K_r) and summed to give the resultant command roll angle correction, ($\Delta\phi_c$).

The ability of the rider model to provide stable path guidance depends on the predictor model's ability to accurately project the future bicycle path. With an inaccurate predictor model, differences between predicted and actual locations of the bicycle result in incorrect error estimates and control inputs which had to inaccurate or unstable tracking performance. Predictor model accuracy is strongly dependent on the predicted bicycle roll angle (ϕ_p) which varies with predictor time (t_p).

In the initial studies, very simplified functions of ϕ_p were used. Two of these functions were:

$$\phi_p = \phi_c \quad \text{and} \quad \phi_p = \phi + \dot{\phi}\, t_p$$

The use of neither of these proved successful because they predicted much faster lateral response than actually occurred. A close study of actual system performance indicated that the bicycle achieved a roll angle equal to the command roll angle after approximately 0.5 seconds, thus, the adoption of the current ϕ_p function.

Two observations were made with regard to the selection of the ϕ_p function and the rider preview time increment: (1) The use of preview time increments less than about 0.3 seconds is likely to result in unstable tracking performance since the system response will be too slow to make the required corrections, (2) Although the command roll angle, in fact, varies with time, a constant value (ϕ_c @ $t_p = 0$) is used in the ϕ_p function. This modeling technique represents the limitation of human precognitive ability. It was observed that the predicted path became increasingly inaccurate for predictor times greater than 0.7 seconds, depending on the magnitude of $\dot{\phi}_c$.

The rider model guidance function was programmed for the computer simulation and several test runs were performed to check tracking performance. A single maneuver consisting of a straight path leading into a wide right turn immediately followed by a tight left turn was chosen. Successive variations of guidance function coefficients (primarily K_e, K_ψ and K_r) were made until satisfactory tracking performance was achieved, Figure 27 . During these guidance function checks, it was found that the stabilization function coefficients had a greater influence on tracking <u>stability</u> than did the guidance function coefficients. Naturally, K_e and K_ψ had the greatest influence on tracking <u>accuracy</u>.

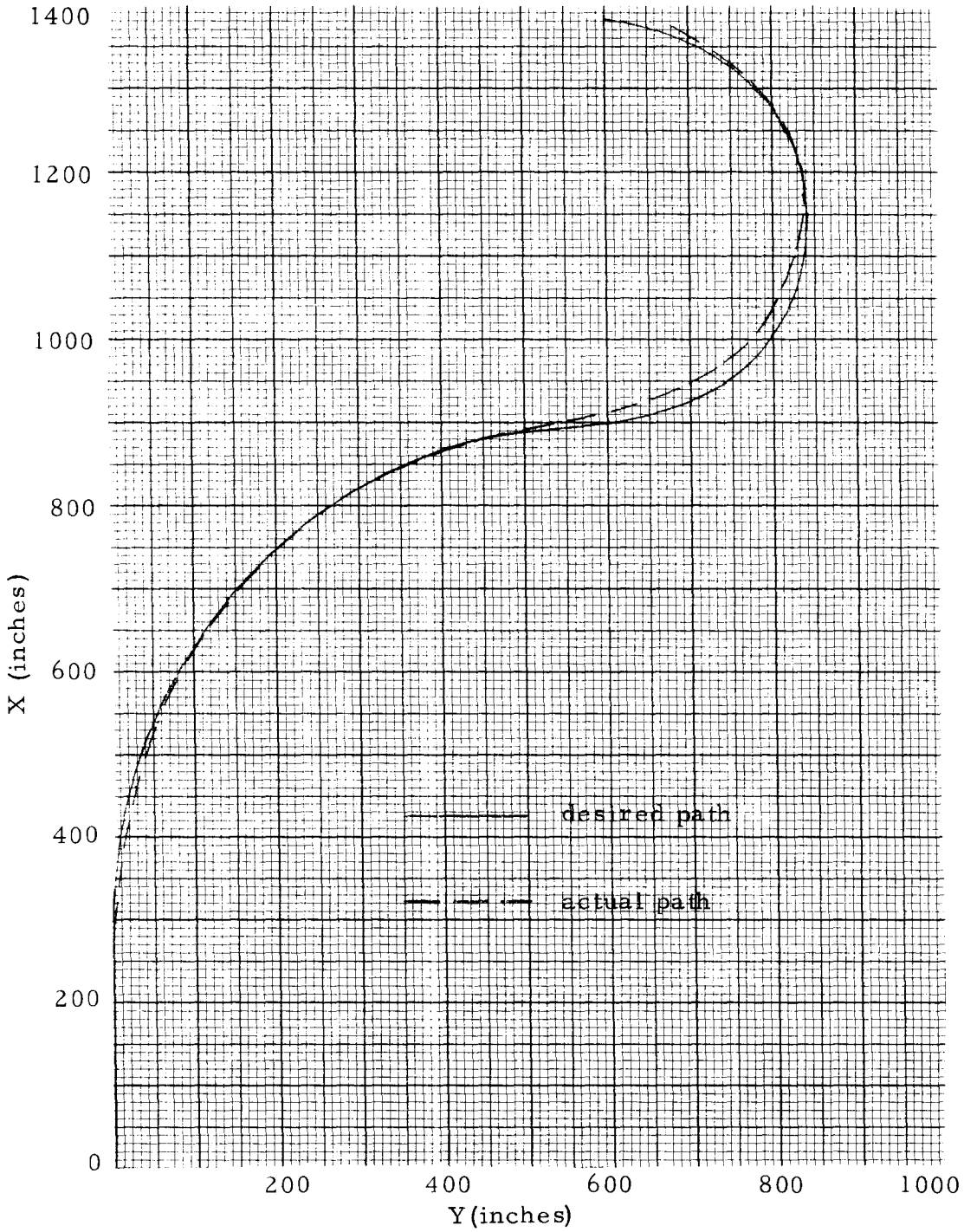

FIGURE 27. TYPICAL SIMULATION PATH FOLLOWING PERFORMANCE (10 mph)

3.2 Lean Control Mode

The lean mode of the rider control model was formulated on the basis of riding techniques observed in the experimental test program and on previous mathematical analyses of rider lean control of two-wheel vehicles (Reference 3 and 4). The following factors were considered in the development of the lean control mode. The modeling techniques employed are then discussed. Refer to Figure 28.

1. Rider lean motion is an independent degree-of-freedom of the model with torque control inputs (rather than a position control input). Thus the output of the rider lean control mode is lean torque. ($N\phi_d$).

2. The primary inputs to the lean control mode for the active control torques are the same as to the steer control mode: ϕ_c, ϕ, $\dot{\phi}$ and $\ddot{\phi}$.

3. Other inputs to the lean control mode for the passive control torques (see 4, 5 and 6 below) are rider lean angle and angular velocity: ϕ_d and $\dot{\phi}_d$.

4. The human has a physical hip restraint which limits rider lean angles to about 20 degrees. This is modeled by a restoring torque which is a cubic function of lean angle ($K_{1\phi_d^3} \phi_d^3$). The coefficient is adjusted to cause a sharp rise in restoring torque at about $\pm$ 20 degrees with almost no torque being exerted in the normal lean angle range.

5. It was observed in the experimental tests that the rider tends to stay in plane with the bicycle ($\phi_d = 0$)

in steady state turns* as well as in straight line travel. This is probably a matter of comfort since this position tends to reduce the steady state lean torque to zero. This condition was modeled mathematically as a torsional spring (with an effective rate of $K_{1\phi_d}$) which is continuously forcing the rider into the in-plane position. The value of $K_{1\phi_d}$ was set between that needed to overcome lean moments due to gravity and centrifugal forces and that which could cause simulation solution instabilities (resultant rider lean natural frequency was about 2 Hz.).

6. In order to assure smooth motion and prevent possible high frequency lean instabilities, the capability of generating a lean damping torque ($K_{1\phi_d}\ \phi_d$) was included. $K_{1\phi_d}$ was initially adjusted to provide ciritcal damping of the lean motion as determined by rider upper body inertia at the 2 Hz. natural frequency.

7. As in the steer control mode the primary active control torque is proportional to the difference between command roll angle and actual roll angle ($K_{1\phi}\ (\phi - \phi_c)$. $K_{1\phi}$ was adjusted on the basis of lean angles and roll angle achieved in transient turning maneuvers.

8. Roll velocity feedback ($K_{1\dot{\phi}}\ \dot{\phi}$) and roll acceleration feedback ($K_{1\ddot{\phi}}\ \ddot{\phi}$) are also included for active control torque. $K_{1\dot{\phi}}$ was adjusted during check-out of the lean control mode. $K_{1\ddot{\phi}}$ is currently set to zero.

* Although there were indications that in very tight turns at high roll angles the rider would lean out of the turn as much as one half the roll angle.

Figure 28 shows the revised rider roll stabilization function. The lean control mode was programmed for computer simulation and several check-out runs were made to adjust coefficients. With the final coefficients the resultant performance for a 20 degree command roll angle input (same as used for steer control mode alone in Phase II) is shown in Figure 29 .

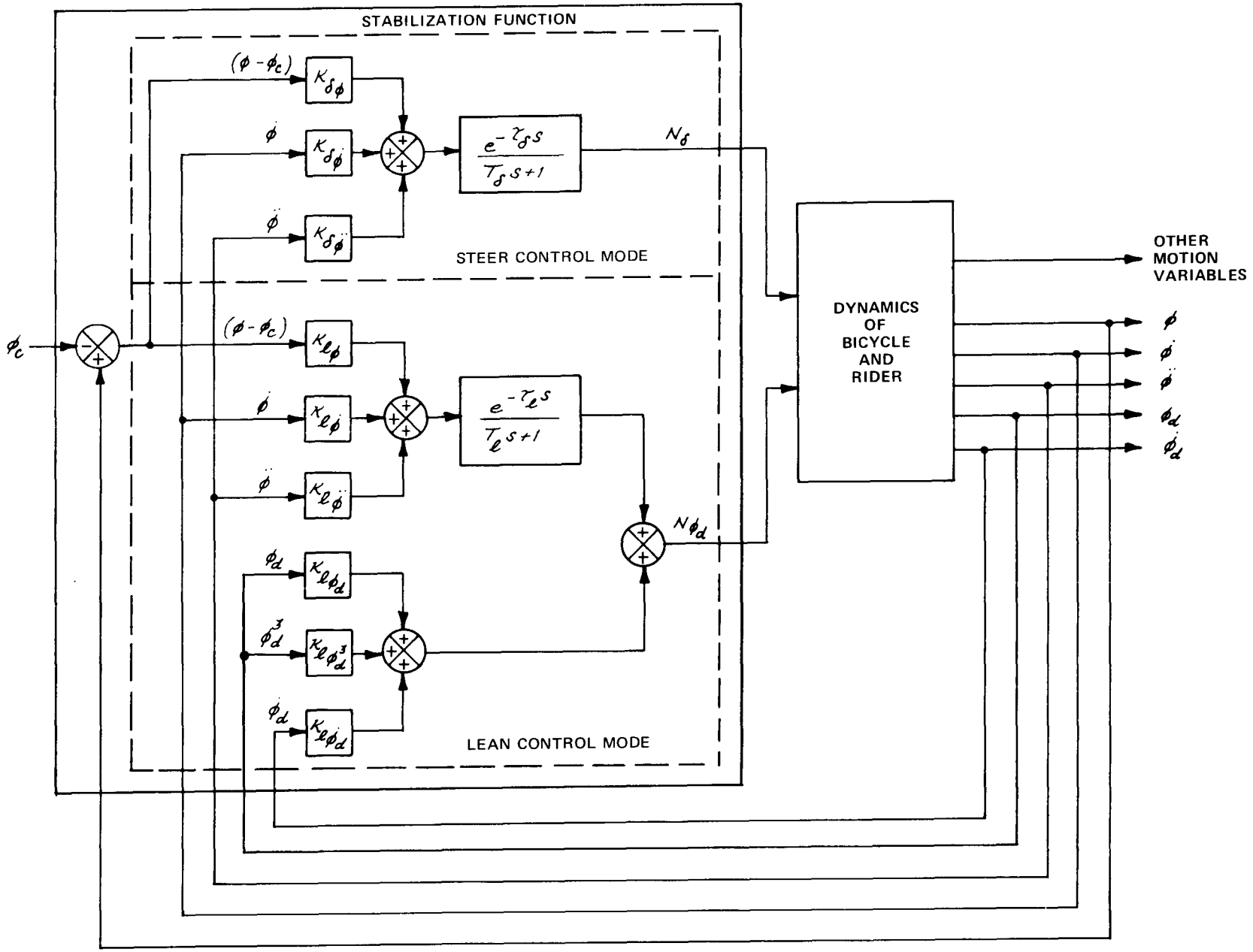

FIGURE 28. BLOCK DIAGRAM OF STABILIZATION FUNCTION OF RIDER CONTROL MODEL

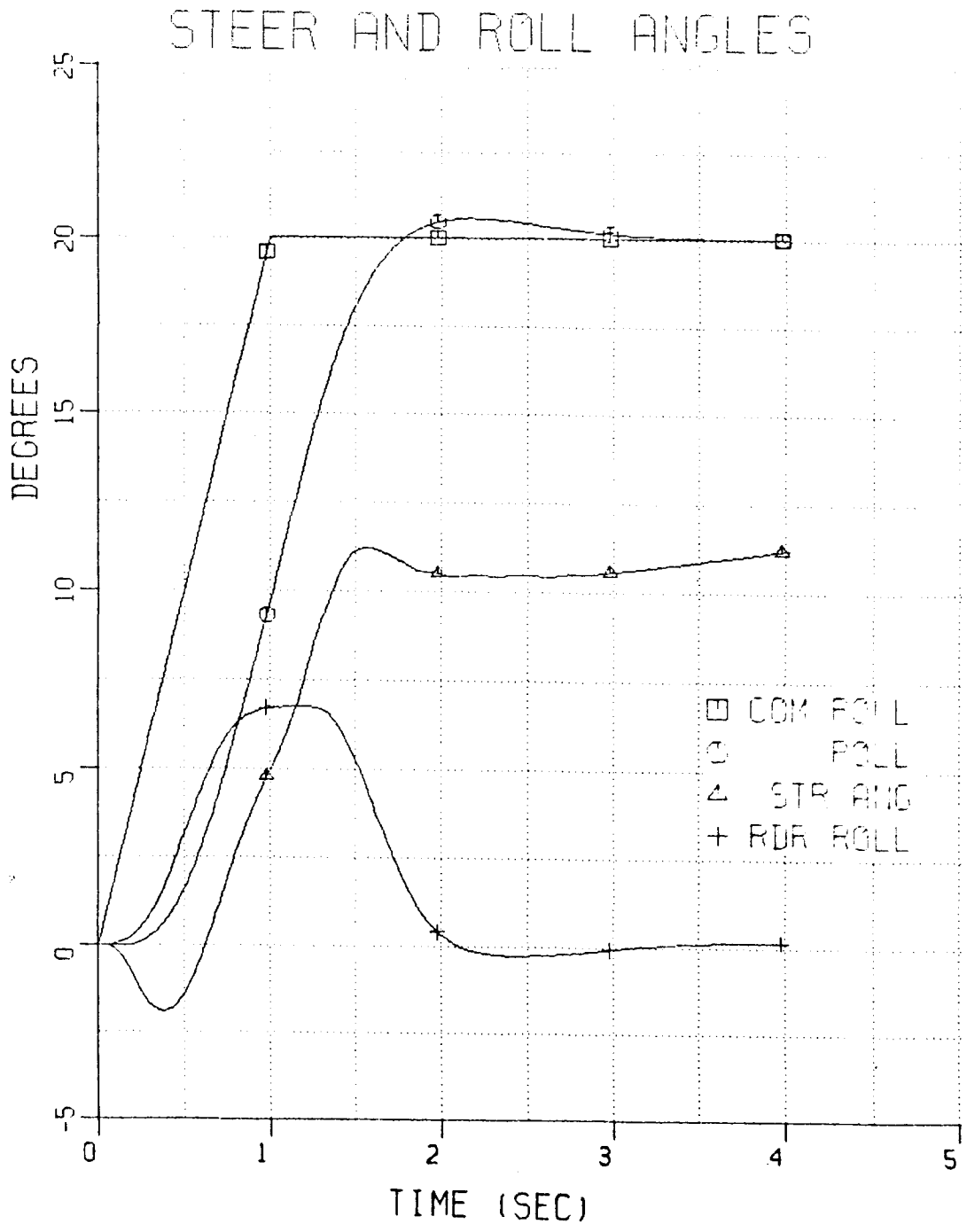

Figure 29: Steer and Lean Control Response

4.0 RIDER CONTROL MODEL PARAMETER STUDY

A simulation study was performed in which the rider control model coefficients were varied from run to run to determine their influence and system performance. Included in this study were the following parameters:

1. τ - reaction time delay
2. t_δ - compensation time lag
3. t_s - preview time increment
4. K_p - path error coefficient
5. K_ψ - heading angle error coefficient
6. K_r - yaw velocity error coefficient
7. $K_{\delta\phi}$ - roll angle - steer moment coefficient
8. $K_{\delta\dot{\phi}}$ - roll velocity - steer moment coeffcient
9. $K_{\delta\ddot{\phi}}$ - roll acceleration - steer moment coefficient

In general, the variation of each of these parameters was a $\pm$ 50% change from a nominal set of "workable" coefficients which had evolved from the rider control model check-out runs. In a broad sense, the rider control model check-out runs were also part of the rider model parameter study. In fact, the level of rider performance which evolved from the control model development was very close to that selected for the bicycle stability parameter study which was performed later. The simulated maneuver for this study was a straight path tracking task with a side force disturbance input. Although the guidance function had the capability for curved path tracking, the straight path task was selected because the experimental tests had shown that, subjectively, there was little difference in disturbance-response behavior for the two riding situations. Further, the straight path task caused less confusion in

interpreting the results. A single speed of 10 mph was used in this study (the bicycle stability parameter study performed later showed that the influence of speed is of primary importance). The standard Suburban was used as the base bicycle configuration. Appendix C contains plots of the time histories of steer and roll angles for 19 runs of this study.

A primary objective of the rider model parameter study was to derive a set of coefficients which would produce performance representative of an "average rider". This was to be done by comparing the simulation results with the experimental test data from the side force disturbance response tests. Simulation performance levels were to be classified (poor, average, superior) an the basis of bicycle stability and rider control responsiveness and damping. Because of the variability in the experimental data representing actual rider performance, was not meaningful to classify the simulation results on this basis. It is speculated that the inconsistancy in rider behavior in this task is due to the small magnitude of the disturbing force. The required recovery maneuver was too easy. Therefore, many variations in control response which provided successful recovery were possible. If the disturbance had been greater and the task more difficult, it might have resulted in a more consistant pattern of control response.

Therefore, rather than classifying on the basis of actual rider performance, a technical classification was made of the stability parameter study (Section 5.0) and allows comparisons of the relative effects of rider control model changes versus bicycle parameter changes. Table 1 is a summary of the results.

Run No.	RIDER CONTROL MODEL COEFFICIENTS									Response*
	$\hat{C}$	T_s	t_s	K_p	K_ψ	K_r	K_{s_ϕ}	$K_{s_{\dot{\phi}}}$	$K_{s_{\ddot{\phi}}}$	
1	0	0.1	1.0	0.004	-0.2	-0.4	400	200	50	S
2	0	0.1	1.0	0.004	-0.2	-0.4	800	280	50	OS (1.0)
3	0	0.1	1.0	0.004	-0.2	-0.4	144	120	50	OU (.25)
4	0	0.1	1.0	0.004	-0.2	-0.4	400	280	50	S
5	0	0.1	1.0	0.004	-0.2	-0.4	400	120	50	OU (.57)
6	0	0.1	1.0	0.004	-0.2	-0.4	400	200	70	OS (.48)
7	0	0.1	1.0	0.004	-0.2	-0.4	400	200	30	OS (1.0)
8	0	.05	1.0	0.004	-0.2	-0.4	400	200	50	S
9	0	0.2	1.0	0.004	-0.2	-0.4	400	200	50	S
10	.05	0.1	1.0	0.004	-0.2	-0.4	400	200	50	OS (2.0)
11	0.1	0.1	1.0	0.004	-0.2	-0.4	400	200	50	OU (1.7)
12	0	0.1	0.5	0.004	-0.2	-0.4	400	200	50	S
13	0	0.1	2.0	0.004	-0.2	-0.4	400	200	50	OU
14	0	0.1	1.0	0.002	-0.2	-0.4	400	200	50	S
15	0	0.1	1.0	0.006	-0.2	-0.4	400	200	50	OS (1.3)
16	0	0.1	1.0	0.004	-0.1	-0.4	400	200	50	S
17	0	0.1	1.0	0.004	-0.3	-0.4	400	200	50	S
18	0	0.1	1.0	0.004	-0.2	-0.2	400	200	50	OS (.74)
19	0	0.1	1.0	0.004	-0.2	-0.6	400	200	50	OU

* Response code:

S	-	nonoscillatory stable	
OS	-	oscillatory stable	(oscillation frequency, Hz.)
OU	-	oscillatory unstable	

TABLE 1. RIDER CONTROL MODEL PARAMETER STUDY RESULT MATRIX

5.0 BICYCLE-RIDER DISTURBANCE RESPONSE STABILITY STUDY

A simulated bicycle stability study was performed to compare three standard bicycle configurations and to determine the effects of certain bicycle design parameter changes. Three basic bicycle configurations were used in this study: (1) standard bicycle - single speed Schwinn Suburban with conventional handle bars and coaster brakes (the same bicycle used in Phase I study, Ref. 1.), (2) high rise bicycle - single speed Schwinn Sting-Ray with high handle bars and coaster brakes, (3) racer - 15 speed Schwinn Paramount with drop handle bars and caliper brakes. Experimental measurements of the physical characteristics (weights, dimensions, moments of inertia) of the high rise and racer bicycles were made as was done in Phase I for the standard bicycle. The characteristics of the bicycles are shown in Figures 30, 31 and 32.

The parameter study consisted of the same variations which were used in the Phase I study of the stability of a riderless bicycle. The base configuration for the parameter study was the standard Suburban. All simulated maneuvers had a single parameter variation with other data remaining the same as the standard configuration. For each parameter a value higher and one lower than the standard were run. In some cases the high and low values represented the range of this parameter in current production bicycles. In other cases, arbitrary values of 80% and 120% of the standard were used.

The simulated maneuver consisted of a straight path following task in which a side force disturbance was imposed on the frame of the bicycle, see Section 2.2 .

This disturbance response maneuver was performed at speeds of 6, 10 and 15 mph for each bicycle configuration. Plots of the time histories of steer and roll angles are shown in Appendix D for all 63 runs of the study.

WHEELBASE (IN)	41.5	WEIGHT OF RIDER (LB)	102.00
TOTAL WEIGHT OF BICYCLE (LB)	46.60	LOCATION OF RIDER C.G. FORWARD OF REAR WHEEL CENTER (IN)	11.30
LOCATION OF TOTAL BICYCLE C.G. FORWARD OF REAR WHEEL CENTER (IN)	18.03	HEIGHT OF RIDER C.G. ABOVE GROUND (IN)	46.60
LOCATION OF TOTAL BICYCLE C.G. ABOVE GROUND (IN)	20.76	HEIGHT OF SADDLE ABOVE GROUND (IN)	46.70
ROLL MOMENT OF INERTIA OF THE TOTAL BICYCLE ABOUT AXIS THROUGH TOTAL C.G. (LB-IN-SEC SQ)	12.64	ROLL MOMENT OF INERTIA OF RIDER ABOUT AN AXIS THROUGH HIS C.G. (LB-IN-SEC SQ)	27.80
PITCH MOMENT OF INERTIA OF THE TOTAL BICYCLE ABOUT AXIS THROUGH TOTAL C.G. (LB-IN-SEC SQ)	35.95	PITCH MOMENT OF INERTIA OF RIDER ABOUT AN AXIS THROUGH HIS C.G. (LB-IN-SEC SQ)	39.90
YAW MOMENT OF INERTIA OF THE TOTAL BICYCLE ABOUT AXIS THROUGH TOTAL C.G. (LB-IN-SEC SQ)	25.70	YAW MOMENT OF INERTIA OF RIDER ABOUT AN AXIS THROUGH HIS C.G. (LB-IN-SEC SQ)	18.40
ROLL-YAW PRODUCT OF INERTIA OF THE TOTAL BICYCLE ABOUT AXIS THROUGH TOTAL C.G. (LB-IN-SEC SQ)	-1.62	ROLL-YAW PRODUCT OF INERTIA OF RIDER ABOUT AN AXIS THROUGH HIS C.G. (LB-IN-SEC SQ)	0.0
WEIGHT OF FRONT FORK ASSEMBLY (FORK,WHEEL,AND HANDLE BARS),(LB)	11.40	CASTER ANGLE OF THE STEER AXIS (DEG)	21.00
PERPENDICULAR DISTANCE FROM C.G. OF FRONT FORK ASSEMBLY TO STEER AXIS (IN)	1.50	FORK OFFSET (IN)	1.87
DISTANCE PARALLEL TO STEER AXIS FROM C.G. OF FRONT FORK ASSEMBLY TO FRONT WHEEL CENTER (IN)	9.50	UNDEFLECTED WHEEL ROLLING RADIUS (IN)	13.62
ROLL MOMENT OF INERTIA OF FRONT FORK ASSEMBLY ABOUT AN AXIS PERPENDICULAR TO THE STEER AXIS THROUGH C.G. OF ASSEMBLY (LB-IN-SEC SQ)	4.59	TIRE SECTION WIDTH (IN)	1.60
		RADIAL STIFFNESS OF TIRE (LB/IN)	100.00
		SPIN MOMENT OF INERTIA OF THE FRONT WHEEL (LB-IN-SEC SQ)	1.76
PITCH MOMENT OF INERTIA OF FRONT FORK ASSEMBLY ABOUT AN AXIS THROUGH THE C.G. OF THE ASSEMBLY (LB-IN-SEC SQ)	5.56	SPIN MOMENT OF INERTIA OF THE REAR WHEEL (LB-IN-SEC SQ)	1.76
		VERTICAL LOAD-TIRE SIDE FORCE COEF. (LB/LB/LB)	-0.00
YAW MOMENT OF INERTIA OF FRONT FORK ASSEMBLY ABOUT THE STEER AXIS (LB-IN-SEC SQ)	1.86	SLIP ANGLE-TIRE SIDE FORCE COEF. (LB/LB/DEG)	0.226
ROLL-YAW PRODUCT OF INERTIA OF FRONT FORK ASSEMBLY ABOUT AN AXIS THROUGH THE C.G. OF THE ASSEMBLY (LB-IN-SEC SQ)	-0.52	SLIP ANGLE CUBED-TIRE SIDE FORCE COEFFICIENT (LB/LB/DEG SQ)	-0.00232
		INCLINATION ANGLE-TIRE SIDE FORCE COEFFICIENT (LB/LB/DEG)	0.00325

FIGURE 30 - Physical Characteristics of the Suburban

PHYSICAL CHARACTERISTICS OF THE SCHWINN J38-6 STING-RAY 22JUN'72

WHEELBASE (IN)	35.00
TOTAL WEIGHT OF BICYCLE (LB)	36.70
LOCATION OF TOTAL BICYCLE C.G. FORWARD OF REAR WHEEL CENTER (IN)	15.10
LOCATION OF TOTAL BICYCLE C.G. ABOVE GROUND (IN)	15.50
ROLL MOMENT OF INERTIA OF THE TOTAL BICYCLE ABOUT AXIS THROUGH TOTAL C.G. (LB-IN-SEC SQ)	8.54
PITCH MOMENT OF INERTIA OF THE TOTAL BICYCLE ABOUT AXIS THROUGH TOTAL C.G. (LB-IN-SEC SQ)	24.16
YAW MOMENT OF INERTIA OF THE TOTAL BICYCLE ABOUT AXIS THROUGH TOTAL C.G. (LB-IN-SEC SQ)	17.22
ROLL-YAW PRODUCT OF INERTIA OF THE TOTAL BICYCLE ABOUT AXIS THROUGH TOTAL C.G. (LB-IN-SEC SQ)	-1.96

WEIGHT OF RIDER (LB)	0.0
LOCATION OF RIDER C.G. FORWARD OF REAR WHEEL CENTER (IN)	0.0
HEIGHT OF RIDER C.G. ABOVE GROUND (IN)	0.0
HEIGHT OF SADDLE ABOVE GROUND (IN)	0.0
ROLL MOMENT OF INERTIA OF RIDER ABOUT AN AXIS THROUGH HIS C.G. (LB-IN-SEC SQ)	0.0
PITCH MOMENT OF INERTIA OF RIDER ABOUT AN AXIS THROUGH HIS C.G. (LB-IN-SEC SQ)	0.0
YAW MOMENT OF INERTIA OF RIDER ABOUT AN AXIS THROUGH HIS C.G. (LB-IN-SEC SQ)	0.0
ROLL-YAW PRODUCT OF INERTIA OF RIDER ABOUT AN AXIS THROUGH HIS C.G. (LB-IN-SEC SQ)	0.0

WEIGHT OF FRONT FORK ASSEMBLY (FORK,WHEEL,AND HANDLE BARS),(LB)	10.20
PERPENDICULAR DISTANCE FROM C.G. OF FRONT FORK ASSEMBLY TO STEER AXIS (IN)	1.50
DISTANCE PARALLEL TO STEER AXIS FROM C.G. OF FRONT FORK ASSEMBLY TO FRONT WHEEL CENTER (IN)	10.30
ROLL MOMENT OF INERTIA OF FRONT FORK ASSEMBLY ABOUT AN AXIS PERPENDICULAR TO THE STEER AXIS THROUGH C.G. OF ASSEMBLY (LB-IN-SEC SQ)	3.87
PITCH MOMENT OF INERTIA OF FRONT FORK ASSEMBLY ABOUT AN AXIS THROUGH THE C.G. OF THE ASSEMBLY (LB-IN-SEC SQ)	4.05
YAW MOMENT OF INERTIA OF FRONT FORK ASSEMBLY ABOUT THE STEER AXIS (LB-IN-SEC SQ)	1.29
ROLL-YAW PRODUCT OF INERTIA OF FRONT FORK ASSEMBLY ABOUT AN AXIS THROUGH THE C.G. OF THE ASSEMBLY (LB-IN-SEC SQ)	0.41

CASTER ANGLE OF THE STEER AXIS (DEG)	21.00
FORK OFFSET (IN)	1.60
UNDEFLECTED WHEEL ROLLING RADIUS (IN)	10.00
TIRE SECTION WIDTH (IN)	1.75
RADIAL STIFFNESS OF TIRE (LB/IN)	500.00
SPIN MOMENT OF INERTIA OF THE FRONT WHEEL (LB-IN-SEC SQ)	0.69
SPIN MOMENT OF INERTIA OF THE REAR WHEEL (LB-IN-SEC SQ)	0.69
FIRST AND SECOND ORDER COEFFICIENTS RELATING TIRE SIDE FORCE AND SLIP ANGLE	0.0 0.0
FIRST AND SECOND ORDER COEFFICIENTS RELATING TIRE SIDE FORCE AND INCLINATION ANGLE	0.0 0.0
COEFFICIENT OF ROLLING RESISTANCE (LB/LB)	0.0
AERODYNAMIC DRAG COEFFICIENT (LB/MPH-SQ)	0.0

FIGURE 31 - Physical Characteristics of the Sting-Ray

PHYSICAL CHARACTERISTICS OF THE 26 INCH SCHWINN P15 PARAMOUNT 22JUN'72

WHEELBASE (IN)	42.00
TOTAL WEIGHT OF BICYCLE (LB)	25.50
LOCATION OF TOTAL BICYCLE C.G. FORWARD OF REAR WHEEL CENTER (IN)	19.20
LOCATION OF TOTAL BICYCLE C.G. ABOVE GROUND (IN)	21.00
ROLL MOMENT OF INERTIA OF THE TOTAL BICYCLE ABOUT AXIS THROUGH TOTAL C.G. (LB-IN-SEC SQ)	8.51
PITCH MOMENT OF INERTIA OF THE TOTAL BICYCLE ABOUT AXIS THROUGH TOTAL C.G. (LB-IN-SEC SQ)	25.04
YAW MOMENT OF INERTIA OF THE TOTAL BICYCLE ABOUT AXIS THROUGH TOTAL C.G. (LB-IN-SEC SQ)	18.07
ROLL-YAW PRODUCT OF INERTIA OF THE TOTAL BICYCLE ABOUT AXIS THROUGH TOTAL C.G. (LB-IN-SEC SQ)	-2.57

WEIGHT OF RIDER (LB)	0.0
LOCATION OF RIDER C.G. FORWARD OF REAR WHEEL CENTER (IN)	0.0
HEIGHT OF RIDER C.G. ABOVE GROUND (IN)	0.0
HEIGHT OF SADDLE ABOVE GROUND (IN)	0.0
ROLL MOMENT OF INERTIA OF RIDER ABOUT AN AXIS THROUGH HIS C.G. (LB-IN-SEC SQ)	0.0
PITCH MOMENT OF INERTIA OF RIDER ABOUT AN AXIS THROUGH HIS C.G. (LB-IN-SEC SQ)	0.0
YAW MOMENT OF INERTIA OF RIDER ABOUT AN AXIS THROUGH HIS C.G. (LB-IN-SEC SQ)	0.0
ROLL-YAW PRODUCT OF INERTIA OF RIDER ABOUT AN AXIS THROUGH HIS C.G. (LB-IN-SEC SQ)	0.0

WEIGHT OF FRONT FORK ASSEMBLY (FORK,WHEEL,AND HANDLE BARS),(LB)	7.30
PERPENDICULAR DISTANCE FROM C.G. OF FRONT FORK ASSEMBLY TO STEER AXIS (IN)	1.90
DISTANCE PARALLEL TO STEER AXIS FROM C.G. OF FRONT FORK ASSEMBLY TO FRONT WHEEL CENTER (IN)	11.00
ROLL MOMENT OF INERTIA OF FRONT FORK ASSEMBLY ABOUT AN AXIS PERPENDICULAR TO THE STEER AXIS THROUGH C.G. OF ASSEMBLY (LB-IN-SEC SQ)	2.59
PITCH MOMENT OF INERTIA OF FRONT FORK ASSEMBLY ABOUT AN AXIS THROUGH THE C.G. OF THE ASSEMBLY (LB-IN-SEC SQ)	2.75
YAW MOMENT OF INERTIA OF FRONT FORK ASSEMBLY ABOUT THE STEER AXIS (LB-IN-SEC SQ)	0.71
ROLL-YAW PRODUCT OF INERTIA OF FRONT FORK ASSEMBLY ABOUT AN AXIS THROUGH THE C.G. OF THE ASSEMBLY (LB-IN-SEC SQ)	-0.17

CASTER ANGLE OF THE STEER AXIS (DEG)	17.40
FORK OFFSET (IN)	2.10
UNDEFLECTED WHEEL ROLLING RADIUS (IN)	13.50
TIRE SECTION WIDTH (IN)	1.00
RADIAL STIFFNESS OF TIRE (LB/IN)	1000.00
SPIN MOMENT OF INERTIA OF THE FRONT WHEEL (LB-IN-SEC SQ)	0.73
SPIN MOMENT OF INERTIA OF THE REAR WHEEL (LB-IN-SEC SQ)	0.73
FIRST AND SECOND ORDER COEFFICIENTS RELATING TIRE SIDE FORCE AND SLIP ANGLE	0.0 0.0
FIRST AND SECOND ORDER COEFFICIENTS RELATING TIRE SIDE FORCE AND INCLINATION ANGLE	0.0 0.0
COEFFICIENT OF ROLLING RESISTANCE (LB/LB)	0.0
AERODYNAMIC DRAG COEFFICIENT (LB/MPH-SQ)	0.0

FIGURE 32 - Physical Characteristics of the Paramount

It is well known that the human rider is adaptive and that his characteristics change with the task, speed, etc. as well as with the dynamics of the bicycle. It should be kept in mind that these simulated responses were made with a set of rider model coefficients which remained constant throughout the study. Nevertheless, these data are a measure of bicycle stability since they indicate the degree of adaption which would be required to achieve a level of performance equal to that of the base configuration.

Before discussing the results of this parameter study in detail several significant observations will be made about the results in general.

1. Bicycle speed had a more pronounced effect on stability than did any of the changes in bicycle configuration tested. Typically, all configurations were stable and well behaved at 15 mph and oscillatory unstable at 6 mph.

2. The Sting-Ray had remarkably superior performance at 6 mph compared to all other configurations tested. This was the only configuration to exhibit stable nonoscillatory disturbance response behavior at 6 mph. However, at the higher speeds, particularly 15 mph, this bicycle showed significantly inferior performance.

3. Wheelbase was the single parameter having the greatest effect on stability. The short wheelbase configuration of the suburban (33.2 in.) exhibited damped oscillatory response at 6 mph whereas the long wheelbase configuration (44.8 in.) was oscillatory unstable. Further, the amplitude of the steering correction was almost twice as large for the long wheelbase as for the short wheelbase. With increasing

speed the difference in performance became smaller, with the difference between these two configurations becoming insignificant at 15 mph.

4. Three configurations were so unstable at 6 mph that they eventually fell over. These were the Paramount, the light weight (25.0 lb.) configuration, and the high c.g. (24.9 in.) configuration.

5. Four configurations exhibited significantly more stable performance at 6 mph than the others. As previously discussed the Sting-Ray had superior performance. The short wheelbase (33.2 in.) configuration, the short steering trail (2.87 in. fork offset) configuration, and the small wheel diameter (20.0 in.) configuration showed damped oscillatory response whereas all others were oscillatory unstable.

6. The amplitude of the required steering correction became considerably smaller with increasing speed. 27° - 56° at 6 mph, 8° - 14° at 10 mph, and 4° - 6° at 15 mph.

7. The amplitude of the roll response showed a slight increase with increasing speed: 8° - 12° at 6 mph and 10 mph, and 10° - 15° at 15 mph.

Table 2 summarizes the disturbance response behavior of the bicyle-rider system at 6, 10 and 15 mph for the three bicycles and several configurations of the Surburban with various parameter changes. The following code was used in abbreviating the results.

#A-B
(C/D)

where:

A - simulation run number

B - { S nonoscillatory stable
OS oscillatory stable
OU oscillatory unstable

C - amplitude (peak to peak) of steering correction in degrees

D - amplitude (peak to peak) of the first cycle of roll response; * indicates bicycle fell over.

The responses of the three bicycles and the effects of the parameter variations on the Suburban are discussed below.

1. The standard Suburban configuration was oscillatory unstable at 6 mph, and nonoscillatory stable at 10 mph and 15 mph.

2. The Paramount was oscillatory unstable at 6 mph and eventually fell over. At 10 mph and 15 mph the stability of the Paramount was equivalent to the standard Suburban.

3. The Sting-Ray was nonoscillatory stable at 6 mph but had larger roll response amplitude than the standard Suburban at 10 mph and 15 mph.

For the Suburban:

4. Reducing the wheelbase from 41.5 to33.2 improved low speed stability and had little effect at 15 mph. Increasing the wheelbase to 49.8 degraded low speed stability with little effect at 15 mph.

BICYCLE CONFIGURATION		SPEED		
		6 mph	10 mph	15 mph
Standard Suburban		#1 - OU (37/9)	#2 - S (12/9)	#3 - S (5/10)
Standard Paramount		#4 - OU (56/*)	#5 - S (12/9)	#6 - S (5/10)
Standard Sting-Ray		#7 - S (30/11)	#8 - S (9/12)	#9 - S (5/15)
Wheelbase	33.2 in.	#10 - OS (27/8)	#11 - S (8/9)	#12 - S (4/11)
	49.8 in.	#13 - OU (47/12)	#14 - S (15/8)	#15 - S (6/10)
Total Weight	25.0 lb.	#16 - OU (42/*)	#17 - S (13/9)	#18 - S (5/10)
	55.0 lb.	#19 - OU (34/9)	#20 - S (10/8)	#21 - S (4/10)
Total C.G. Height	16.6 in.	#22 - OU (37/10)	#23 - S (12/9)	#24 - S (4/10)
	24.9 in.	#25 - OU (44/*)	#26 - S (11/9)	#27 - S (4/10)
Steer Moment of Inertia	1.49 $lb\text{-}in\text{-}sec^2$	#28 - OU (35/9)	#29 - S (11/8)	#30 - S (4/10)
	2.23 $lb\text{-}in\text{-}sec^2$	#31 - OU (38/10)	#32 - S (12/8)	#33 - S (4/10)
Caster Angle	15.0 deg.	#34 - OU (36/10)	#35 - S (11/8)	#36 - S (4/10)
	25.0 deg.	#37 - OU (38/9)	#38 - S (12/9)	#39 - S (5/10)
Fork Offset	0.87 in.	#40 - OU (39/12)	#41 - S (12/8)	#42 - S (5/10)
	2.87 in.	#43 - OS (34/8)	#44 - S (12/9)	#45 - S (4/10)
Undeflected Rolling Radius	10.0 in.	#46 - OS (34/7)	#47 - S (10/9)	#48 - S (4/11)
	14.6 in.	#49 - OU (37/10)	#50 - S (12/8)	#51 - S (4/10)
Wheel Moment of Inertia	1.41 $lb\text{-}in\text{-}sec^2$	#52 - OU (37/9)	#53 - S (12/8)	#54 - S (5/10)
	2.11 $lb\text{-}in\text{-}sec^2$	#55 - OU (36/9)	#56 - S (13/9)	#57 - S (4/10)
Tire Cornering Stiffness	low	#58 - OU (36/9)	#59 - S (14/9)	#60 - S (5/10)
	high	#61 - OU (36/9)	#62 - S (12/9)	#63 - S (4/10)

TABLE 2. BICYCLE STABILITY PARAMETER STUDY RESULT MATRIX

5. Reducing the total bicycle weight from 40.8 lb to 25.0 lb degraded low speed stability, increasing bicycle weight to 55.0 lb caused a slight improvement in low speed stability. Weight had little effect on stability at 15 mph.

6. Lowering the height of the bicycle center of gravity had little effect; however, raising the c.g. from 20.8 in.to 24.9 in.reduced low speed stability and caused the bicycle to eventually fall over. Center of gravity height had little effect at 15 mph.

7. Reducing the steer moment of inertia from 1.86 to 1.49 lb-in-sec^2 or increasing it to 2.23 lb-in-sec^2 had little effect at any speed tested. There was a slight trend of improved performance with reduced inertia.

8. Reducing caster angle from 21.0 degrees to 15.0 degrees or increasing it to 25.0 degrees while maintaining constant steering trail had little effect on stability throughout the speed range tested.

9. Reducing steering trail (by increasing fork offset) from 2.9 in.to 1.9 in.resulted in damped oscillatory response at 6 mph. Increasing steering trail to 3.9 in.degraded stability at low speed causing an increase in roll response amplitude. Steering trail had little effect at 10 mph and 15 mph.

10. Reducing the rolling radii from 13.6 in.to 10.0 in. resulted in damped oscillatory response at 6 mph with little effect at 10 mph and 15 mph. Increasing the rolling radii to 14.6 in.had little effect at any speed tested.

11. Reducing the front wheel spin moment of inertia from 1.76 to 1.41 lb-in-sec^2 or increasing it to 2.11 lb-in-sec^2 had little effect at any speed tested.

12. Reducing or increasing the tire cornering stiffness by 20% had little effect at any speed tested.

6.0 HIGH SPEED BICYCLE STEERING STABILITY

The potential for the existence of a high speed instability in single track vehicles has been long recognized by theoretical dynamicists. This condition, which was called "speedman's wobble" by Pearsall and defined as the "weave" mode of oscillation by Sharp has been treated in a number of studies but no clear and complete understanding of it has resulted, primarily because of limitations in the mathematical models used for analysis.

The low speed roll stability of the bicycle has been a subject of considerable analytical research. Published work on the single track vehicle dates back to the turn of the century. Unfortunately many of these mathematical treatments did not consider the effects of gyroscopic moments, tire mechanics and high speed operation. In 1956, Dohring discussed the steering wobble of high speed motorcycles. However, he neglected the interaction between the front fork assembly and the rear frame and the tire mechanics were greatly oversimplified. Collins performed a mathematical analysis of the effects of motorcycle parameters on stability. Singh's analysis, published in 1964, was the most comprehensive at that time. However, this study was not directly related to the effects of design on high speed stability.

This phenomenon, which is manifested as coupled roll-yaw motions of the unit at high speed, is characterized by near-zero damping of oscillations of the steering system. Motion pictures of the weave oscillation as it occurred in experimental tests were made by Schwinn personnel. These movies were analyzed and the frequency of oscillation was determined to be approximately 2 Hz. This frequency is consistent with reports of motorcycle weave frequencies of 2-3 Hz.

A preliminary simulation study was made with the objectives of demonstrating the occurrence of the weave oscillation and determining the influence of speed and certain design parameters. The following conditions were used in the simulation tests. Initially the bicycle was traveling in a straight line at constant speed. The rider control model was set up for "hands off" steering control, i.e., no rider steering torques. Rider lean movement was constrained to keep the rider in the plane of the bicycle. A side force disturbance was imposed on the frame to excite the weave oscillation. The point of application of the distrubance input was the approximate location of the saddle. The disturbance input was one cycle of a 2 Hz.sinusoidal force with an amplitude of 50 pounds. The duration of the side force input was 0.5 seconds after which the bicycle motion was unrestrained.

The bicycle configuration selected for this series of tests was that of the Paramount. Runs were performed at 30, 40 and 50 mph with the standard Paramount configuration and a 120 pound rider. At all three speeds this configuration was very stable. Figure 33 shows the roll angle and steer angle response at 30 mph. Refer to Appendix E for the complete set of plotted time histories. The maximum angle of the bicycle roll response was from 2.5 to 4 degrees with the magnitude of the response decreasing with increasing bicycle speed. At all three speeds the bicycle had returned to steady state straight line travel within 2 seconds. In these three tests there was no apparent tendency for the standard Paramount configuration to weave.

Preliminary studies of high speed motorcycle stability have shown that steer damping torque between the front fork and the frame at the steering head is a critical factor determining the occurrence of the

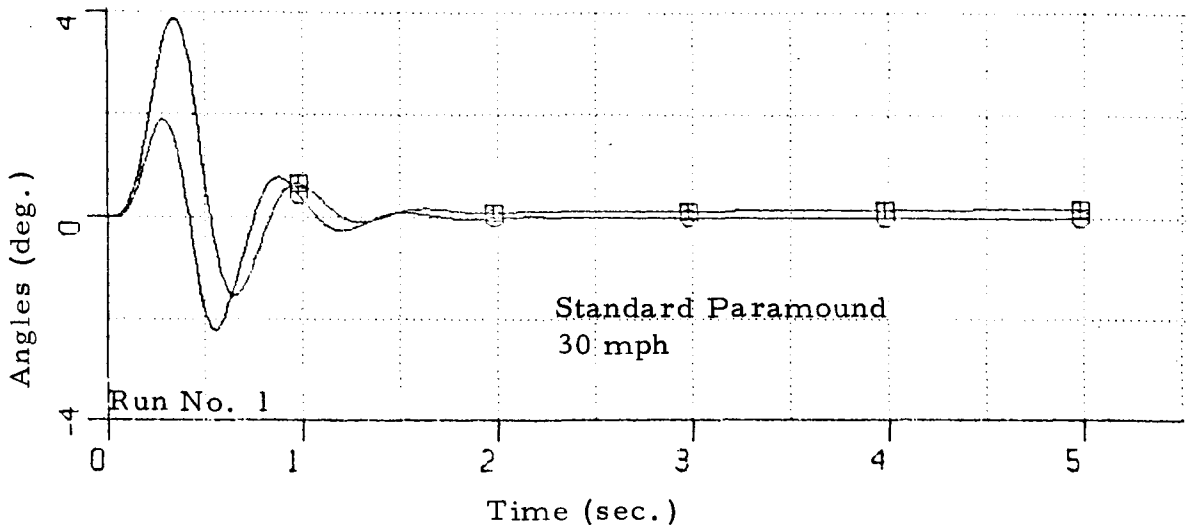

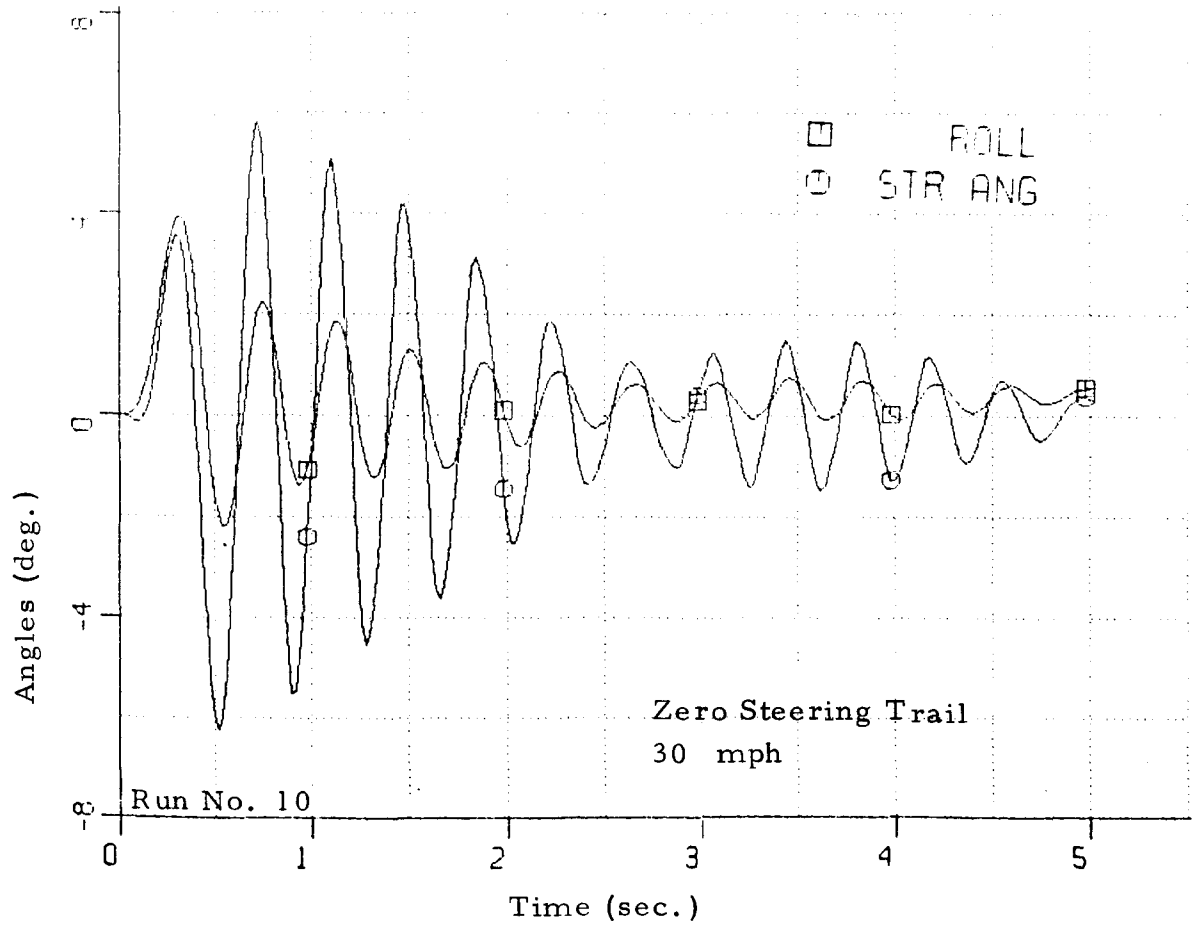

Figure 33 - Roll Angle and Steer Angle Disturbance Response at High Speed

weave oscillation. Two levels of steering damping were tested. Run 4 had a value of 0.1 in-lb-sec/deg which was thought to be representative of an actual bicycle. Run 5 had a level of steering damping ten times greater than Run 4. Both runs were made at 30 mph. Run 4 showed a slight increase in the magnitude of the roll angle response but the oscillation settled out in about 2 seconds as with the standard Paramount configuration Run 1. Run 5 was considerably more oscillatory and did not return to steady state straight line motion within 5 seconds. The magnitude of the initial roll angle response was about 6 degrees compared to 4 degrees for Run 1. It should be noted that the oscillation frequency for this run is about 1 Hz, not 2 Hz as was calculated from the movie of the actual oscillation.

Six additional tests were made at 30 mph with variations in steering head angle and steering trail. Runs 6 and 7 were made with steering head angle decreased and increased 5 degrees from the standard Paramount design of 17.4 degrees. In these two tests the fork offset was compensated to maintain constant steering trail at the design value of 1.71 inches. There was not a significant difference in the response of either of these two configurations compared to the standard Paramount.

The configurations of runs 8 through 11 included variations in steering trail with all other parameters maintained constant. Increasing steering trail by one inch had no apparent effect (run 9). Decreasing the steering trail by one inch to 0.71 inch (run 8) caused only a slight increase in roll oscillation amplitude. However, a further reduction of 0.71 inches to zero steering trail (run 10) caused the steering to oscillate at about 2.5 Hz for several seconds, Figure 33. The initial amplitude of the steering oscillation was about $\pm$ 6 degrees. The amplitude of the bicycle

roll response was about $\pm$ 2 degrees. Run 11 shows that with 0.5 inch negative steering trail the bicycle was highly unstable and fell over after only one oscillation cycle.

These results show that the weave oscillation will occur with the simulated bicycle. However, a large variation from actual design was necessary before the oscillation occurred. Since the oscillation is known to occur on standard design configurations it is believed that there are other influences which have not been accurately modeled in the simulated bicycle. In particular the coupling between the rider and the bicycle frame (in this study the rider was assumed rigidly attached to the frame) and the precise fore and aft location of the rider c.g. should be carefully analyzed for future simulated high speed stability studies.

This study has shown another detrimental effect of negative steering trail. It has been previously been recognized that steering trail had a strong influence on capsize mode stability. However, the effect of steering trail on stability of the oscillatory weave mode had not been previously demonstrated.

7.0 SIMPLIFIED BICYCLE DYNAMICS

A low effort level task to derive simplified expressions for the motions of a bicycle was performed during this phase of study. It was not expected that all aspects of the analysis could be completed in the period, but some interesting progress has been made and is reported in this section.

As pointed out previously, most of the effort on the program to date has been directed toward the development of a complex rider-bicycle simulation for the study of the influences of rider and bicycle characteristics on system dynamics. An approach of this type is essential in developing a capability for quantitative evaluation of bicycle designs. On the other hand, the required sophistication of the mathematical model of the system inhibits easy identification of specific effects via examination of the equations of motion. That is, the bicycle design parameters do not stand out in these nonlinear, higher-ordered, interacting expressions and it is difficult to achieve a ready understanding of design effects. These simplified models are not, in any way, replacements for the nonlinear simulation; they are intended for, and capable of, only providing insight into the probable effects of specific changes in the design of the bicycle and/or the rider-bicycle combination.

Prior to initiating the analytical study, a careful review of several reports and papers on bicycle stability characteristics was made in an effort to identify any pertinent information in the state-of-the-art for direct application. Most of the references, for which brief resumes are given in Appendix B , suffer from omission of various effects which are thought to be significant (e.g., tire characteristics, steering geometry). The work of Sharp is considered to be the lone exception although his results are not in convenient form for use by others.

Effort on the simplified analysis task has been devoted to the development of a set of linear steady-state relationships among yaw rate (r), roll angle (φ), steering angle (δ) and steering torques (T). These expressions have been written in terms of the physical characteristics of the bicycle-rider system - mass, wheelbase, head tube rake angle, mechanical trail, etc. - and include the tire forces due to slip and inclination angles. For fixed control conditions (i.e., positioning of the steering independent of steering torque requirements), the transfer function of r/δ has marked resemblance with that of a simplified automobile model (the so-called bicycle model of the automobile) but it also has additional terms because of the interaction of the roll motion. For free control conditions, (which involve steering torque) the expressions are still very complicated and considerably more effort will be needed to obtain generally valid simplifications.

The equations of motion have been analyzed for both the fixed (position) and free (torque) control modes of operation. The equations have been linearized so that the significant relationships can be presented in the form of transfer functions which retain only the dominant terms. The analyses are based in part on the model of the system which is used in the nonlinear computer simulation and compatible symbols are used where practical. The two principal steady state fixed control expressions are:

$$\frac{r}{\delta} = \frac{V/\ell \left[\cos\sigma + \frac{C_{F\varphi}}{C_{F\alpha}} \sin\sigma - \frac{Z_F \ell_F - W_F O_F}{h\, mg} \left(\frac{C_{F\varphi}}{C_{F\alpha}} - \frac{C_{R\varphi}}{C_{R\alpha}} \right) \right]}{1 + V^2 \left[\frac{M(bC_{R\alpha} - aC_{F\alpha})}{\ell^2 C_{F\alpha} C_{R\alpha}} - \frac{1+K}{\ell g} \left(\frac{C_{F\varphi}}{C_{F\alpha}} - \frac{C_{R\varphi}}{C_{R\alpha}} \right) \right]}$$

$$\frac{\varphi}{\delta} = \frac{V^2/lg\left[\cos\sigma + \frac{C_{F\varphi}}{C_{F\alpha}}\sin\sigma - \frac{Z_p l_F - W_F c_F}{MhV^2}\left(1 + \frac{MV^2(bC_{R\alpha} - aC_{F\alpha})}{l^2 C_{F\alpha} C_{R\alpha}}\right)\right]}{1 + V^2\left[\frac{M(bC_{R\alpha} - aC_{F\alpha})}{l^2 C_{F\alpha} C_{R\alpha}} - \frac{1+K}{lg}\left(\frac{C_{F\varphi}}{C_{F\alpha}} - \frac{C_{R\varphi}}{C_{R\alpha}}\right)\right]}$$

where:

V	=	bicycle velocity
l	=	wheelbase
σ	=	head tube rake angle
C_α	=	tire cornering stiffness
C_φ	=	tire camber thrust
Z_F	=	front wheel normal (vertical) force
g	=	gravity
M	=	total mass of bicycle and rider
M_F	=	mass of steering assembly ($W_F = gM_F$)
h	=	height of center-of-gravity of total mass
c_F	=	offset
l_F	=	trail
K	=	gyroscopic effect $= \frac{2i}{hMr_w}$
i	=	wheel moment of inertias about spin axis
r_w	=	wheel radius
a, b	=	distances from total c.g. to front and rear wheel centers
I_x, I_z	=	total roll and yaw moments of inertia about the total c.g.

Note that the effects of steering geometry are present only in the numerators of these steady state fixed control expressions and, even then, are coupled only in the camber thrust coefficients of the yaw rate expression. Also, the gyroscopic effect has little influence, regardless of speed, on the values of these expressions. With the weight distribution normally found on bicycles (i.e., the center-of-gravity is aft

of the midpoint of the wheelbase, thus $a > b$, the primary term in the denominator identifies them as oversteering machines. At high speeds, control gains become very large and the potential for instability in this mode of operation exists. The implication of this is that the bicycle must be considered in terms of torque control, as is done in the nonlinear simulation developed in this program. It is also of interest to note that the steady state lateral acceleration expression based on the r/δ function ($a_y/\delta = V\, r/\delta$) has a slight variance with that from the ϕ/δ function ($a_y/\delta = g\,\phi/\delta$) reflecting the front fork geometry effects.

The characteristic equation for the bicycle with steering position control has been simplified by retaining only the numerically significant terms* to:

$$\Delta_P = I_x I_z M V^2 s^4 + s^3 \left[V I_z (I_x + M h^2)(C_{F\alpha} + C_{R\alpha}) + M I_x (a^2 C_{F\alpha} + b^2 C_{R\alpha}) \right] + s^2 \left[\ell^2 C_{F\alpha} C_{R\alpha} (I_x + M h^2) + M V^2 \left(I_x + \frac{2 i h}{r_w}\right)(a C_{F\alpha} - b C_{R\alpha}) - M V^2 h I_z (C_{F\phi} + C_{R\phi}) \right] + M V h s \left[a \ell C_{F\alpha} C_{R\phi} - b \ell C_{R\alpha} C_{F\phi} - M g (a^2 C_{F\alpha} + b^2 C_{R\alpha}) - g (C_{F\alpha} + C_{R\alpha}) \left(I_z - \frac{2 i V^2}{g r_w}\right) \right] - M h g \left[\ell^2 C_{F\alpha} C_{R\alpha} - M V (a C_{F\alpha} - b C_{R\alpha}) - \frac{V \ell}{g} (C_{R\alpha} C_{F\phi} - C_{F\alpha} C_{R\phi}) \right]$$

bracket added

where s is the Laplace operator

This fourth order expression identifies the principal bicycle parameters which affect stability in the fixed steering mode of operation. Time and

---

* based on current Schwinn bicycle designs

funding limitations did not permit numerical analyses of this expression for typical bicycle designs but some general observations may be made with regard to the effects of design variables on the coefficients of the equation.

1. Note that the sign of the constant term is opposite to that of the s^4 term. This reflects the basically unstable motion of the bicycle at low speed (since at least one root of this expression must be negative --- a condition for instability according to Routh/Hurwitz criteria).

2. The influence of speed is clearly demonstrated in the expression by its appearance in many of the coefficients. Superficially, at least, this would imply improvement in stability (though it does not assure unconditionally stable operation) as speed is increased.

3. The coefficients of the s^2 and s terms contain the gyroscopic effect, which are significant to dynamic stability. This effect has been omitted from the constant term because of its small influence as indicated previously.

4. Note the important role played by the tire slip angle performance characteristics according to this equation. They demonstrate the futility of performing bicycle stability analyses without access to reasonable tire data. Tire camber coefficients appear to be less important.

5. Clearly, substitution of numerical values into the expression is now needed to gain some insight into the relative effects of design parameters. It would be interesting to evaluate the three designs used in the principal study with this simplified expression.

The bicycle rider is probably not acutely conscious of how he applies steering control to his machine. He steers as necessary to maintain stability but these actions are not considered in terms of displacement or torque. One of the most interesting aspects of bicycle dynamics is the essential role of free (force) control in bicycle behavior. In contrast with the automobile, which can be studied almost entirely in the fixed (position) control mode, the design characteristics of bicycles (and many other single track machines) require that handling studies involve examination of both control modes.

The linearized torque control equations are considerably more cumbersome than the position control expressions. At this time, we have carried them through only to the point of deriving a few of the more important steady state transfer functions. It should be noted that the nonlinear mathematical model on which the simulation studies are based is a torque-control model - a feature which is essential for maneuvering analyses - and further work on the simplified model in this mode of operation is strongly recommended.

8.0 BICYCLE PERFORMANCE EFFICIENCY STUDY

The current renaissance of bicycle transportation has emphasized the significance of minimizing the effort in bicycle riding. Since it has been widely accepted that the weight of a bicycle is the prime consideraton in determining pedaling effort, the trend has been toward the reduction of bicycle weight. However, there are other factors whose effects on pedaling effort are equal to or greater than that of weight. One important factor is the rolling resistance of the tires. Unfortunately, there has been little or no information upon which one could objectively evaluate the effects of rolling resistance, weight or other factors.

The literature contains a few simple analyses which show the power requirements of various bicycle resistances as a function of speed. However, no comprehensive analytical formulation of bicycle speed and power input which includes the effects of mechanical friction, tire rolling resistance, bicycle weight, aerodynamic drag, road grade has been found. The objective of this study was not only to perform such an analysis but also to present the results in such a format that the quantitative effects could easily be recognized.

The primary resistances to bicycle motion are aerodynamic drag, tire rolling resistance, mechanical friction in the drive train, road grade and total weight. Nonweiler concluded from experimental tests using a wind tunnel that the aerodynamic drag force on a bicycle and rider was proportional to the square of the velocity and only slightly influenced by the size of the rider, Reference 5 . However, the position ("racing" or "touring") taken by the rider had a considerable effect on the drag force.

Nonweiler measured the drag on several subjects and expressed his results in terms of "drag area" which is equivalent to the quotient ---- drag force/dynamic head. Dynamic head is defined as $1/2\ \rho\ v^2$ where ρ is the density of air and v is the speed. Thus the following equation can be

used for determining the aerodynamic drag force.

$$F_a = 0.00256\ AV^2$$

where

F_a is the drag force in pounds
A is the drag area in square feet
V is the speed in miles per hour

The concept of drag area was used because of the lack of a convenient reference area for the formation of drag coefficients. Using Nonweiler's results, average drag areas were computed for the "racing" position ($A = 3.4$ ft.^{2}) and the "touring" position ($A = 4.2$ ft.^{2}) and estimated for the upright "sitting" position ($A = 5.0$ ft.^{2}).

In the last few years a considerable quantity of bicycle tire rolling resistance data has been measured by the Schwinn Bicycle Company. These data have shown a large range of rolling resistances depending on the tire size, type of construction, inflation pressure, etc. In general, these data have shown that rolling resistance varies nonlinearly with tire loading. Thus the data have been presented in the form of a graph of rolling resistance coefficient (resisting force/load) as a function of load, Figure 34 .

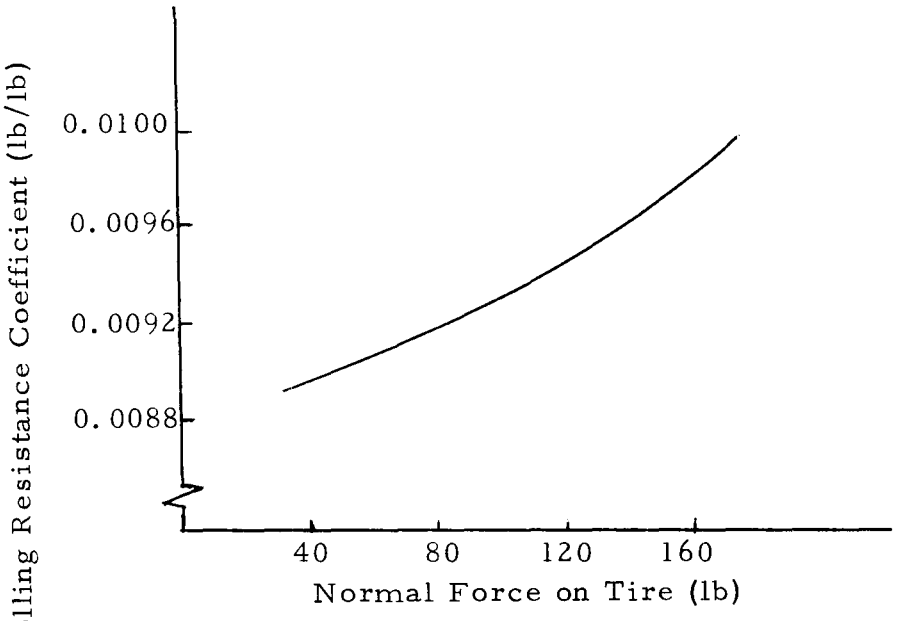

Figure 34: Typical Variation of Rolling Resistance with Tire Load

For the purposes of this study a nominal weight of 200 pounds was chosen for the bicycle and rider. The front tire load was assumed to be 1/3 of this weight and the rear tire load to be 2/3. Based on these tire loads and data supplied by Schwinn, average rolling resistance coefficients (r) were calculated for several tires, see table below.

Tire (Tube)	Pressure (psi)	r (lb/lb)
Breeze	65	0.0190
Puff	75	0.0091
Letour (National)	85	0.0076
Letour (National)	105	0.0067
Letour (Clement Road #13)	85	0.0064
Letour (Clement Road #13)	105	0.0058
Letour (Clement Track #3)	85	0.0063
Letour (Clement Track #3)	105	0.0056
Clement Road Tire #50	105	0.0070

The force required to overcome road grade is equal to the total weight (w) of the bicycle and rider times the grade (g). Thus the following equation gives the total force (F) required to propel the bicycle. The wind speed (W) relative to the ground has been added to the bicycle velocity so that the "air speed" is used in determining the aerodynamic drag force.

$$F = (r + g)\, w + 0.00256\, A\, (V + W)^2$$

The total power (P) required is equal to this force (F) times the forward velocity divided by the overall mechanical efficiency of the bicycle drive train (e). A conversion factor to get the expression in terms of horsepower is included.

Then:

$$P = 0.00267 \frac{V}{e} (r + g) w + 0.00256 A (V + W)^2$$

where

P - power (hp)
V - bicycle velocity (mph)
e - drive train efficiency
r - rolling resistance coefficient (lb/lb)
g - road grade (tangent of the road inclination angle)
w - total weight of bicycle and rider (lb)
A - drag area (ft^2)
W - wind velocity (mph)

Using a digital computer this equation was solved to determine power as a function of bicycle velocity for various tire rolling resistance coefficients, bicycle weights, riding positions, wind velocities, and road grades. The results of these computations are plotted in Figure 35a through 40a (the figures with "b" are explained later). Several curves are shown on each graph. One curve represents the power-velocity function for a set of "base conditions" or coefficients in the horsepower equation. The other curves have the same base conditions except for a single coefficient which has a different value. Thus on the figures whose numbers have "a" subscripts each curve shows the horsepower required to pedal the bicycle at any speed up to 40 mph.

Unfortunately, most cyclists have little understanding of how much power they actually put out when riding or what their power capabilities are. Therefore, they find curves such as these difficult to relate to their riding experience. A more natural format for presenting this information is to assume constant horsepower input to several bicycle configurations and to observe the speed differences between them. For the base bicycle, using Figure 35a , it can be seen that one would be going about 18.7 mph in the touring position (base condition) but only about 17.9 mph in the upright

sitting position. With the 105 psi sew-up tires the speed would be about 21.9 mph with the same 0.4 hp input.

Another way if interpreting this is that if the base condition speed was 18.7 mph one would lose 0.8 mph by sitting upright or gain 3.2 mph by changing to 105 psi sew-up tires if the power input remained constant. Thus another format is a plot of speed changes as functions of the speed of the base condition. This is equivalent to plotting speed change as a function of power input but base condition speed is a more desireable independent variable since it is easier to relate to actual riding experience.

Figures 35 through 40 with "b" subscripts are plots of this type. If a person were accustomed to riding under certain base conditions at a certain speed he can easily determine from these figures how much faster or slower he would be going if he made a change in riding position, tires (rolling resistance), total weight or if he encountered a change in grade or wind. For example, using Figure 35 b, at 10 mph he could expect that by changing to 105 psi sew-up tires he could be moving about 3.9 mph faster but by reducing the weight of his bike by ten pounds he would only gain about 0.3 mph.

Thus the "speed change versus base speed" plots express quantitatively the effects of different bicycle resistances in a format which is intuitively understood by cyclists. By using these plots, questions such as "how much faster can I go on these tires?" or "how much slower will I go in a headwind?" can be easily answered. Example plots are shown in Figures 35b through 40b and 41.

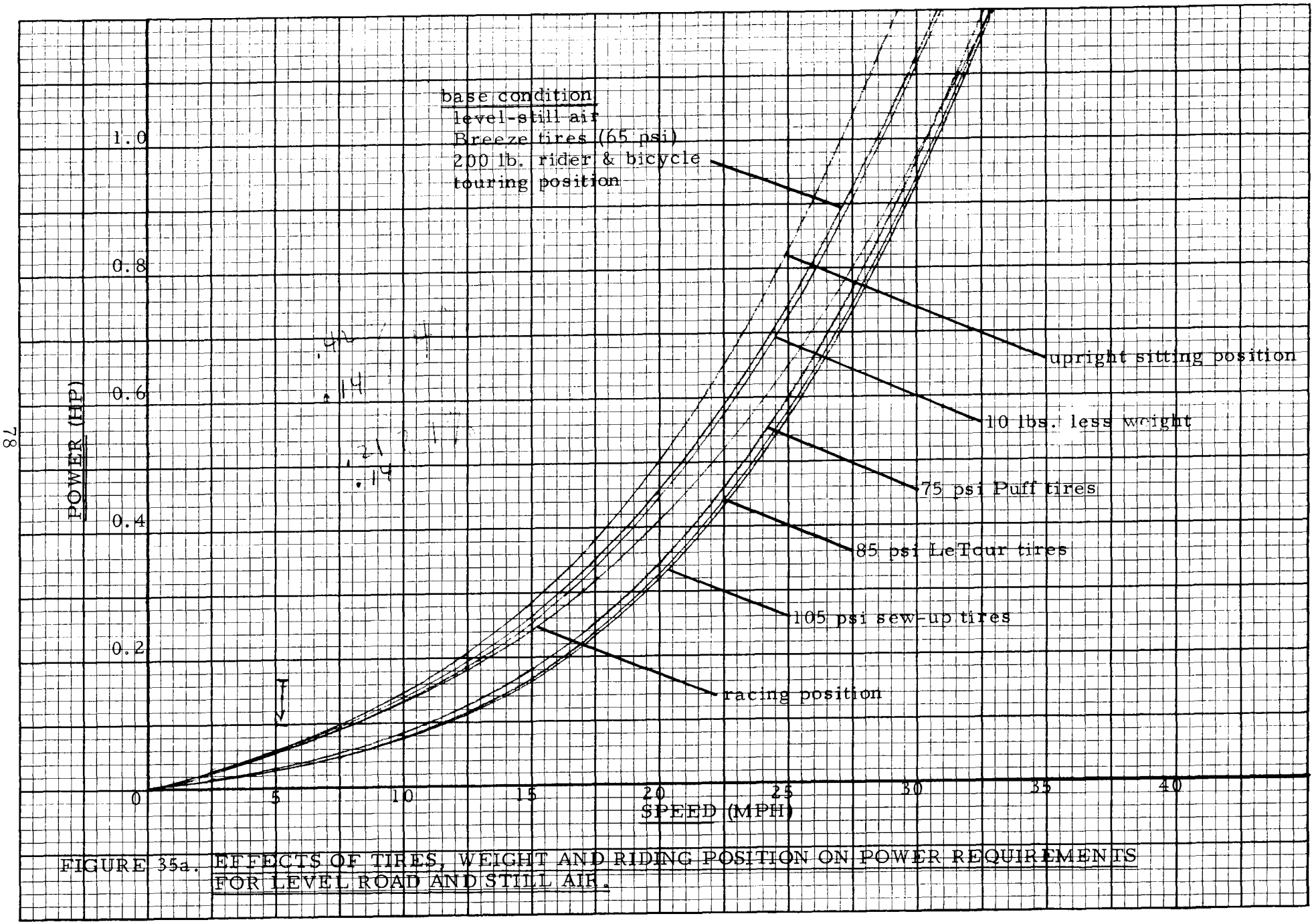

FIGURE 35a. EFFECTS OF TIRES, WEIGHT AND RIDING POSITION ON POWER REQUIREMENTS FOR LEVEL ROAD AND STILL AIR.

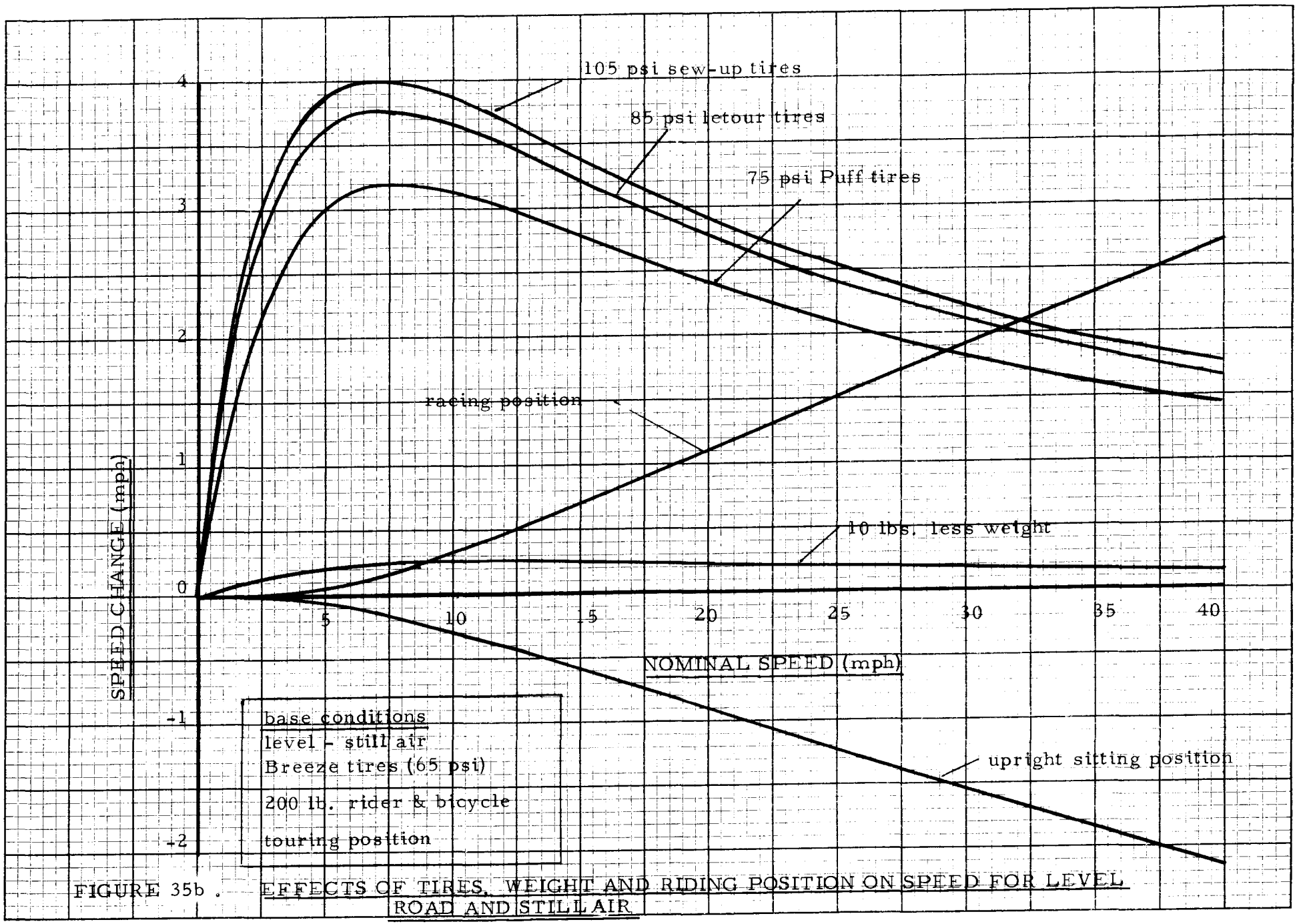

FIGURE 35b . EFFECTS OF TIRES, WEIGHT AND RIDING POSITION ON SPEED FOR LEVEL ROAD AND STILL AIR

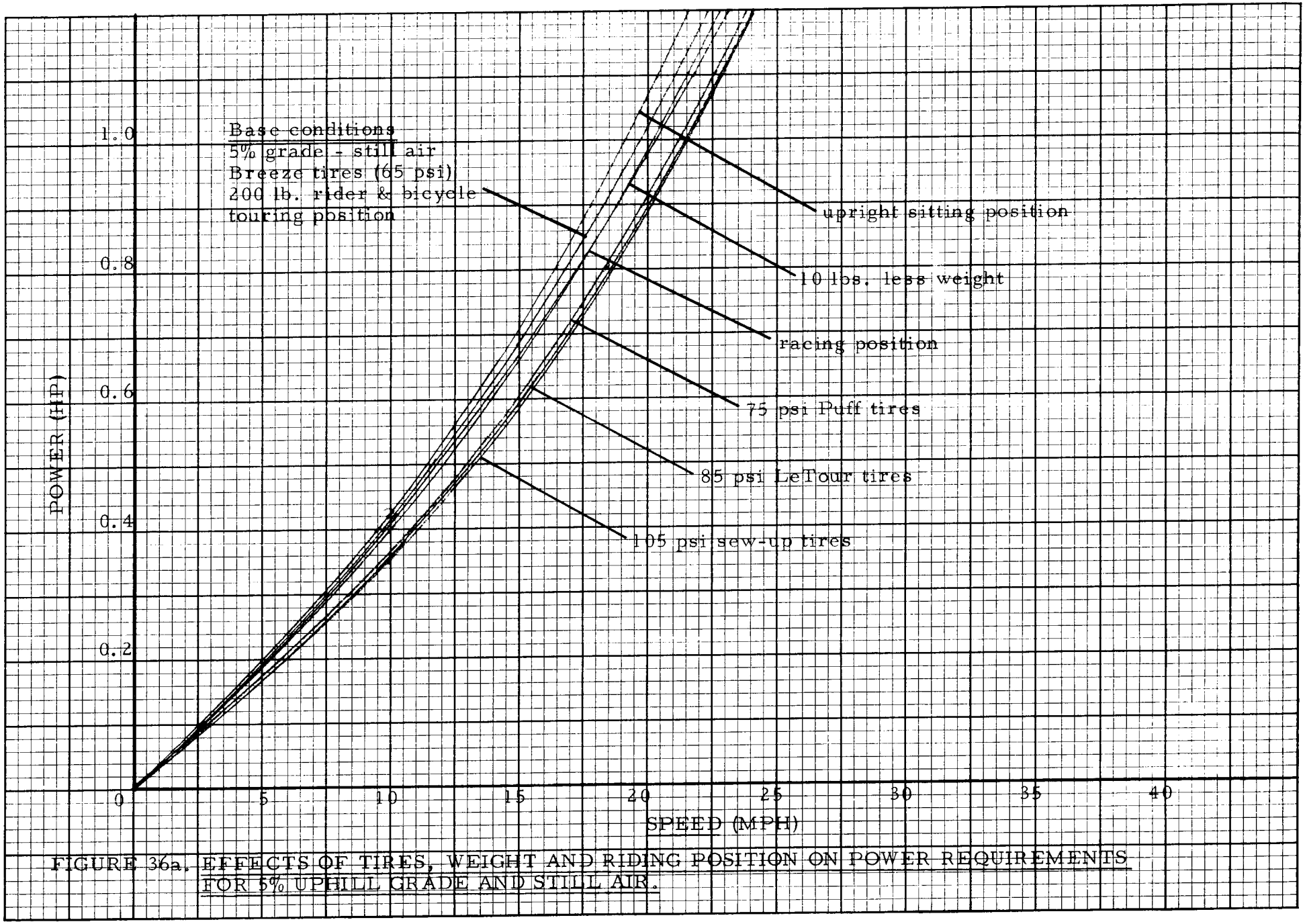

FIGURE 36a. EFFECTS OF TIRES, WEIGHT AND RIDING POSITION ON POWER REQUIREMENTS FOR 5% UPHILL GRADE AND STILL AIR.

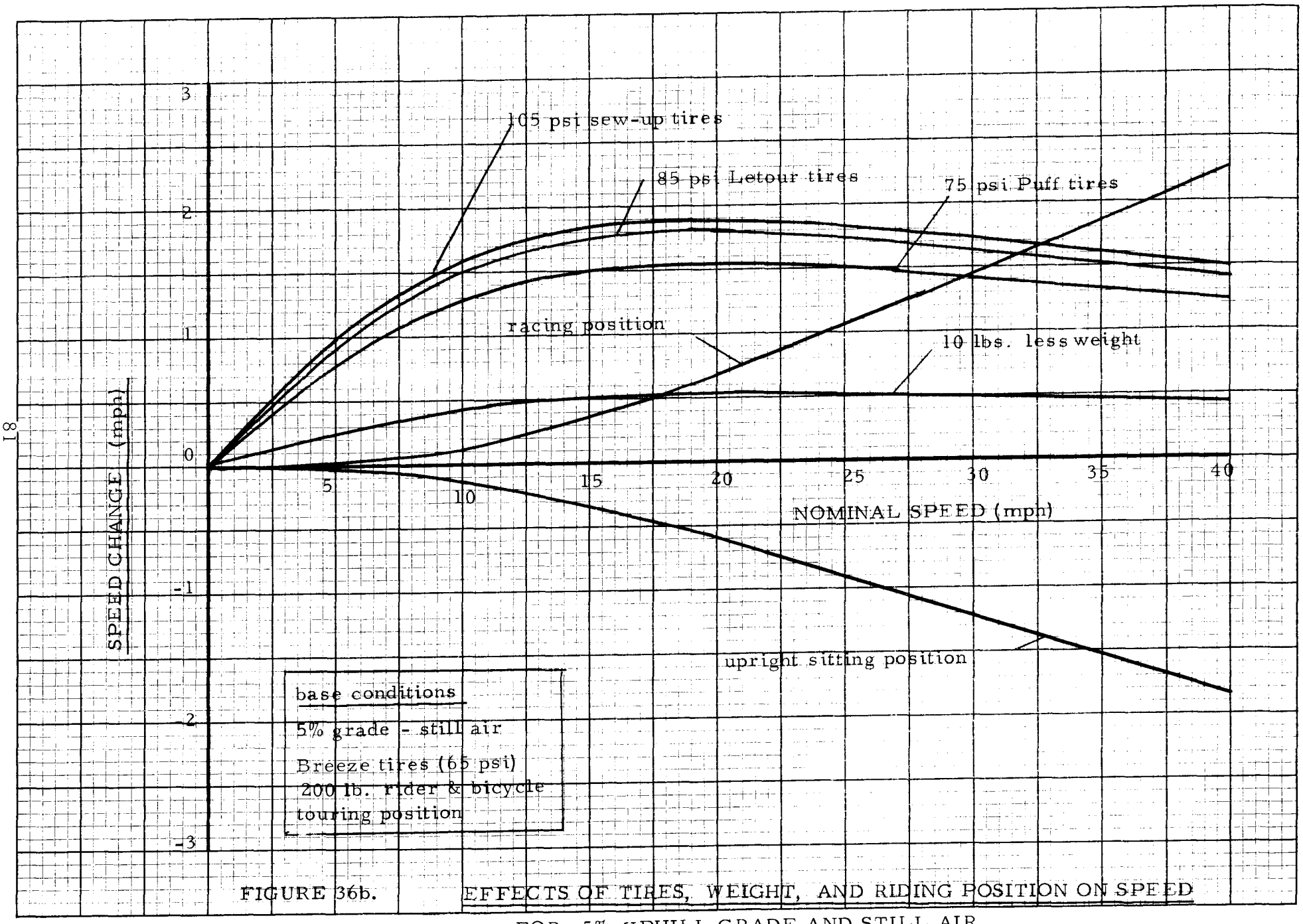

FIGURE 36b. EFFECTS OF TIRES, WEIGHT, AND RIDING POSITION ON SPEED FOR 5% UPHILL GRADE AND STILL AIR

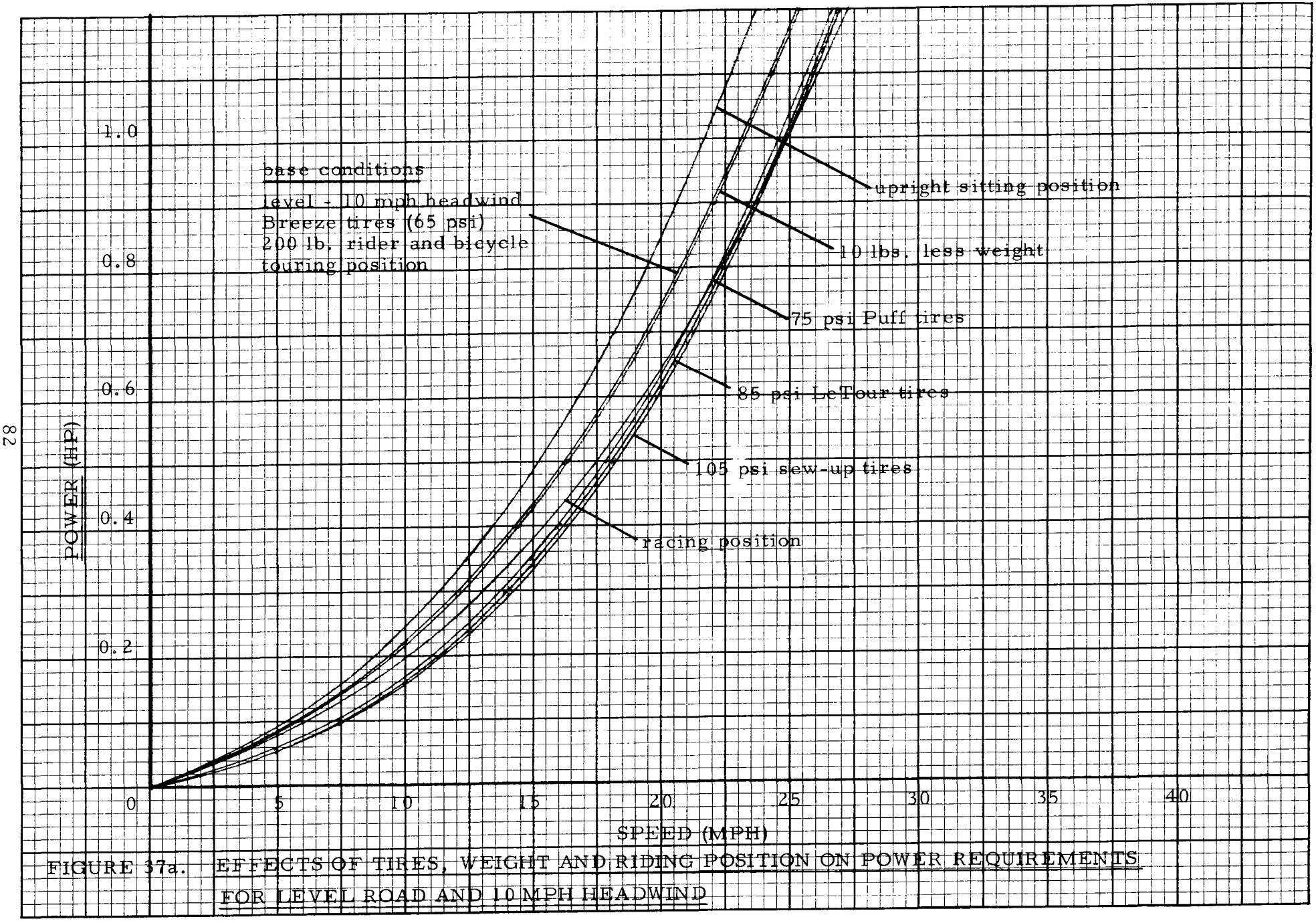

FIGURE 37a. EFFECTS OF TIRES, WEIGHT AND RIDING POSITION ON POWER REQUIREMENTS FOR LEVEL ROAD AND 10 MPH HEADWIND

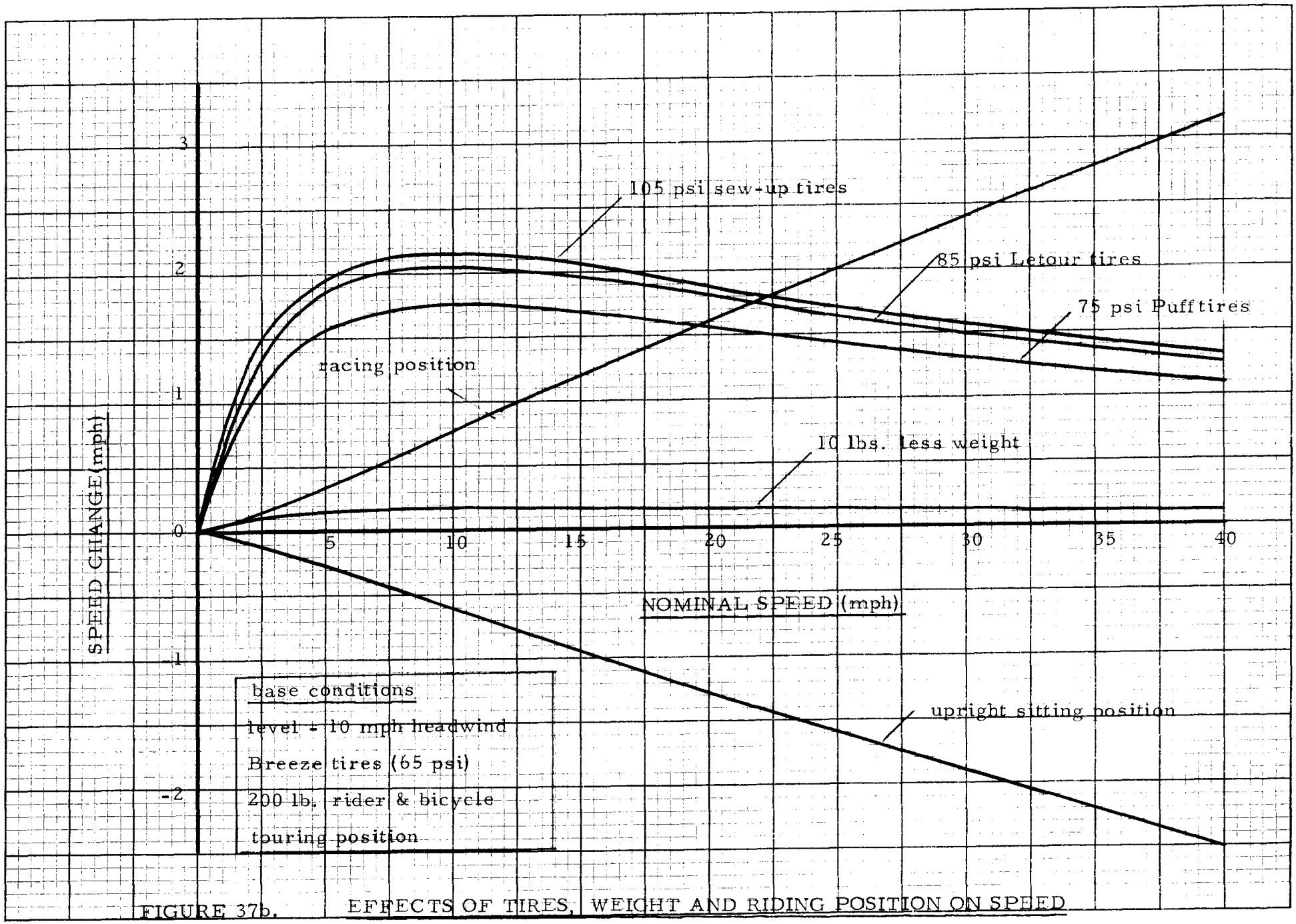

FIGURE 37b. EFFECTS OF TIRES, WEIGHT AND RIDING POSITION ON SPEED FOR LEVEL ROAD AND 10 MPH HEADWIND

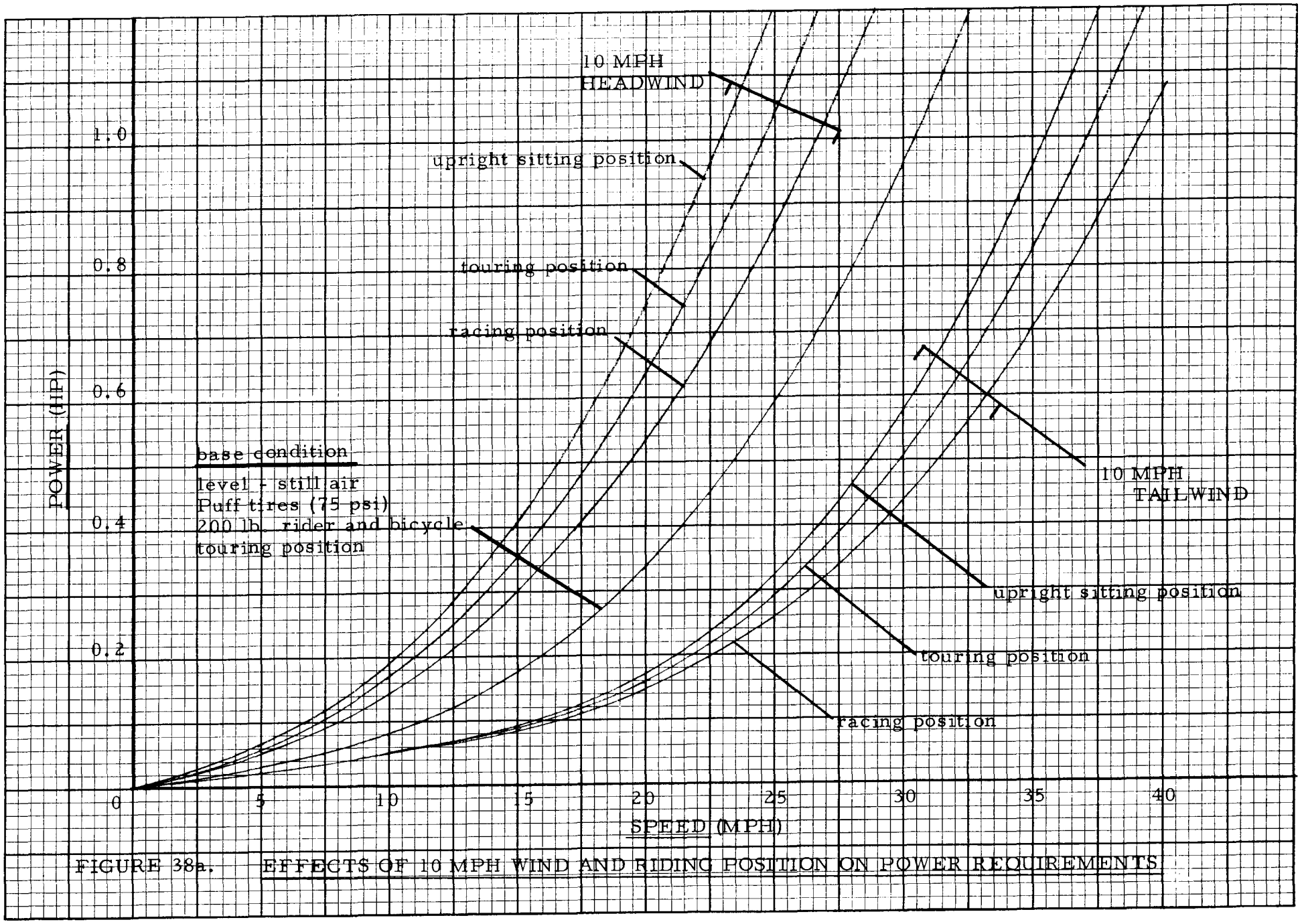

FIGURE 38a. EFFECTS OF 10 MPH WIND AND RIDING POSITION ON POWER REQUIREMENTS

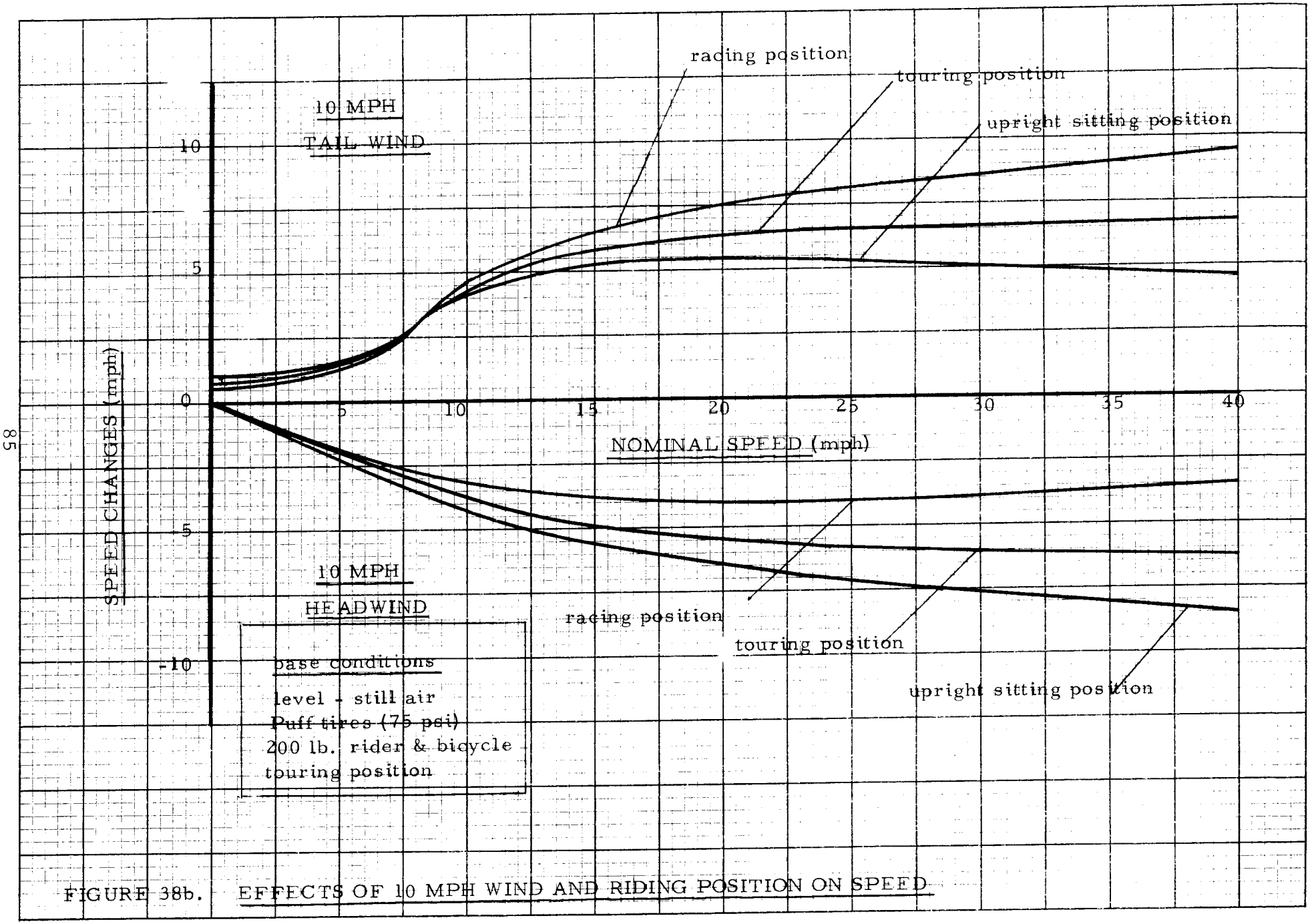

FIGURE 38b. EFFECTS OF 10 MPH WIND AND RIDING POSITION ON SPEED

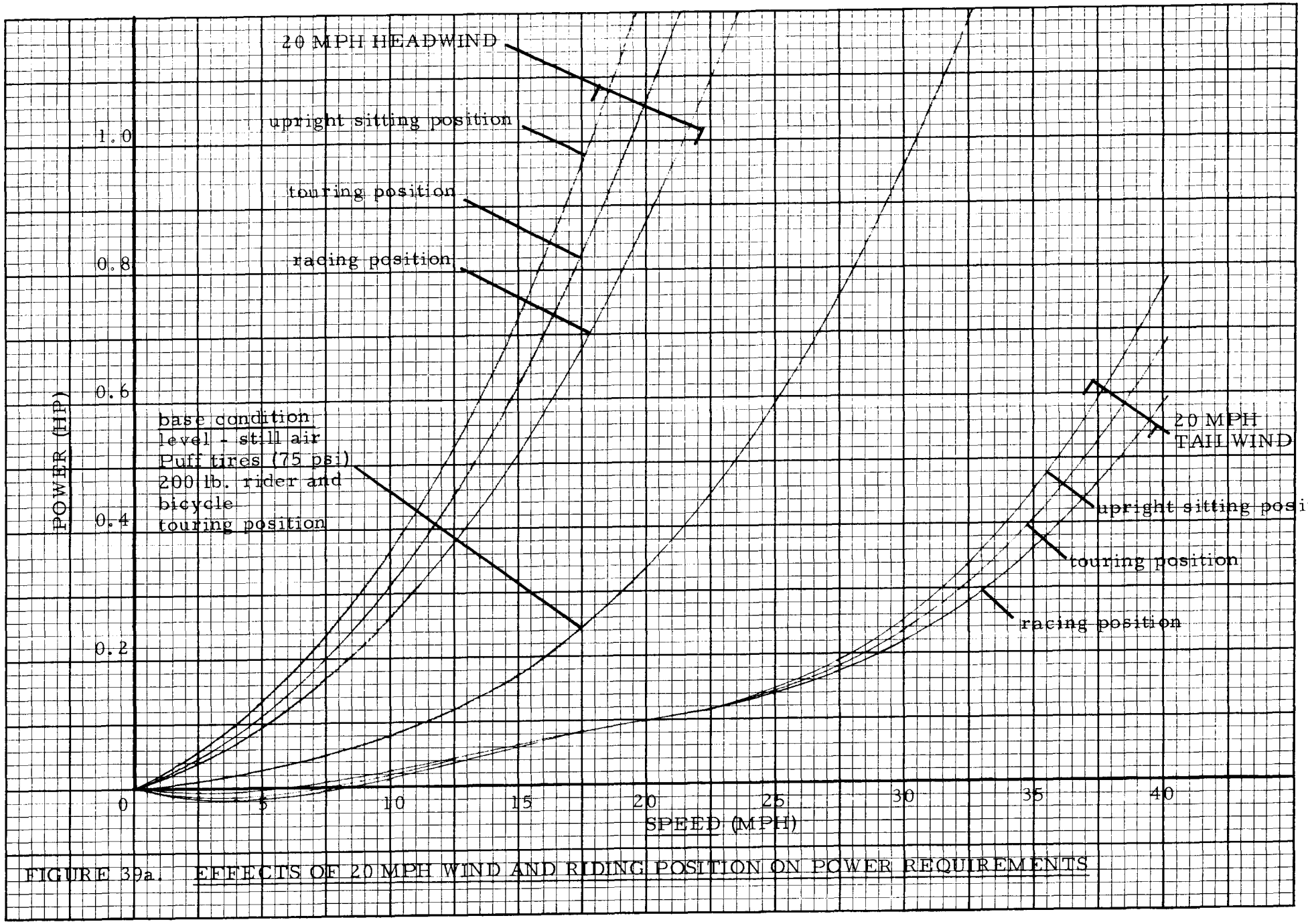

FIGURE 39a. EFFECTS OF 20 MPH WIND AND RIDING POSITION ON POWER REQUIREMENTS

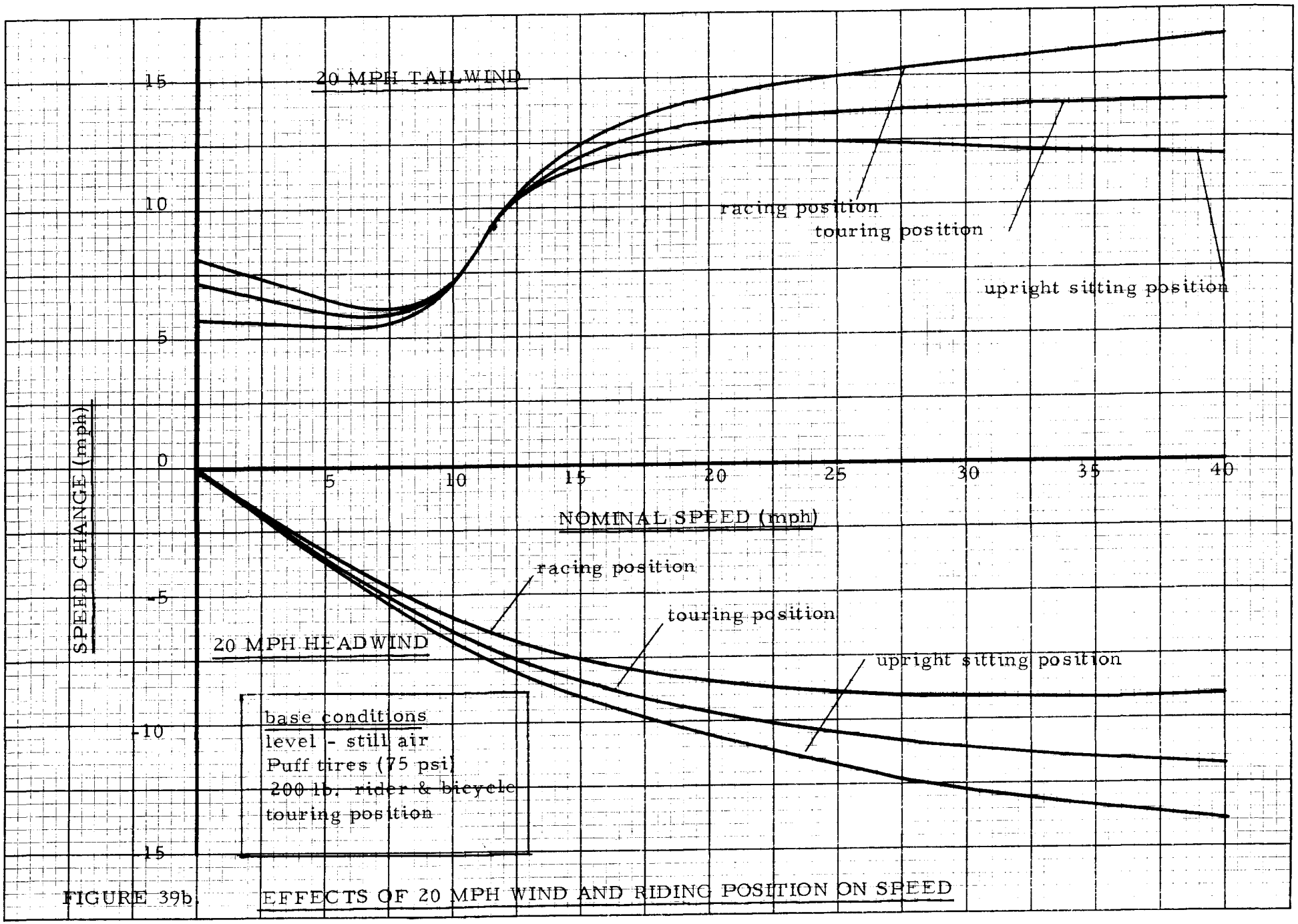

FIGURE 39b. EFFECTS OF 20 MPH WIND AND RIDING POSITION ON SPEED

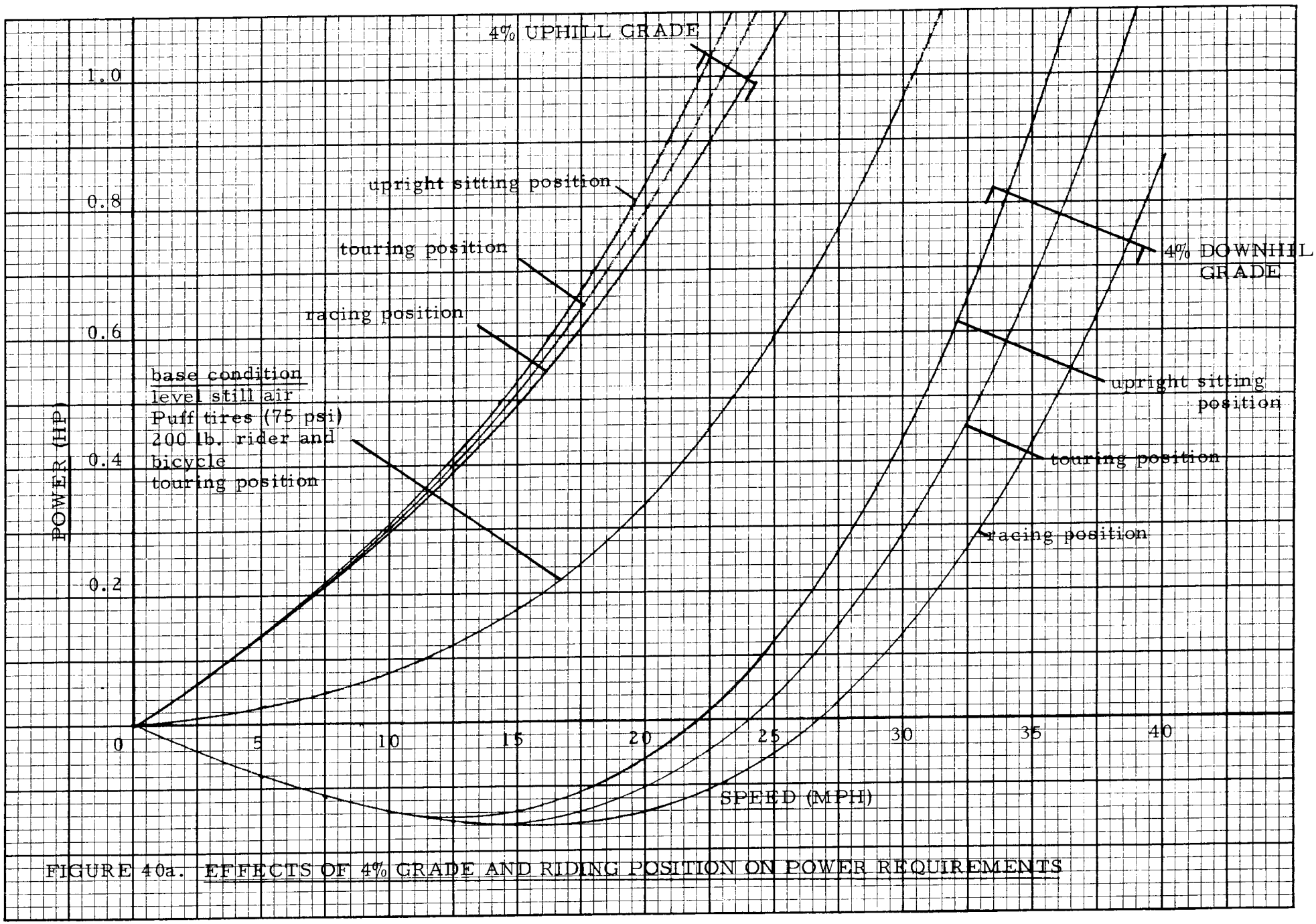

FIGURE 40a. EFFECTS OF 4% GRADE AND RIDING POSITION ON POWER REQUIREMENTS

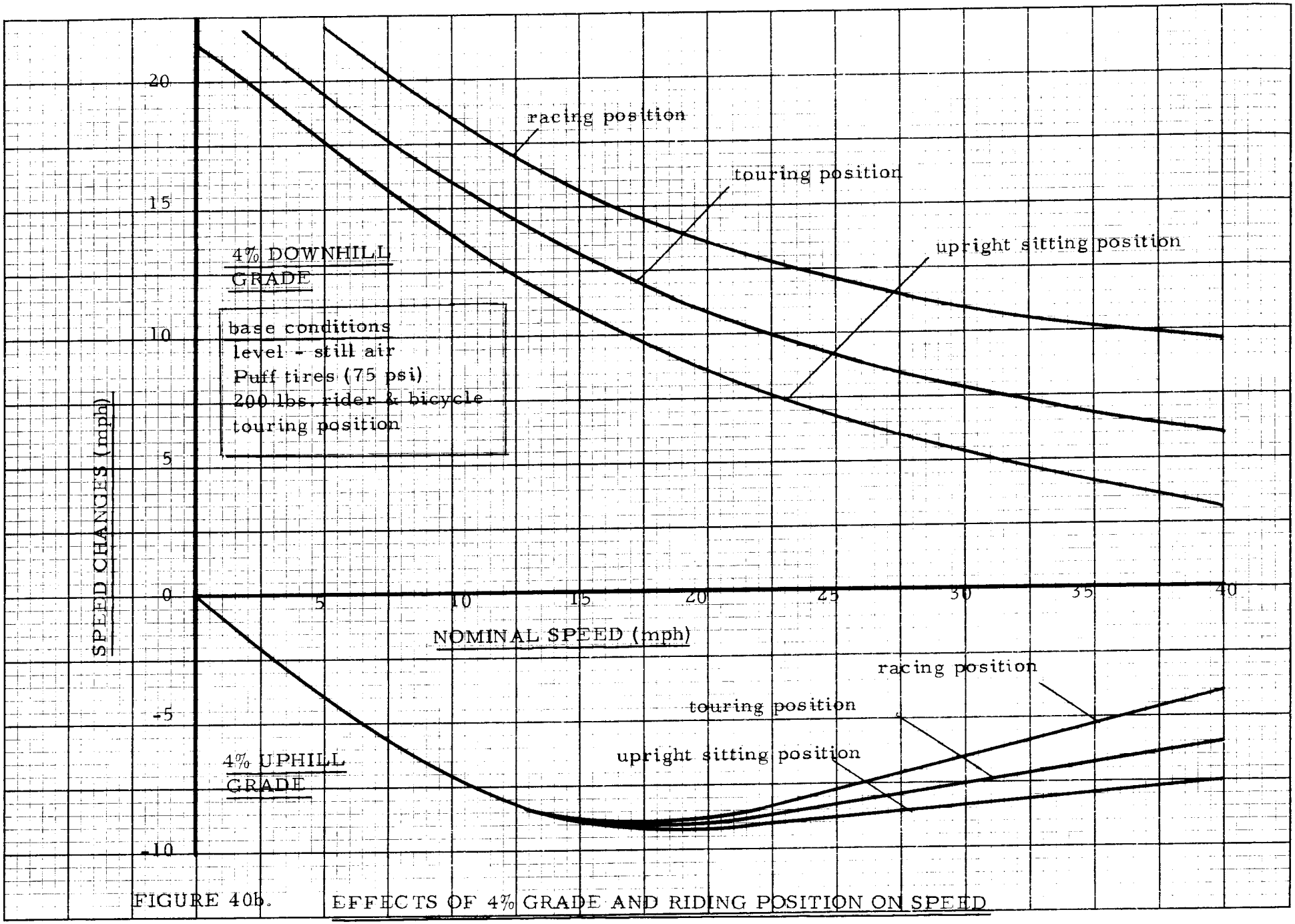

FIGURE 40b. EFFECTS OF 4% GRADE AND RIDING POSITION ON SPEED

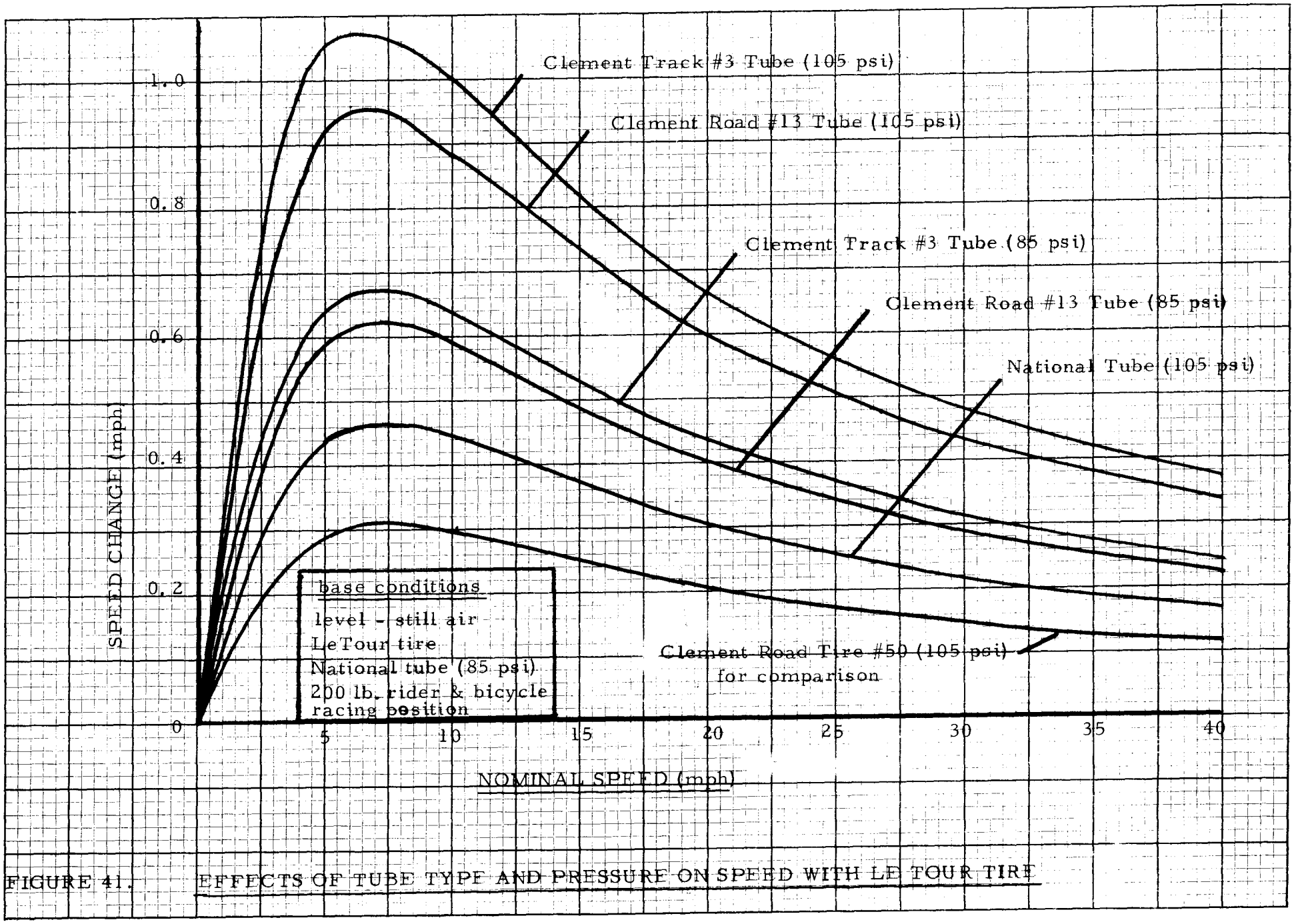

FIGURE 41. EFFECTS OF TUBE TYPE AND PRESSURE ON SPEED WITH LE TOUR TIRE

REFERENCES

1. Roland, R. D., Jr. and Lynch, J. P.: "Bicycle Dynamics - Tire Characteristics and Rider Modeling" Cornell Aeronautical Laboratory, Inc., Technical Report No. YA-3063-K-2, March 1972.

2. Roland, R. D., Jr. and Massing, D. E.: "A Digital Computer Simulation of Bicycle Dynamics" Cornell Aeronautical Laboratory, Inc., Technical Report No. YA-3063-K-1, June 1971.

3. Van Lunteren, A. and Stassen, H. G.: "Investigations of the Characteristics of a Human Operator Stabilizing a Bicycle Model" Intern. Symp. on Ergonomics in Machine Design, Prague, 1967.

4. Weir, D. M.: "Motorcycle Handling Dynamics and Rider Control and the Effect of Design Configuration on Response and Performance" University of California, Los Angeles, 1972.

5. Nonweiler, T.: "The Air Resistance of Racing Cyclists" The College of Aeronautics, Cranfield, England, Report No. 106, October 1956.

6. Sharp, R. S.: "The Stability and Control of Motorcycles" Journal of Mechanical Engineering Science, Vol. 13, No. 5, 1971.

APPENDIX A

Experimental Measurement of the Aerodynamic Drag of Spinning Bicycle Wheels

Experimental measurements were made to determine the aerodynamic resistance of bicycle wheel spinning in still air. The objective of this study was to determine what portion of the total aerodynamic resistance of the bicycle might be due to the spinning wheels and whether the use of wheel covers (on both sides completely enclosing the spokes) might significantly reduce this resistance.

Experimental data were obtained by spinning each wheel configuration at constant speed with a d.c. motor and measuring power consumption (voltage times current to drive motor) and wheel rpm, Figure A-1. These data were corrected for the power to drive the motor alone and converted to horsepower and equivalent forward bike speed in mph. Figure A-2, shows curves of power versus speed for wheels with and without the covers. For comparison, one other configuration was tested. This was a wheel with four 4 inch by 10 inch cardboard paddles inserted in the spokes (90 degrees apart). Power consumption with this configuration is considerably higher than with the others.

This comparison shows that the effect of the wheel covers is small. The reduction in wheel spin drag horsepower is of the order of 0.010 horsepower at 30 mph and 0.025 horsepower at 50 mph. The effect of the wheel covers on bicycle speed (at constant horsepower) can be determined by using the power versus speed graph for bicycle riding made in the performance efficiency study. This shows that at 30 mph the use of wheel covers (on both wheels) would increase speed about 0.15 mph and at 50 mph a speed increase of about 0.75 mph would be obtained. It is interesting to note that in the 20 to 30 mph speed range the power consumption due to wheel spin drag is about 7% of the total power input.

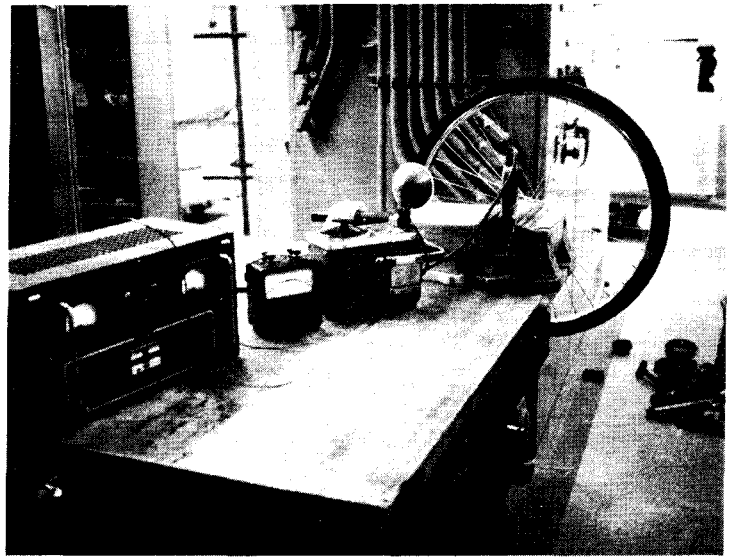

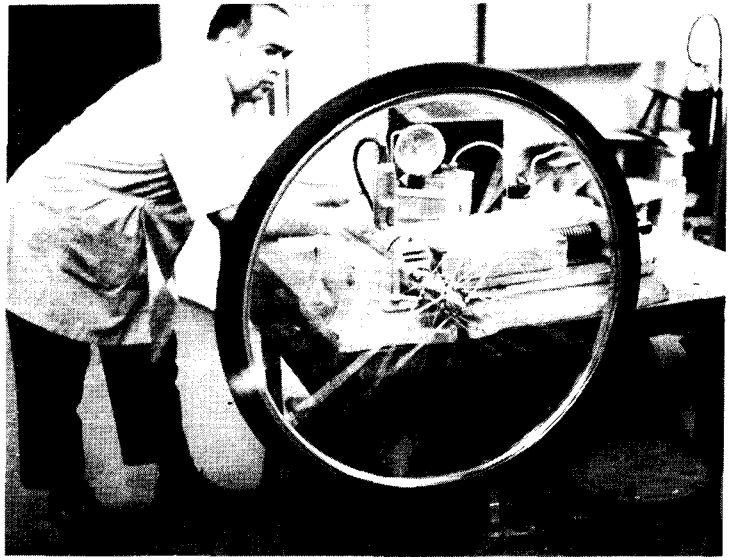

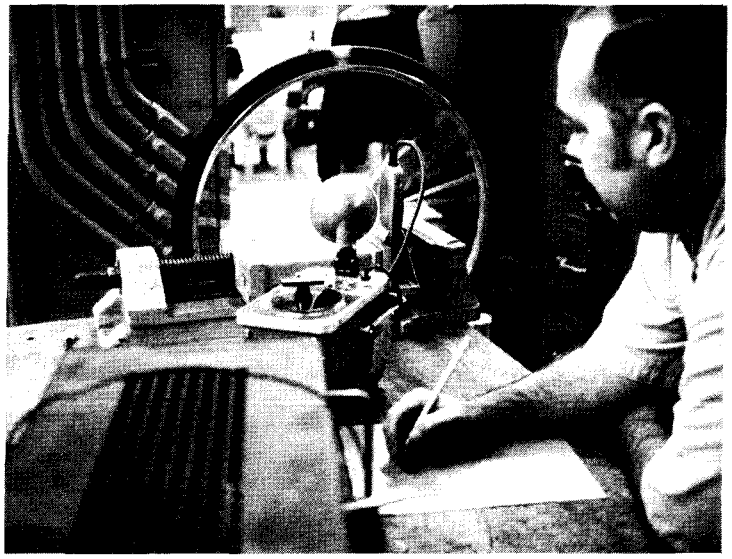

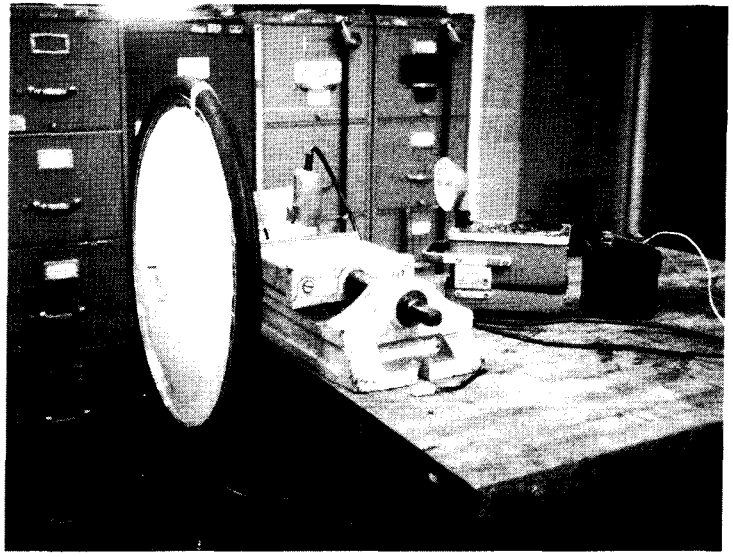

Figure A-1 TEST APPARATUS FOR MEASURING WHEEL SPIN POWER CONSUMPTION

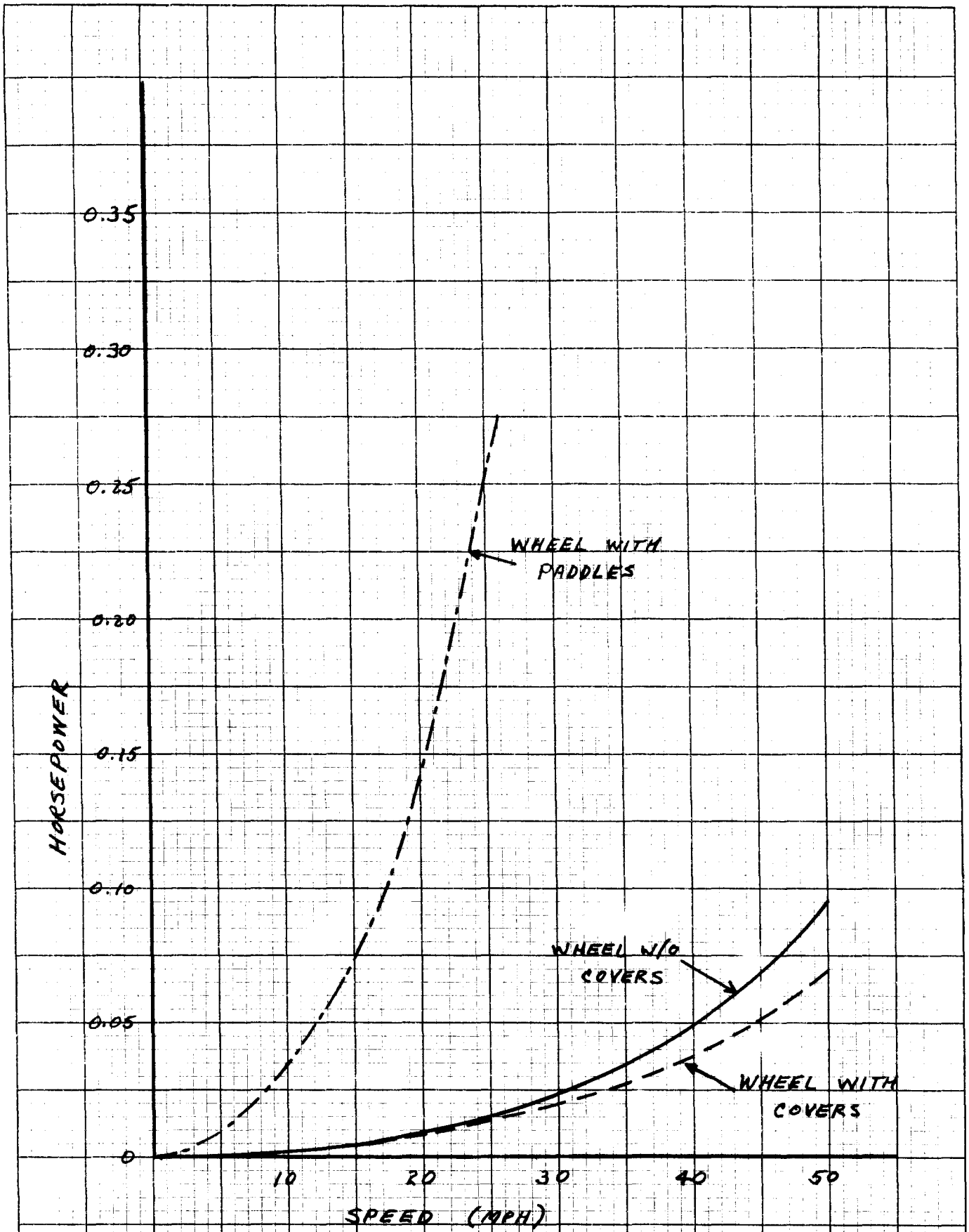

Figure A-2 POWER CONSUMPTION IN SPINNING BICYCLE WHEEL

It can be concluded from these results that although the use of covered wheels for power reduction has no practical advantage for normal riding speeds, it can give a slight advantage at racing speeds. (Furthermore, using paddles on the wheels produces an excellent exerciser).

APPENDIX B

Abstracts and Comments on Previous Bicycle Analyses

Steering and Stability of Single-Track Vehicles - R. A. Wilson-Jones

This is generally considered to be one of the classic papers on single-track vehicles but it contains no analytical treatment of stability. Some full-scale experimental results are given for a motorcycle and the control phenomenon of reversed steering torque for initiating a fast turn (which is supported by the Calspan-Schwinn tests and simulation) is discussed.

Fundamental Characteristics of Single-Track Vehicles in Steady Turning - H. Fu.

This paper provides an analysis of the steady state equations of motion in the six rigid body degrees of freedom. The analysis includes a simplified treatment of aerodynamic and tire slip angle and inclination angle effects. Steering angle is used as an input, so the approach is basically a representation of the two wheel vehicle as a position control system.

Investigations of the Characteristics of a Human Operator Stabilizing a Bicycle Model - Van Lunteran

In conjunction with studies of man-machine systems, Van Lunteran utilized a "bicycle simulator" for which he devised a simplified set of linear differential equations involving vehicle roll angle, steering angle, and rider lean angle (claimed to be based on Whipple's work but the connection is difficult to follow). This model attempts to represent the basic roll stability problem of the bicycle but, in our opinion, falls far short of this goal. The expression is written in "black box" terms (i.e., basically, input-output relationships) without any details of bicycle design showing up explicity. Although the representation may be satisfactory for its

application (the study of human operator characteristics) it cannot be used for bicycle design and performance analyses.

The Stability and Control of Motorcycles - R. S. Sharp

This mathematical model of the two-wheeled vehicle is a linear four degree-of freedom representation developed for vehicle-only stability analysis. The equations of motion are written for lateral force, roll moment, yaw moment, and steering torque incorporating tire performance, (including tire dynamic response) and passive rider weight. Sharp identifies three basic regions of operation for the two-wheel vehicle -

1. Low speed instability (which is the basic static instability in roll)

2. Wobble (a mid-speed oscillation of the steering system)

3. Weave (a high-speed, coupled roll-yaw oscillation of the system)

The equations of motion are presented in terms of the vehicle's physical characteristics and solutions for a range of values of the characteristics are given in the form of stability plots.

Motorcycle Handling Dynamics and Rider Control and the Effect of Design Configuration on Response and Performance - D. Weir

The mathematical model of two-wheel vehicles used by Weir in his doctorate dissertation follows the form of the four degrees of freedom model developed by Sharp. Generalized transfer functions for lateral translation, roll rotation, yaw rotation, and steering angle motions are derived from the differential equations for the appropriate forces and moments. Constant velocity operation is assumed since emphasis is placed on stability analyses. Weir utilizes the stability derivative notation for combining system parameters to permit the generation of concise equations of motion.

APPENDIX C

Plotted Results of Rider Control Model Parameter Study

(Table 1, Section 4 lists rider model configuration by run number)

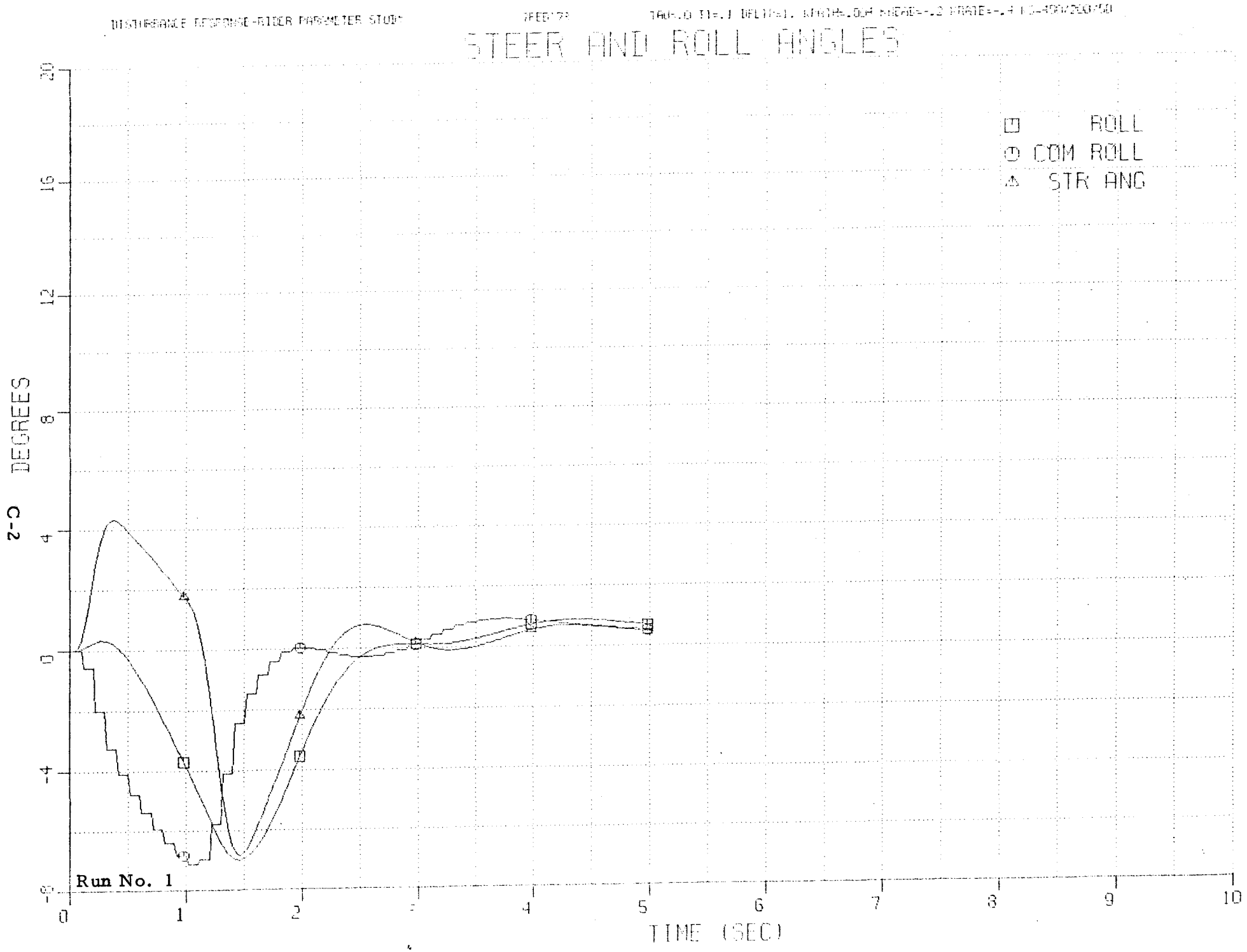
STEER AND ROLL ANGLES
ROLL
COM ROLL
STR ANG
DEGREES
TIME (SEC)
Run No. 1
C-2

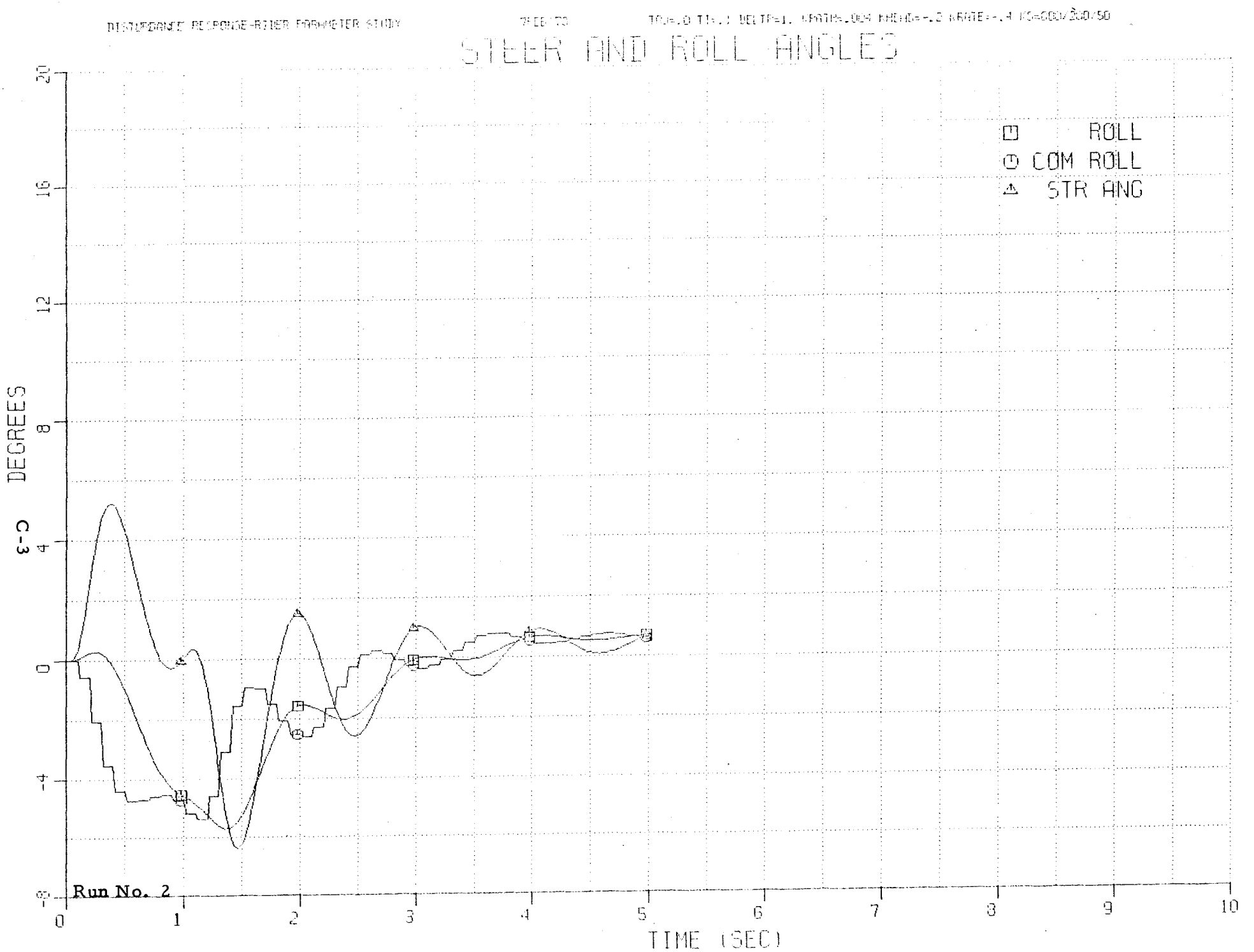
STEER AND ROLL ANGLES
ROLL
COM ROLL
STR ANG
DEGREES
TIME (SEC)
Run No. 2
C-3

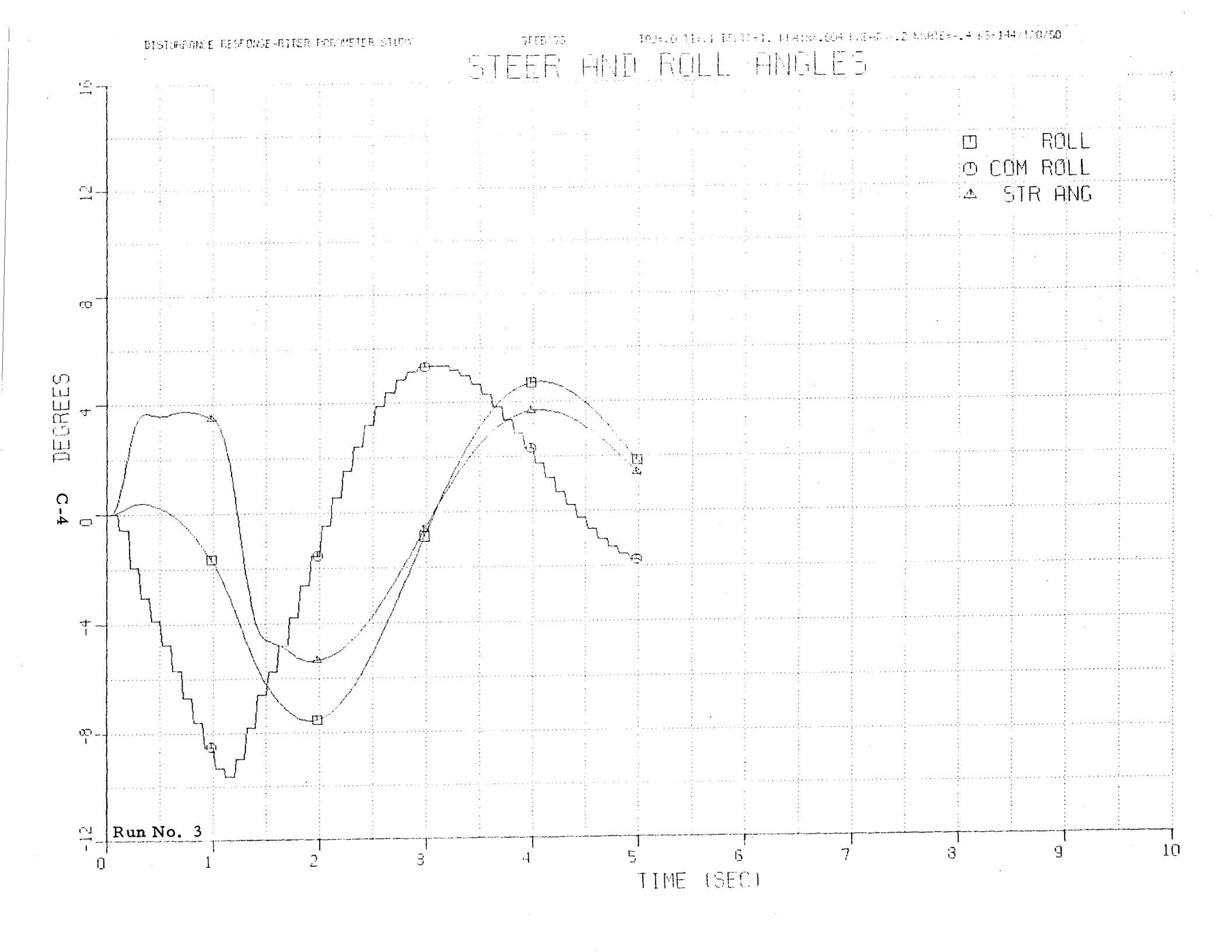
STEER AND ROLL ANGLES
ROLL
COM ROLL
STR ANG
DEGREES
TIME (SEC)
Run No. 3

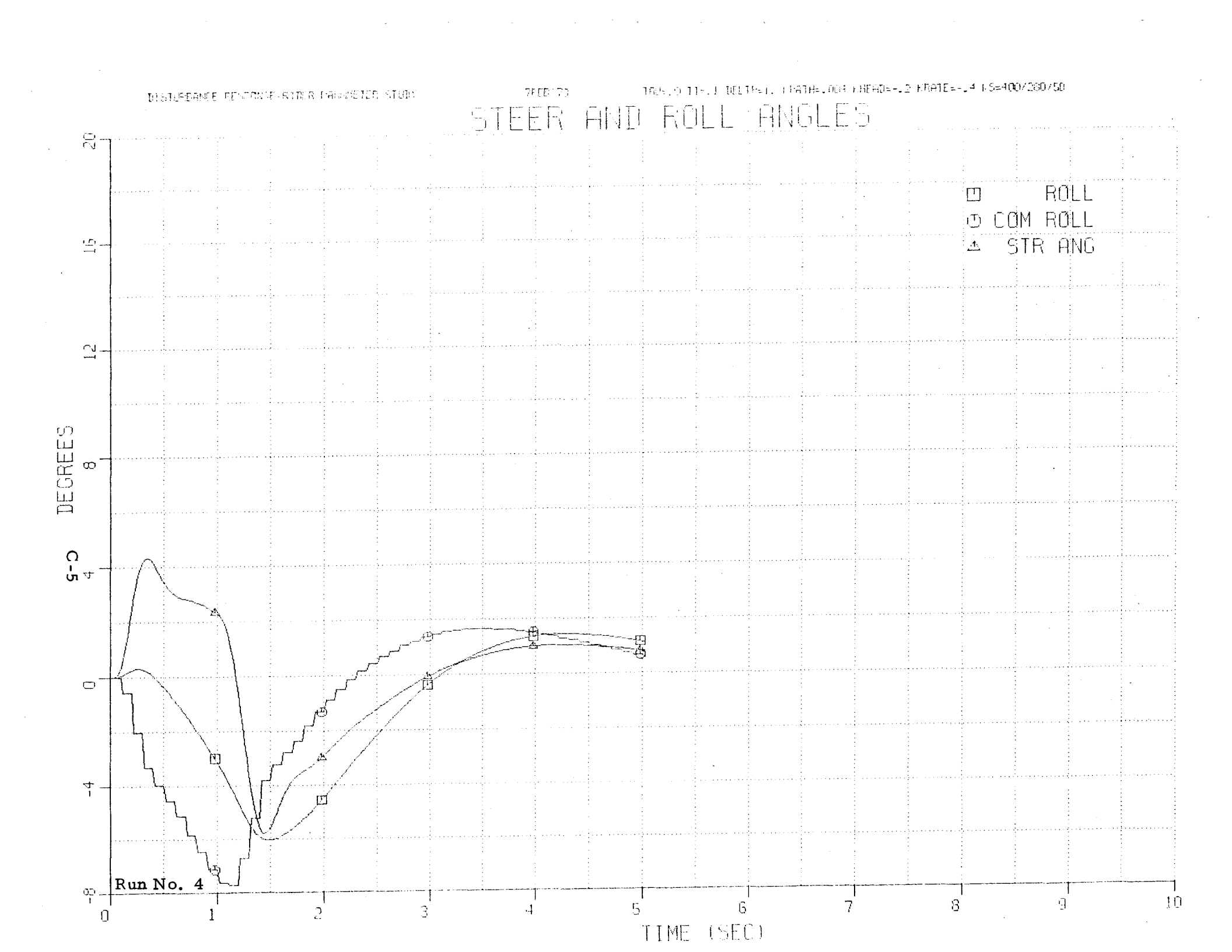
STEER AND ROLL ANGLES
ROLL
COM ROLL
STR ANG
DEGREES
TIME (SEC)
Run No. 4
20
16
12
8
4
0
-4
-8
0
1
2
3
4
5
6
7
8
9
10

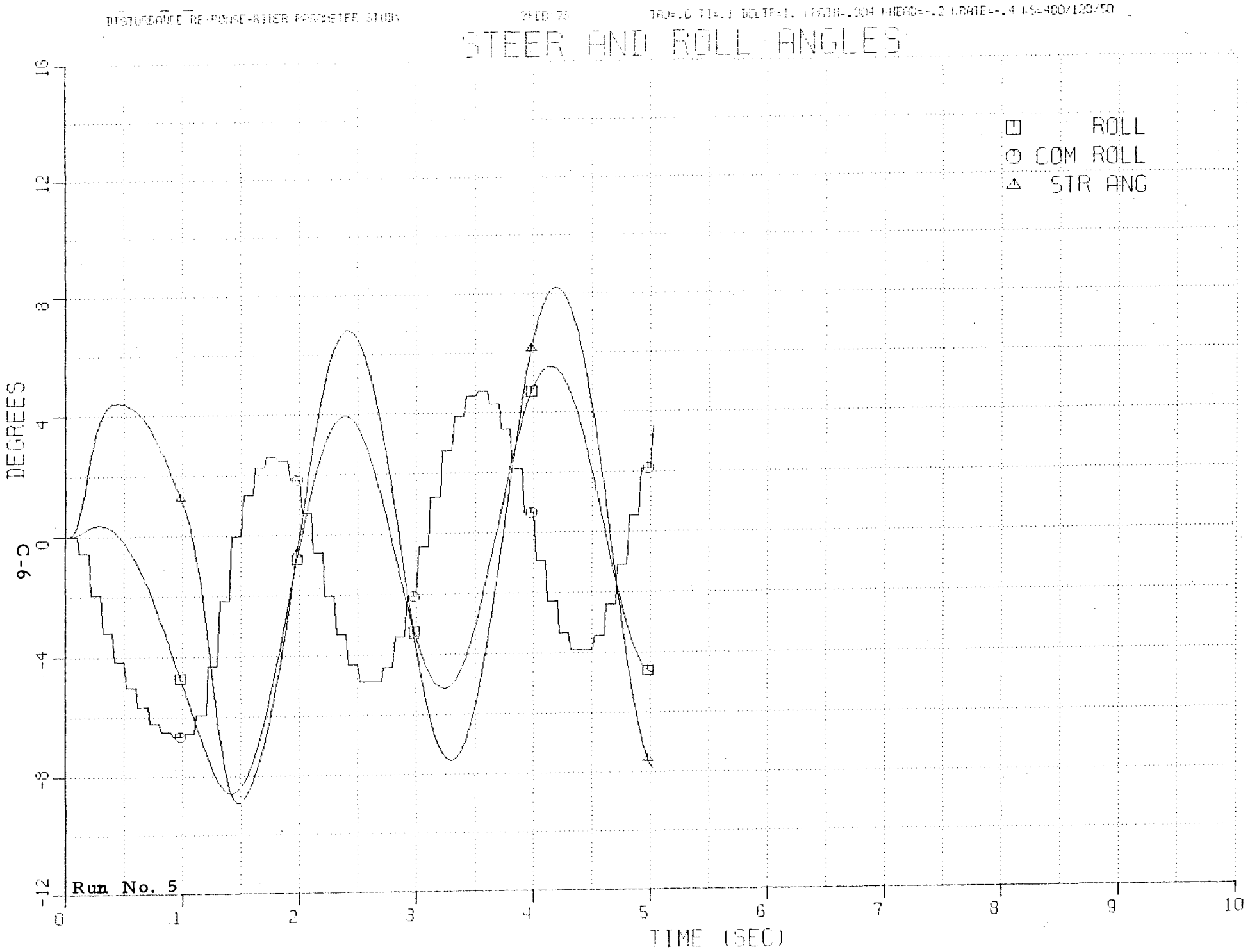
STEER AND ROLL ANGLES
ROLL
COM ROLL
STR ANG
DEGREES
TIME (SEC)
Run No. 5
16
12
8
4
0
-4
-8
-12
0
1
2
3
4
5
6
7
8
9
10

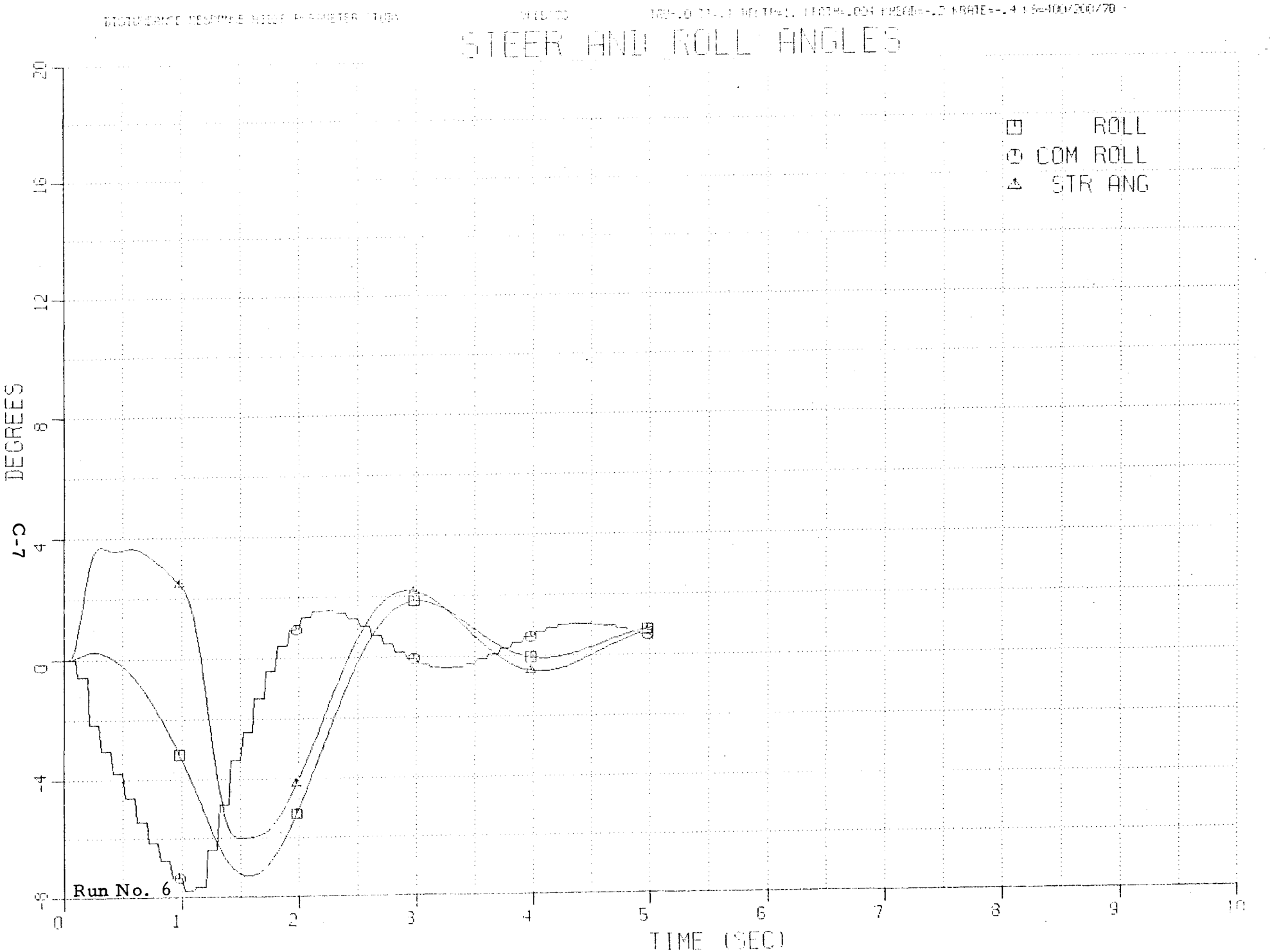
STEER AND ROLL ANGLES
ROLL
COM ROLL
STR ANG
DEGREES
TIME (SEC)
Run No. 6
20
16
12
8
4
0
-4
-8
0
1
2
3
4
5
6
7
8
9
10

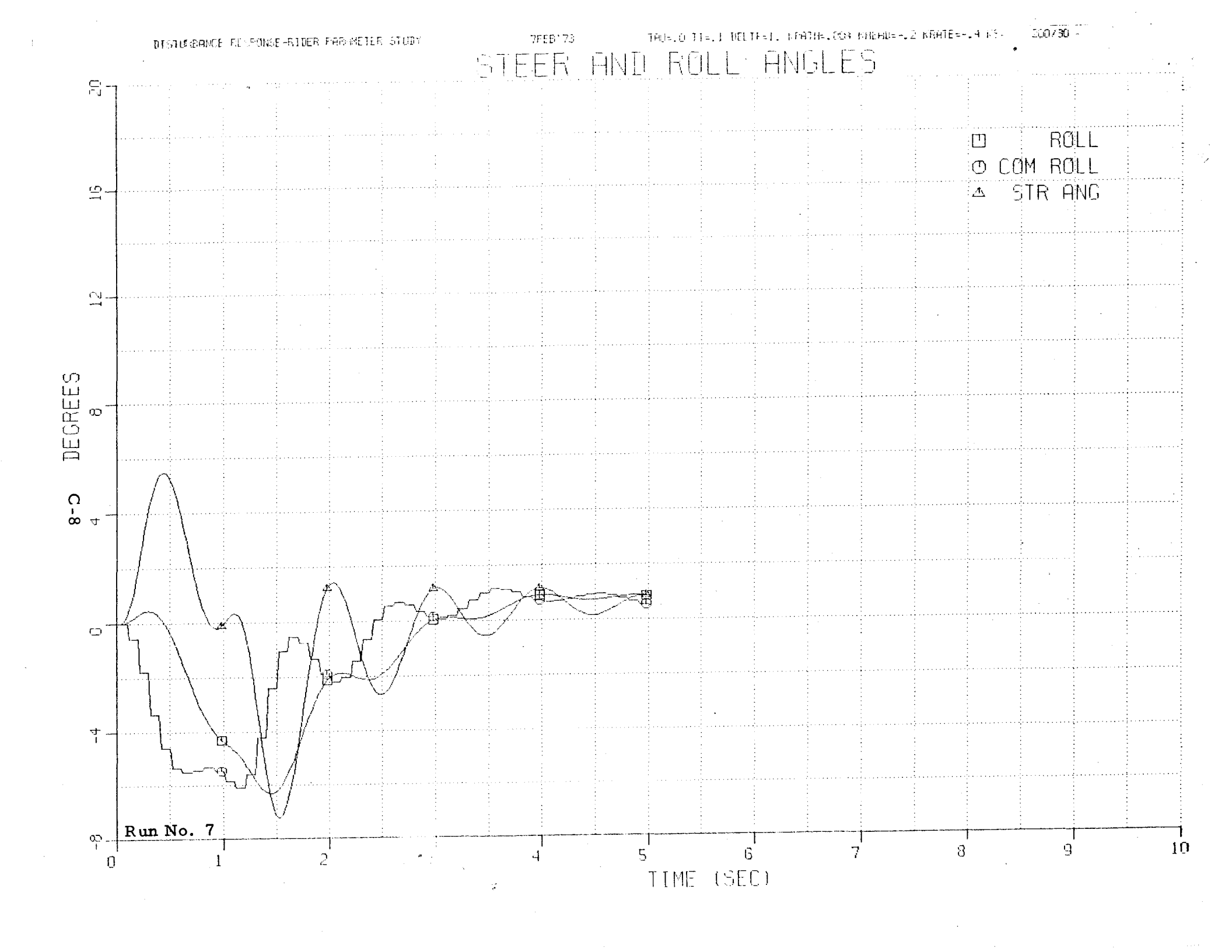
DISTURBANCE RESPONSE-RIDER PARAMETER STUDY
7FEB'73
TAU=.0 TI=.1 DELTA=1. KPATH=.005 KHEAD=-.2 KRATE=-.4 KS=
300/30
STEER AND ROLL ANGLES
ROLL
COM ROLL
STR ANG
8-C DEGREES
20
16
12
8
4
0
-4
-8
0
1
2
4
5
6
7
8
9
10
TIME (SEC)
Run No. 7

STEER AND ROLL ANGLES

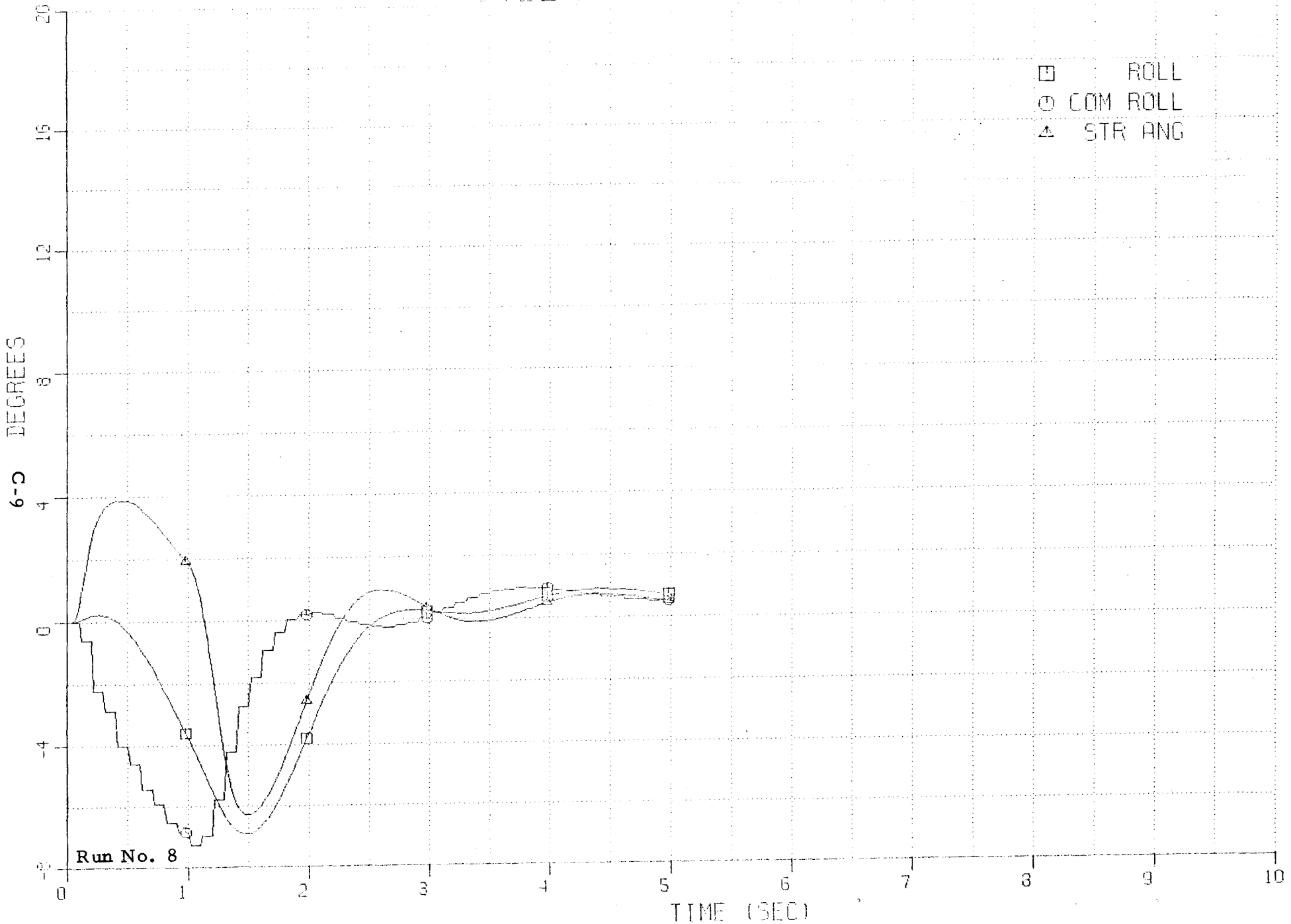

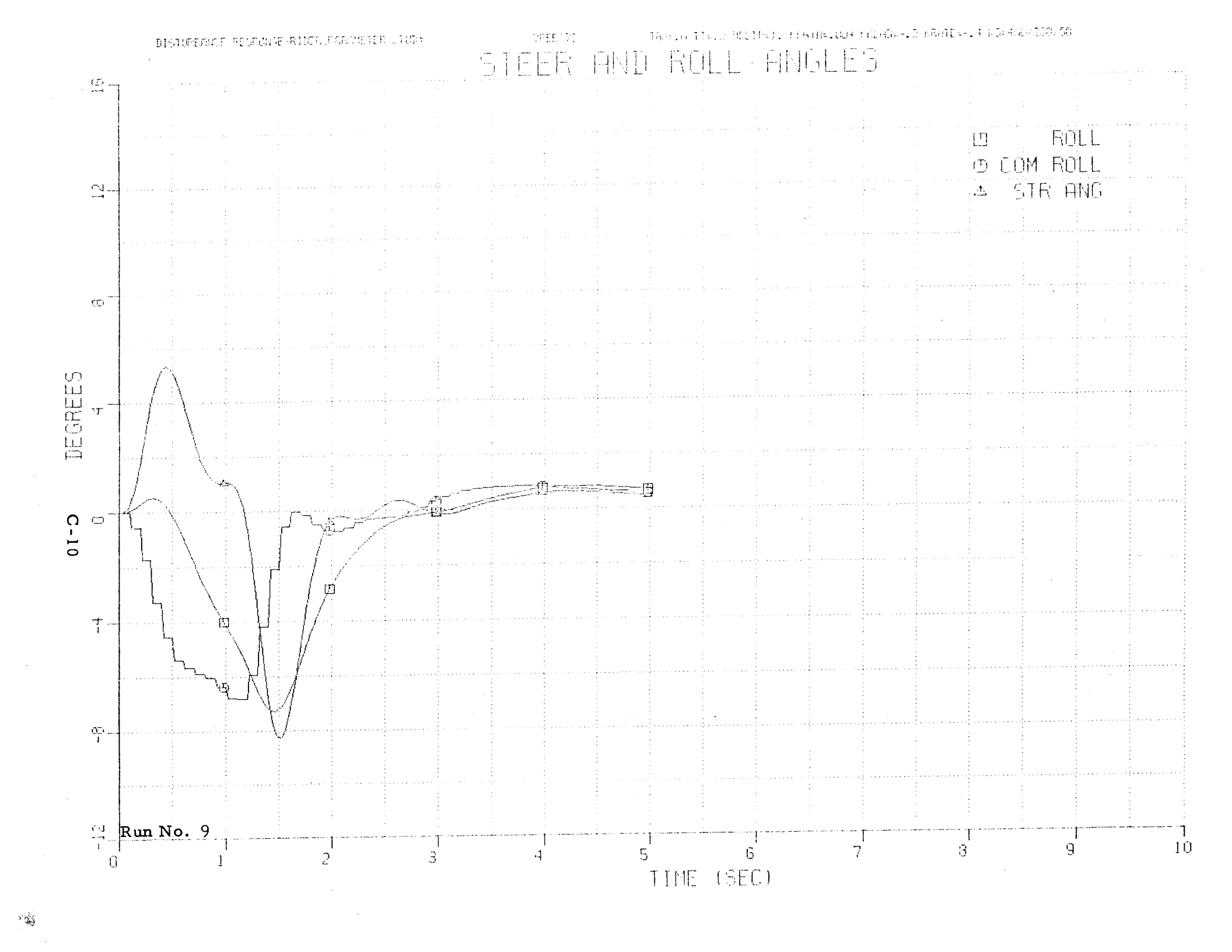
STEER AND ROLL ANGLES
ROLL
COM ROLL
STR ANG
DEGREES
TIME (SEC)
Run No. 9
C-10

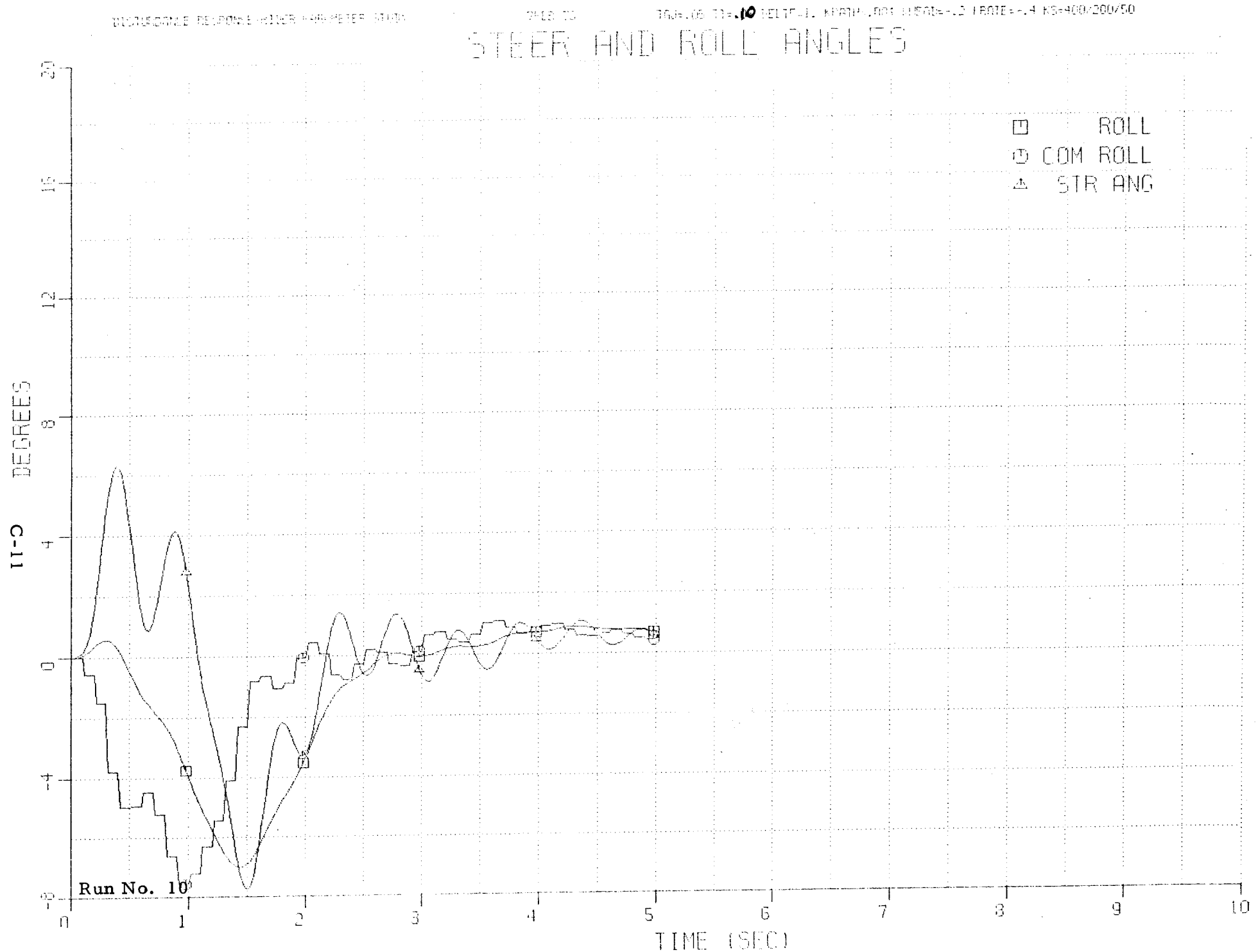
STEER AND ROLL ANGLES
ROLL
COM ROLL
STR ANG
DEGREES
TIME (SEC)
Run No. 10
20
16
12
8
4
0
-4
-8
0
1
2
3
4
5
6
7
8
9
10

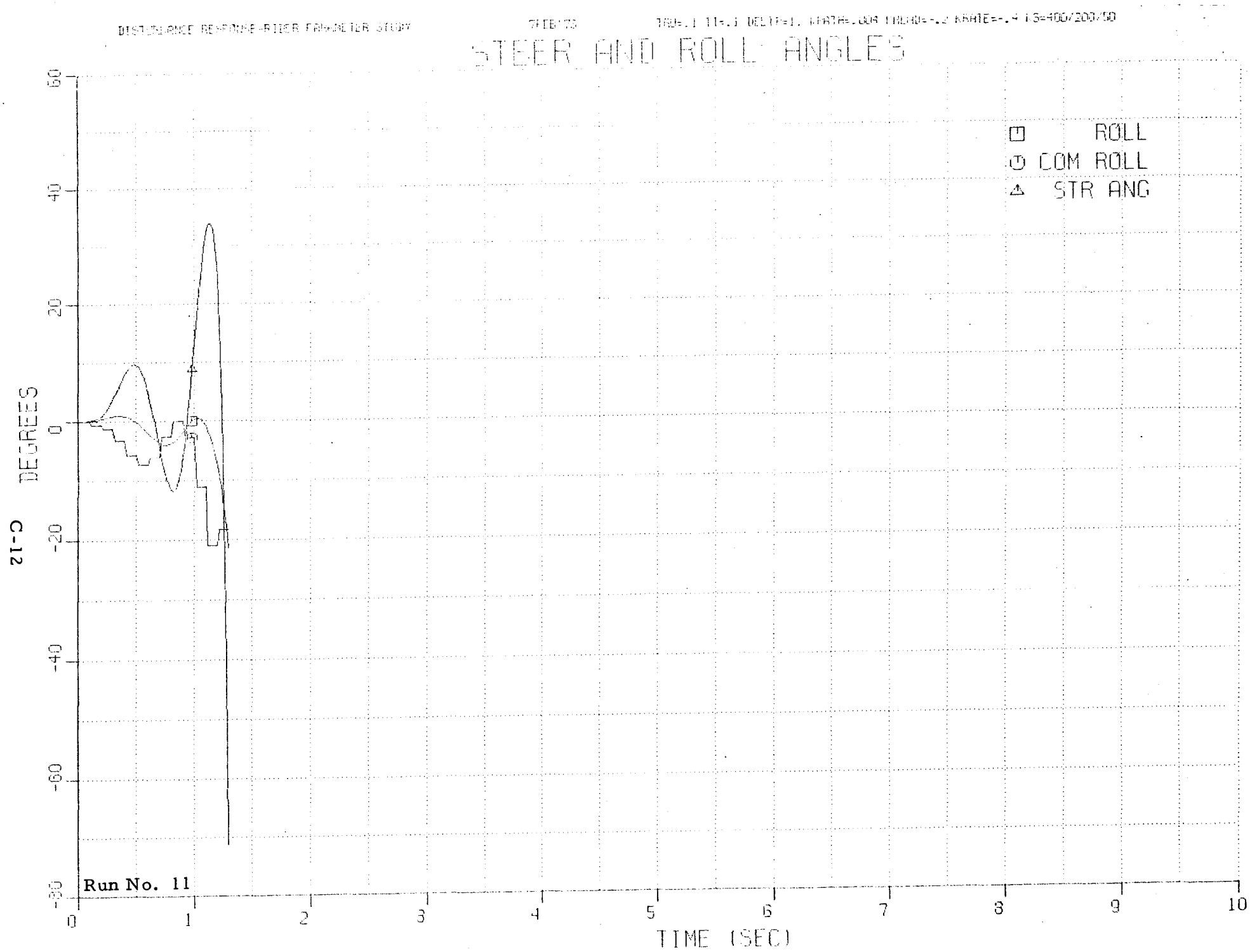
STEER AND ROLL ANGLES
ROLL
COM ROLL
STR ANG
DEGREES
60
40
20
0
-20
-40
-60
-80
0
1
2
3
4
5
6
7
8
9
10
TIME (SEC)
Run No. 11

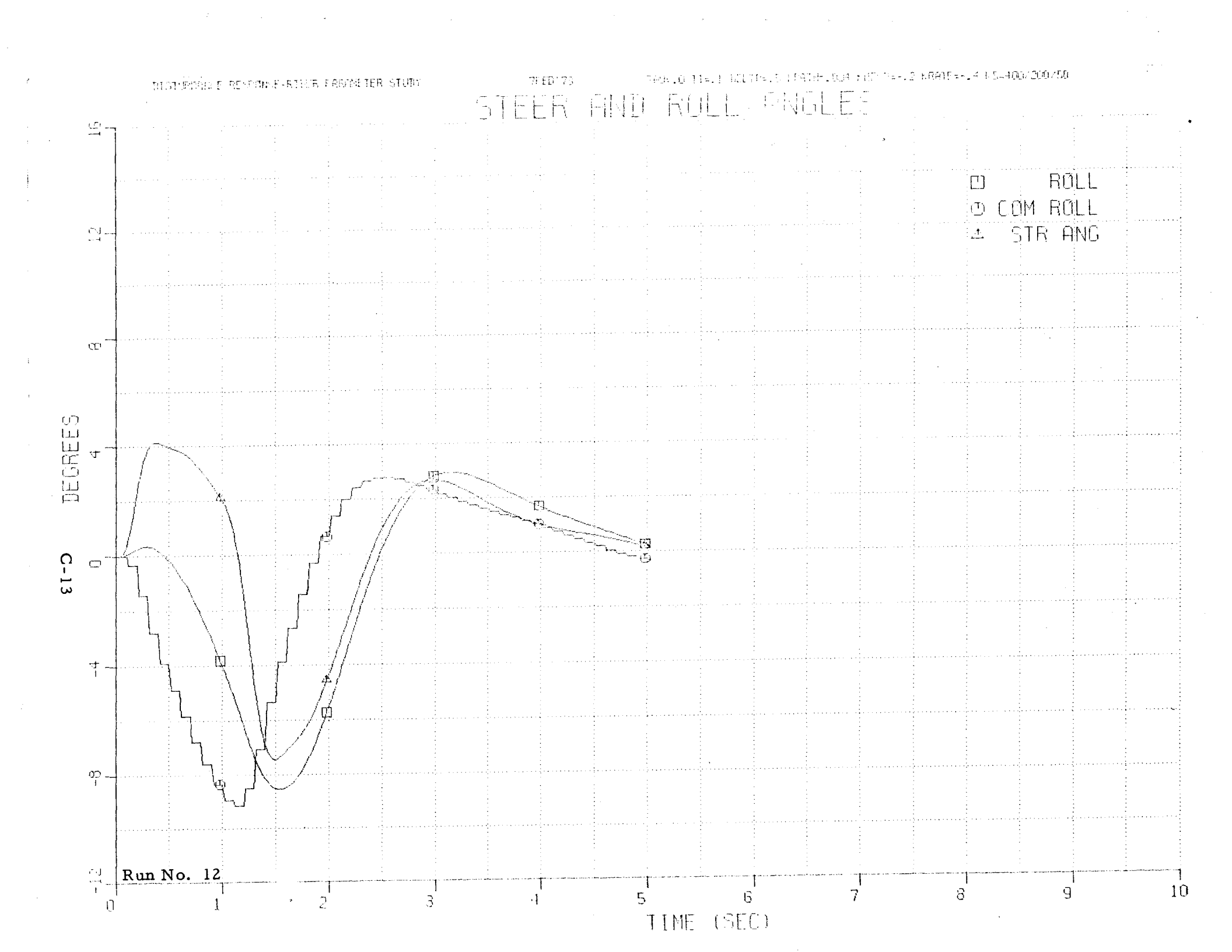
STEER AND ROLL ANGLES
ROLL
COM ROLL
STR ANG
DEGREES
TIME (SEC)
Run No. 12
16
12
8
4
0
-4
-8
-12
0
1
2
3
4
5
6
7
8
9
10

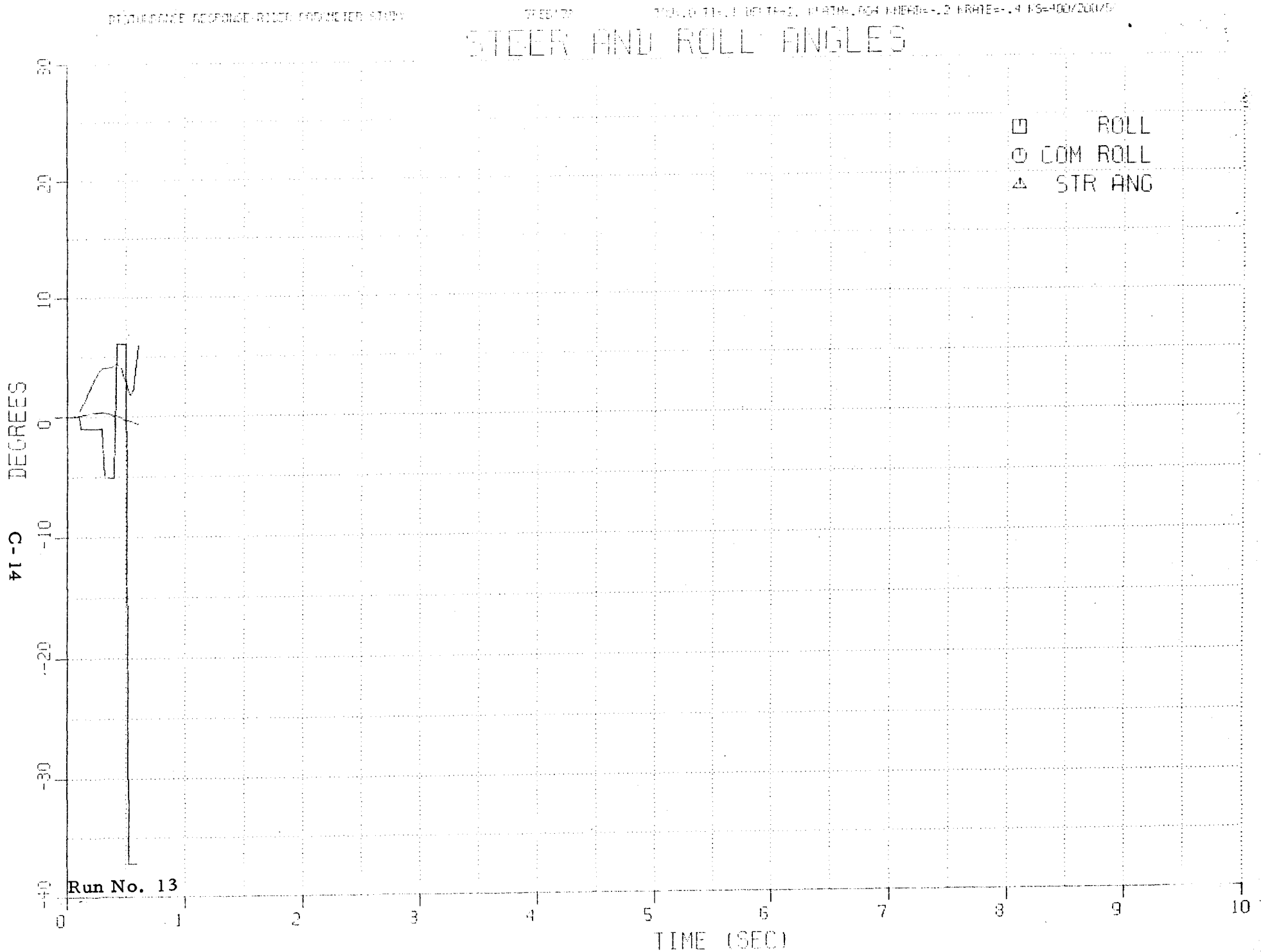
STEER AND ROLL ANGLES
ROLL
COM ROLL
STR ANG
DEGREES
30
20
10
0
-10
-20
-30
-40
0
1
2
3
4
5
6
7
8
9
10
TIME (SEC)
Run No. 13

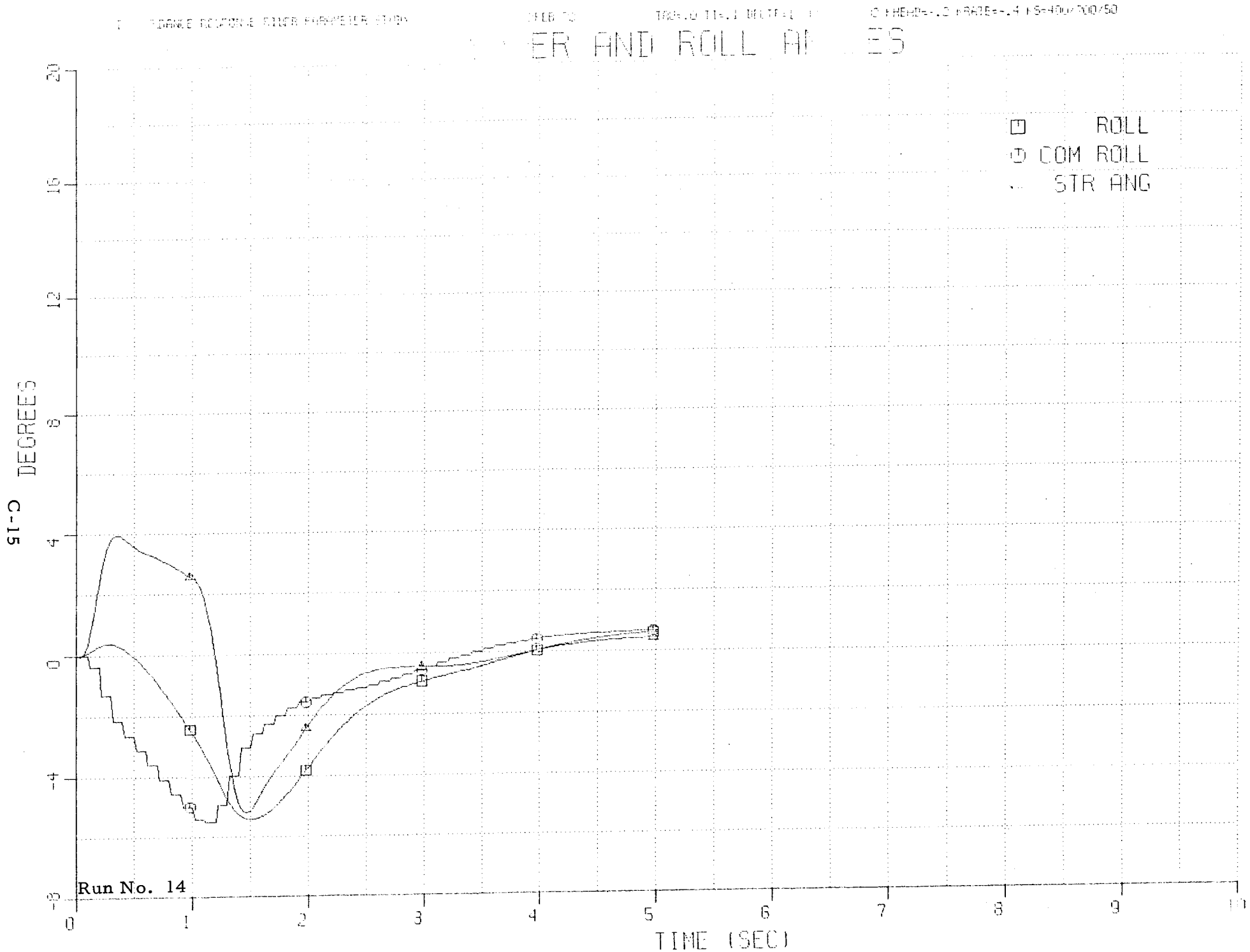
ER AND ROLL AN ES
ROLL
COM ROLL
STR ANG
DEGREES
TIME (SEC)
Run No. 14
20
16
12
8
4
0
-4
-8
0
1
2
3
4
5
6
7
8
9

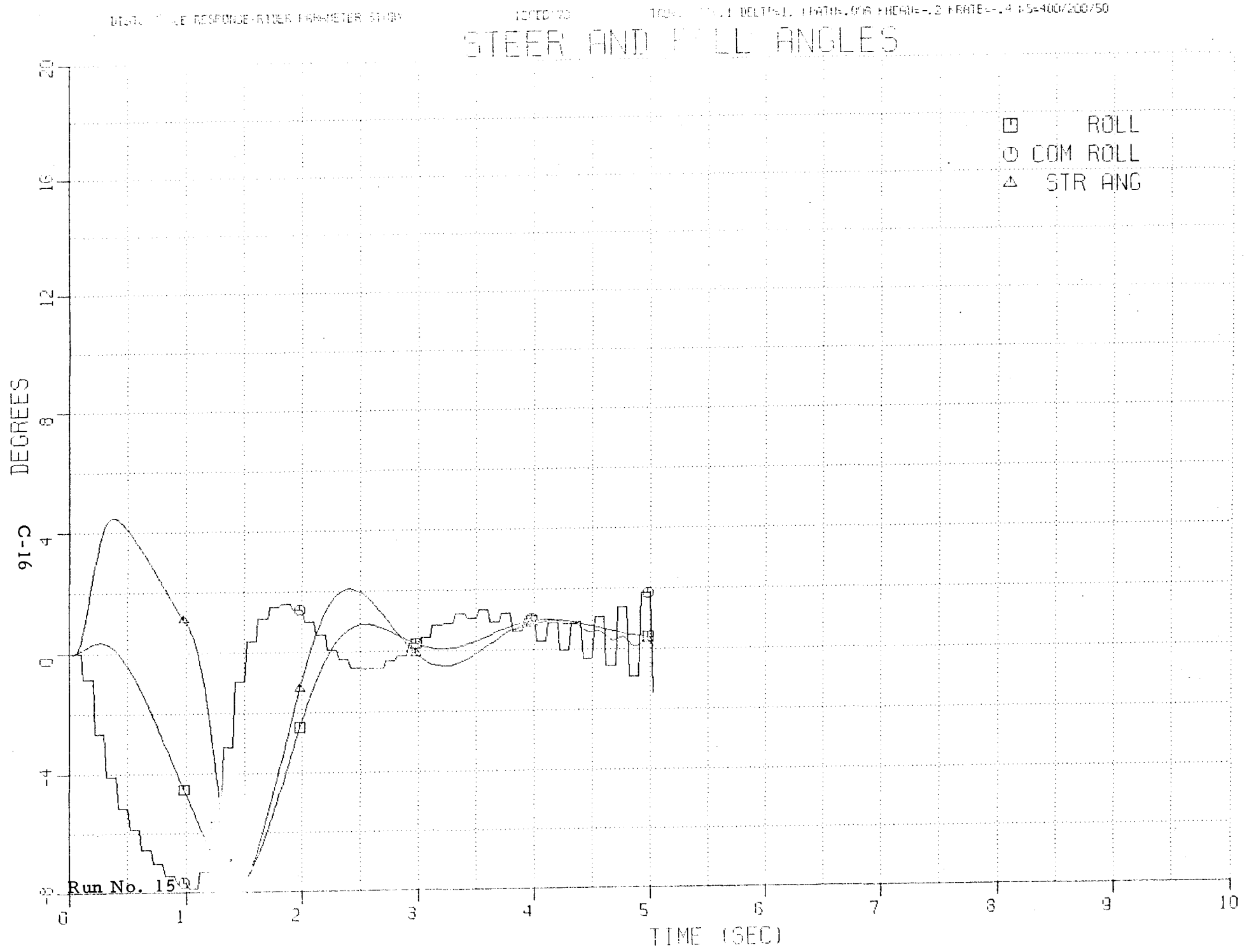
STEER AND ROLL ANGLES
ROLL
COM ROLL
STR ANG
DEGREES
TIME (SEC)
Run No. 15
20
16
12
8
4
0
-4
-8
0
1
2
3
4
5
6
7
8
9
10

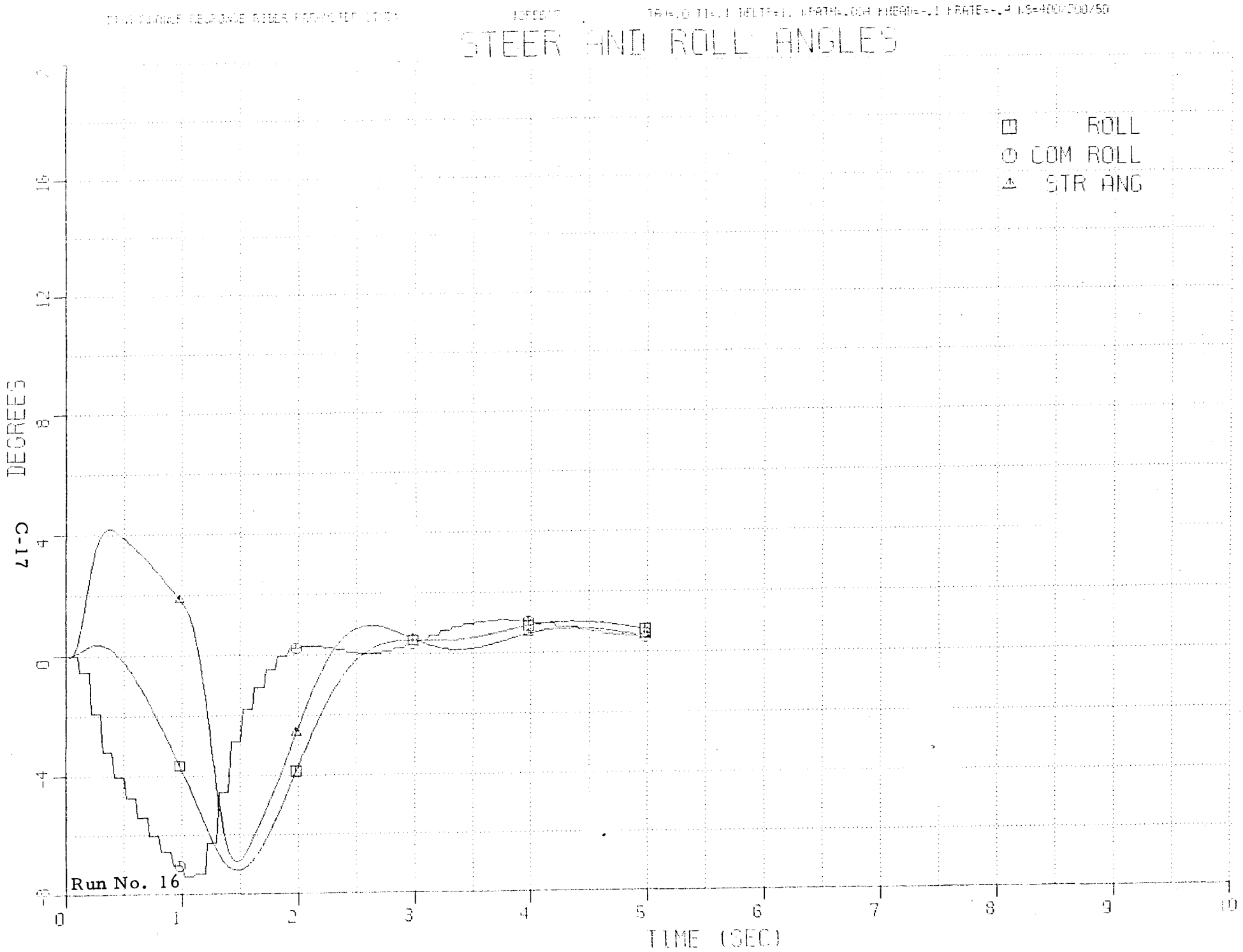
STEER AND ROLL ANGLES
ROLL
COM ROLL
STR ANG
DEGREES
TIME (SEC)
Run No. 16
16
12
8
4
0
-4
-8
0
1
2
3
4
5
6
7
8
9
10

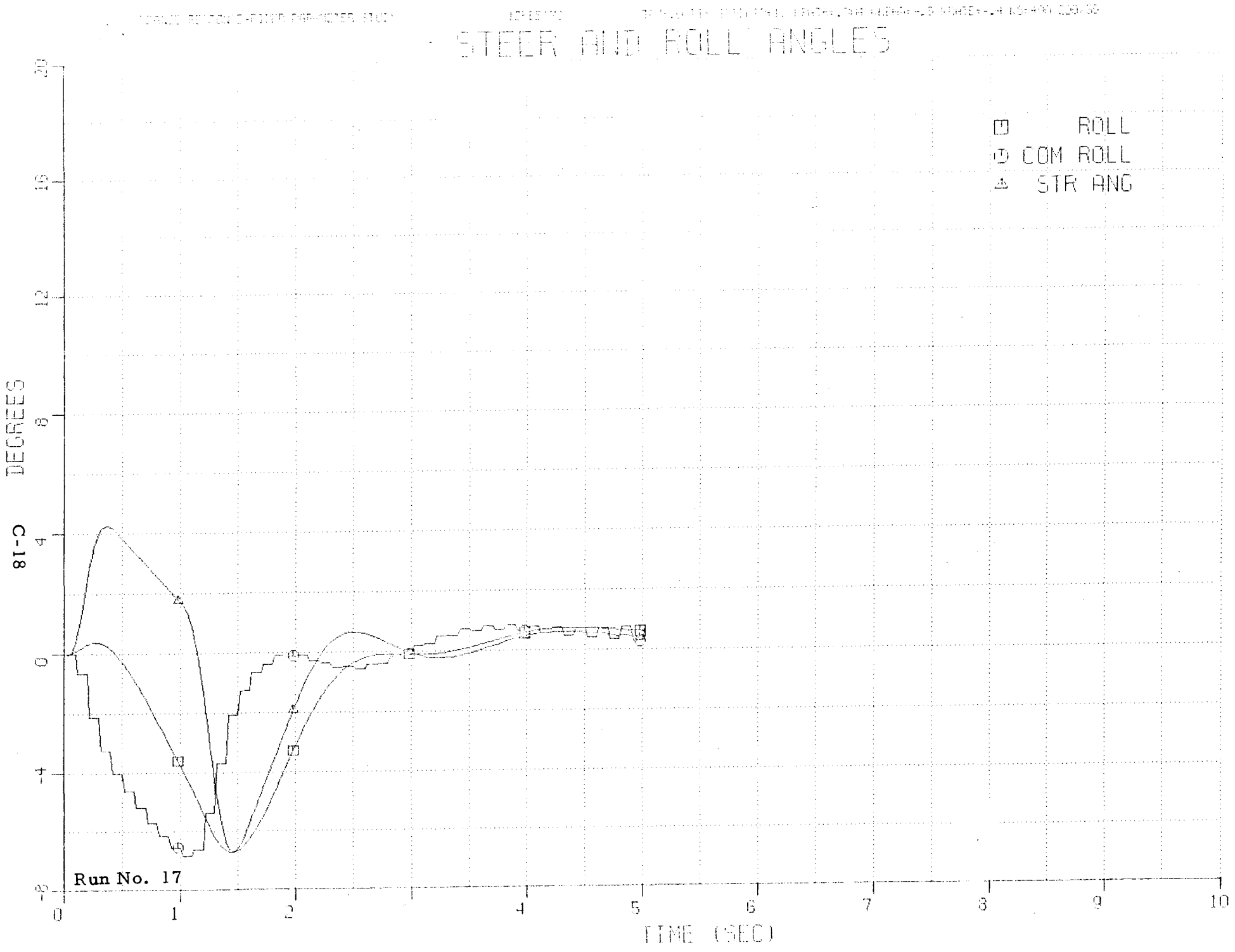
STEER AND ROLL ANGLES
ROLL
COM ROLL
STR ANG
DEGREES
TIME (SEC)
Run No. 17
20
16
12
8
4
0
-4
-8
0
1
2
4
5
6
7
8
9
10

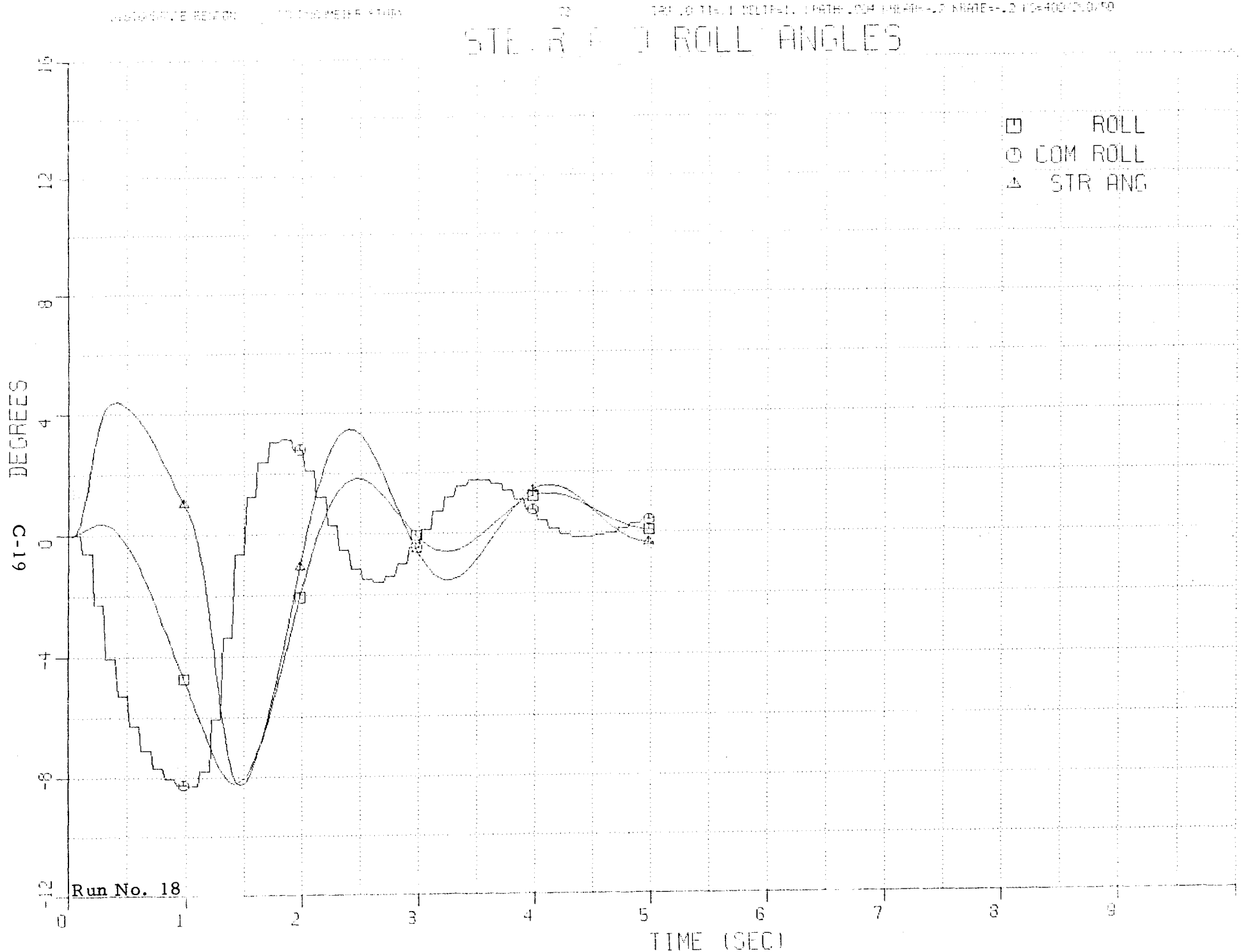
ROLL
COM ROLL
STR ANG
DEGREES
TIME (SEC)
Run No. 18
16
12
8
4
0
-4
-8
-12
0
1
2
3
4
5
6
7
8
9

STEER AND ROLL ANGLES

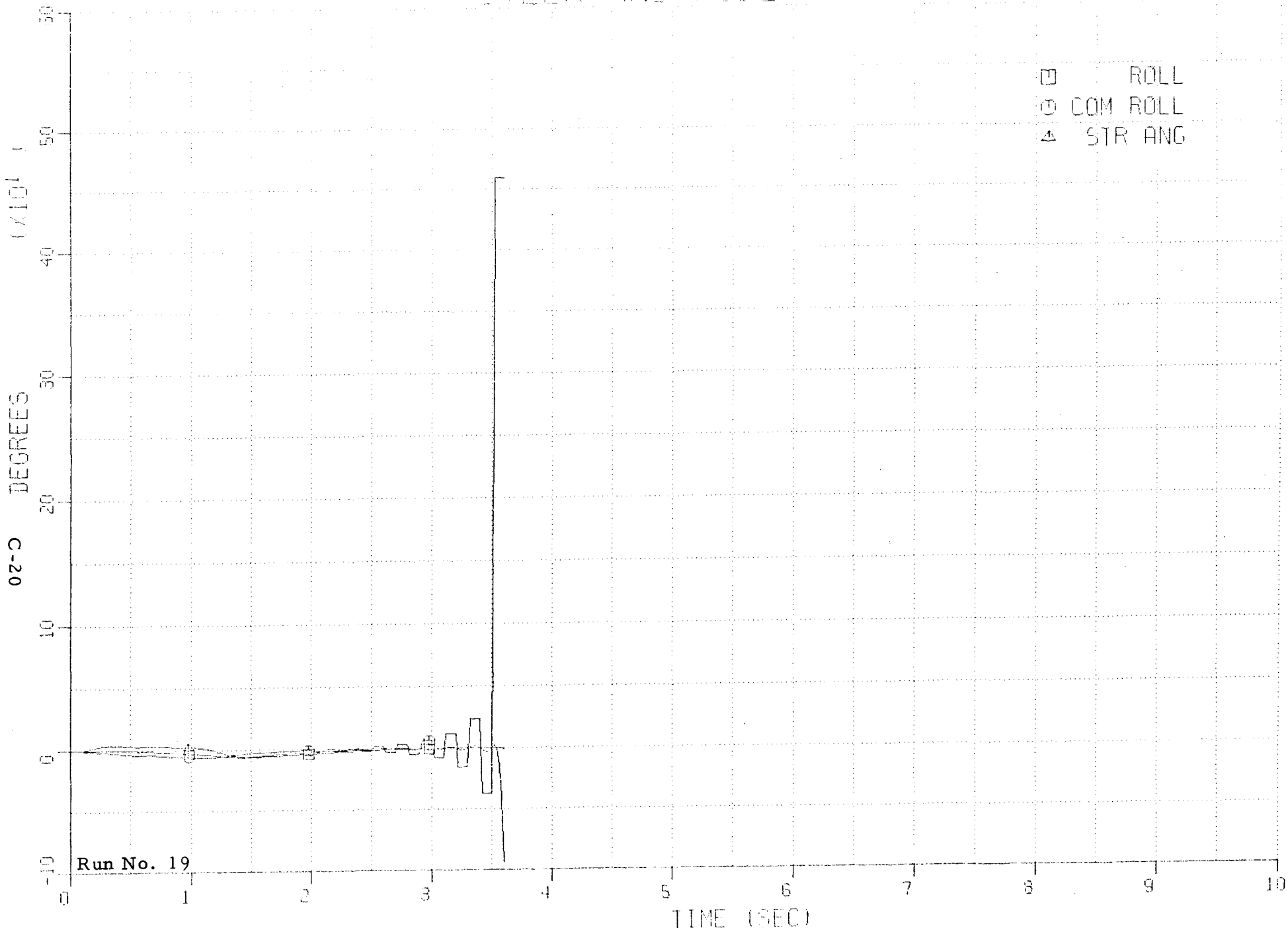

APPENDIX D

Plotted Results of Simulated Bicycle-Rider Disturbance Response Stability Study

SUBURBAN	STANDARD CONFIGURATION	ST. PATH	6 MPH	(1)
SUBURBAN	STANDARD CONFIGURATION	ST. PATH	10 MPH	(2)
SUBURBAN	STANDARD CONFIGURATION	ST. PATH	15 MPH	(3)
PARAMOUNT	STANDARD CONFIGURATION	ST. PATH	6 MPH	(4)
PARAMOUNT	STANDARD CONFIGURATION	ST. PATH	10 MPH	(5)
PARAMOUNT	STANDARD CONFIGURATION	ST. PATH	15 MPH	(6)
STING-RAY	STANDARD CONFIGURATION	ST. PATH	10 MPH	(8)
STING-RAY	STANDARD CONFIGURATION	ST. PATH	6 MPH	(7)
STING-RAY	STANDARD CONFIGURATION	ST. PATH	15 MPH	(9)
SUBURBAN	33.2 IN. WHEELBASE	ST. PATH	6 MPH	(10)
SUBURBAN	33.2 IN. WHEELBASE	ST. PATH	10 MPH	(11)
SUBURBAN	33.2 IN. WHEELBASE	ST. PATH	15 MPH	(12)
SUBURBAN	49.8 IN. WHEELBASE	ST. PATH	6 MPH	(13)
SUBURBAN	49.8 IN. WHEELBASE	ST. PATH	10 MPH	(14)
SUBURBAN	49.8 IN. WHEELBASE	ST. PATH	15 MPH	(15)
SUBURBAN	25 LB. BICYCLE	ST. PATH	6 MPH	(16)
SUBURBAN	25 LB. BICYCLE	ST. PATH	10 MPH	(17)
SUBURBAN	25 LB. BICYCLE	ST. PATH	15 MPH	(18)
SUBURBAN	55 LB. BICYCLE	ST. PATH	6 MPH	(19)
SUBURBAN	55 LB. BICYCLE	ST. PATH	10 MPH	(20)
SUBURBAN	55 LB. BICYCLE	ST. PATH	15 MPH	(21)
SUBURBAN	16.6 IN. CG HEIGHT	ST. PATH	6 MPH	(22)
SUBURBAN	16.6 IN. CG HEIGHT	ST. PATH	10 MPH	(23)
SUBURBAN	16.6 IN. CG HEIGHT	ST. PATH	15 MPH	(24)
SUBURBAN	24.9 IN. CG HEIGHT	ST. PATH	6 MPH	(25)
SUBURBAN	24.9 IN. CG HEIGHT	ST. PATH	10 MPH	(26)
SUBURBAN	24.9 IN. CG HEIGHT	ST. PATH	15 MPH	(27)
SUBURBAN	1.49 LB-IN-SEC2 STEER INERTIA	ST. PATH	6 MPH	(28)
SUBURBAN	1.49 LB-IN-SEC2 STEER INERTIA	ST. PATH	10 MPH	(29)
SUBURBAN	1.49 LB-IN-SEC2 STEER INERTIA	ST. PATH	15 MPH	(30)
SUBURBAN	2.23 LB-IN-SEC2 STEER INERTIA	ST. PATH	6 MPH	(31)
SUBURBAN	2.23 LB-IN-SEC2 STEER INERTIA	ST. PATH	10 MPH	(32)
SUBURBAN	2.23 LB-IN-SEC2 STEER INERTIA	ST. PATH	15 MPH	(33)
SUBURBAN	15 DEG. CASTER ANGLE	ST. PATH	6 MPH	(34)
SUBURBAN	15 DEG. CASTER ANGLE	ST. PATH	10 MPH	(35)
SUBURBAN	15 DEG. CASTER ANGLE	ST. PATH	15 MPH	(36)
SUBURBAN	25 DEG. CASTER ANGLE	ST. PATH	6 MPH	(37)
SUBURBAN	25 DEG. CASTER ANGLE	ST. PATH	10 MPH	(38)
SUBURBAN	25 DEG. CASTER ANGLE	ST. PATH	15 MPH	(39)
SUBURBAN	0.87 IN. FORK OFFSET	ST. PATH	6 MPH	(40)
SUBURBAN	0.87 IN. FORK OFFSET	ST. PATH	10 MPH	(41)
SUBURBAN	0.87 IN. FORK OFFSET	ST. PATH	15 MPH	(42)
SUBURBAN	2.87 IN. FORK OFFSET	ST. PATH	6 MPH	(43)
SUBURBAN	2.87 IN. FORK OFFSET	ST. PATH	10 MPH	(44)
SUBURBAN	2.87 IN. FORK OFFSET	ST. PATH	15 MPH	(45)
SUBURBAN	20.0 IN. WHEEL DIAMETER	ST. PATH	6 MPH	(46)
SUBURBAN	20.0 IN. WHEEL DIAMETER	ST. PATH	10 MPH	(47)
SUBURBAN	20.0 IN. WHEEL DIAMETER	ST. PATH	15 MPH	(48)
SUBURBAN	29.2 IN. WHEEL DIAMETER	ST. PATH	6 MPH	(49)
SUBURBAN	29.2 IN. WHEEL DIAMETER	ST. PATH	10 MPH	(50)
SUBURBAN	29.2 IN. WHEEL DIAMETER	ST. PATH	15 MPH	(51)
SUBURBAN	1.41 LB-IN-SEC2 WHEEL INERTIA	ST. PATH	6 MPH	(52)
SUBURBAN	1.41 LB-IN-SEC2 WHEEL INERTIA	ST. PATH	10 MPH	(53)
SUBURBAN	1.41 LB-IN-SEC2 WHEEL INERTIA	ST. PATH	15 MPH	(54)
SUBURBAN	2.11 LB-IN-SEC2 WHEEL INERTIA	ST. PATH	6 MPH	(55)
SUBURBAN	2.11 LB-IN-SEC2 WHEEL INERTIA	ST. PATH	10 MPH	(56)
SUBURBAN	2.11 LB-IN-SEC2 WHEEL INERTIA	ST. PATH	15 MPH	(57)
SUBURBAN	LOW CORNERING STIFFNESS TIRE	ST. PATH	6 MPH	(58)
SUBURBAN	LOW CORNERING STIFFNESS TIRE	ST. PATH	10 MPH	(59)
SUBURBAN	LOW CORNERING STIFFNESS TIRE	ST. PATH	15 MPH	(60)
SUBURBAN	HIGH CORNERING STIFFNESS TIRE	ST. PATH	6 MPH	(61)
SUBURBAN	HIGH CORNERING STIFFNESS TIRE	ST. PATH	10 MPH	(62)
SUBURBAN	HIGH CORNERING STIFFNESS TIRE	ST. PATH	15 MPH	(63)

TABLE A-1. Test Configurations and Run Numbers

BICYCLE STABILITY PARAMETER STUDY 21FEB'73 SUBURBAN STANDARD CONFIGURATION ST. PATH 6 MPH (1)

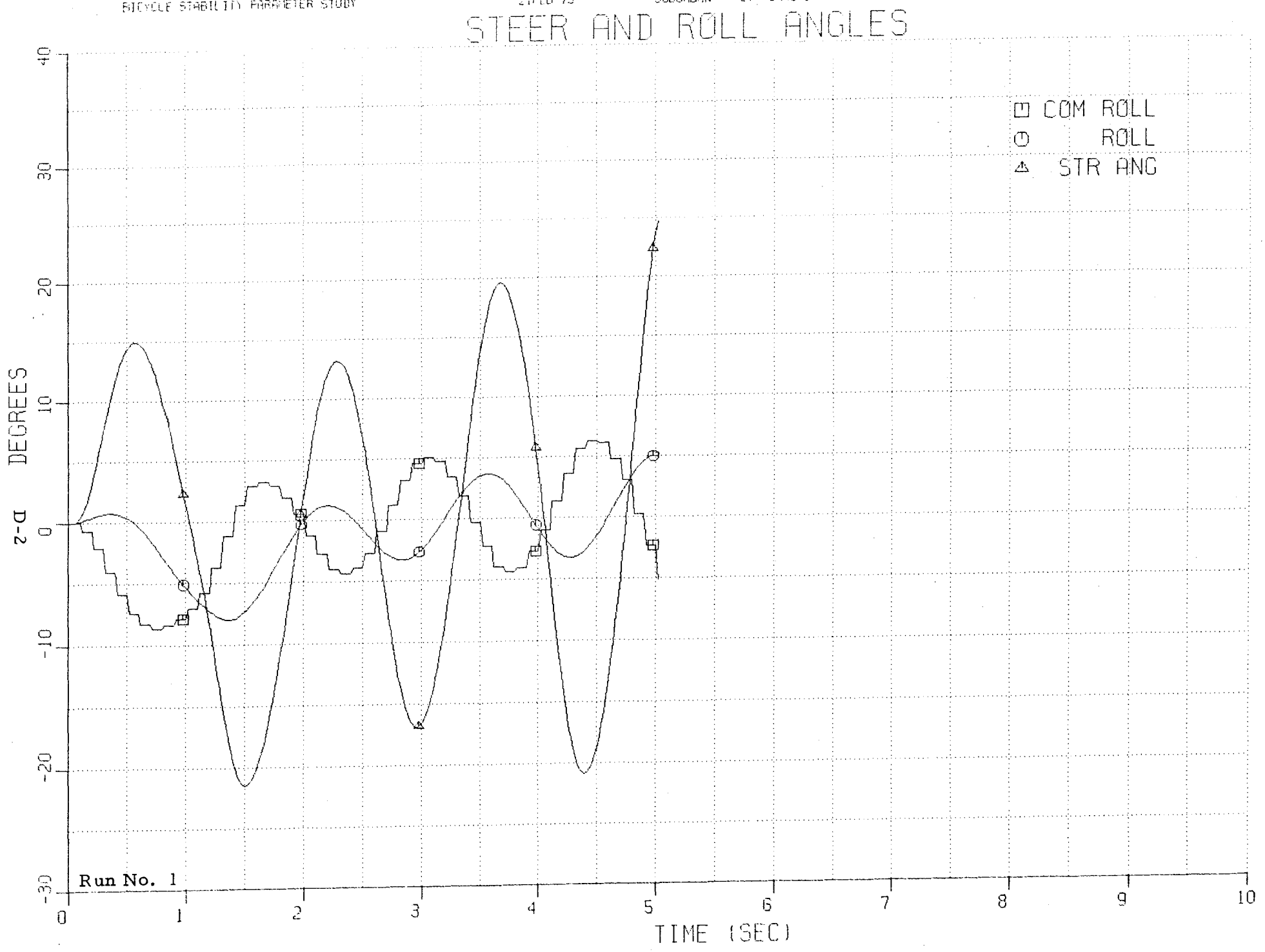

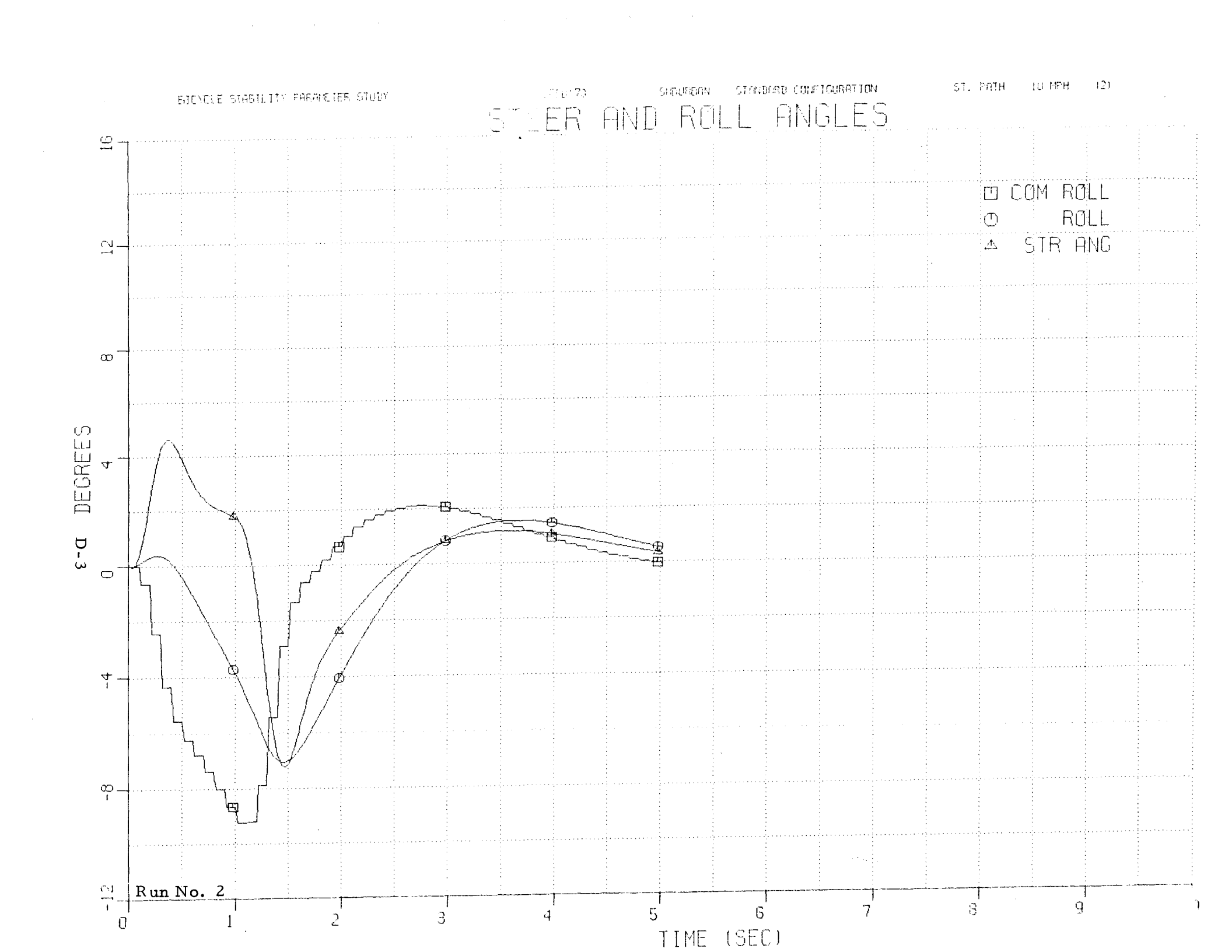
BICYCLE STABILITY PARAMETER STUDY
SUBURBAN STANDARD CONFIGURATION
ST. PATH 10 MPH (2)
STEER AND ROLL ANGLES
COM ROLL
ROLL
STR ANG
D-3 DEGREES
16
12
8
4
0
-4
-8
-12
Run No. 2
0
1
2
3
4
5
6
7
8
9
TIME (SEC)

BICYCLE STABILITY PARAMETER STUDY 21FEB'73 SUBURBAN STANDARD CONFIGURATION ST. PATH 15 MPH (5)

STEER AND ROLL ANGLES

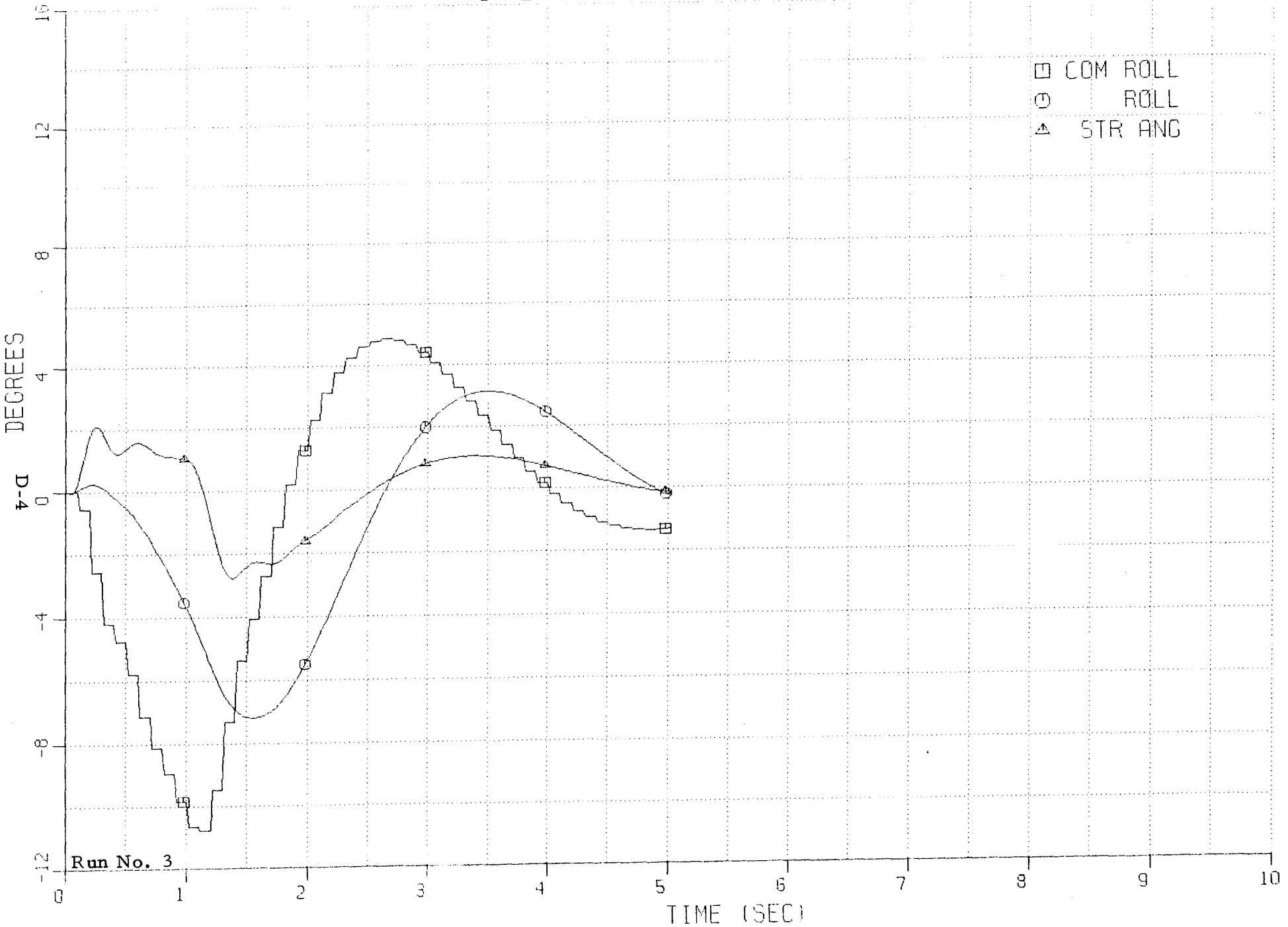

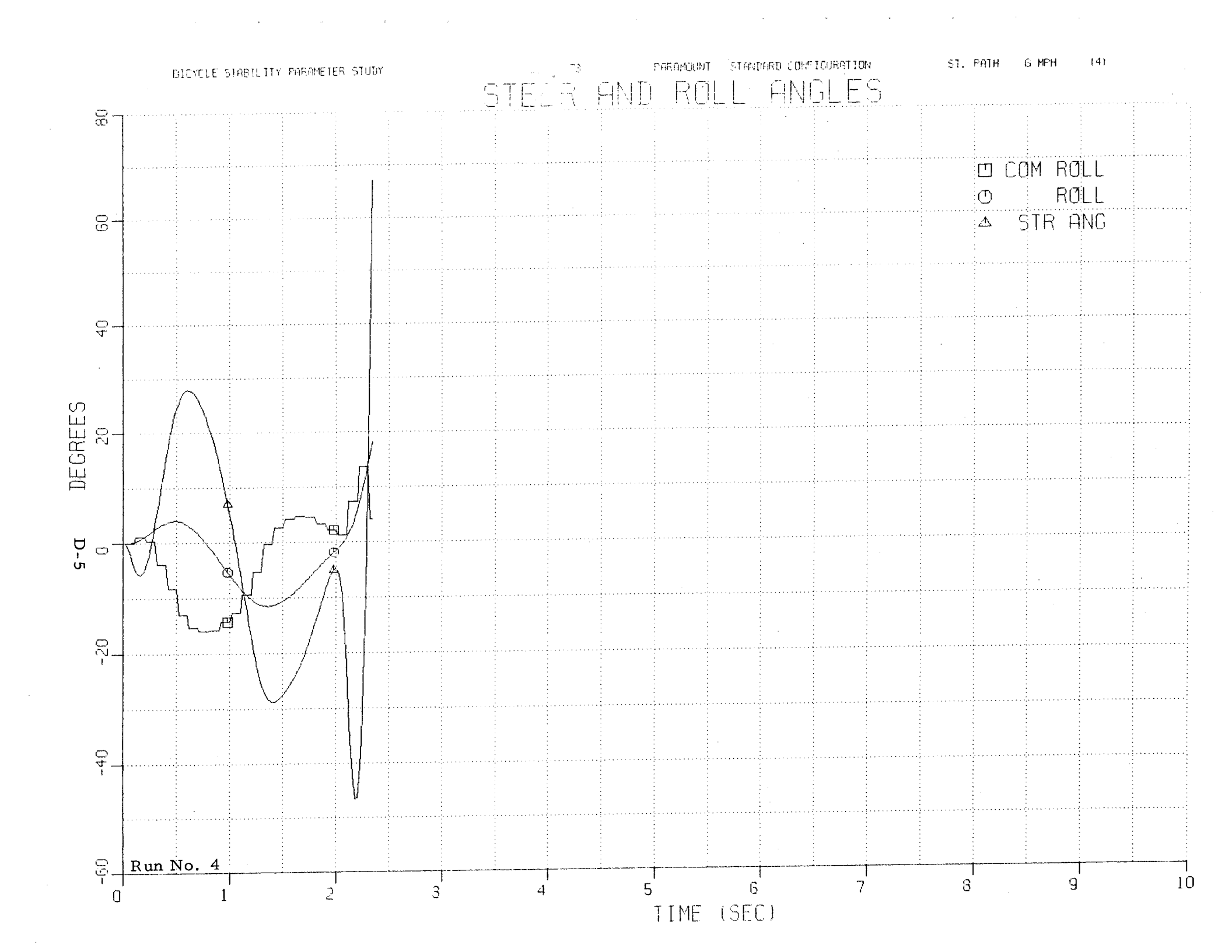
BICYCLE STABILITY PARAMETER STUDY
PARAMOUNT STANDARD CONFIGURATION
ST. PATH 6 MPH (4)
STEER AND ROLL ANGLES
COM ROLL
ROLL
STR ANG
DEGREES
80
60
40
20
0
-20
-40
-60
Run No. 4
0
1
2
3
4
5
6
7
8
9
10
TIME (SEC)

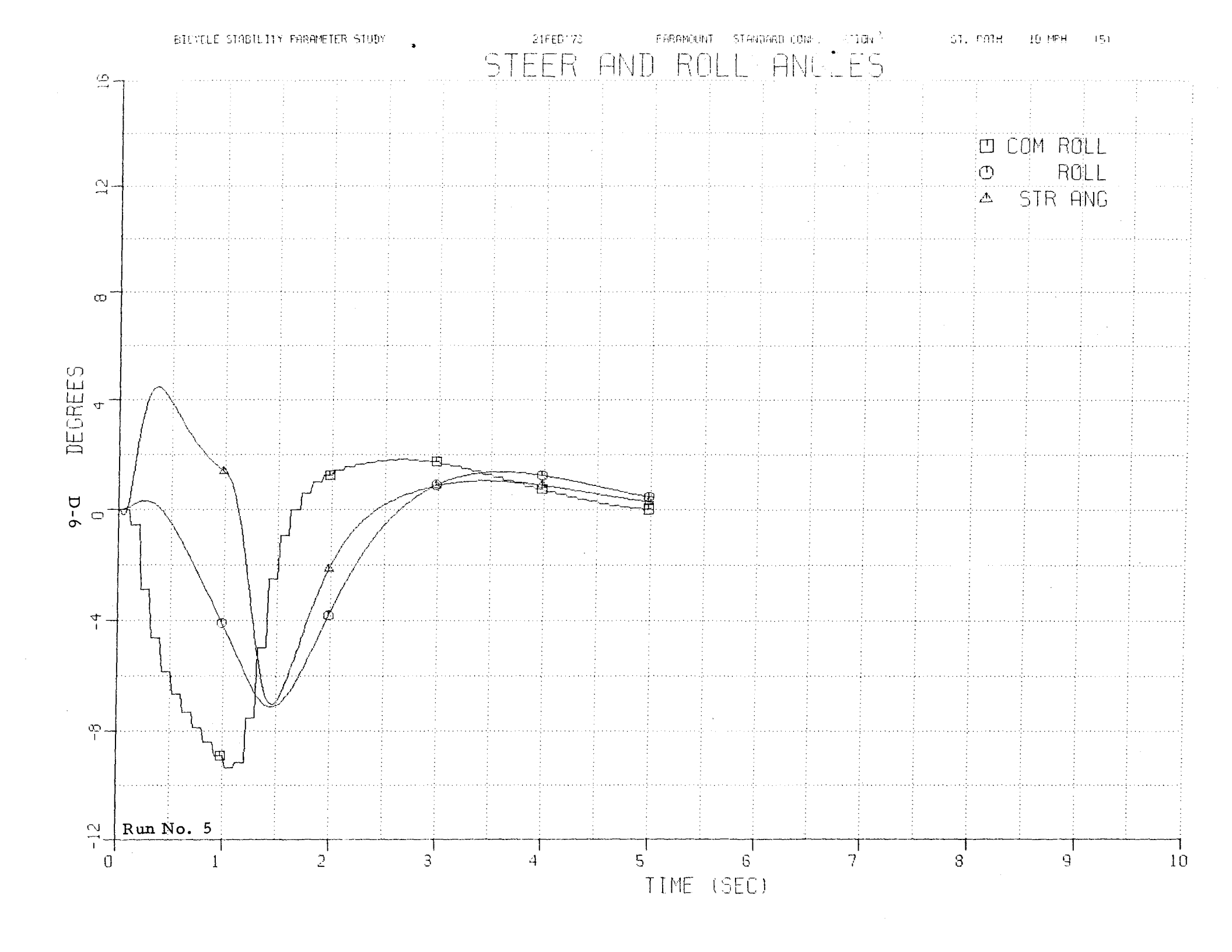
BICYCLE STABILITY PARAMETER STUDY
21FEB'73
PARAMOUNT STANDARD CONF. SECTION
37. 60TH 10 MPH 151
STEER AND ROLL ANGLES
COM ROLL
ROLL
STR ANG
DEGREES
TIME (SEC)
Run No. 5

BICYCLE STABILITY PARAMETER STUDY 21FEB'73 PARAMOUNT STANDARD CONFIGURATION ST. PATH 15 MPH (6)

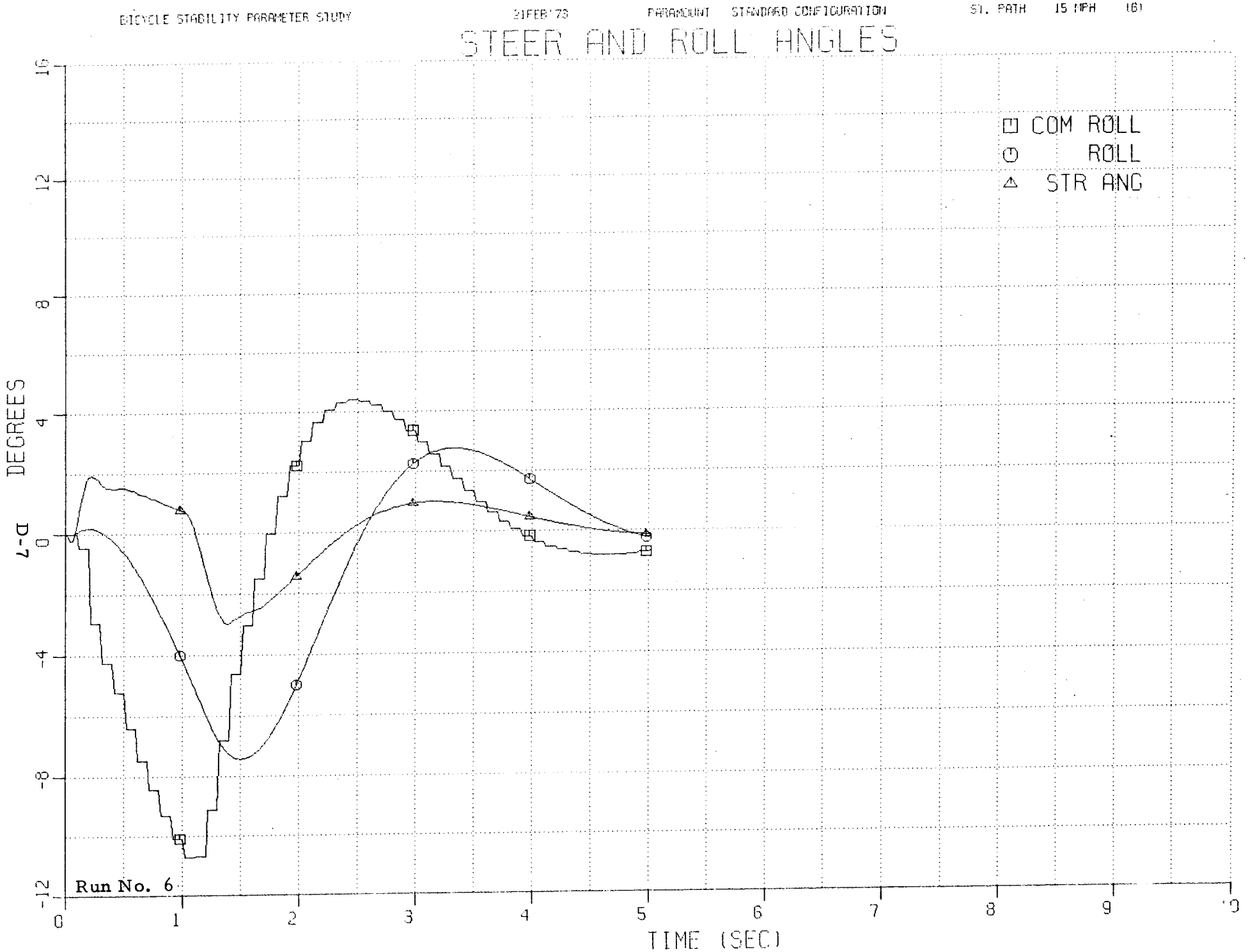

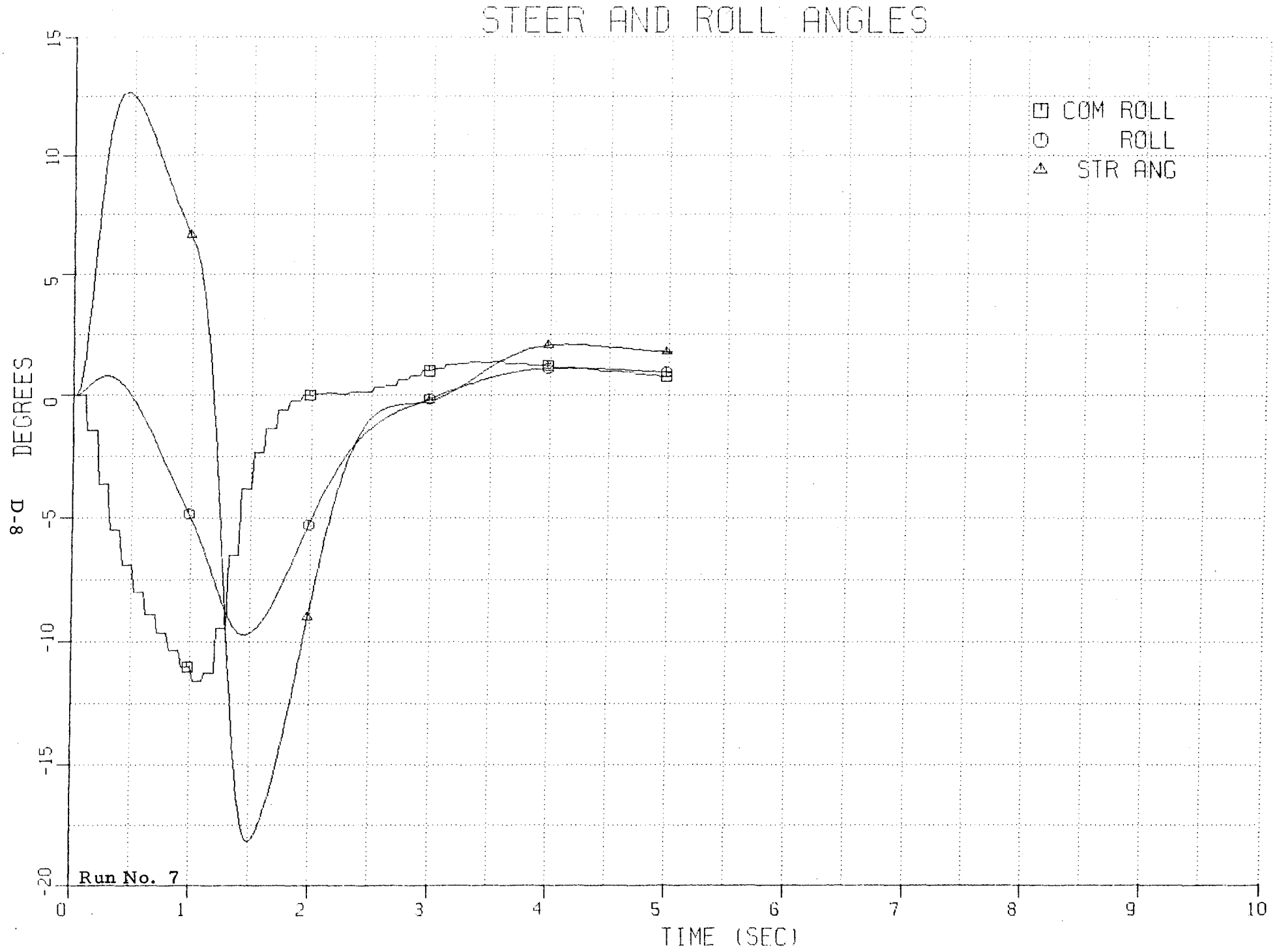
STEER AND ROLL ANGLES
COM ROLL
ROLL
STR ANG
DEGREES
TIME (SEC)
Run No. 7
15
10
5
0
-5
-10
-15
-20
0
1
2
3
4
5
6
7
8
9
10

STEER AND ROLL ANGLES

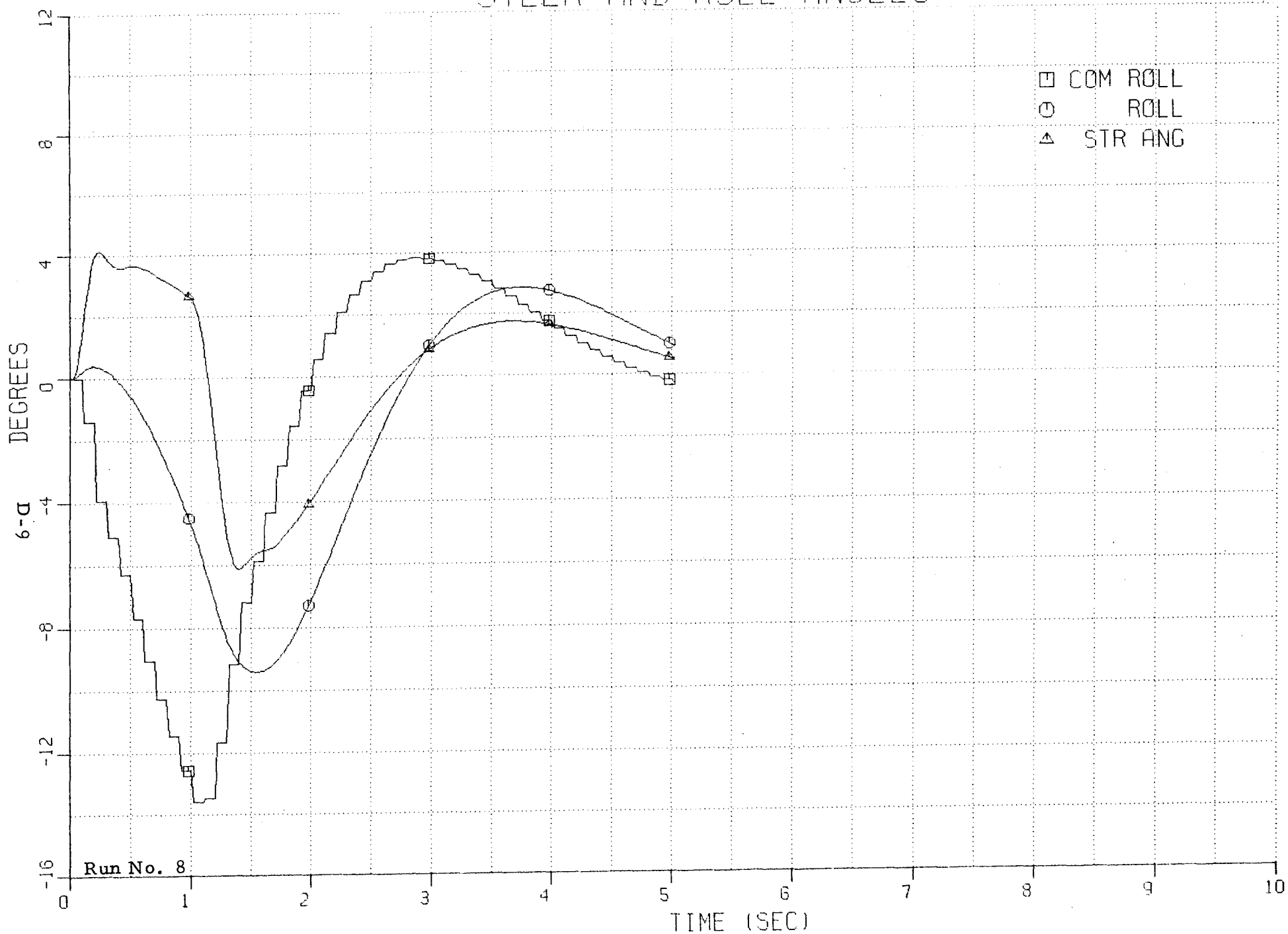

BICYCLE STABILITY PARAMETER STUDY 21FEB'73 STING-RAY STANDARD CONFIGURATION ST. PATH 15 MPH 191

STEER AND ROLL ANGLES

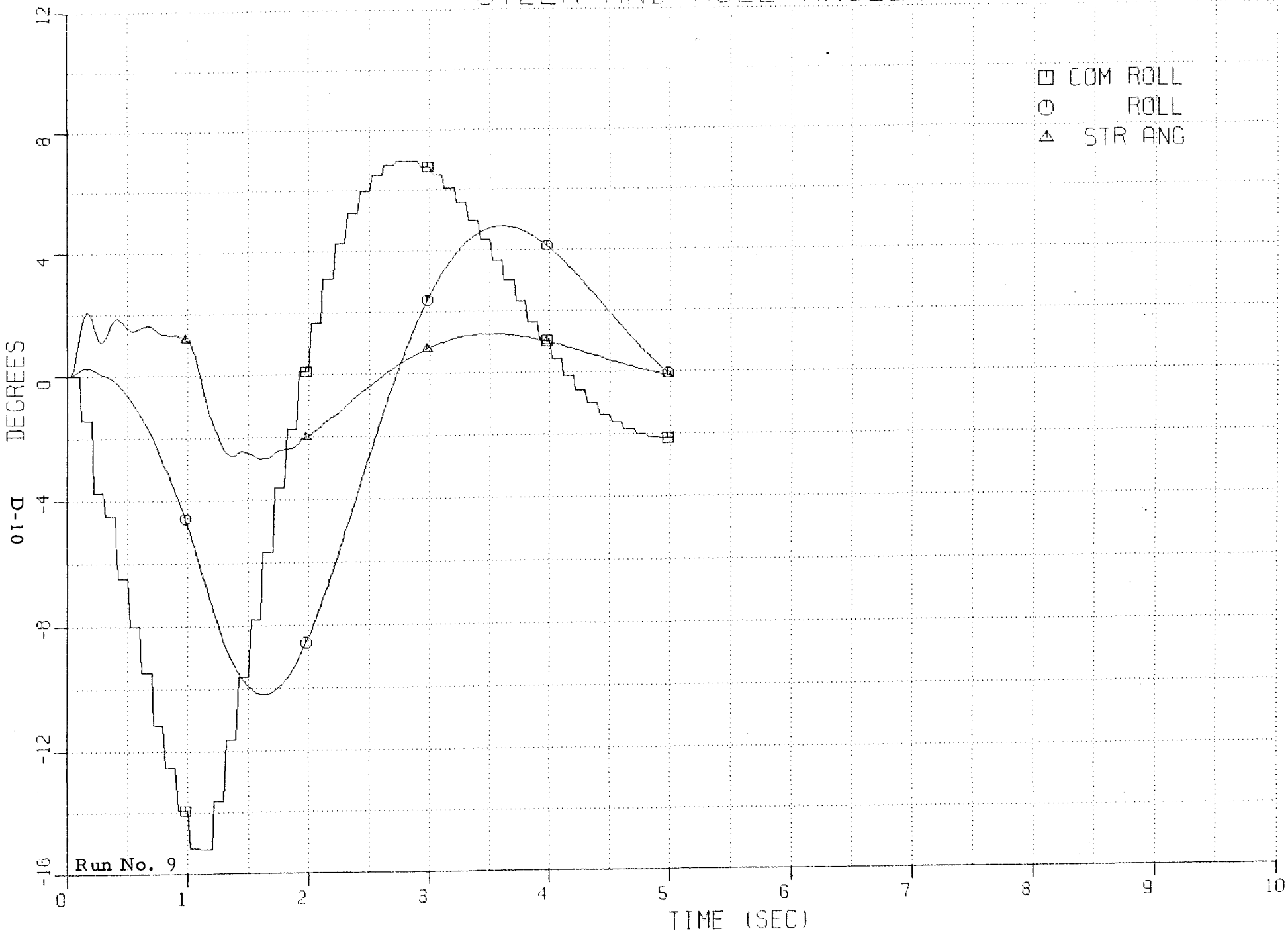

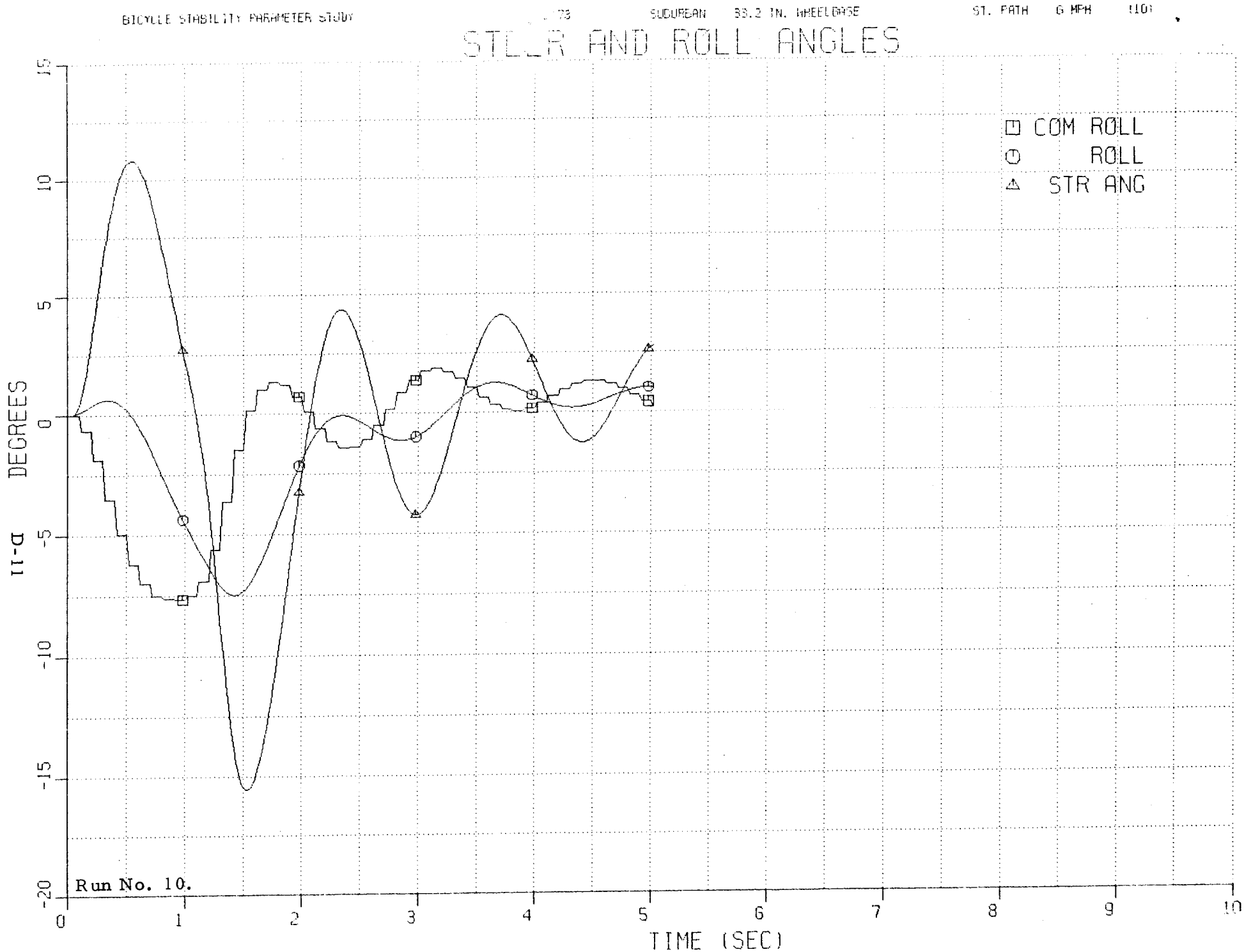
BICYCLE STABILITY PARAMETER STUDY
73 SUBURBAN 88.2 IN. WHEELBASE ST. PATH 6 MPH 1101
STEER AND ROLL ANGLES
COM ROLL
ROLL
STR ANG
DEGREES
TIME (SEC)
Run No. 10.
15
10
5
0
-5
-10
-15
-20
0
1
2
3
4
5
6
7
8
9
10

BICYCLE STABILITY PARAMETER STUDY 21FEB'73 SUBURBAN 89.2 IN. WHEELBASE ST. PATH 10 MPH (11)

STEER AND ROLL ANGLES

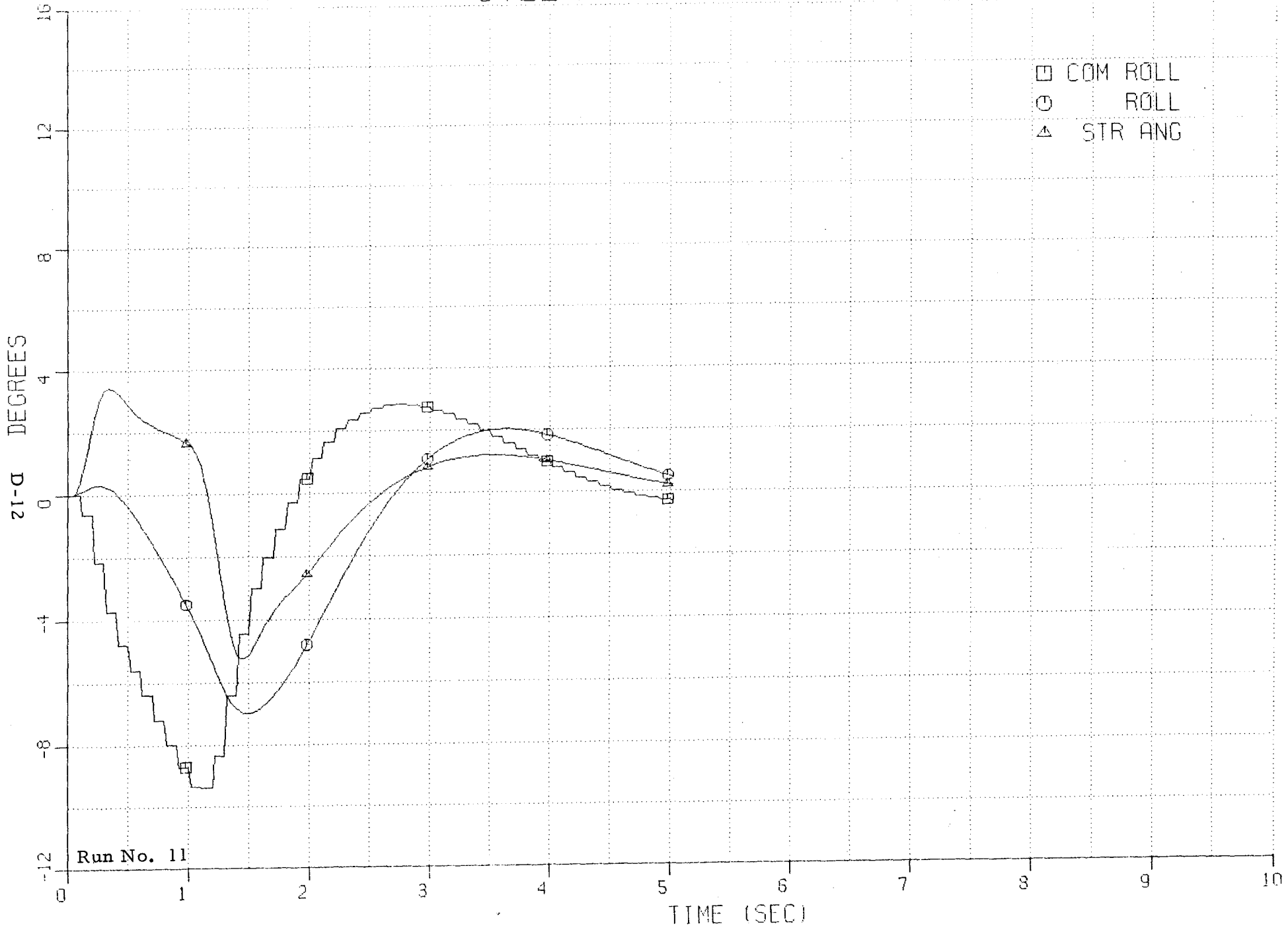

STEER AND ROLL ANGLES

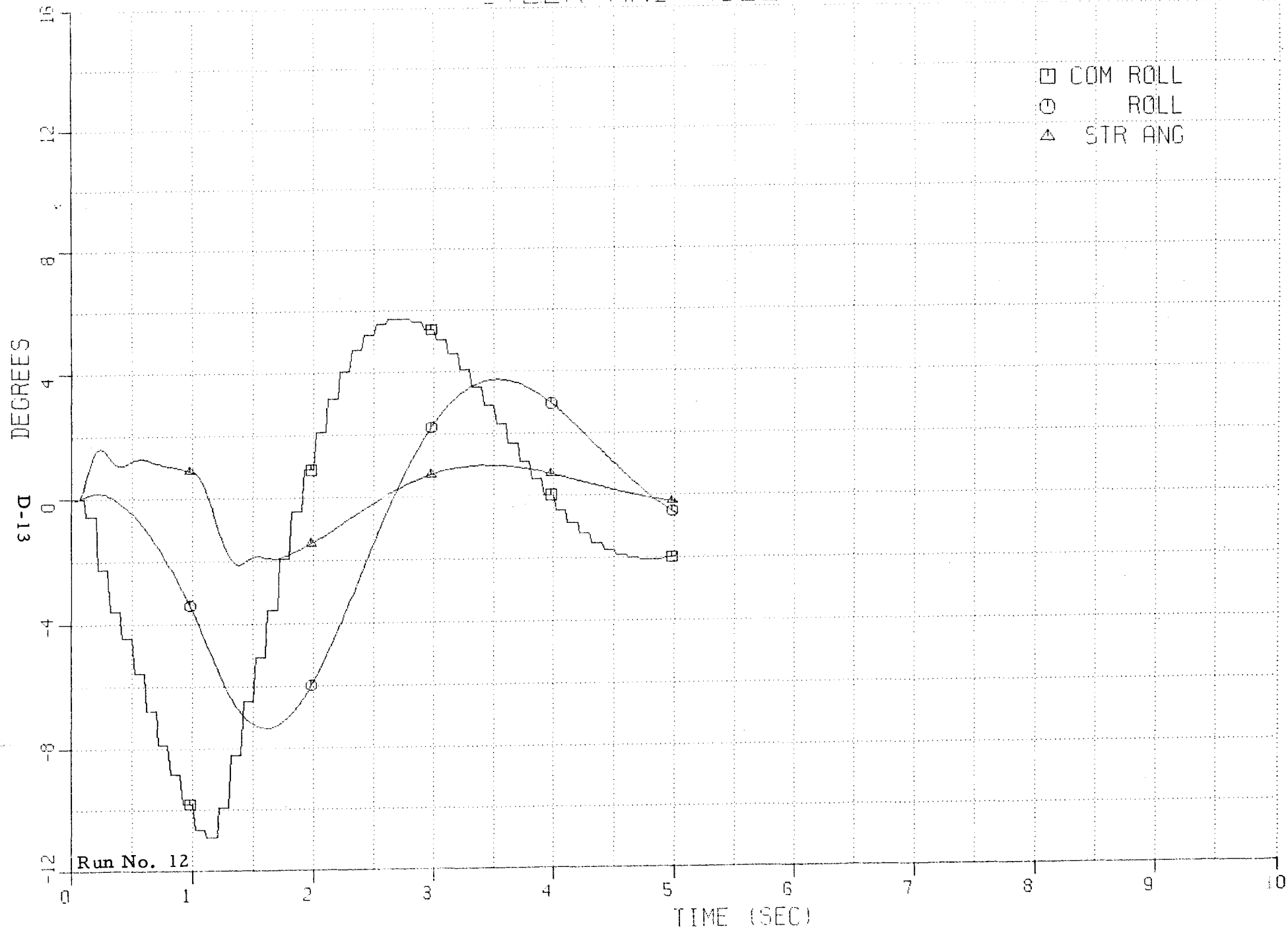

BICYCLE STABILITY PARAMETER .3 21FEB'73 SUBURBAN 48.8 IN. WHEELBASE PATH 0 MPH (13)

STEER AND ROLL ANGLES

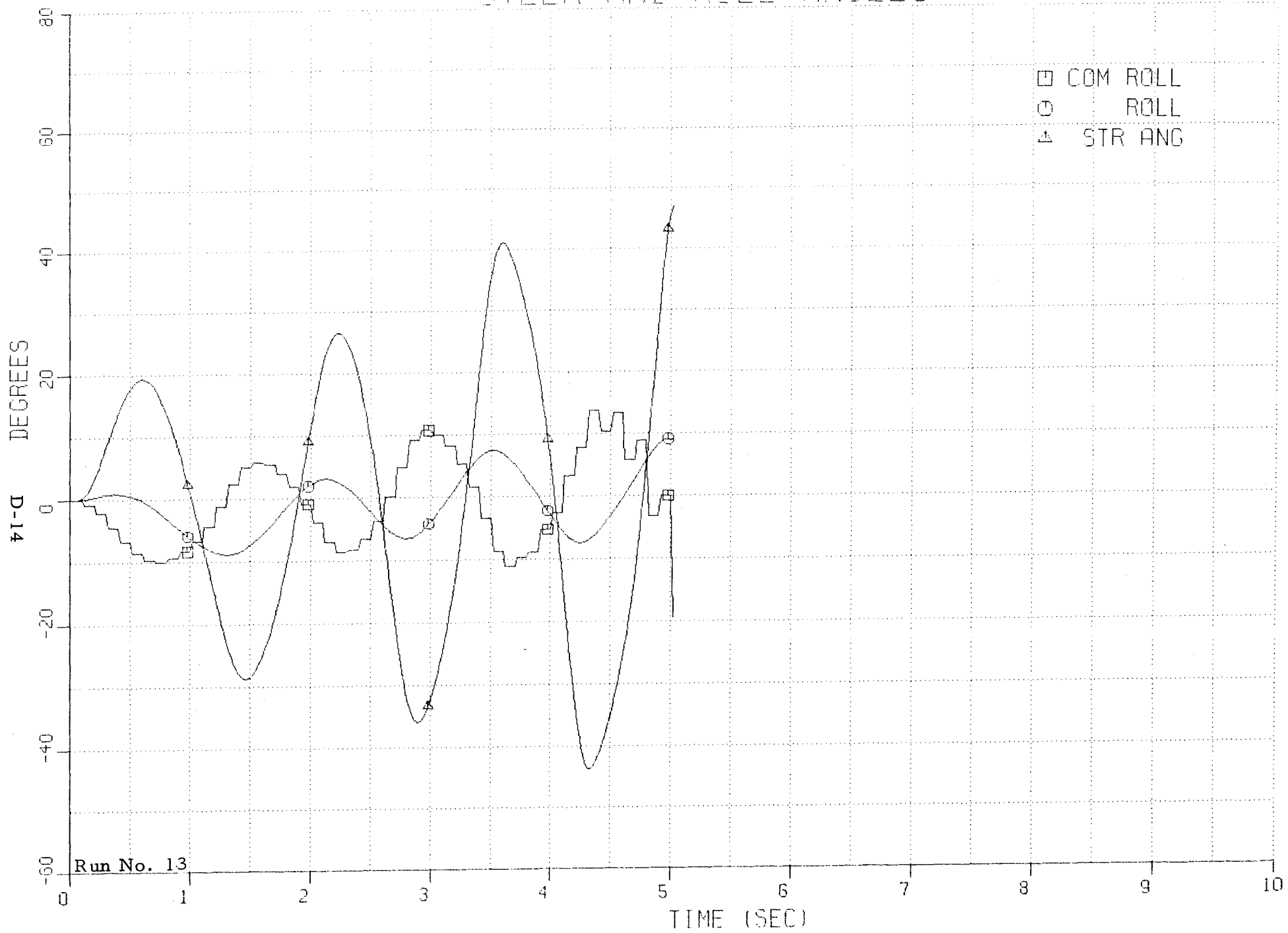

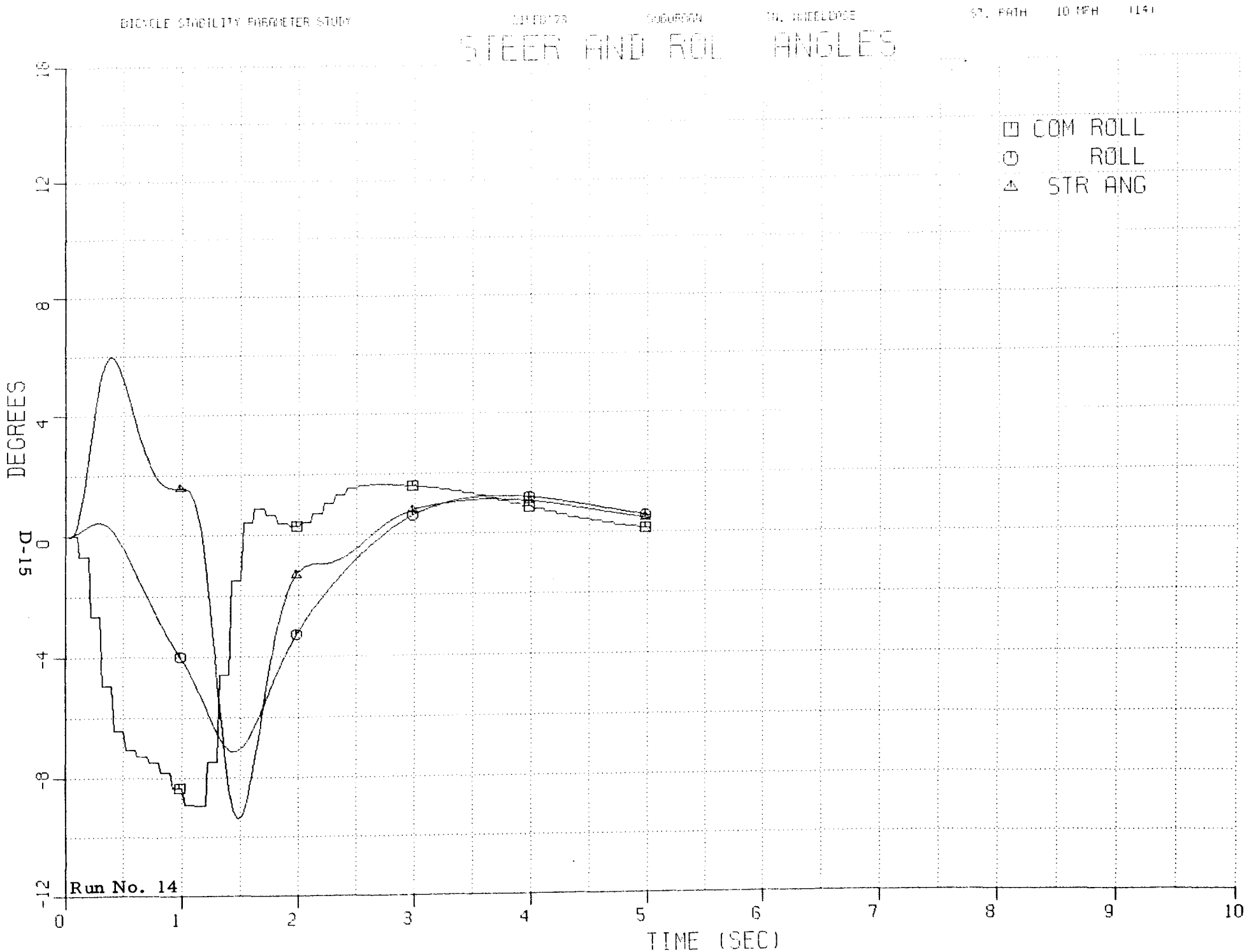
BICYCLE STABILITY PARAMETER STUDY
STEER AND ROL ANGLES
COM ROLL
ROLL
STR ANG
DEGREES
TIME (SEC)
Run No. 14
D-15

BICYCLE STABILITY PARAMETER STUDY 21FEB'73 SUBURBAN 19.8 IN. WHEELBASE ST. PATH 15 MPH (15)

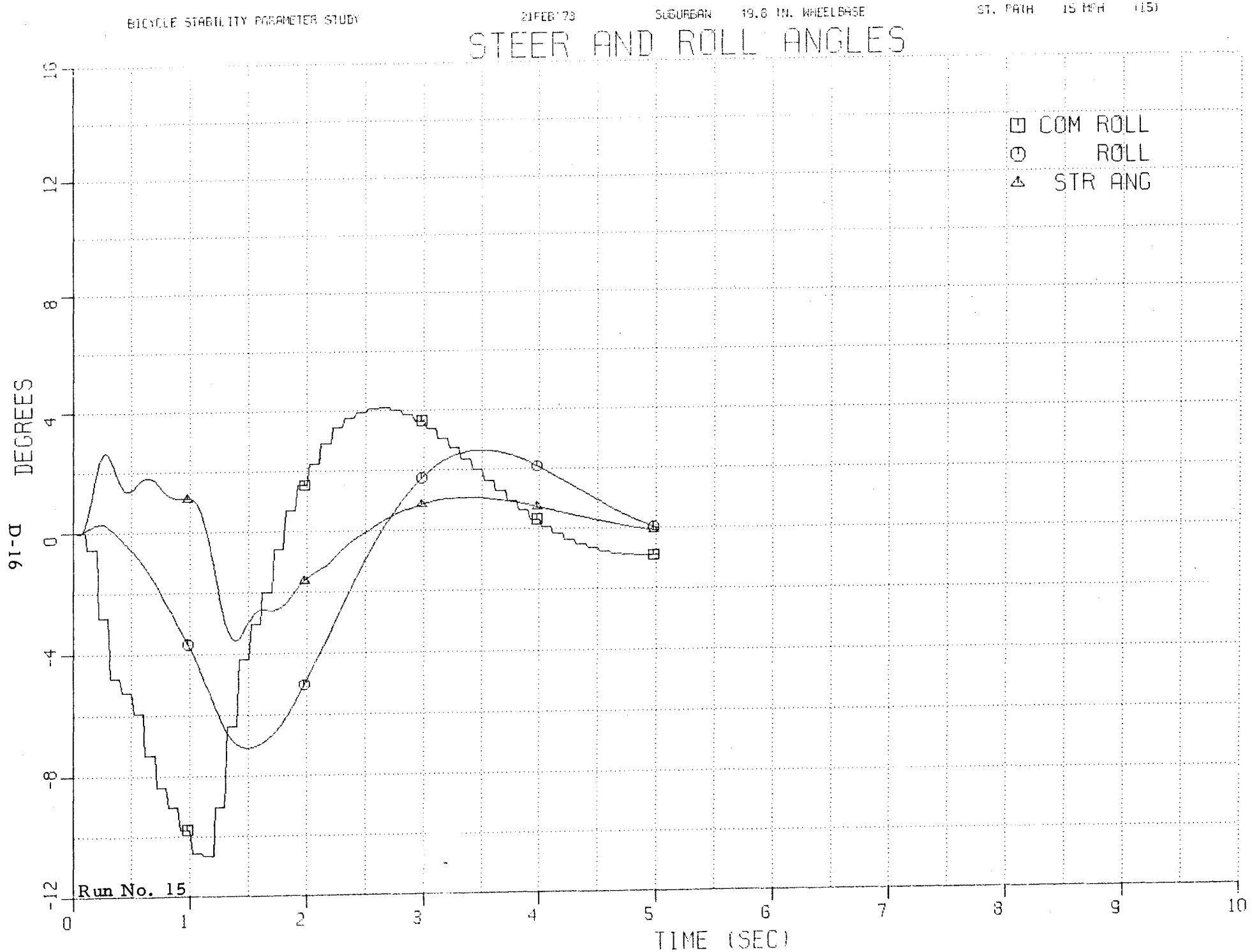

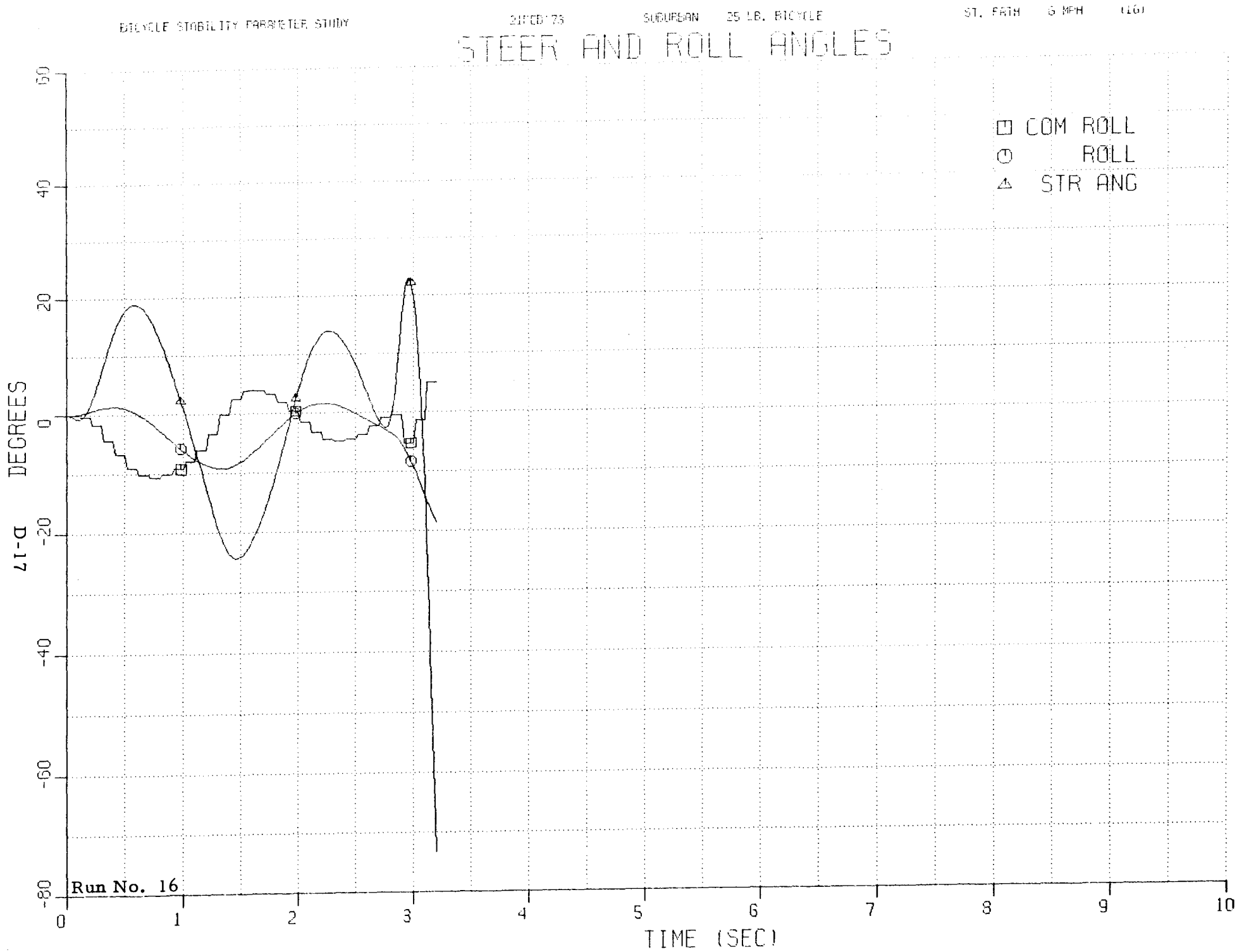
BICYCLE STABILITY PARAMETER STUDY
21FEB'75
SUBURBAN 25 LB. BICYCLE
ST. PATH 5 MPH (16)
STEER AND ROLL ANGLES
COM ROLL
ROLL
STR ANG
DEGREES
60
40
20
0
-20
-40
-60
-80
Run No. 16
0
1
2
3
4
5
6
7
8
9
10
TIME (SEC)

BICYCLE STABILITY PARAMETER STUDY 21FEB'73 SUBURBAN 25 LB. BICYCLE ST. PATH 10 MPH (17)

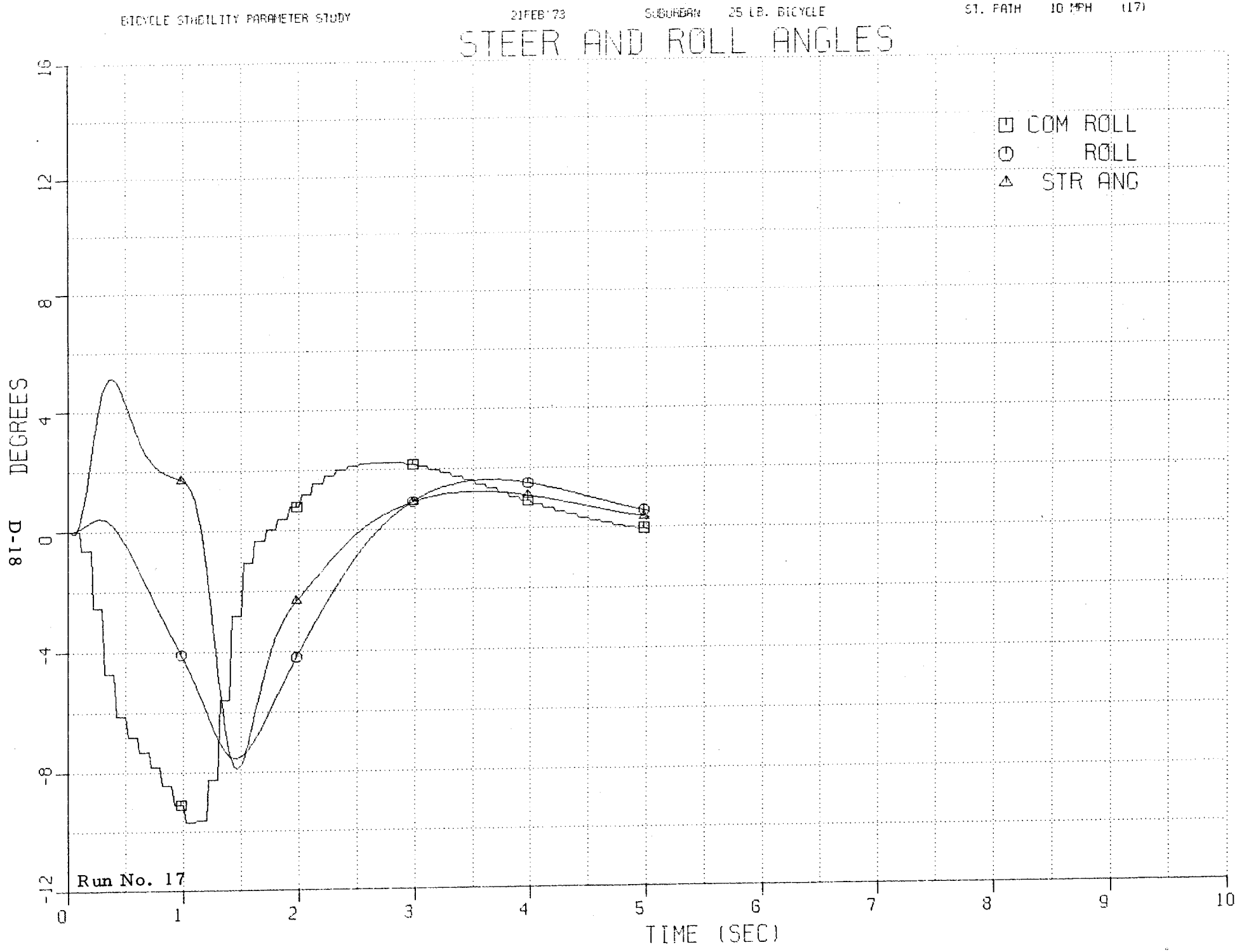

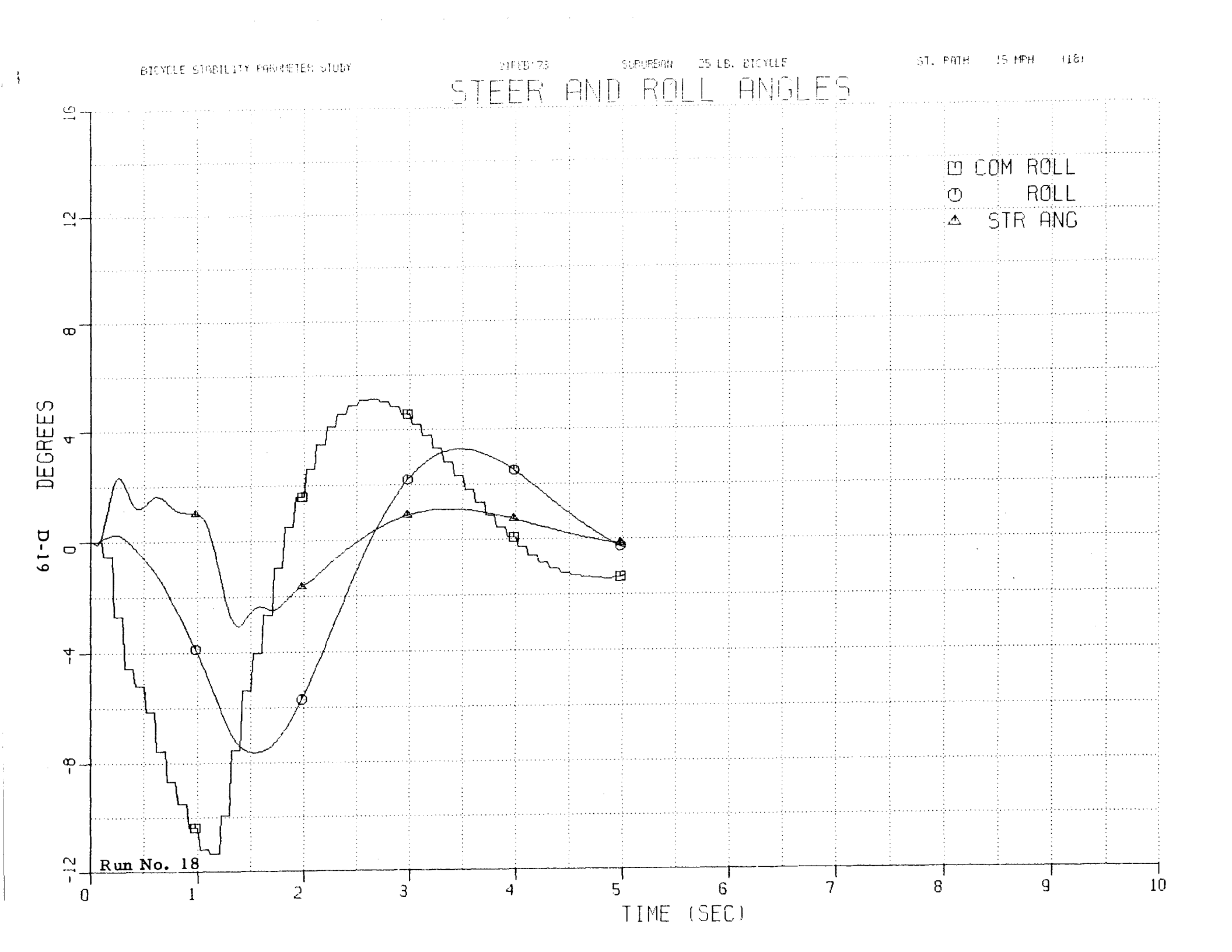
BICYCLE STABILITY PARAMETERS STUDY
21FEB'73 SUBURBAN 25 LB. BICYCLE ST. PATH 15 MPH 116
STEER AND ROLL ANGLES
COM ROLL
ROLL
STR ANG
DEGREES
TIME (SEC)
Run No. 18
D-19

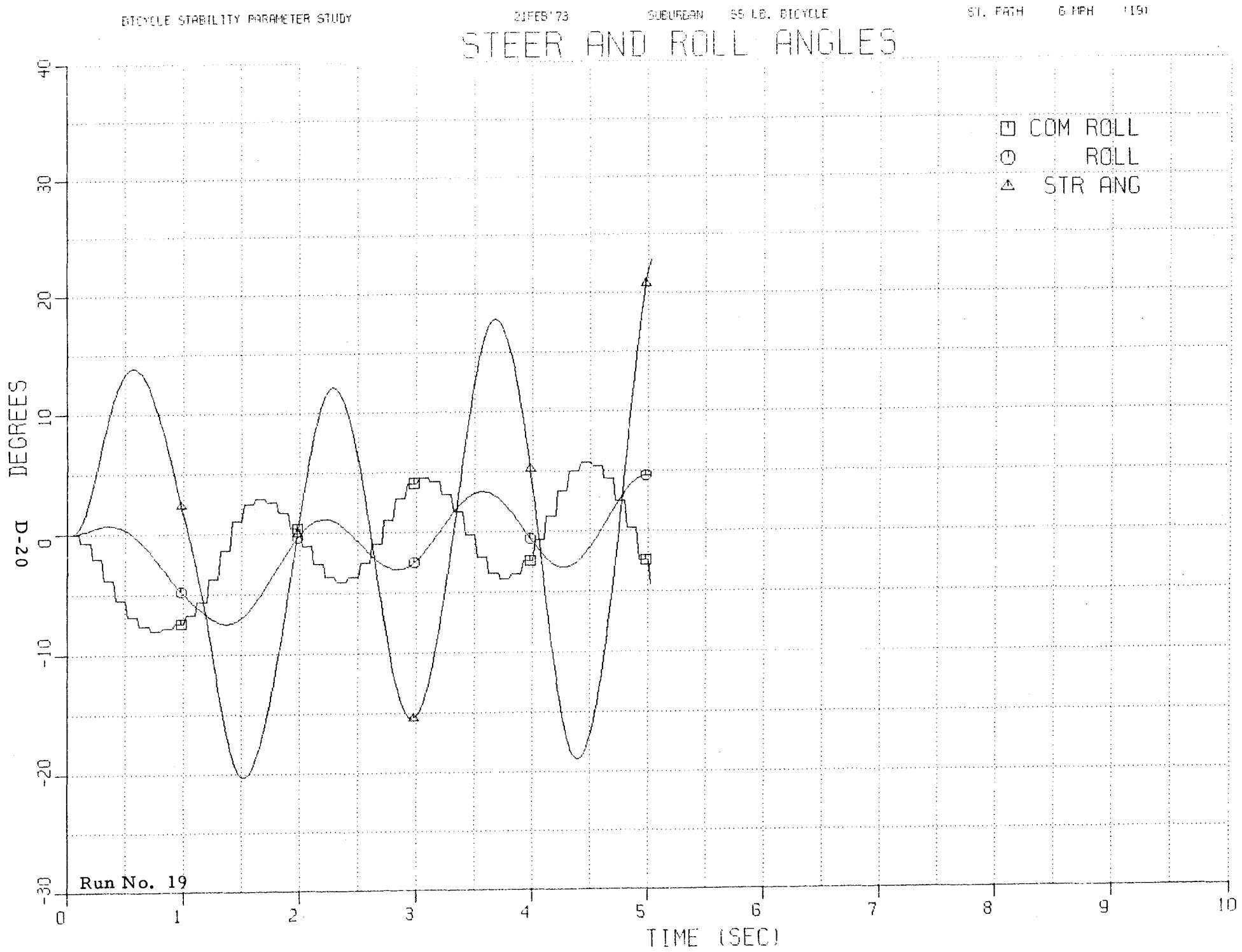
BICYCLE STABILITY PARAMETER STUDY
21FEB'73 SUBURBAN 55 LB. BICYCLE ST. PATH 6 MPH (19)
STEER AND ROLL ANGLES
COM ROLL
ROLL
STR ANG
DEGREES
40
30
20
10
0
-10
-20
-30
Run No. 19
0
1
2
3
4
5
6
7
8
9
10
TIME (SEC)

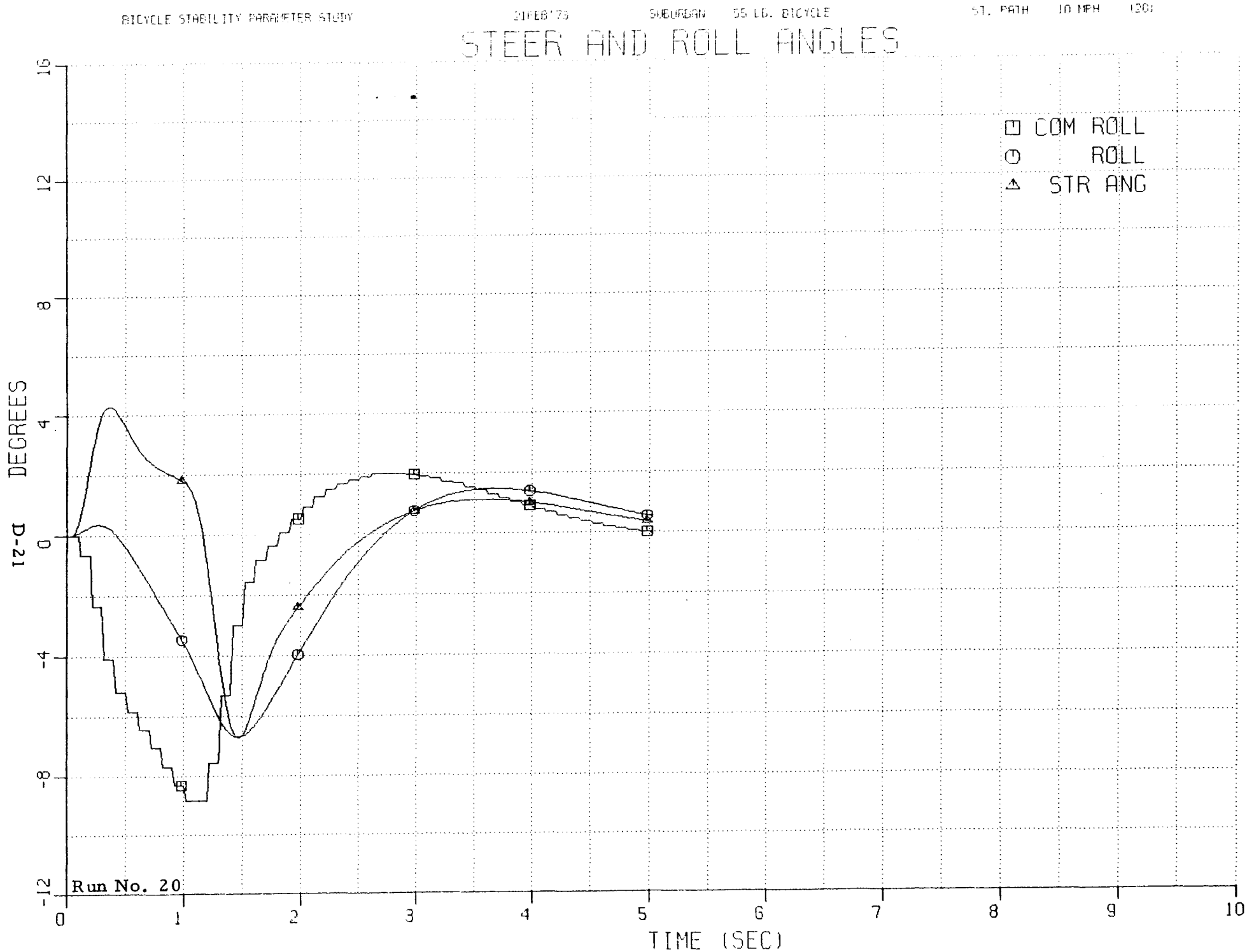
BICYCLE STABILITY PARAMETER STUDY
20FEB'73
SUBURBAN 55 LB. BICYCLE
ST. PATH 10 MPH 120
STEER AND ROLL ANGLES
COM ROLL
ROLL
STR ANG
DEGREES
16
12
8
4
0
-4
-8
-12
Run No. 20
0
1
2
3
4
5
6
7
8
9
10
TIME (SEC)

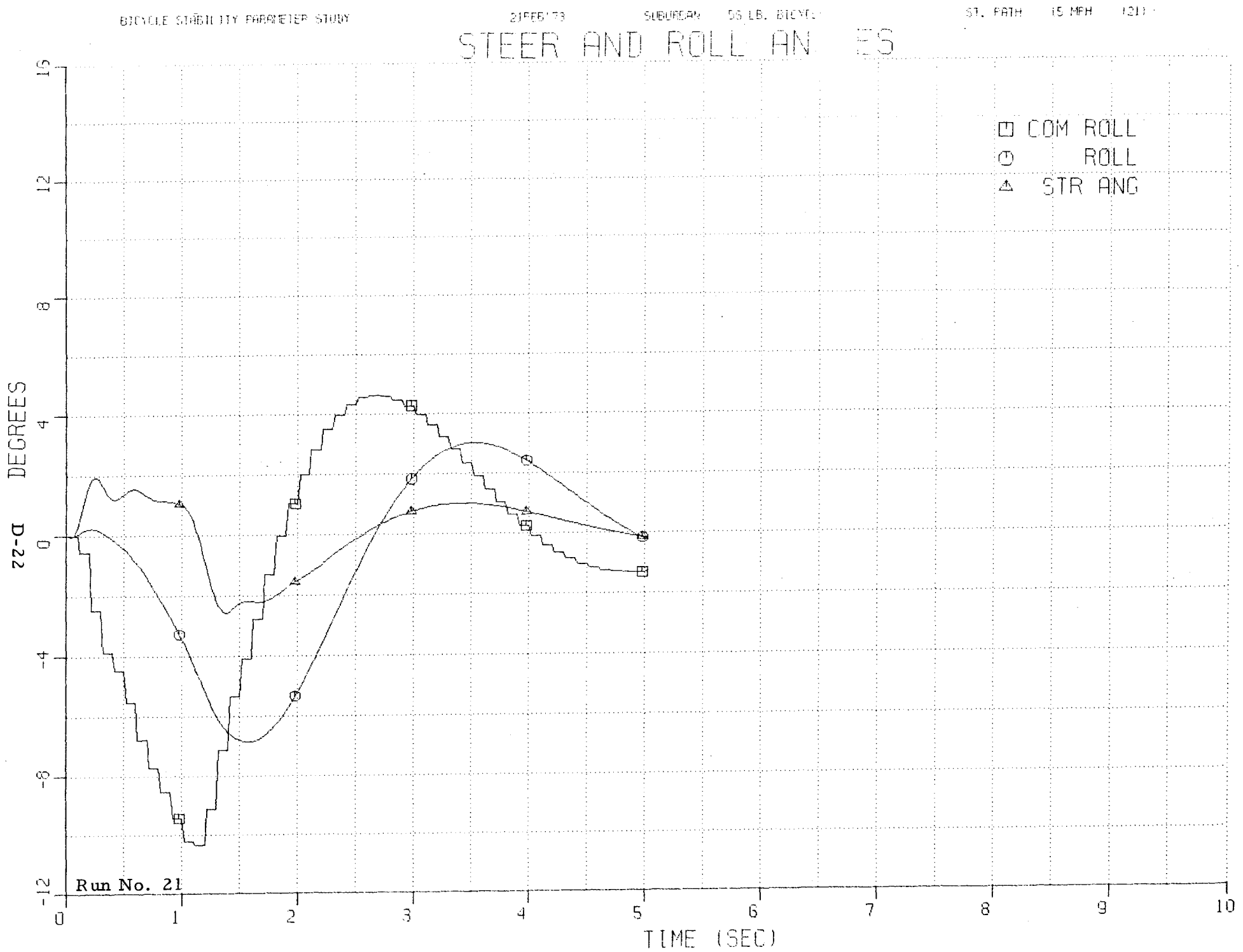
BICYCLE STABILITY PARAMETER STUDY
21FEB'73
SUBURBAN 56 LB. BICYCL
ST. PATH 15 MPH (21)
STEER AND ROLL AN ES
COM ROLL
ROLL
STR ANG
DEGREES
TIME (SEC)
Run No. 21
D-22

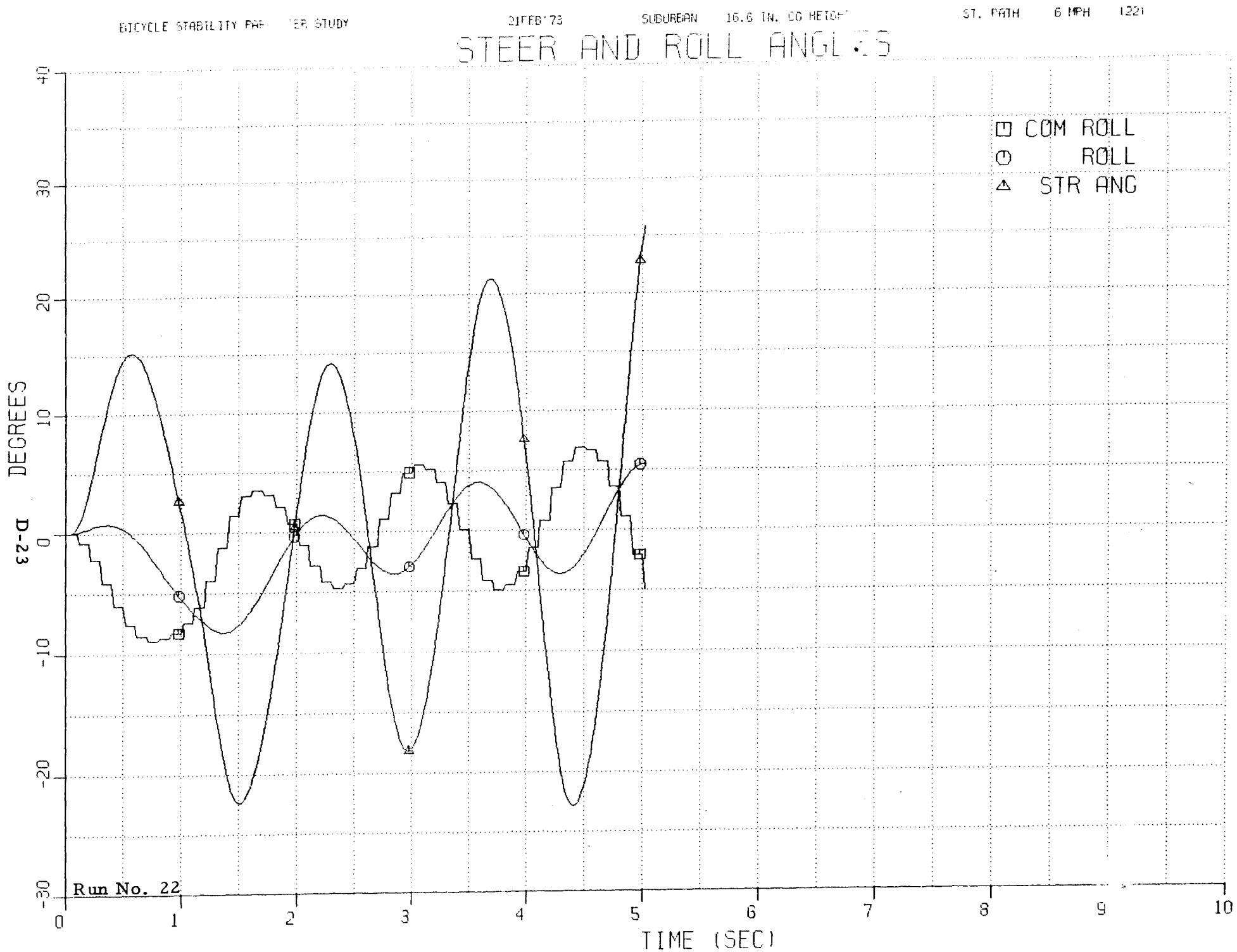
BICYCLE STABILITY PAR TER STUDY
21FEB'73 SUBURBAN 16.6 IN. CG HEIGHT ST. PATH 6 MPH (22)
STEER AND ROLL ANGLES
COM ROLL
ROLL
STR ANG
DEGREES
40
30
20
10
0
-10
-20
-30
Run No. 22
0
1
2
3
4
5
6
7
8
9
10
TIME (SEC)

STEER AND ROLL ANGLES

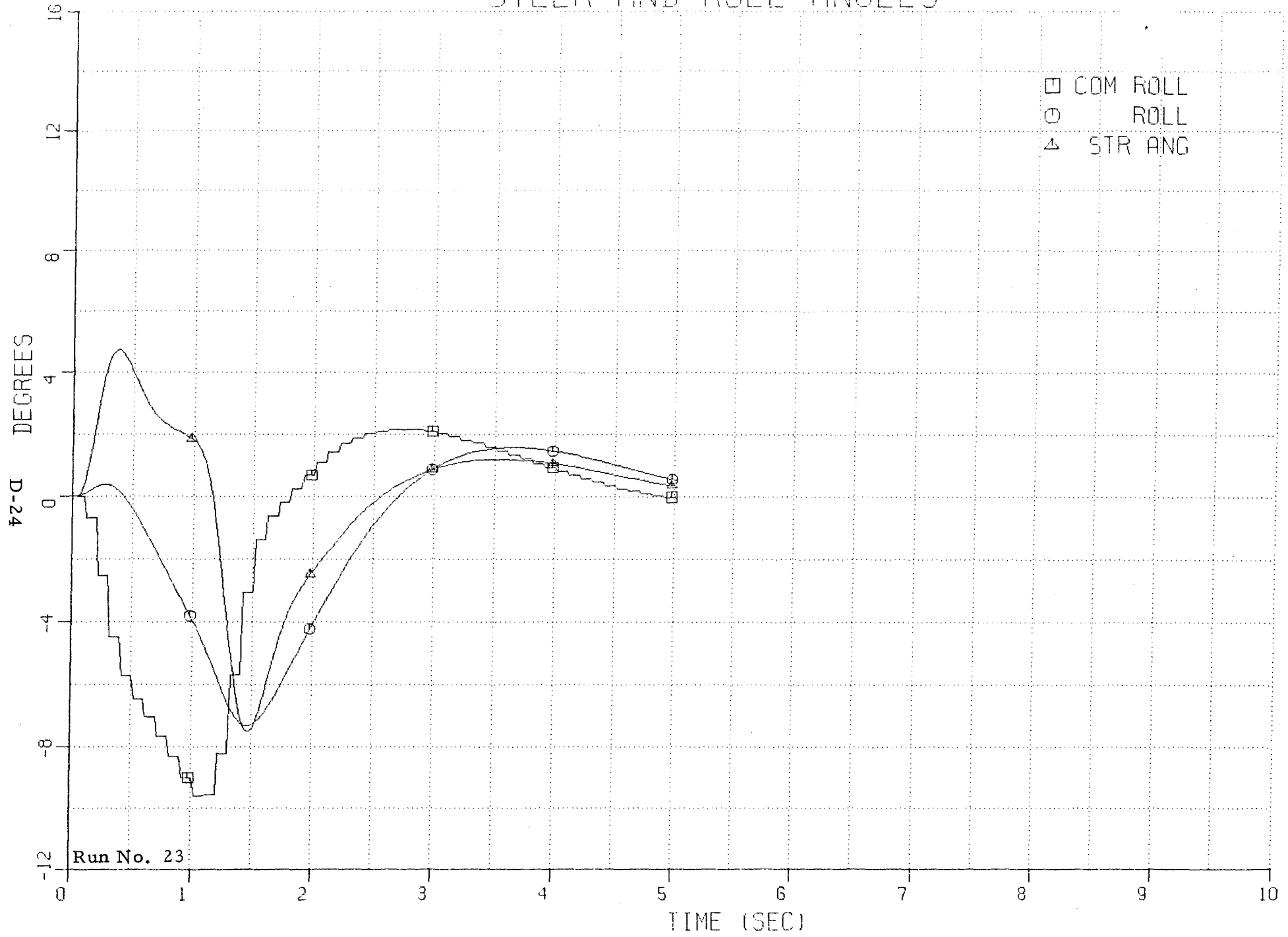

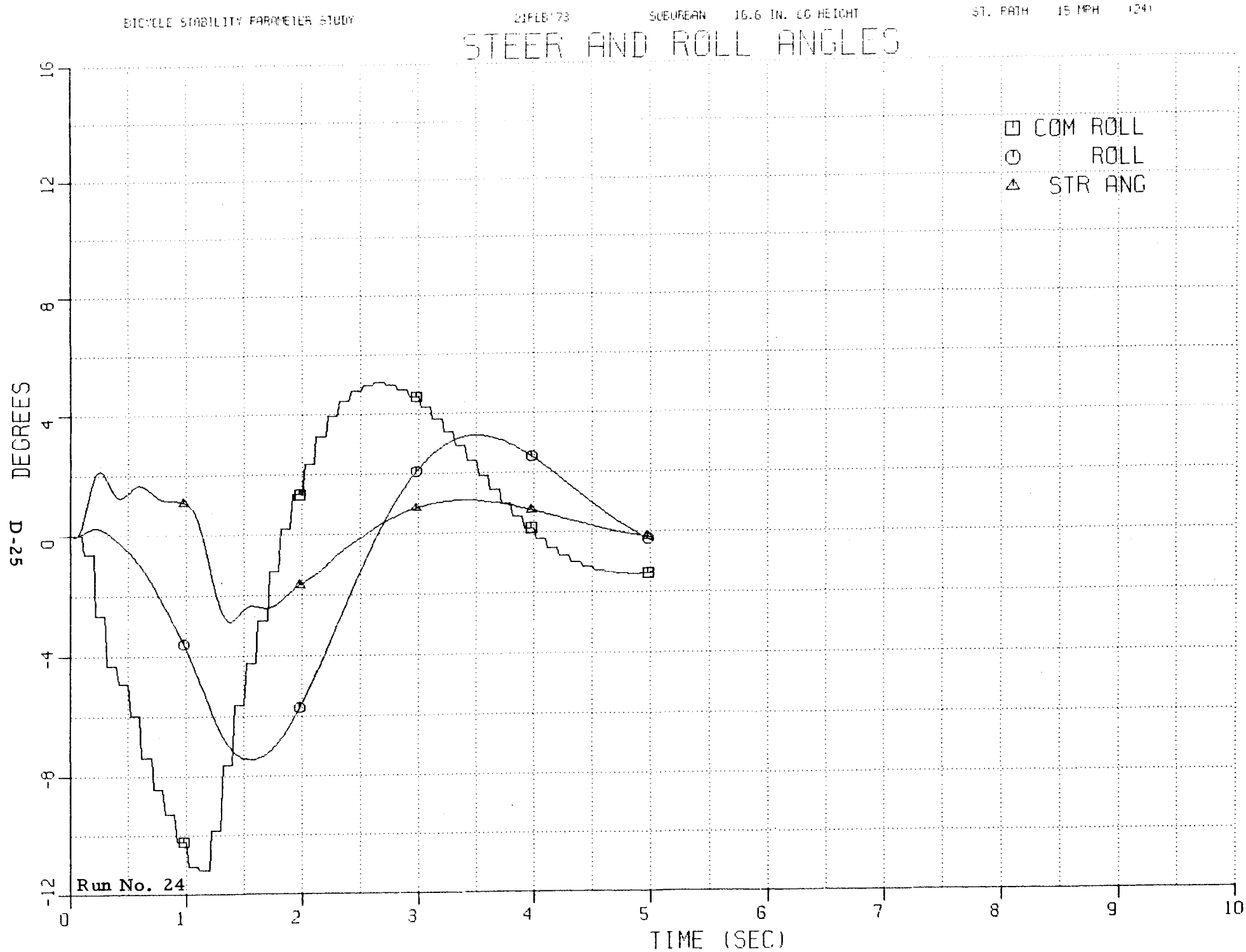
BICYCLE STABILITY PARAMETER STUDY
21FEB'73 SUBUREAN 16.6 IN. CG HEIGHT ST. PATH 15 MPH 1241
STEER AND ROLL ANGLES
COM ROLL
ROLL
STR ANG
DEGREES
16
12
8
4
0
-4
-8
-12
Run No. 24
0
1
2
3
4
5
6
7
8
9
10
TIME (SEC)

BICYCLE STABILITY PARAMETER STUDY 21FEB 73 SUBURBAN 24.9 IN. CG HEIGHT ST. PATH 6 MPH

STEER AND ROLL ANGLES

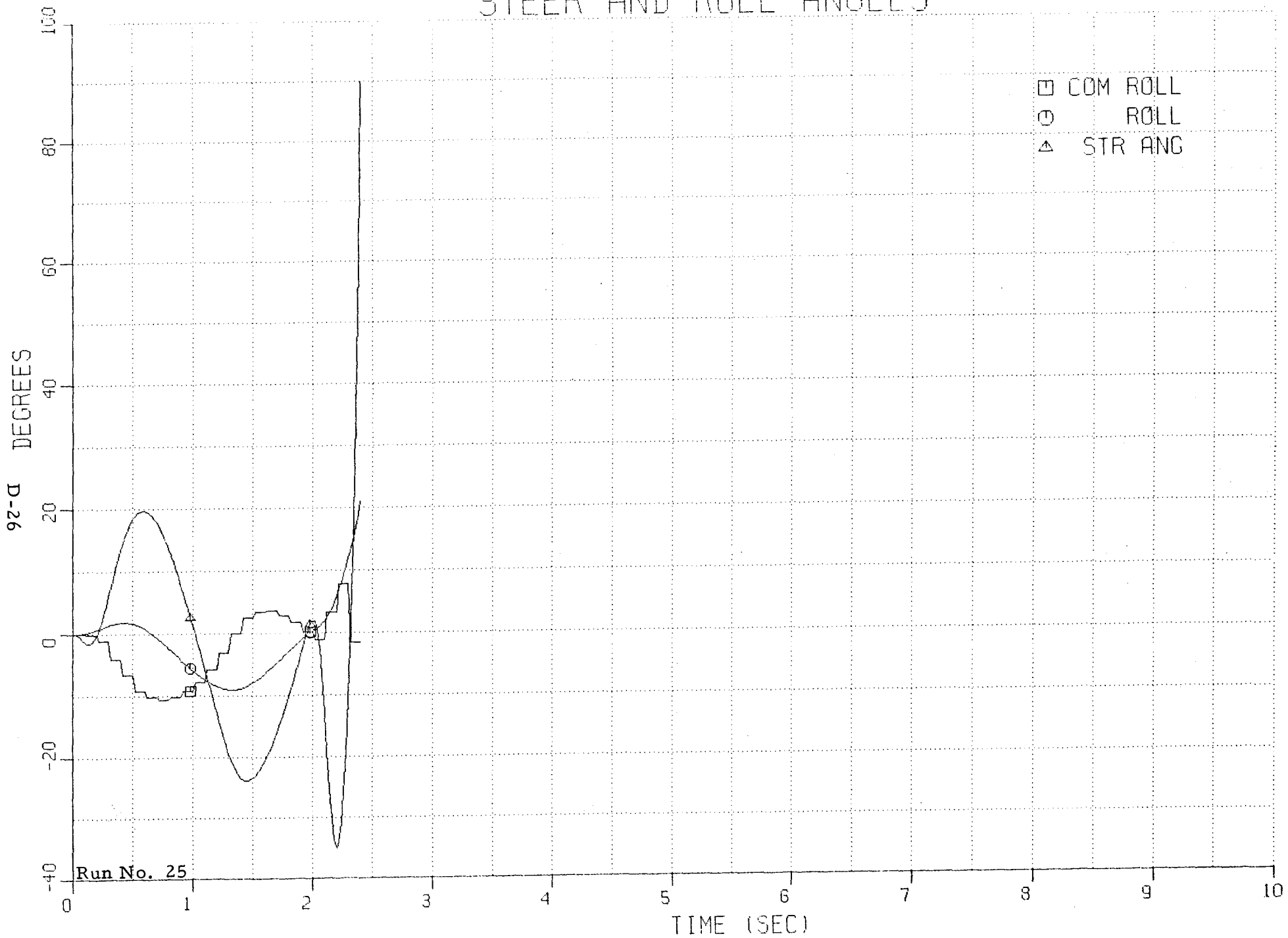

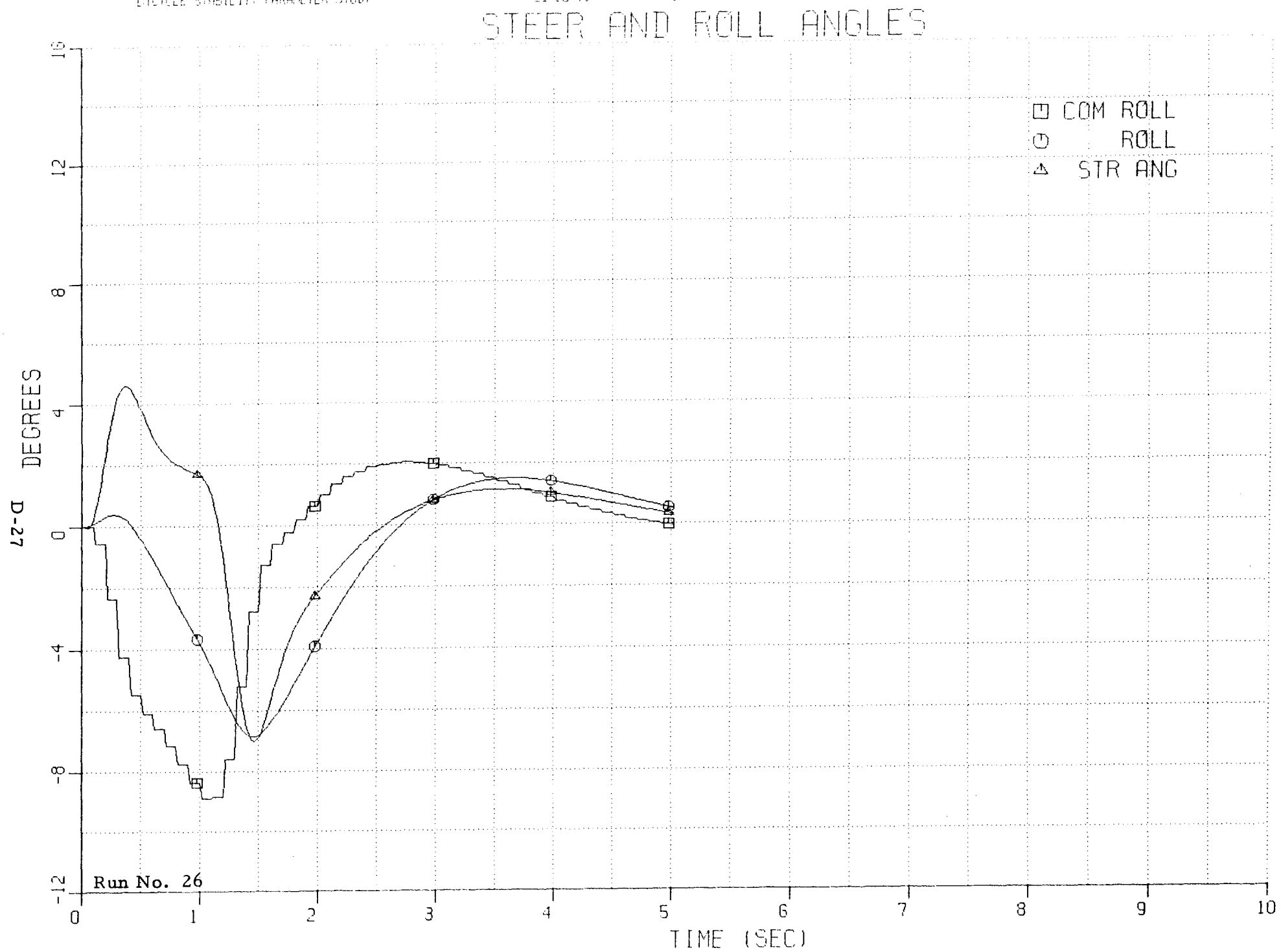
STEER AND ROLL ANGLES
COM ROLL
ROLL
STR ANG
DEGREES
16
12
8
4
0
-4
-8
-12
0
1
2
3
4
5
6
7
8
9
10
TIME (SEC)
Run No. 26

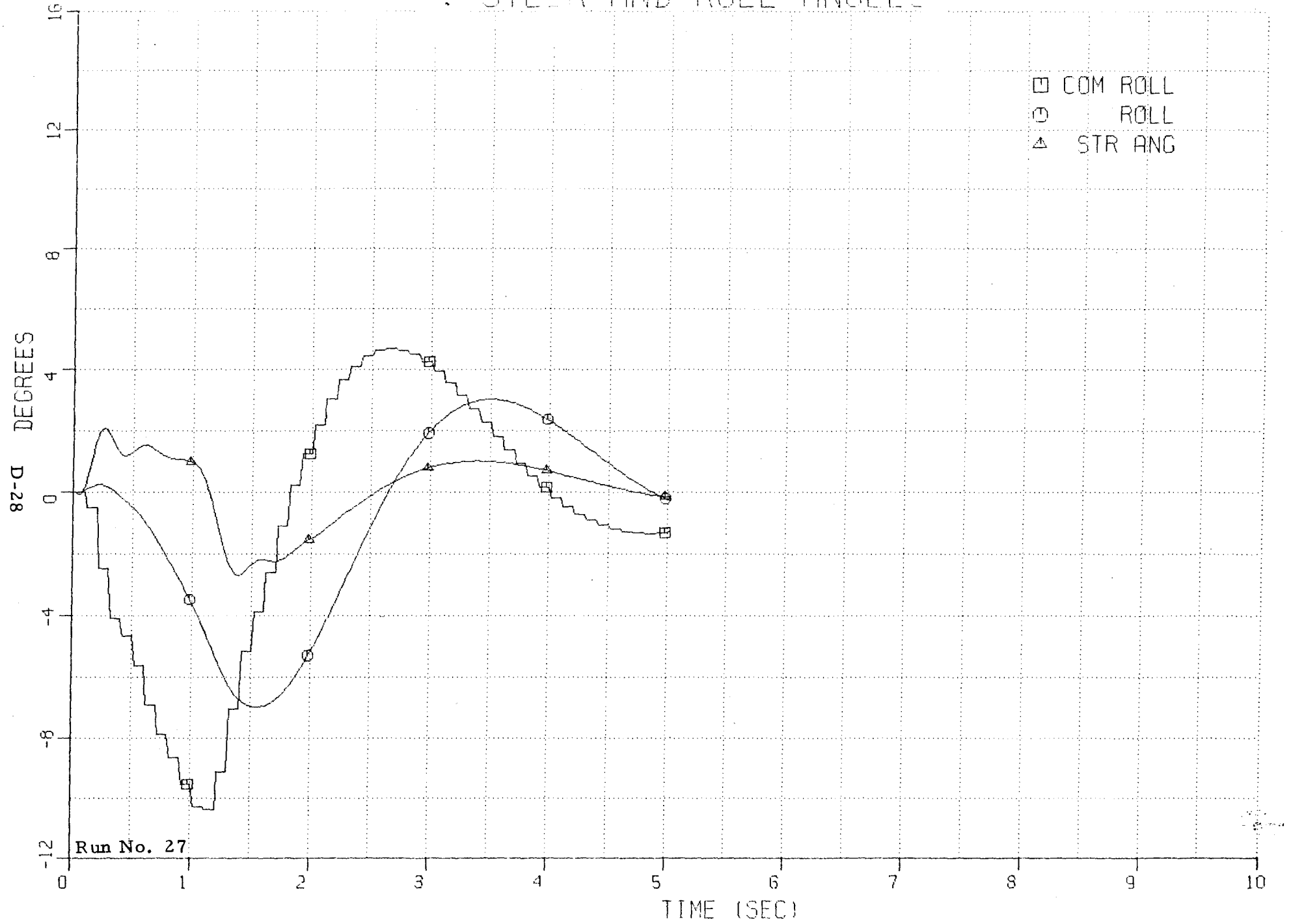
STEER AND ROLL ANGLES
COM ROLL
ROLL
STR ANG
DEGREES
16
12
8
4
0
-4
-8
-12
0
1
2
3
4
5
6
7
8
9
10
TIME (SEC)
Run No. 27

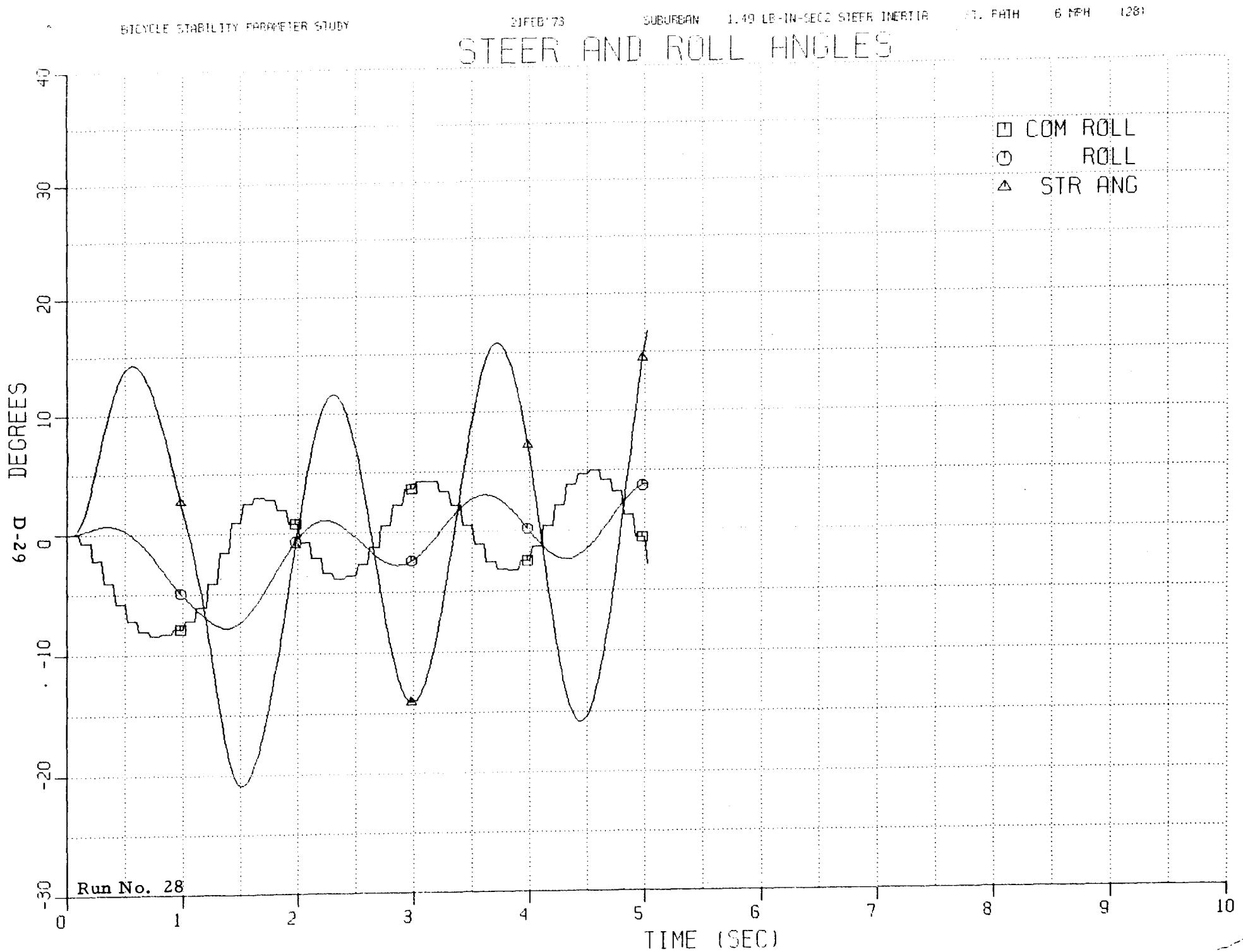
BICYCLE STABILITY PARAMETER STUDY
21FEB'73
SUBURBAN 1.49 LB-IN-SEC2 STEER INERTIA
FLAT PATH
6 MPH
(28)
STEER AND ROLL ANGLES
COM ROLL
ROLL
STR ANG
D-29
DEGREES
40
30
20
10
0
-10
-20
-30
Run No. 28
0
1
2
3
4
5
6
7
8
9
10
TIME (SEC)

STEER AND ROLL ANGLES

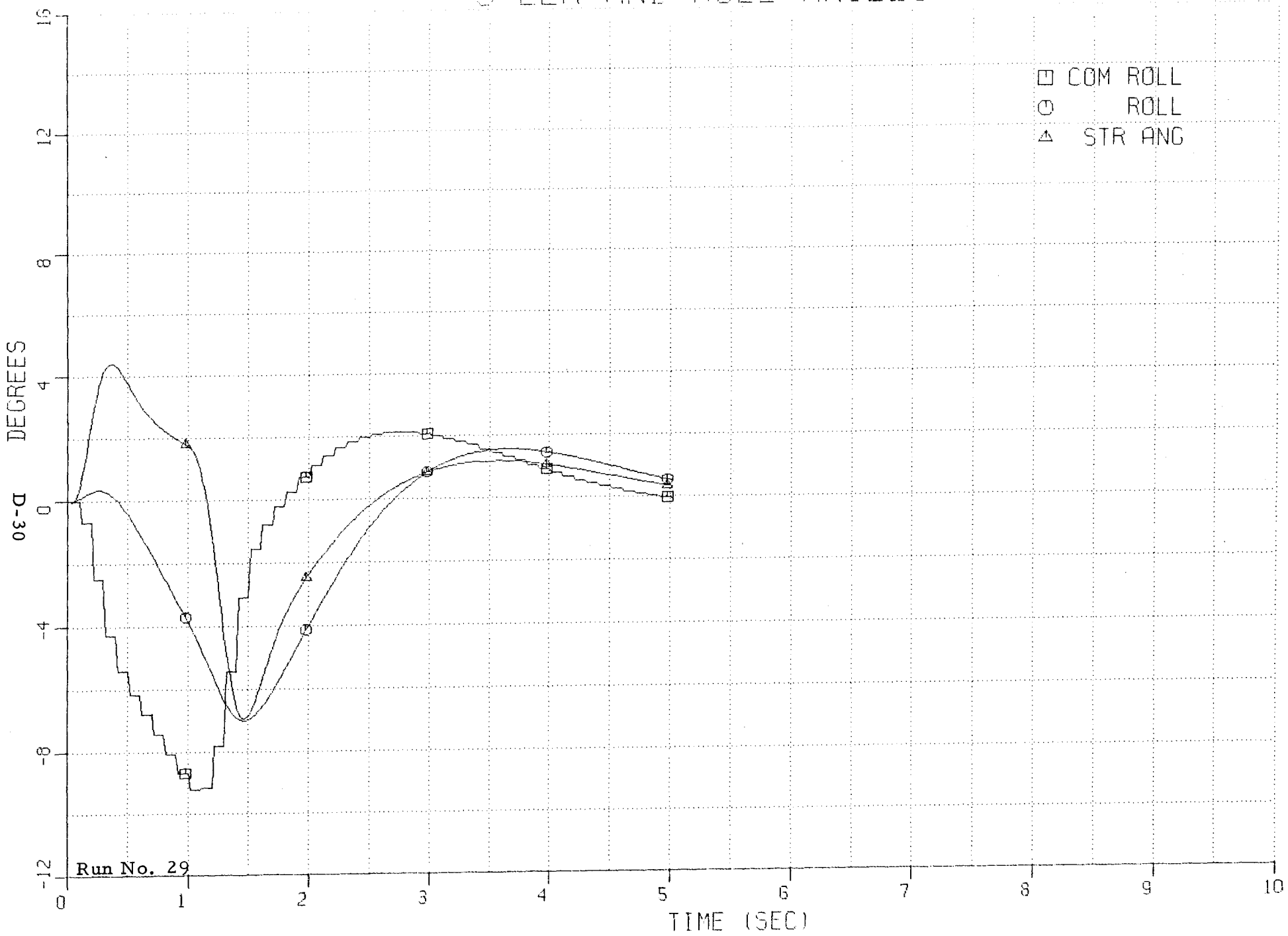

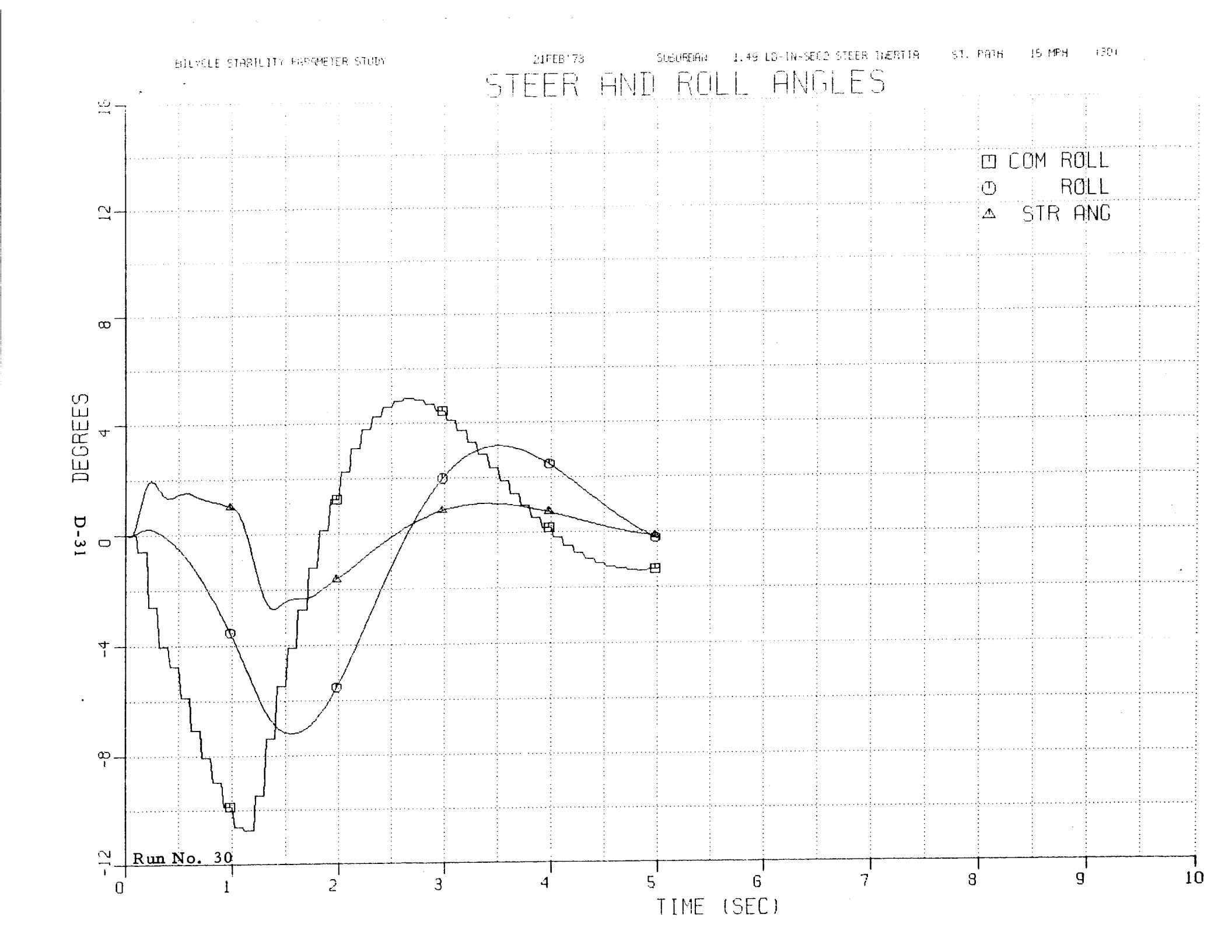
BICYCLE STABILITY PARAMETER STUDY
21FEB'73
SUBURBAN 1.49 LB-IN-SEC2 STEER INERTIA
ST. PATH 15 MPH
STEER AND ROLL ANGLES
COM ROLL
ROLL
STR ANG
DEGREES
TIME (SEC)
Run No. 30
16
12
8
4
0
-4
-8
-12
0
1
2
3
4
5
6
7
8
9
10

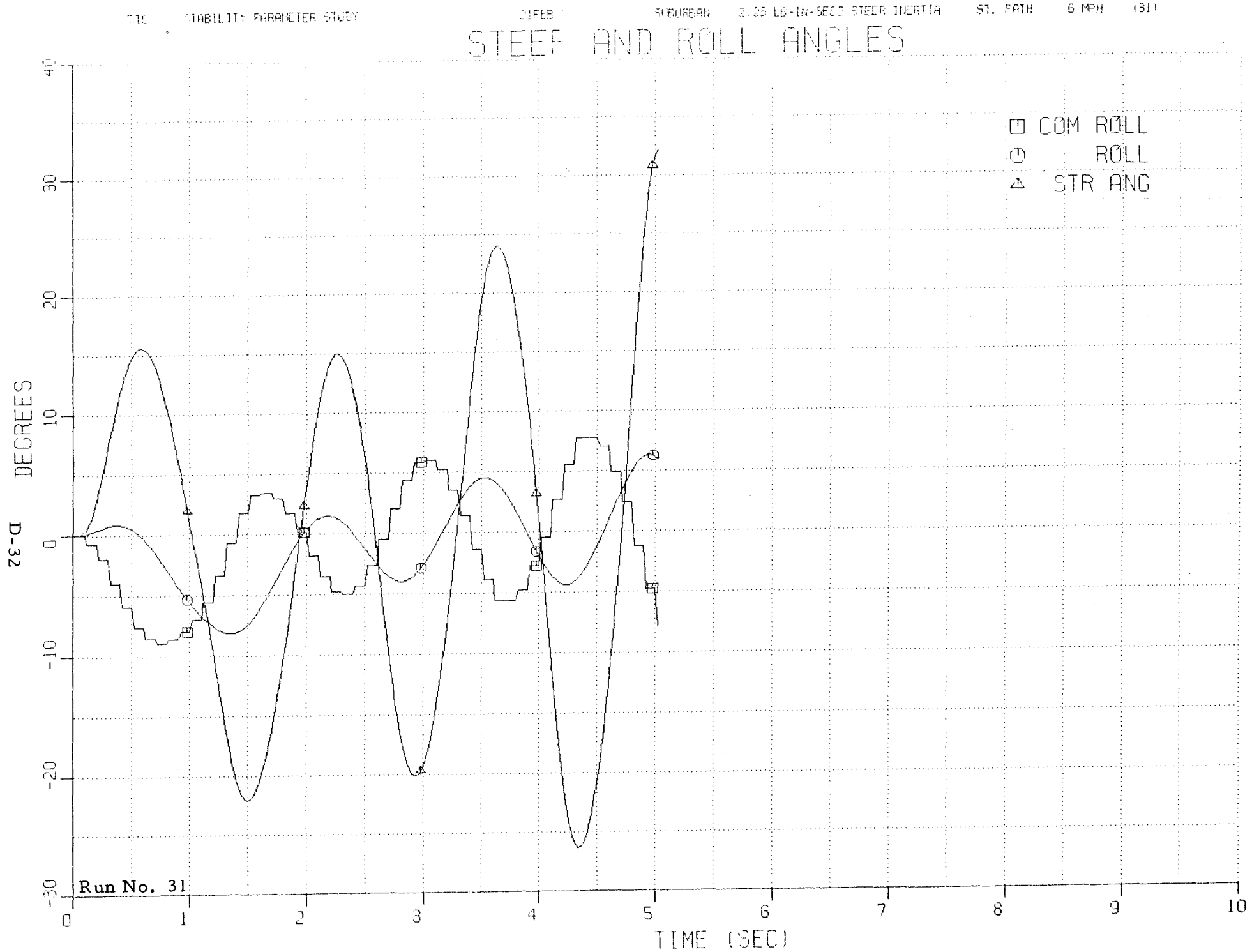
STEER AND ROLL ANGLES
COM ROLL
ROLL
STR ANG
DEGREES
TIME (SEC)
Run No. 31
40
30
20
10
0
-10
-20
-30
0
1
2
3
4
5
6
7
8
9
10

STEER AND ROLL ANGLE

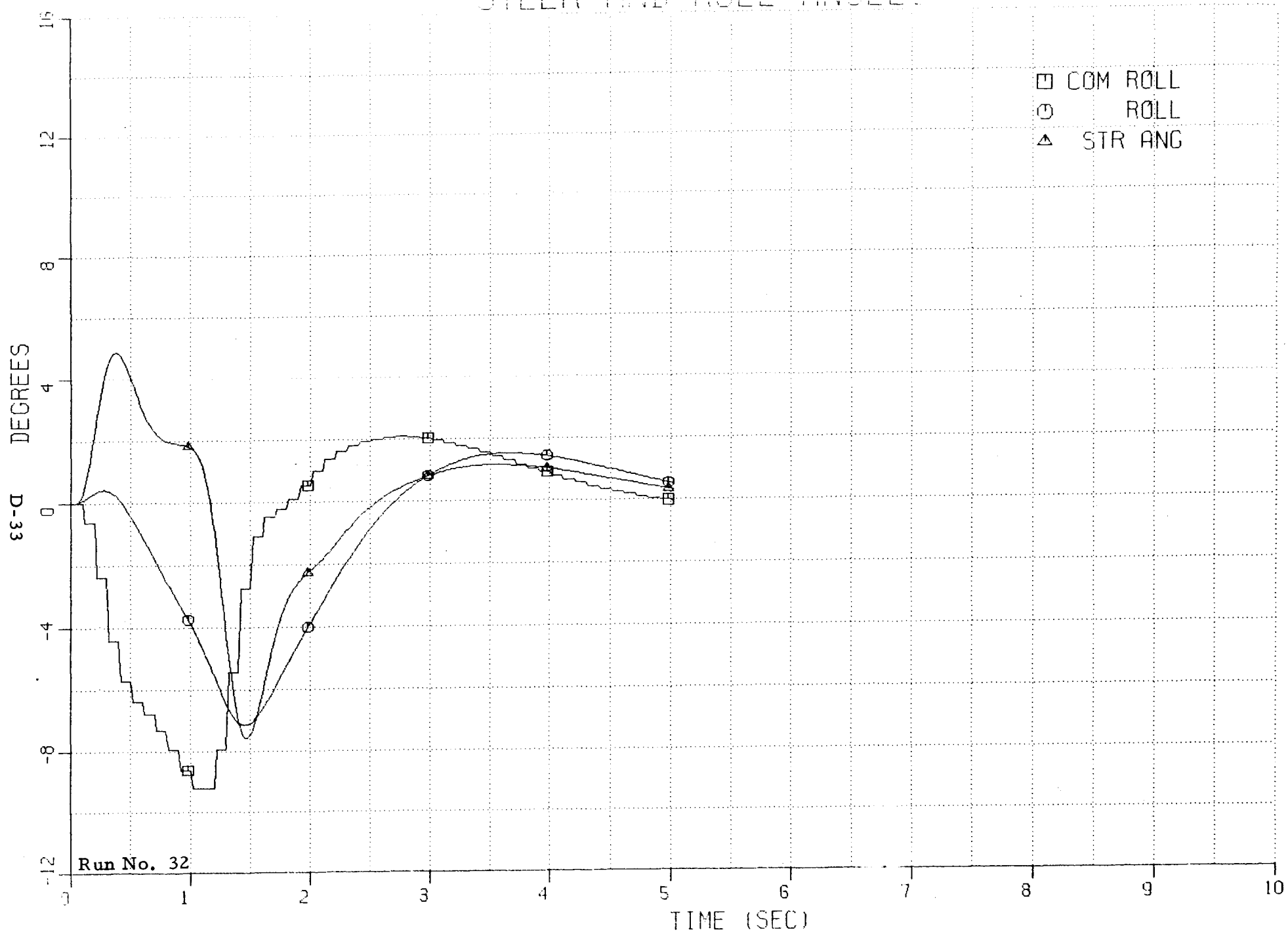

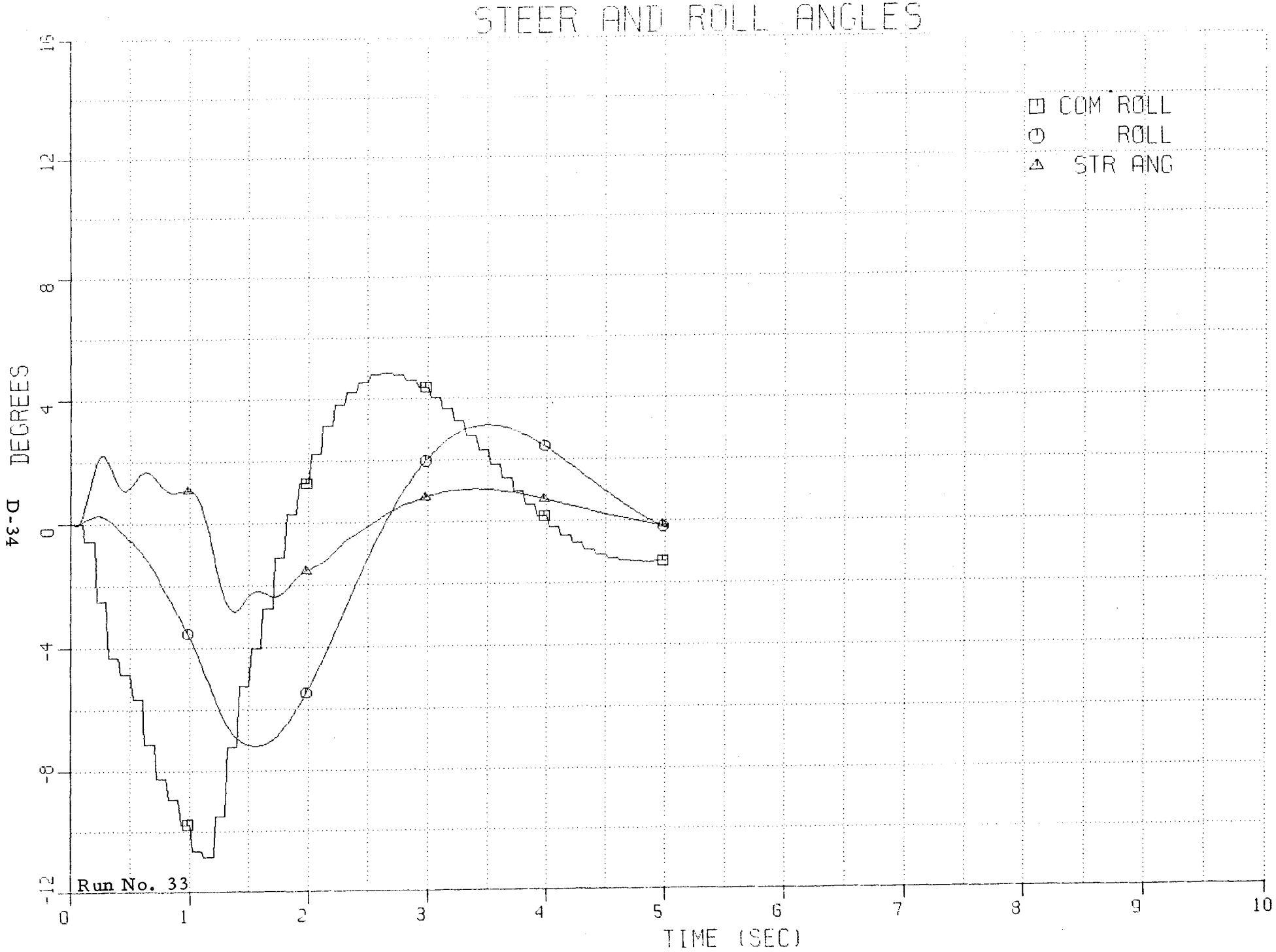
STEER AND ROLL ANGLES
COM ROLL
ROLL
STR ANG
DEGREES
TIME (SEC)
Run No. 33
15
12
8
4
0
-4
-8
-12
0
1
2
3
4
5
6
7
8
9
10

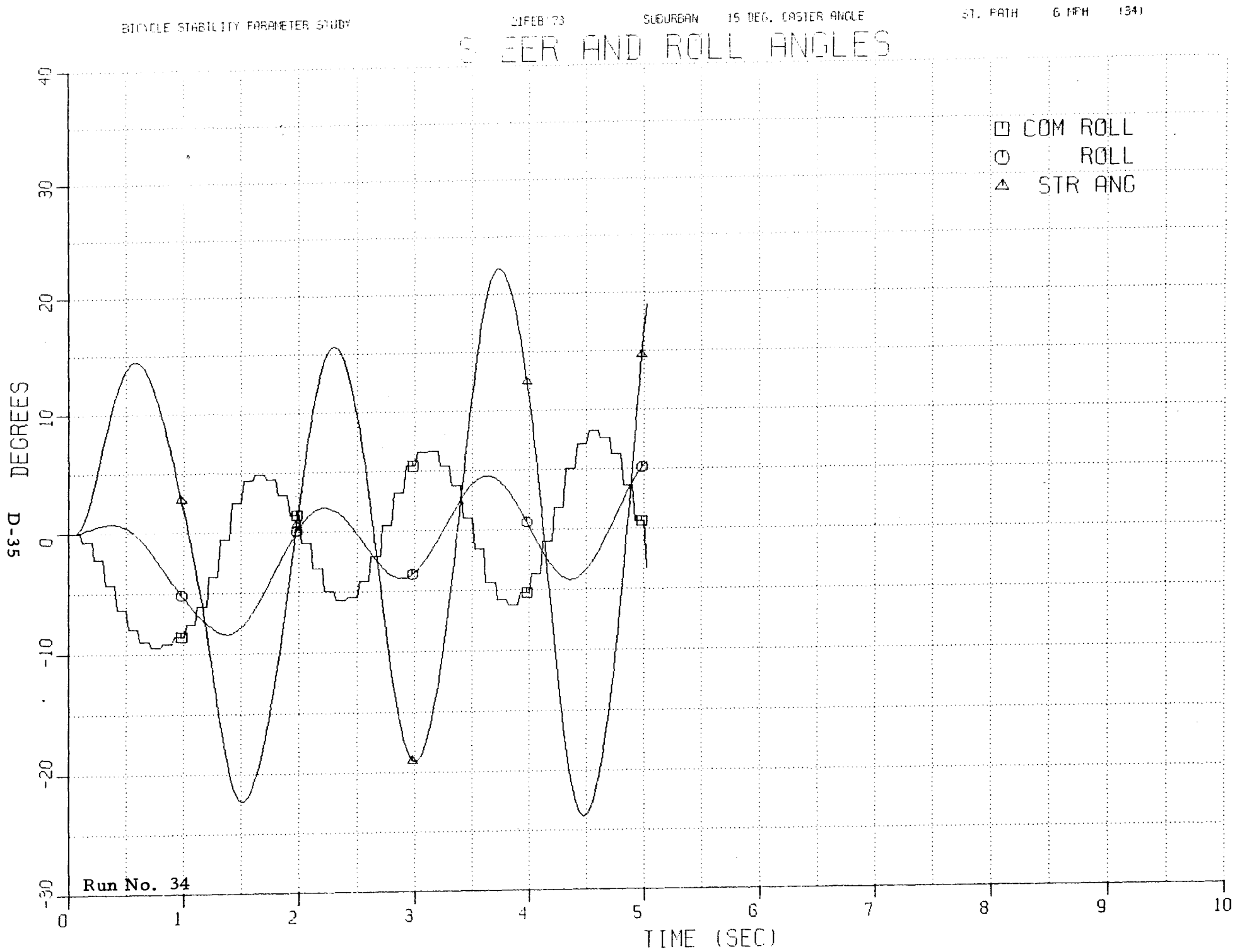
BICYCLE STABILITY PARAMETER STUDY
21FEB 73
SUBURBAN 15 DEG. CASTER ANGLE
ST. PATH 6 MPH (34)
STEER AND ROLL ANGLES
COM ROLL
ROLL
STR ANG
DEGREES
40
30
20
10
0
-10
-20
-30
0
1
2
3
4
5
6
7
8
9
10
TIME (SEC)
Run No. 34

BICYCLE STABILITY PARA[illegible]S STUDY 21FEB 73 SUBURBAN 15 DEG. CASTER ANGLE ST. PATH 10 MPH (35)

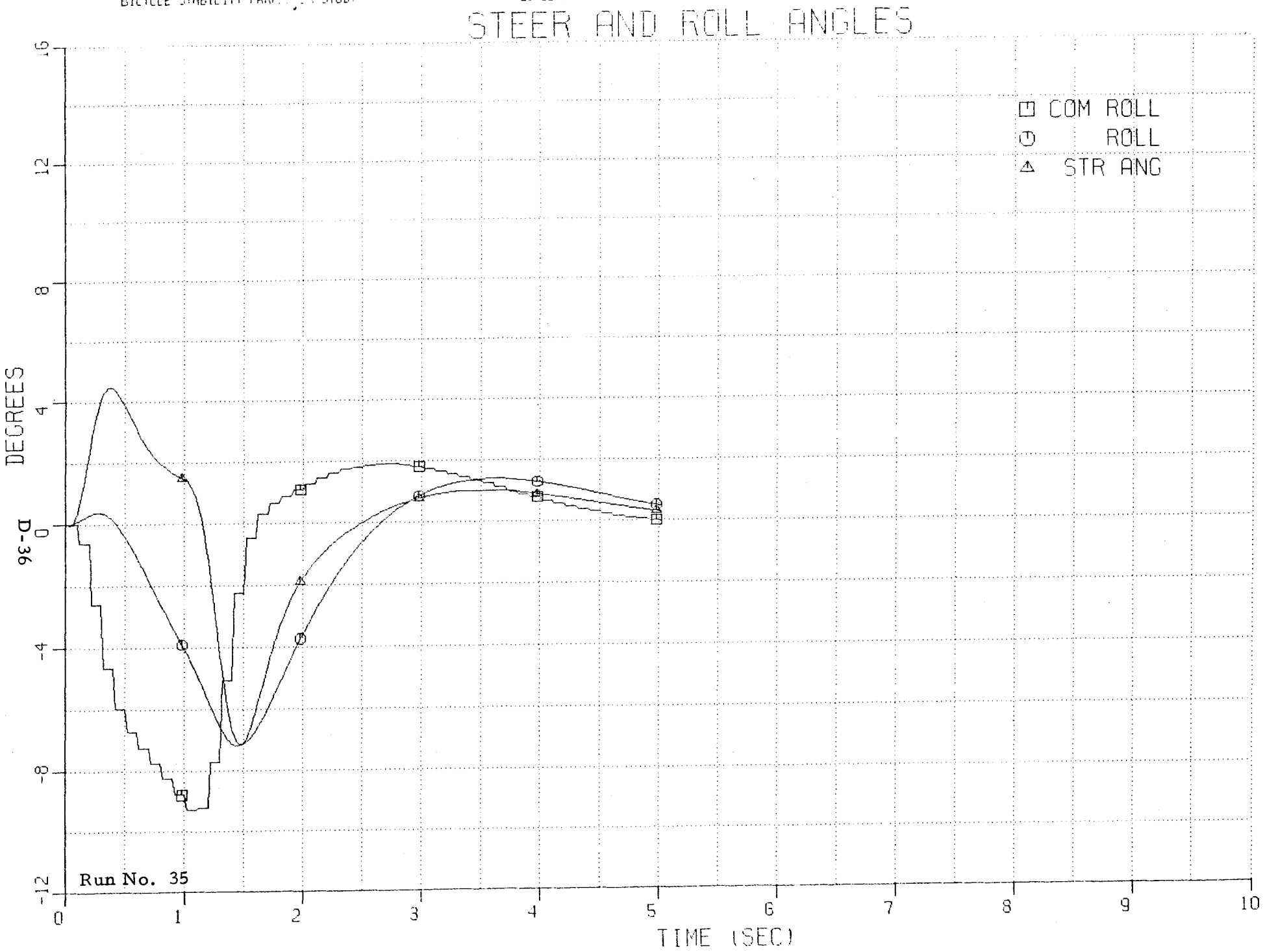

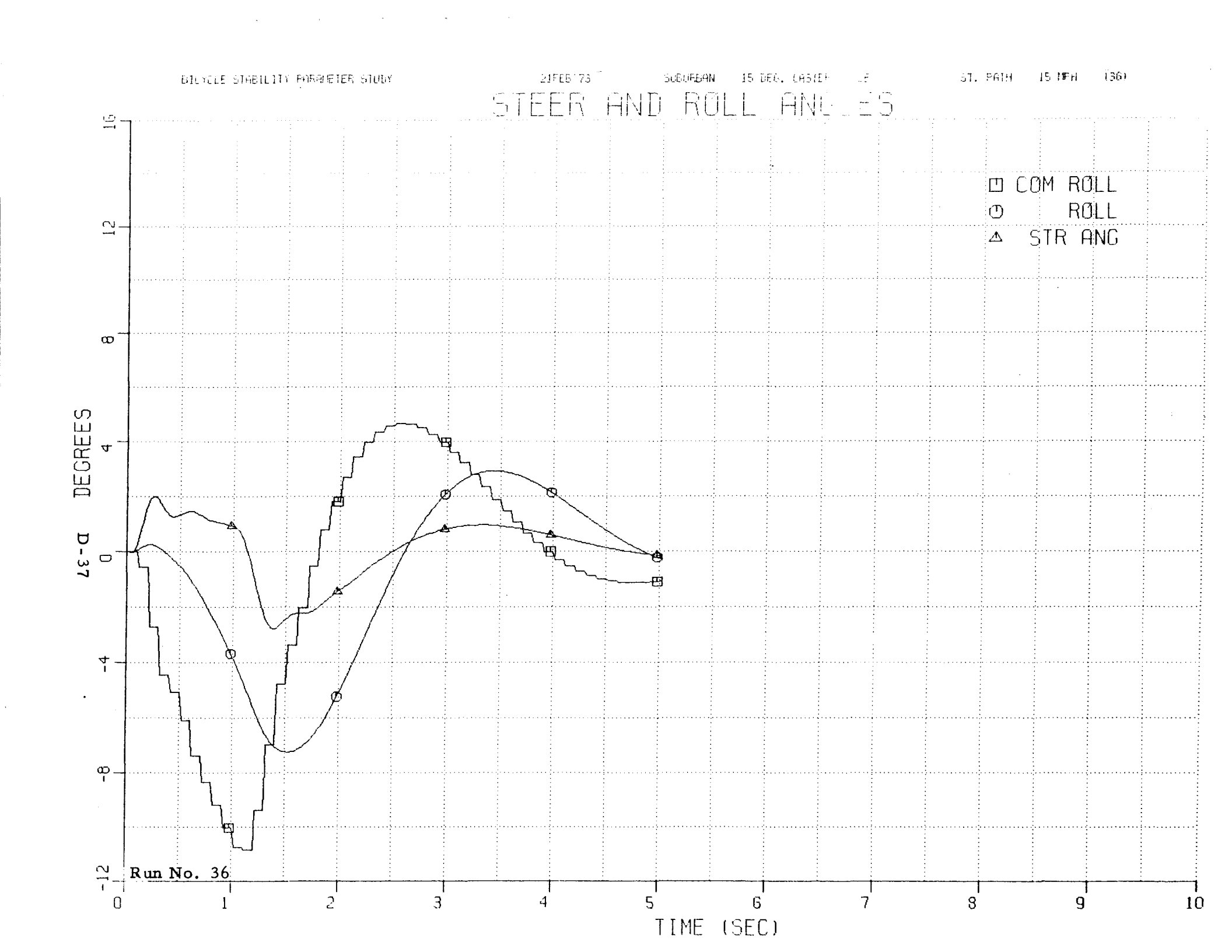
BICYCLE STABILITY PARAMETER STUDY
21FEB 73
SUBURBAN
15 DEG. CASTER
ST. PATH
15 MPH
(36)
STEER AND ROLL ANGLES
COM ROLL
ROLL
STR ANG
DEGREES
TIME (SEC)
Run No. 36
D-37

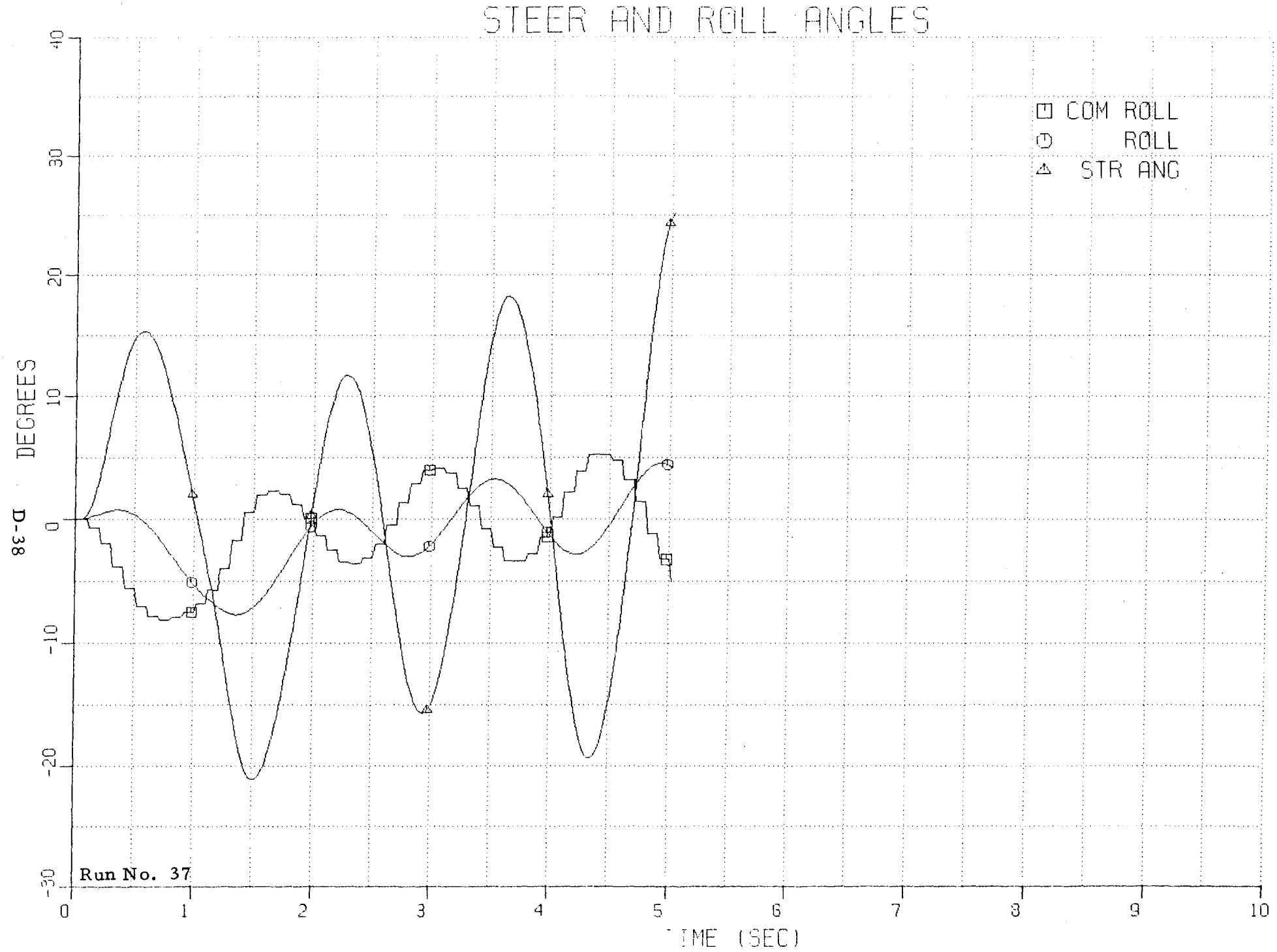
STEER AND ROLL ANGLES
COM ROLL
ROLL
STR ANG
DEGREES
40
30
20
10
0
-10
-20
-30
Run No. 37
0
1
2
3
4
5
6
7
8
9
10
TIME (SEC)

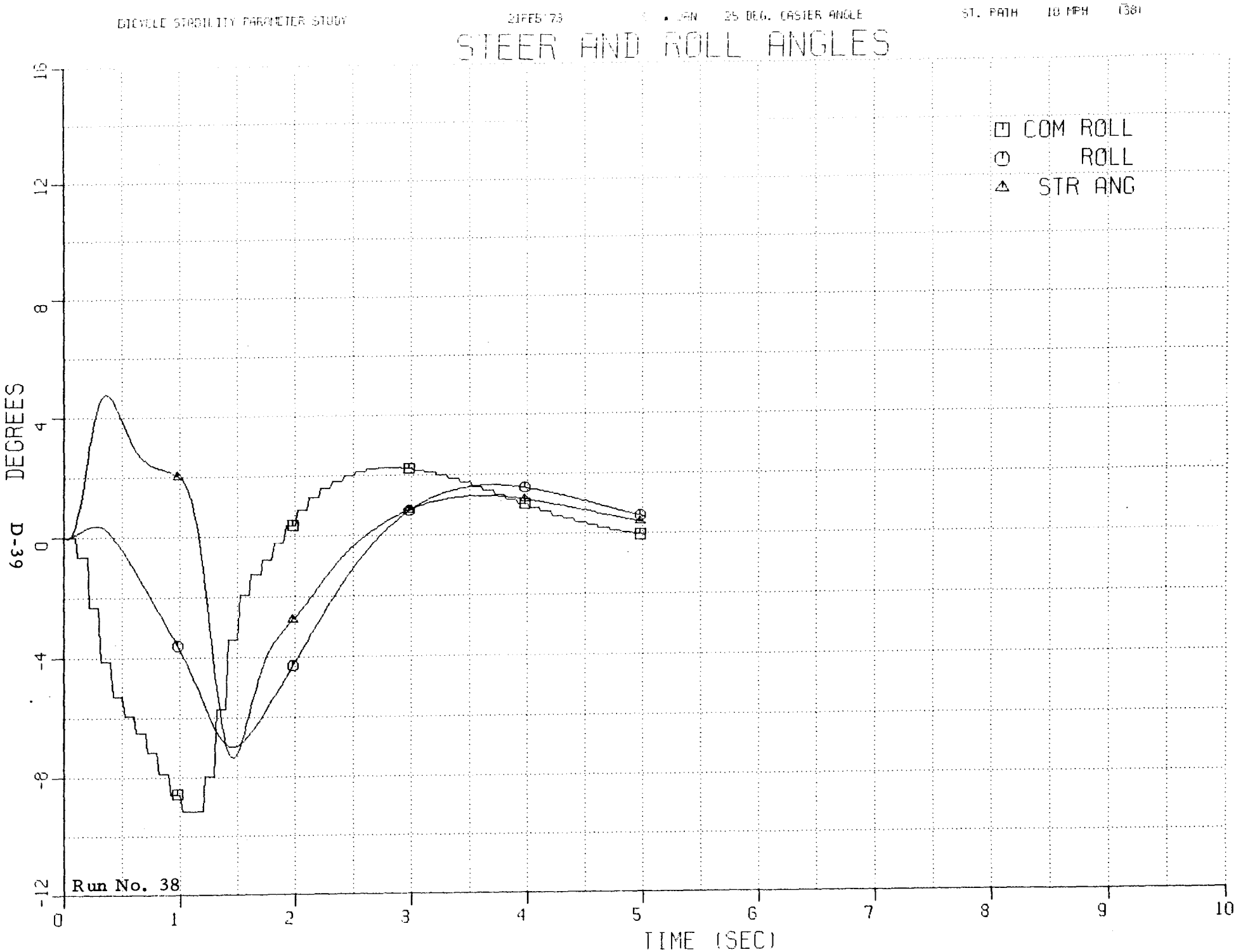
BICYCLE STABILITY PARAMETER STUDY
21FEB 73
• JAN 25 DEG. CASTER ANGLE
ST. PATH 10 MPH (38)
STEER AND ROLL ANGLES
COM ROLL
ROLL
STR ANG
DEGREES
16
12
8
4
0
-4
-8
-12
Run No. 38
0
1
2
3
4
5
6
7
8
9
10
TIME (SEC)

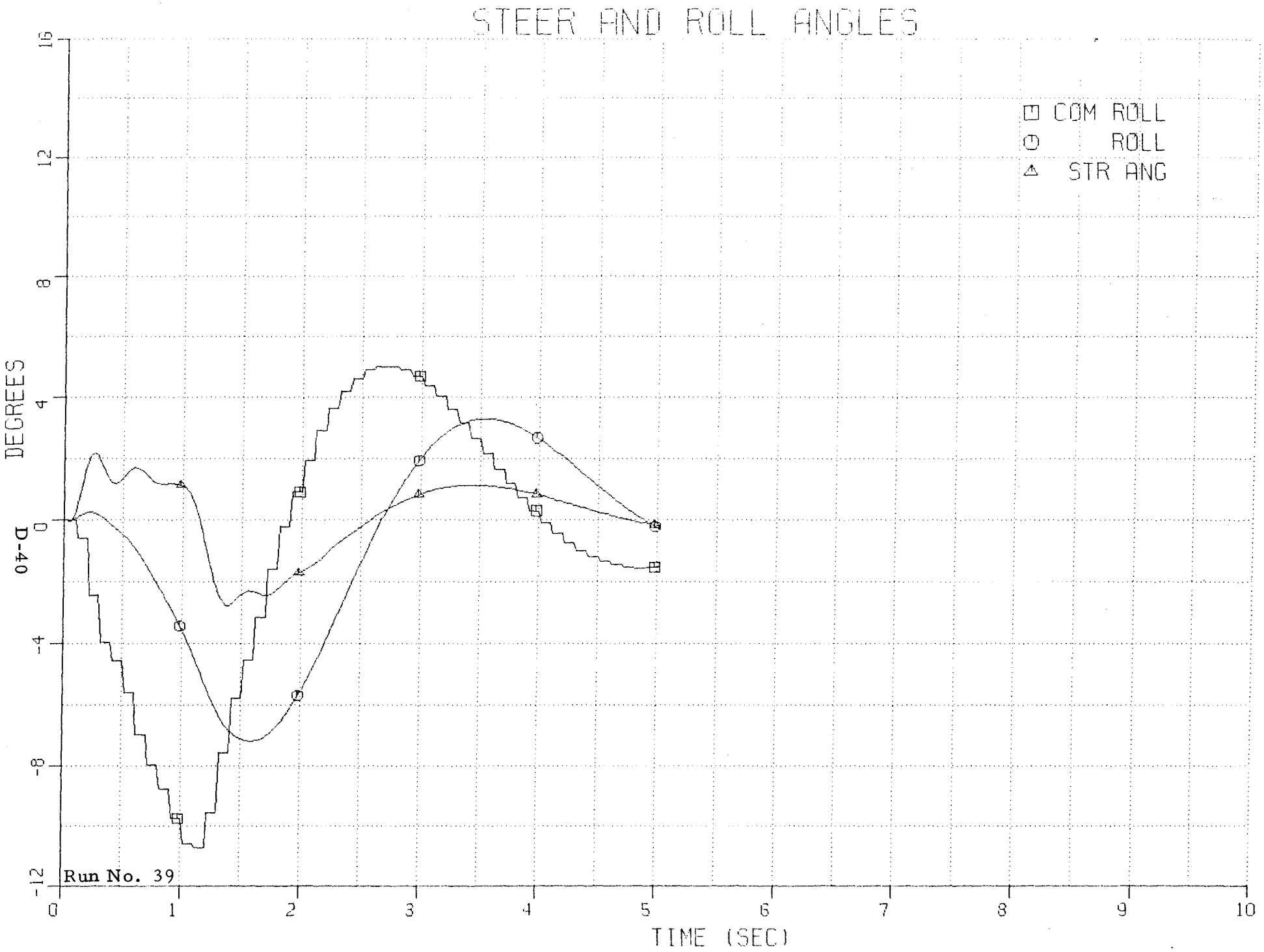
STEER AND ROLL ANGLES
COM ROLL
ROLL
STR ANG
DEGREES
16
12
8
4
0
-4
-8
-12
D-40
Run No. 39
0
1
2
3
4
5
6
7
8
9
10
TIME (SEC)

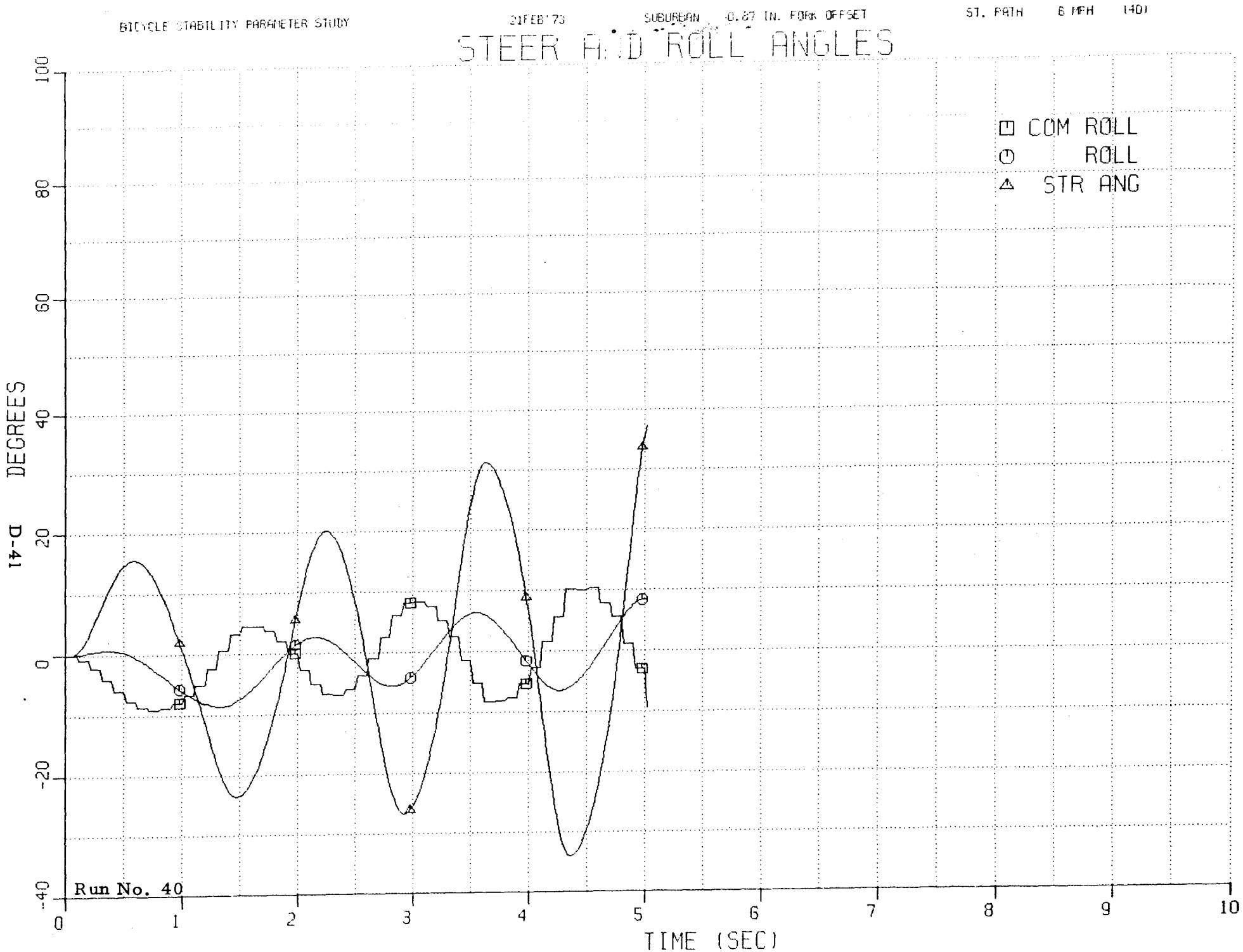
BICYCLE STABILITY PARAMETER STUDY
21FEB'73
SUBURBAN -0.67 IN. FORK OFFSET
ST. PATH 6 MPH (40)
STEER AND ROLL ANGLES
COM ROLL
ROLL
STR ANG
DEGREES
100
80
60
40
20
0
-20
-40
Run No. 40
0
1
2
3
4
5
6
7
8
9
10
TIME (SEC)

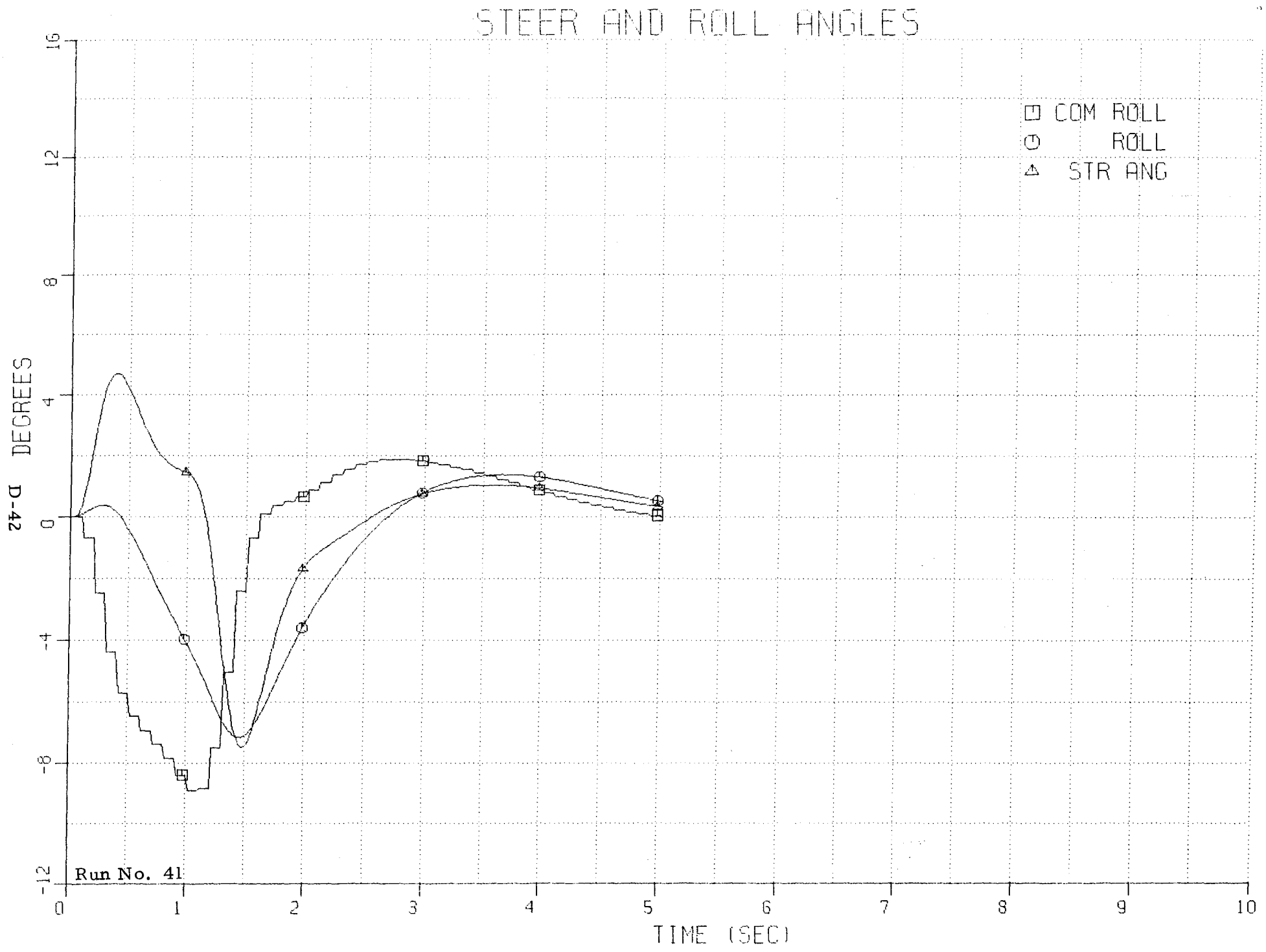
STEER AND ROLL ANGLES
COM ROLL
ROLL
STR ANG
DEGREES
16
12
8
4
0
-4
-8
-12
0
1
2
3
4
5
6
7
8
9
10
TIME (SEC)
Run No. 41

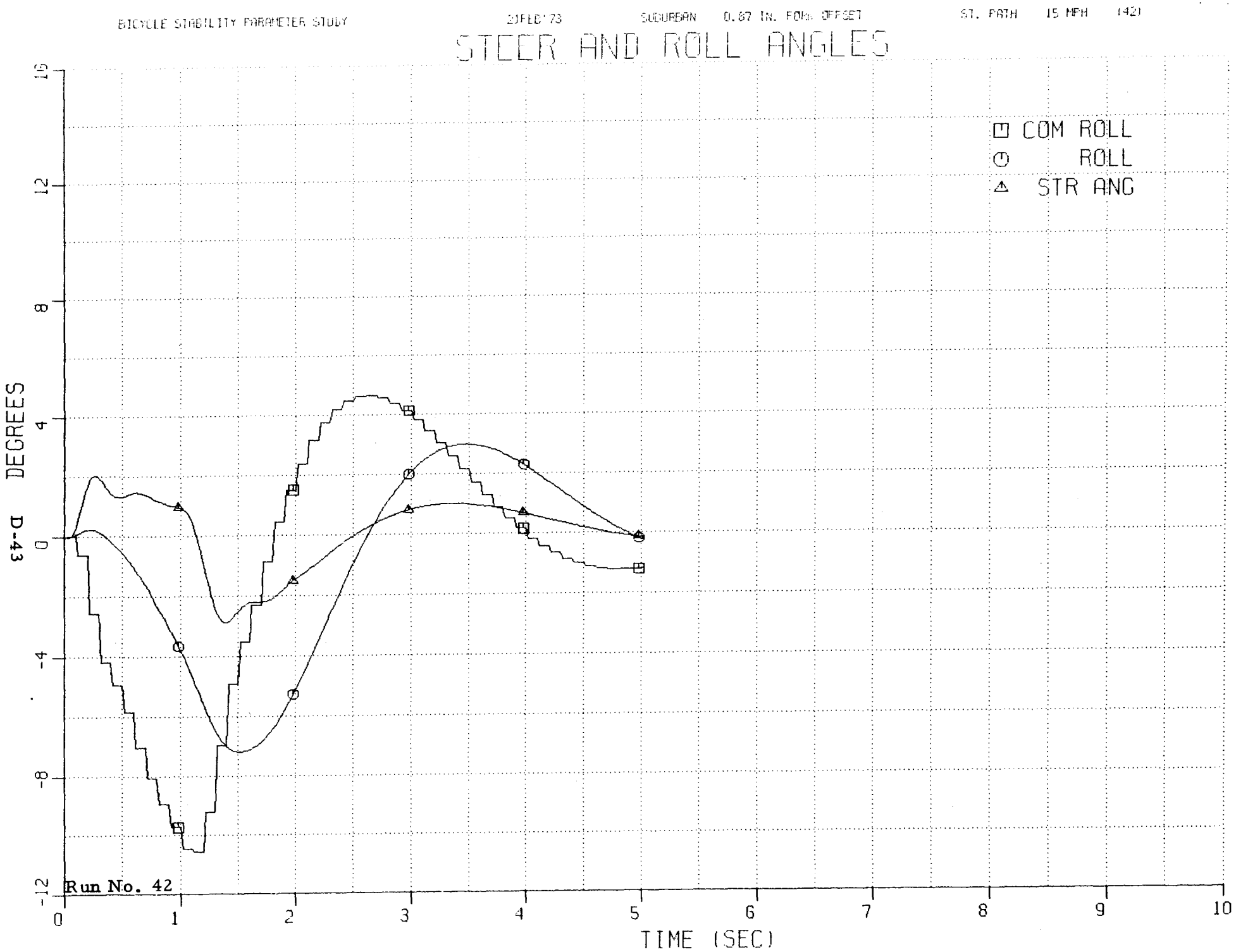
BICYCLE STABILITY PARAMETER STUDY
21FEB'73 SUBURBAN 0.87 IN. FORK OFFSET ST. PATH 15 MPH 1421
STEER AND ROLL ANGLES
COM ROLL
ROLL
STR ANG
DEGREES
16
12
8
4
0
-4
-8
-12
Run No. 42
0
1
2
3
4
5
6
7
8
9
10
TIME (SEC)

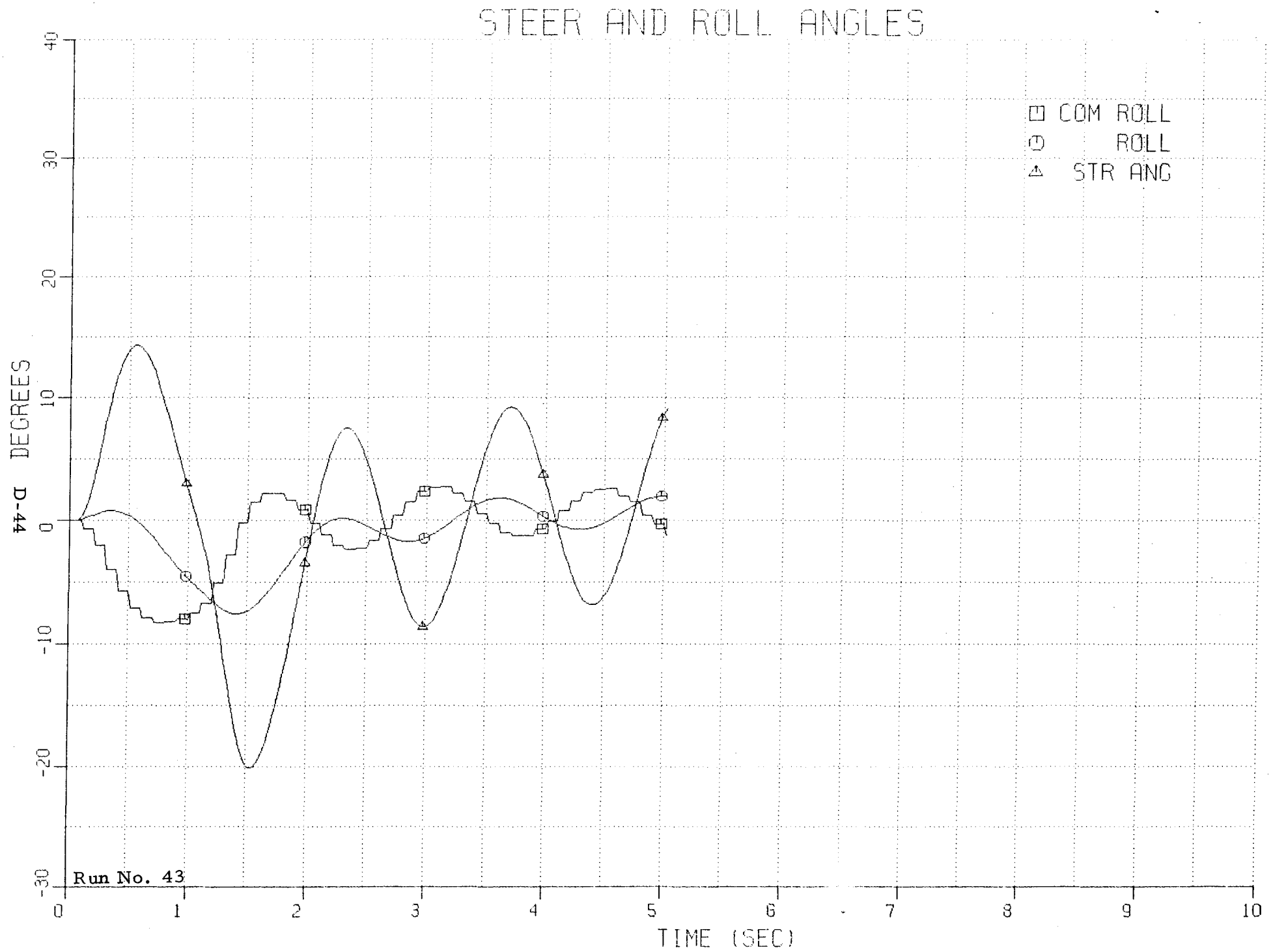
STEER AND ROLL ANGLES
COM ROLL
ROLL
STR ANG
DEGREES
40
30
20
10
0
-10
-20
-30
0
1
2
3
4
5
6
7
8
9
10
TIME (SEC)
Run No. 43

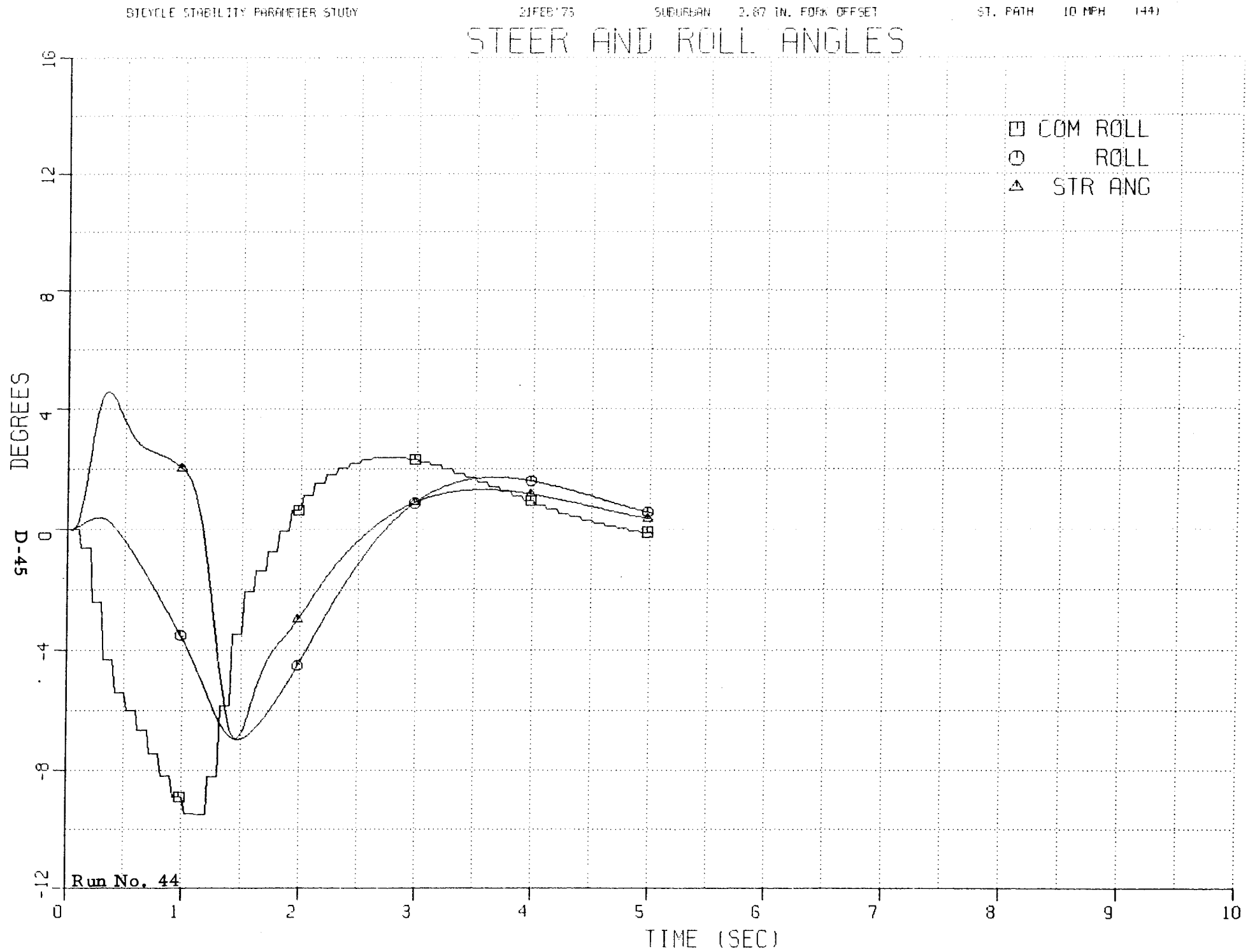
BICYCLE STABILITY PARAMETER STUDY
21FEB'75
SUBURBAN
2.87 IN. FORK OFFSET
ST. PATH
10 MPH
144
STEER AND ROLL ANGLES
COM ROLL
ROLL
STR ANG
DEGREES
16
12
8
4
0
-4
-8
-12
Run No. 44
0
1
2
3
4
5
6
7
8
9
10
TIME (SEC)

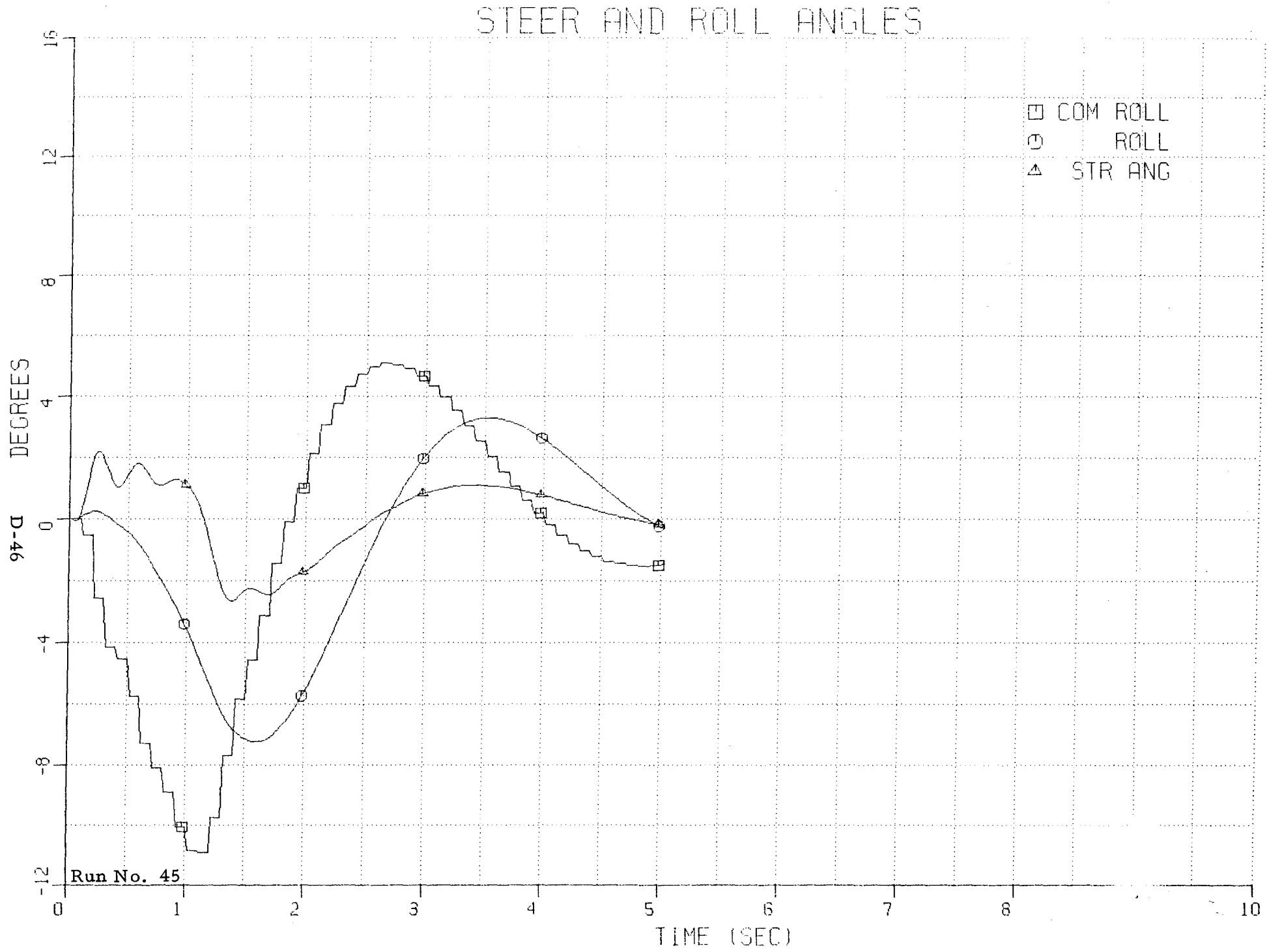
STEER AND ROLL ANGLES
COM ROLL
ROLL
STR ANG
DEGREES
TIME (SEC)
Run No. 45
16
12
8
4
0
-4
-8
-12
0
1
2
3
4
5
6
7
8
10

BICYCLE STABILITY PARAMETER STUDY 21FEB'73 SUBUREAN 20.0 IN. WHEEL DIAMETER ST. PATH 6 MPH (46)

STEER AND ROLL ANGLES

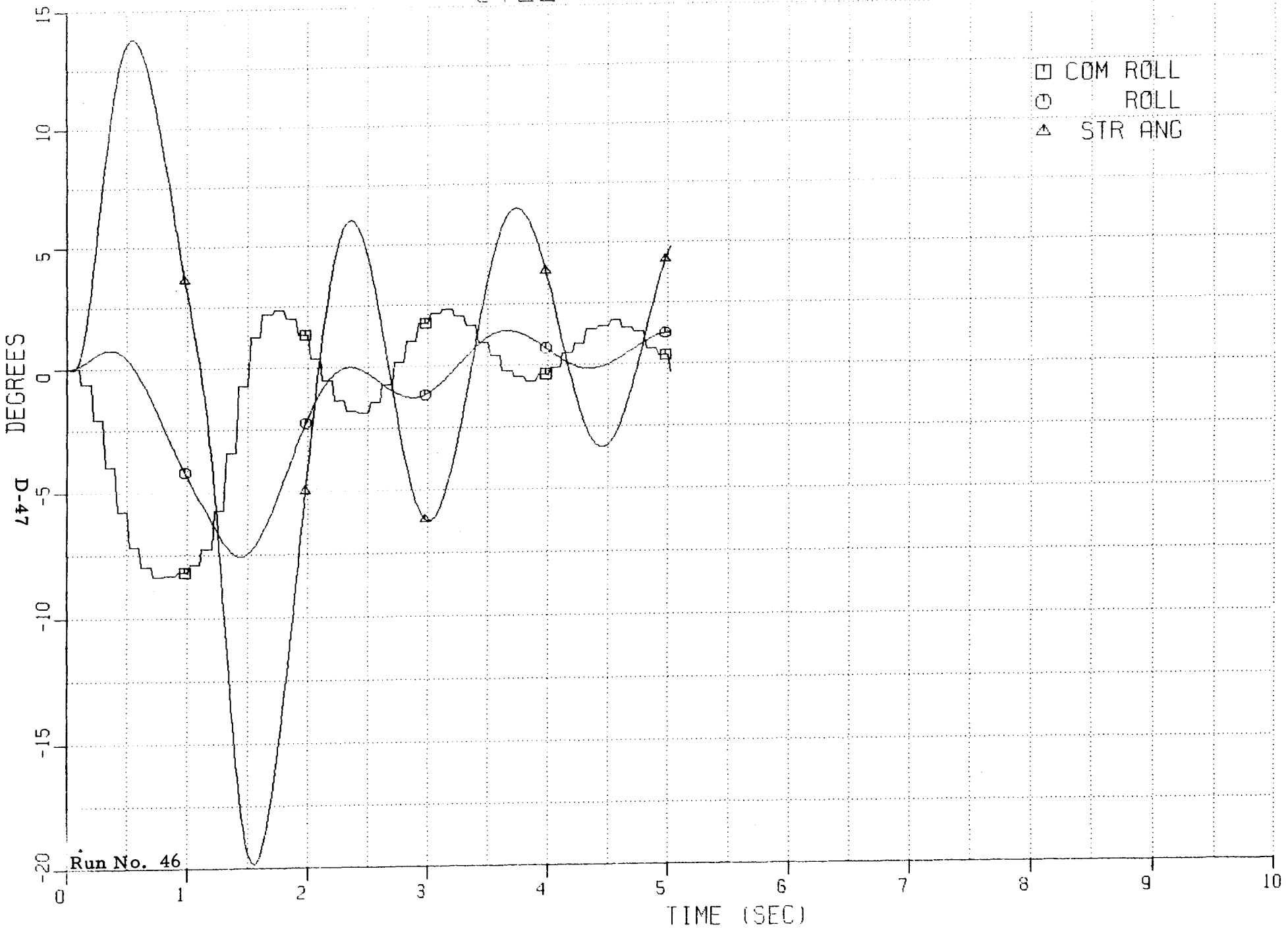

STEER AND ROLL ANGLES

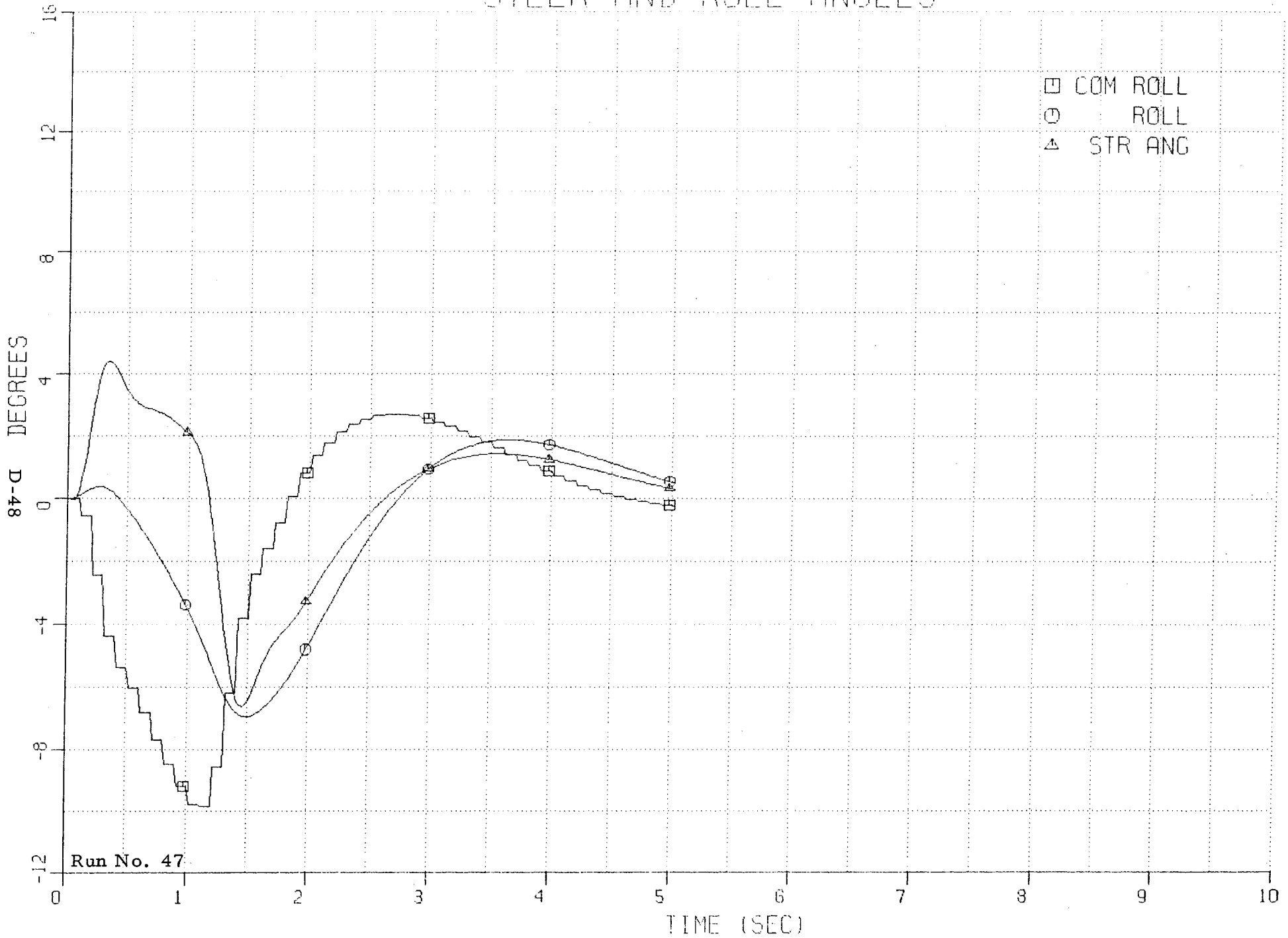

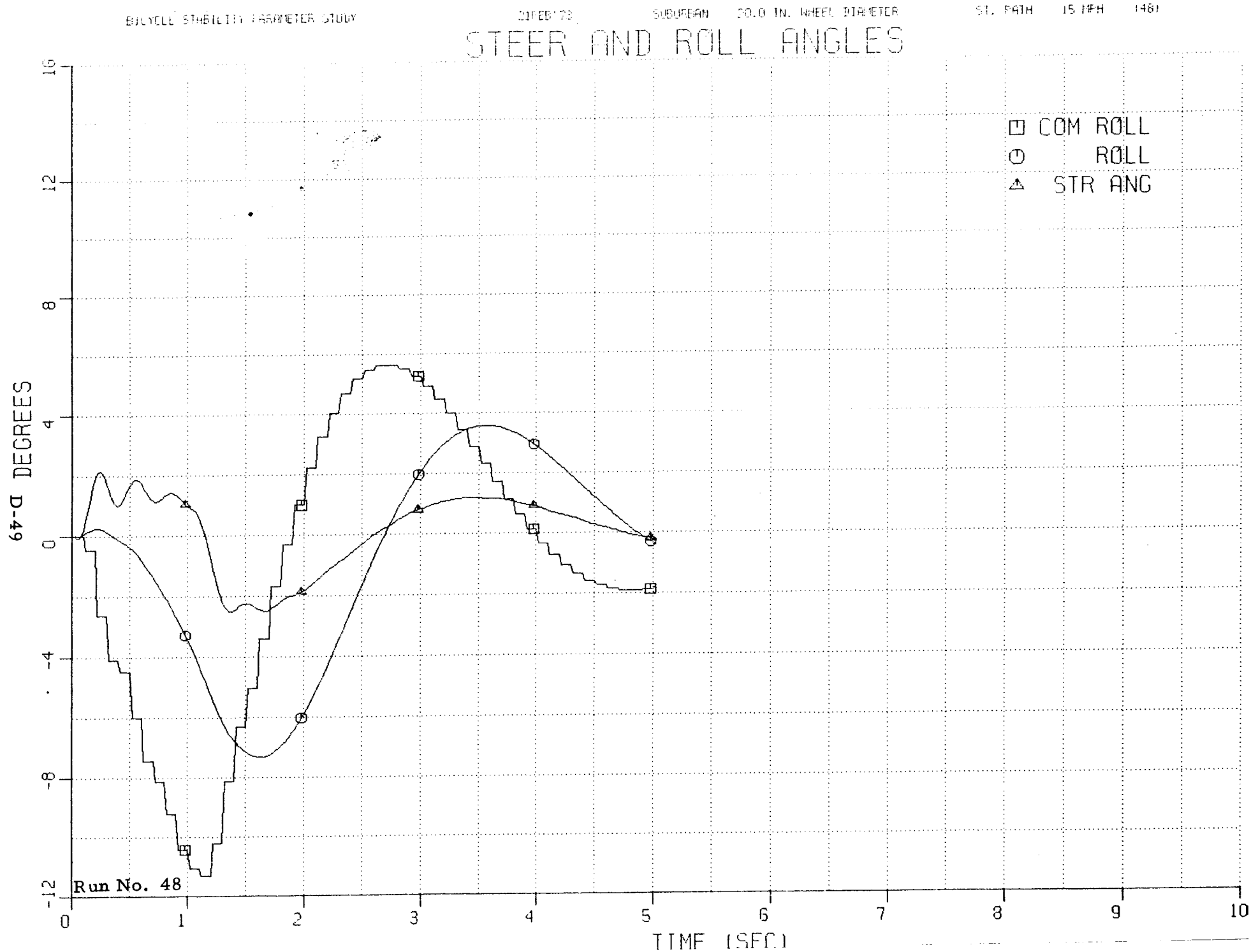
BICYCLE STABILITY PARAMETER STUDY
21FEB'73
SUBURBAN
20.0 IN. WHEEL DIAMETER
ST. PATH
15 MPH
1481
STEER AND ROLL ANGLES
COM ROLL
ROLL
STR ANG
DEGREES
16
12
8
4
0
-4
-8
-12
Run No. 48
0
1
2
3
4
5
6
7
8
9
10
TIME (SEC)

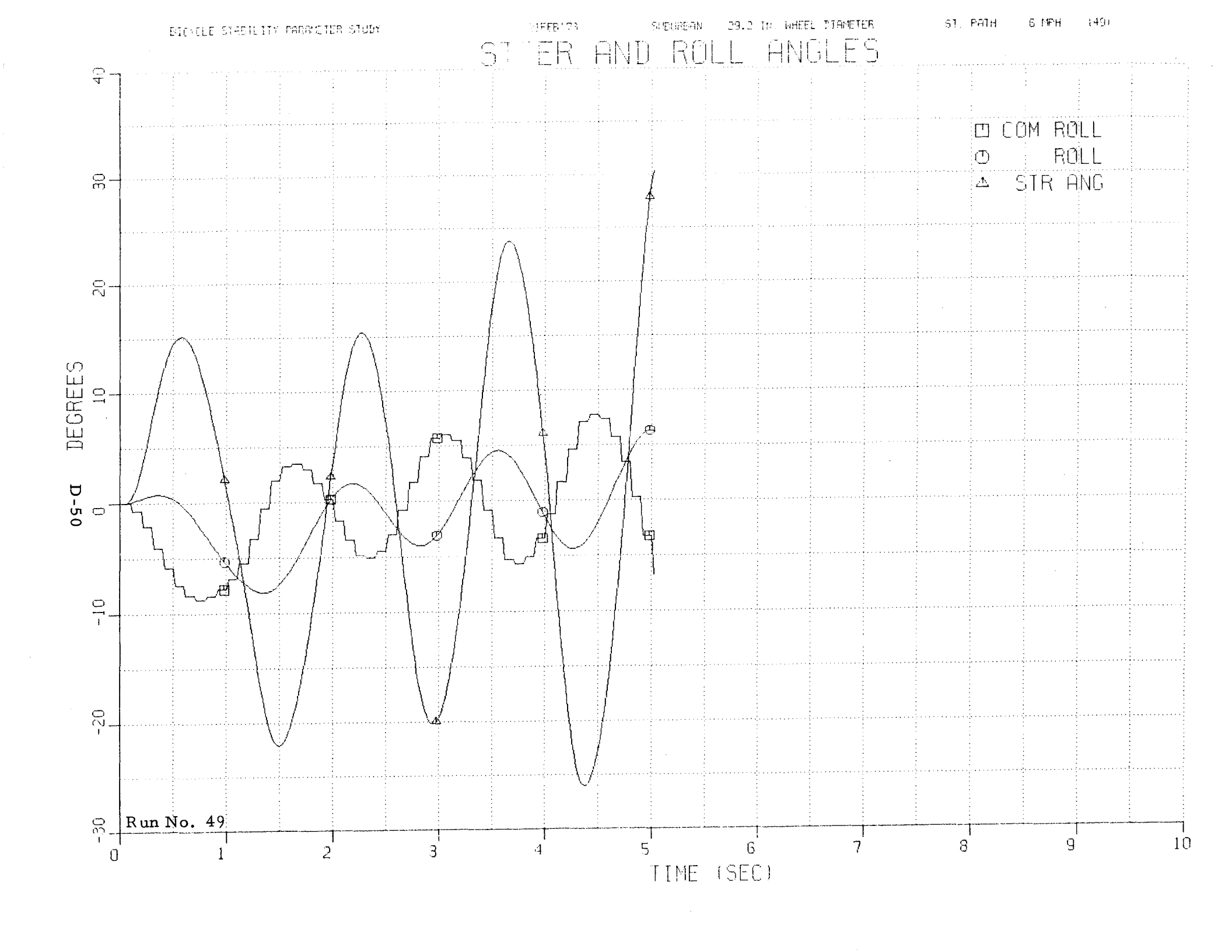
BICYCLE STABILITY PARAMETER STUDY
WHEELING
SWEDEBAN
29.2 IN WHEEL DIAMETER
ST. PATH
6 MPH
149
STEER AND ROLL ANGLES
COM ROLL
ROLL
STR ANG
DEGREES
D-50
40
30
20
10
0
-10
-20
-30
0
1
2
3
4
5
6
7
8
9
10
TIME (SEC)
Run No. 49

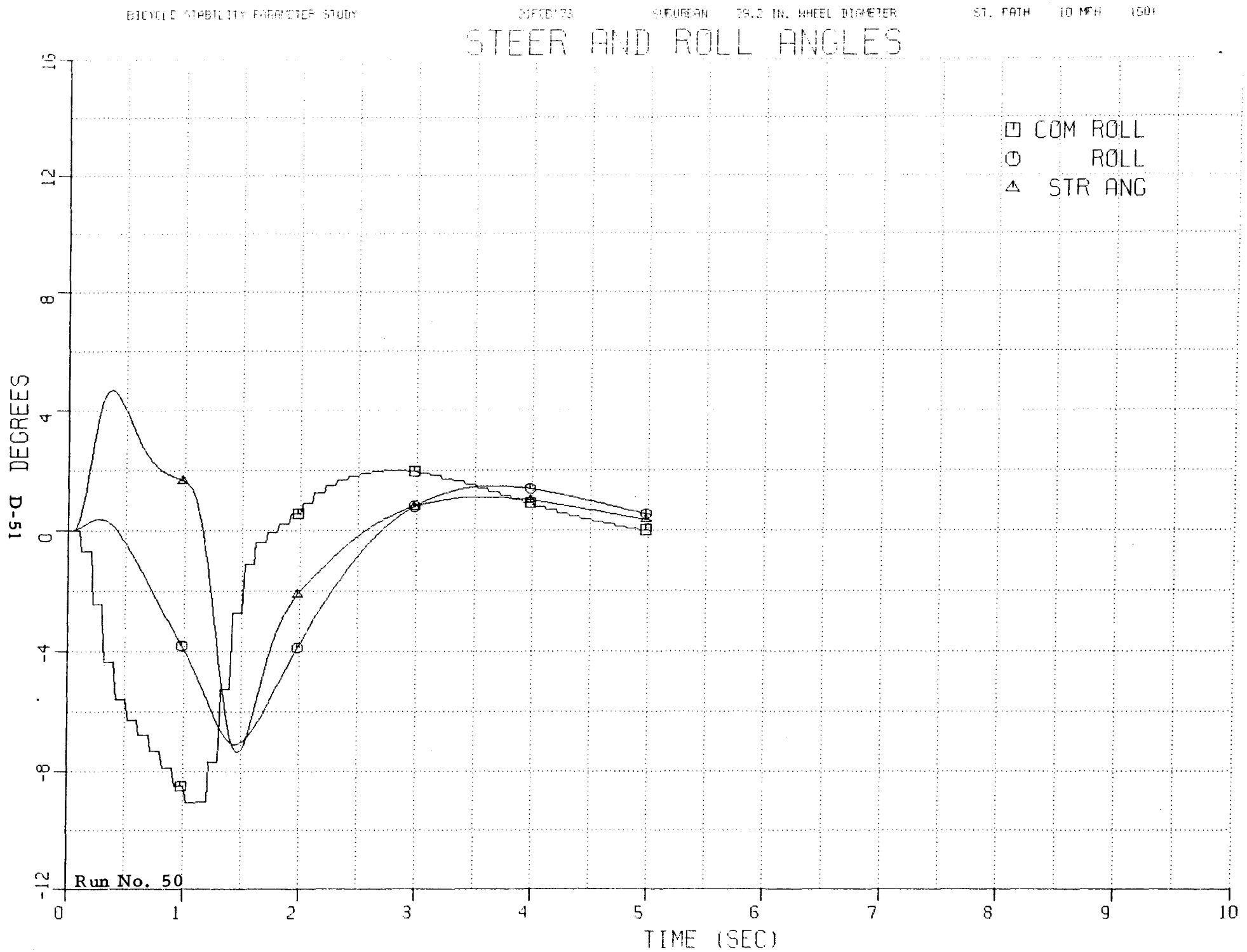
BICYCLE STABILITY PARAMETER STUDY
SUBURBAN 26.0 IN. WHEEL DIAMETER ST. PATH 10 MPH
STEER AND ROLL ANGLES
COM ROLL
ROLL
STR ANG
DEGREES
TIME (SEC)
Run No. 50

STEER AND ROLL ANGLES

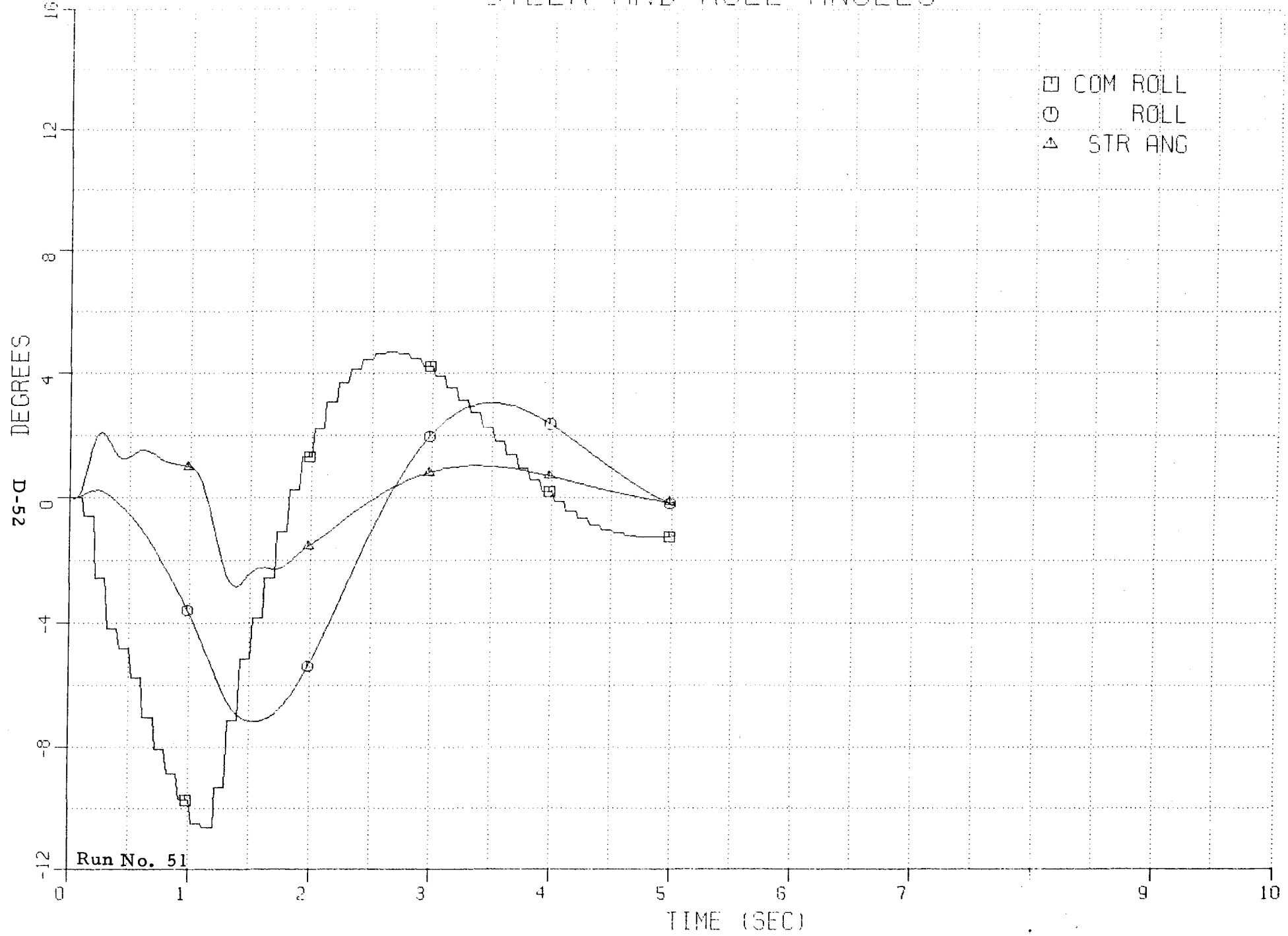

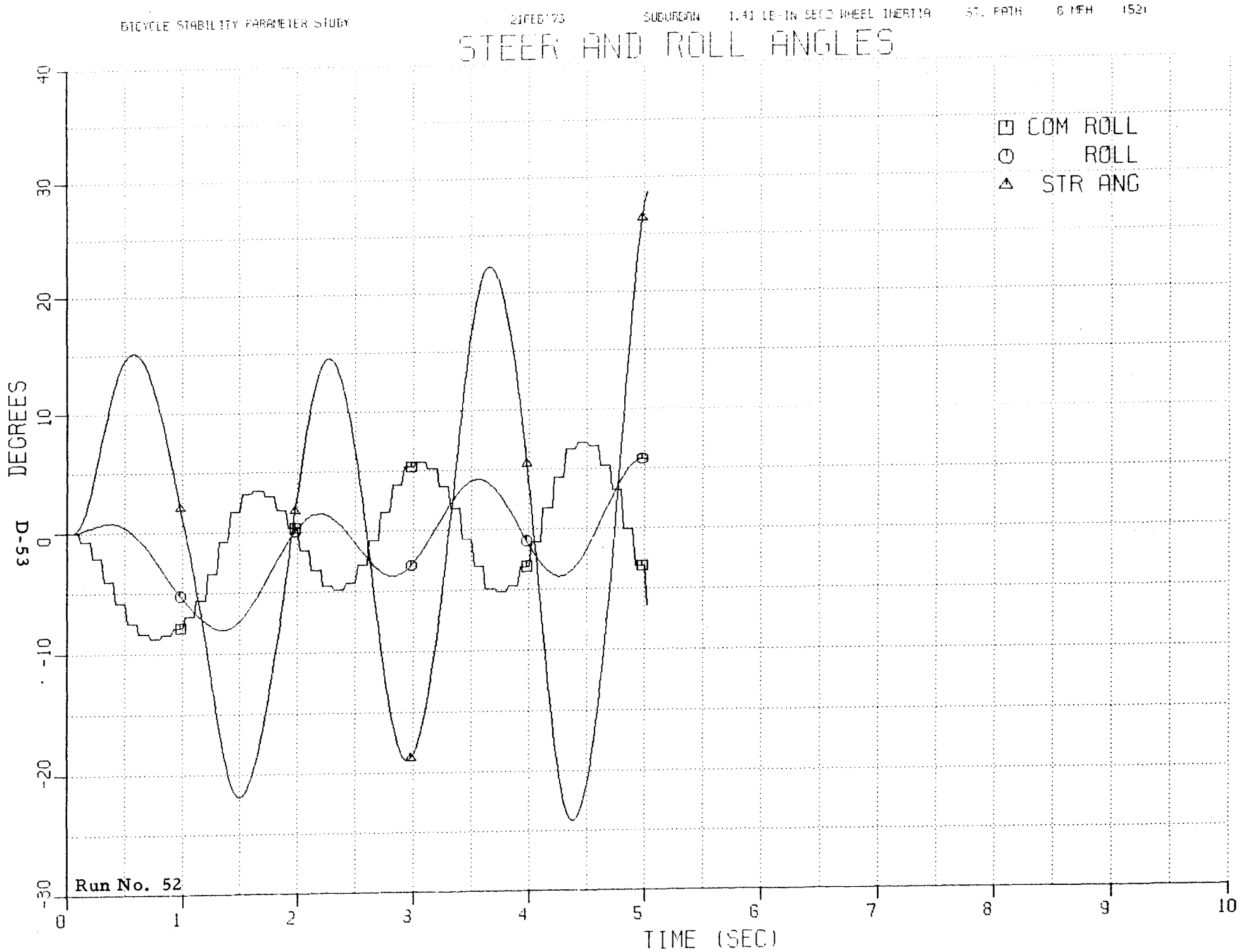
BICYCLE STABILITY PARAMETER STUDY
21FEB'73 SUBURBAN 1.41 LB-IN SEC2 WHEEL INERTIA ST. PATH 6 MPH 1521
STEER AND ROLL ANGLES
COM ROLL
ROLL
STR ANG
DEGREES
TIME (SEC)
Run No. 52
40
30
20
10
0
-10
-20
-30
0
1
2
3
4
5
6
7
8
9
10

BICYCLE STABILITY PARAMETER STUDY 21FEB 73 SHERMSRGN .41 LB-IN-SEC2 WHEEL INERTIA ST. PATH 10 MPH (53)

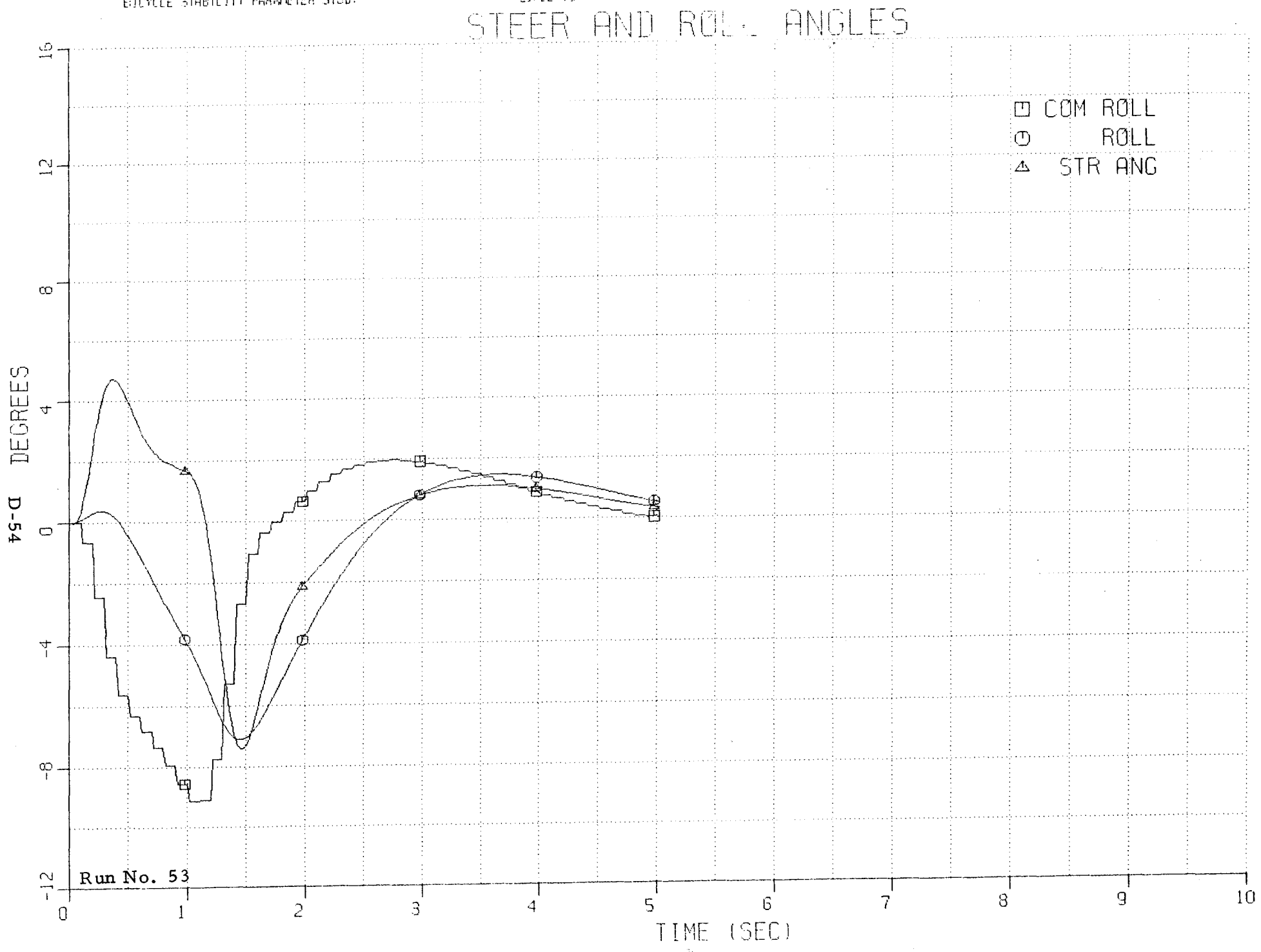

STEER AND ROLL ANGLES

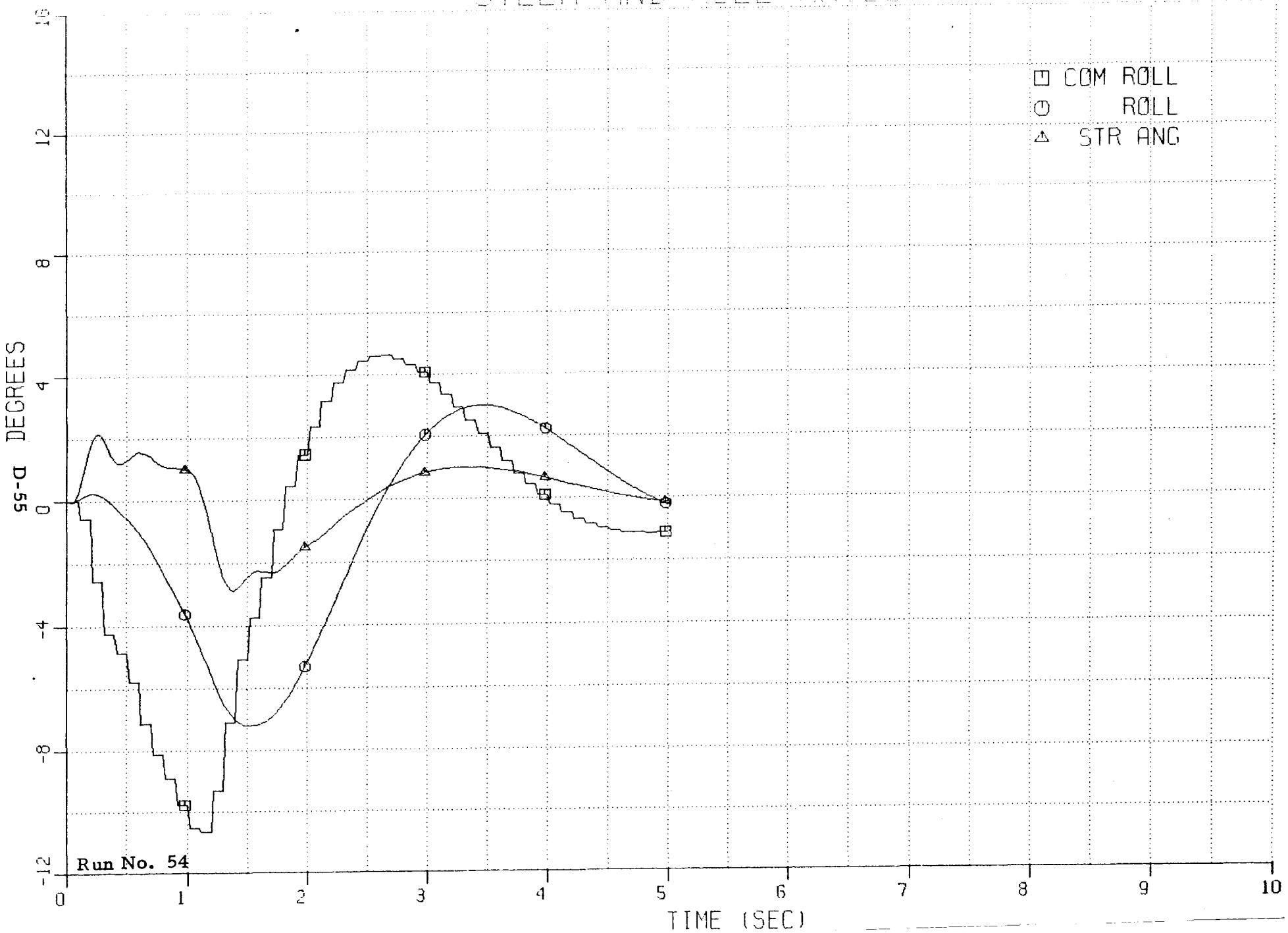

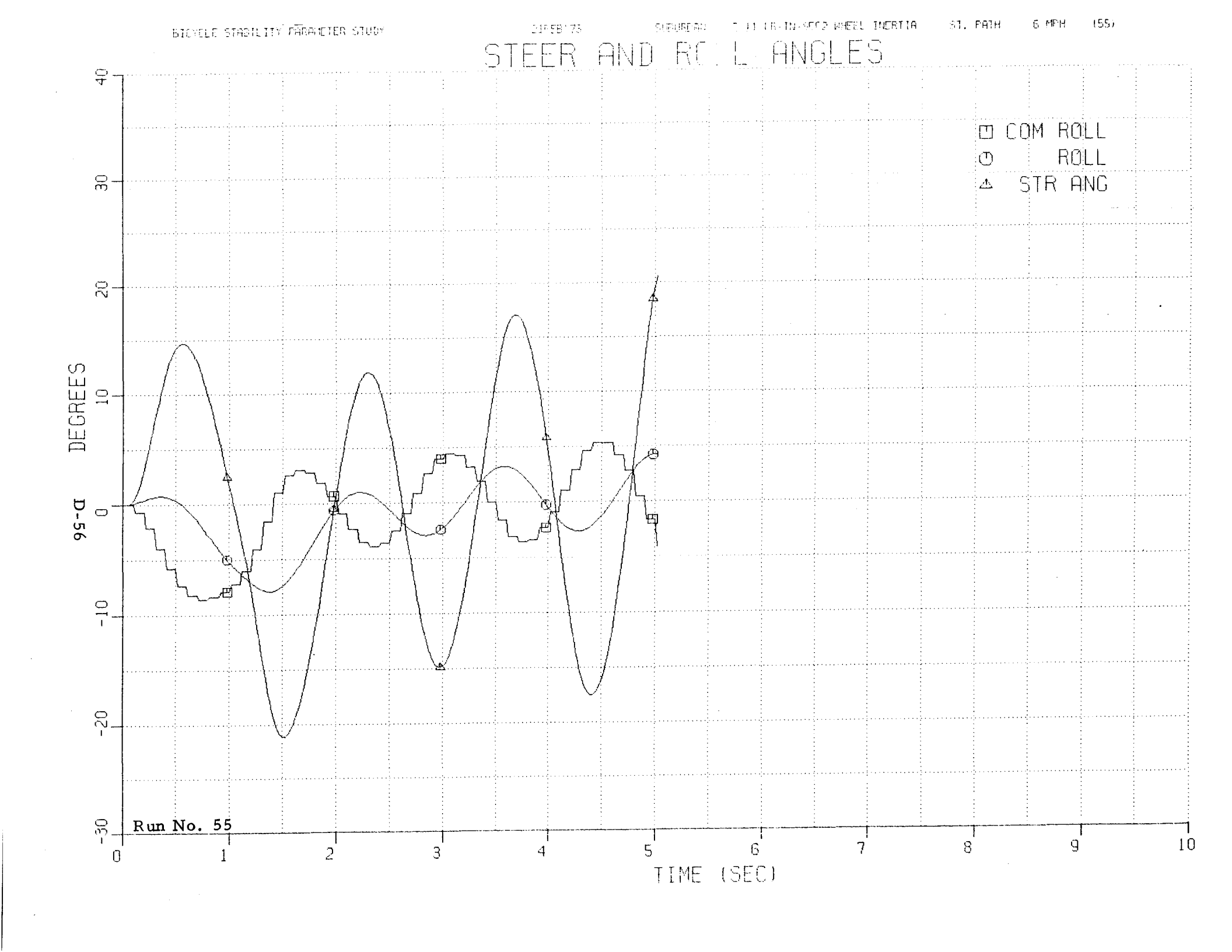
BICYCLE STABILITY PARAMETER STUDY
STEER AND ROLL ANGLES
COM ROLL
ROLL
STR ANG
DEGREES
TIME (SEC)
Run No. 55
40
30
20
10
0
-10
-20
-30
0
1
2
3
4
5
6
7
8
9
10

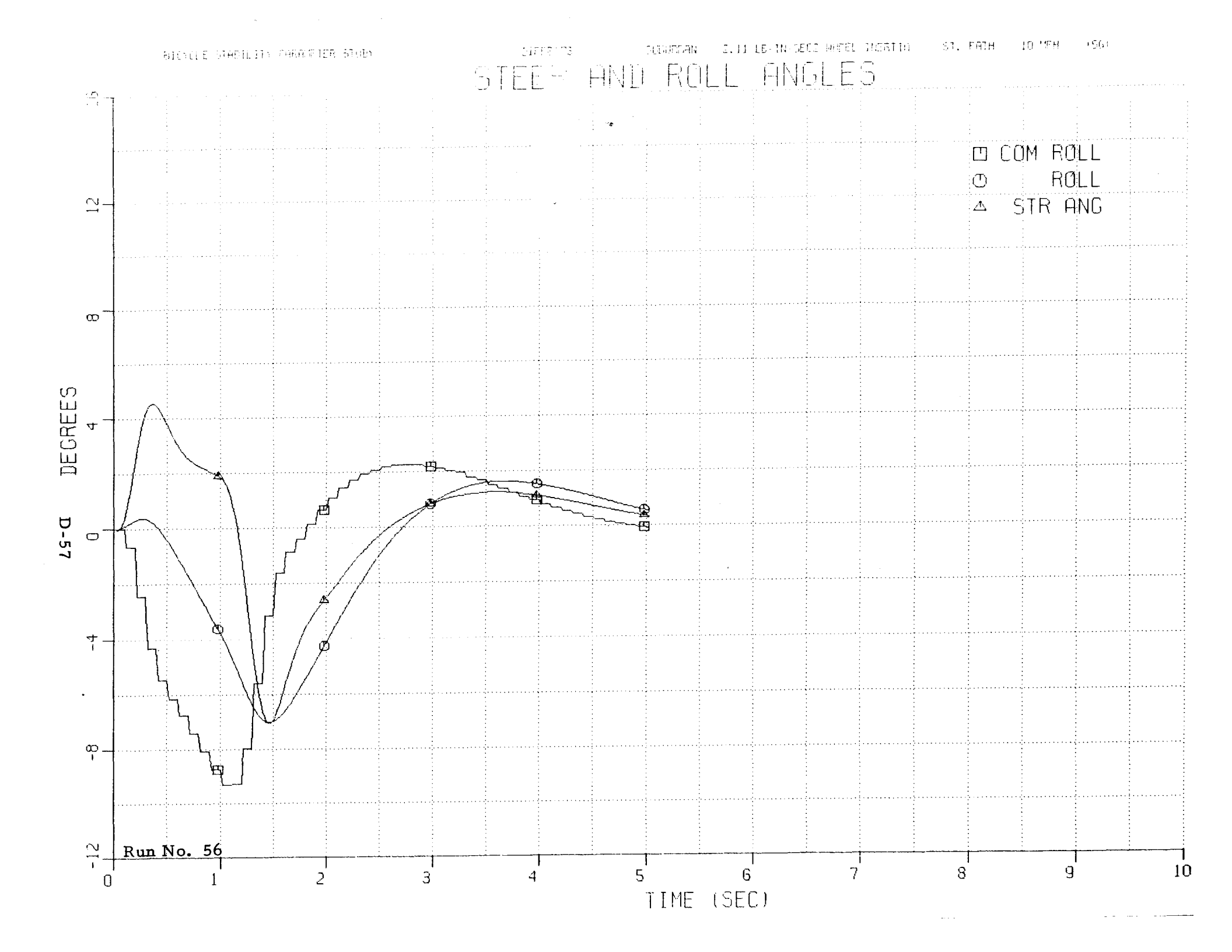
STEER AND ROLL ANGLES
COM ROLL
ROLL
STR ANG
DEGREES
TIME (SEC)
Run No. 56
12
8
4
0
-4
-8
-12
0
1
2
3
4
5
6
7
8
9
10

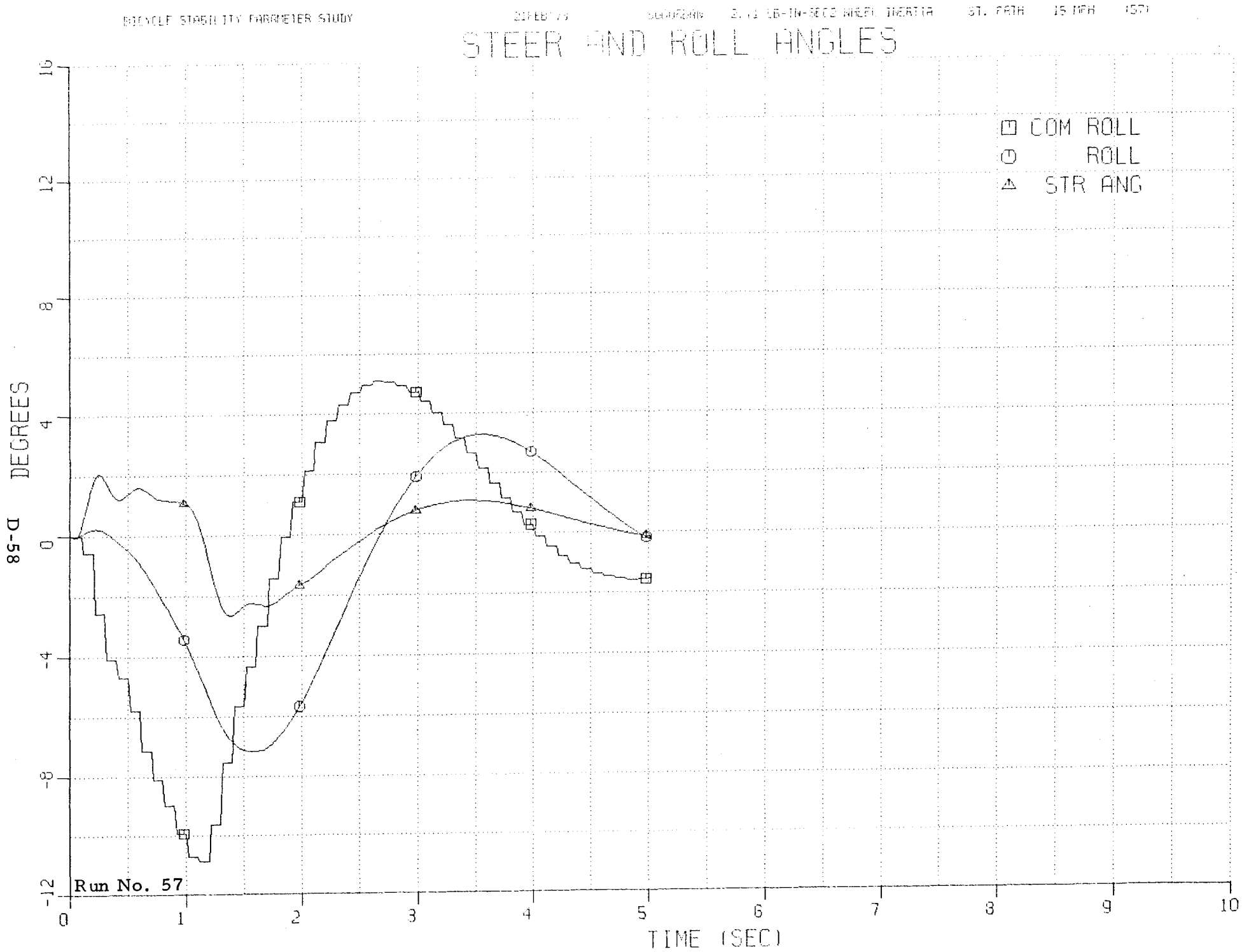
STEER AND ROLL ANGLES
COM ROLL
ROLL
STR ANG
DEGREES
16
12
8
4
0
-4
-8
-12
0
1
2
3
4
5
6
7
8
9
10
TIME (SEC)
Run No. 57

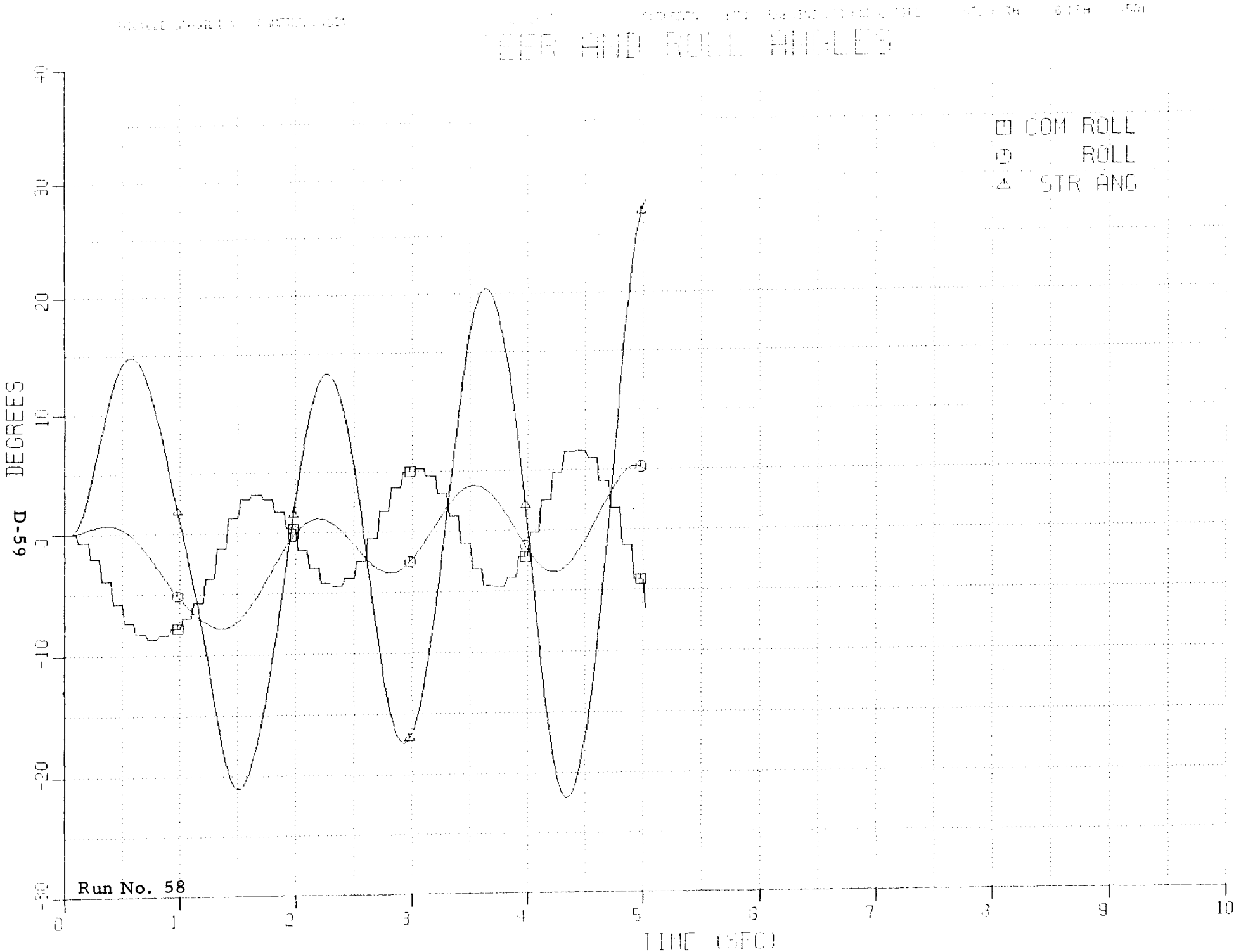
ER AND ROLL ANGLES
COM ROLL
ROLL
STR ANG
DEGREES
TIME (SEC)
Run No. 58

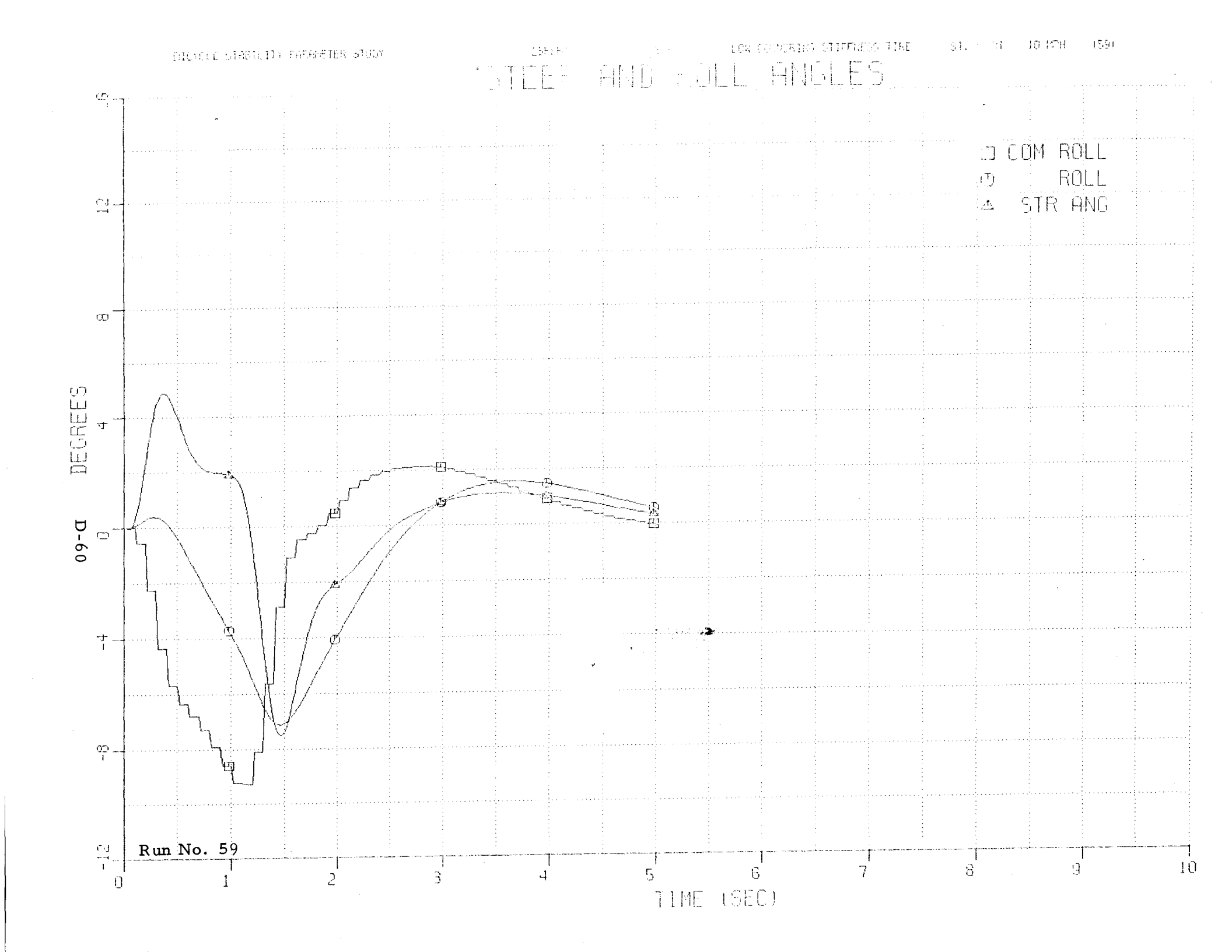
STEER AND ROLL ANGLES
COM ROLL
ROLL
STR ANG
DEGREES
TIME (SEC)
Run No. 59
D-60

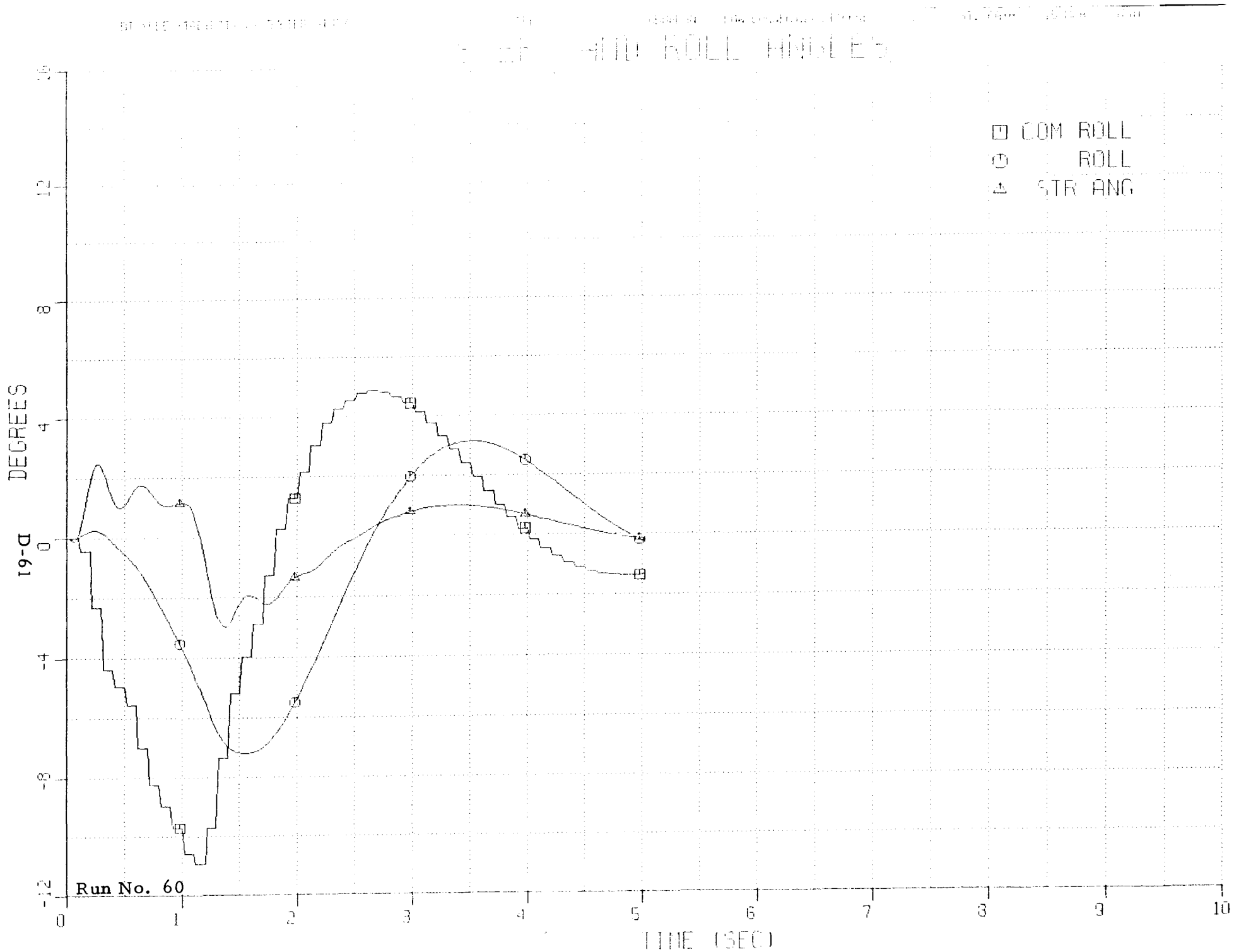
ROLL ANGLES
COM ROLL
ROLL
STR ANG
DEGREES
12
8
4
0
-4
-8
-12
0
1
2
3
4
5
6
7
8
9
10
TIME (SEC)
Run No. 60

BICYCLE STABILITY PARAMETER STUDY 21FEB'75 SUBURBAN HIGH CORNERING STIFFNESS TIRE ST. PATH 6 MPH 1611

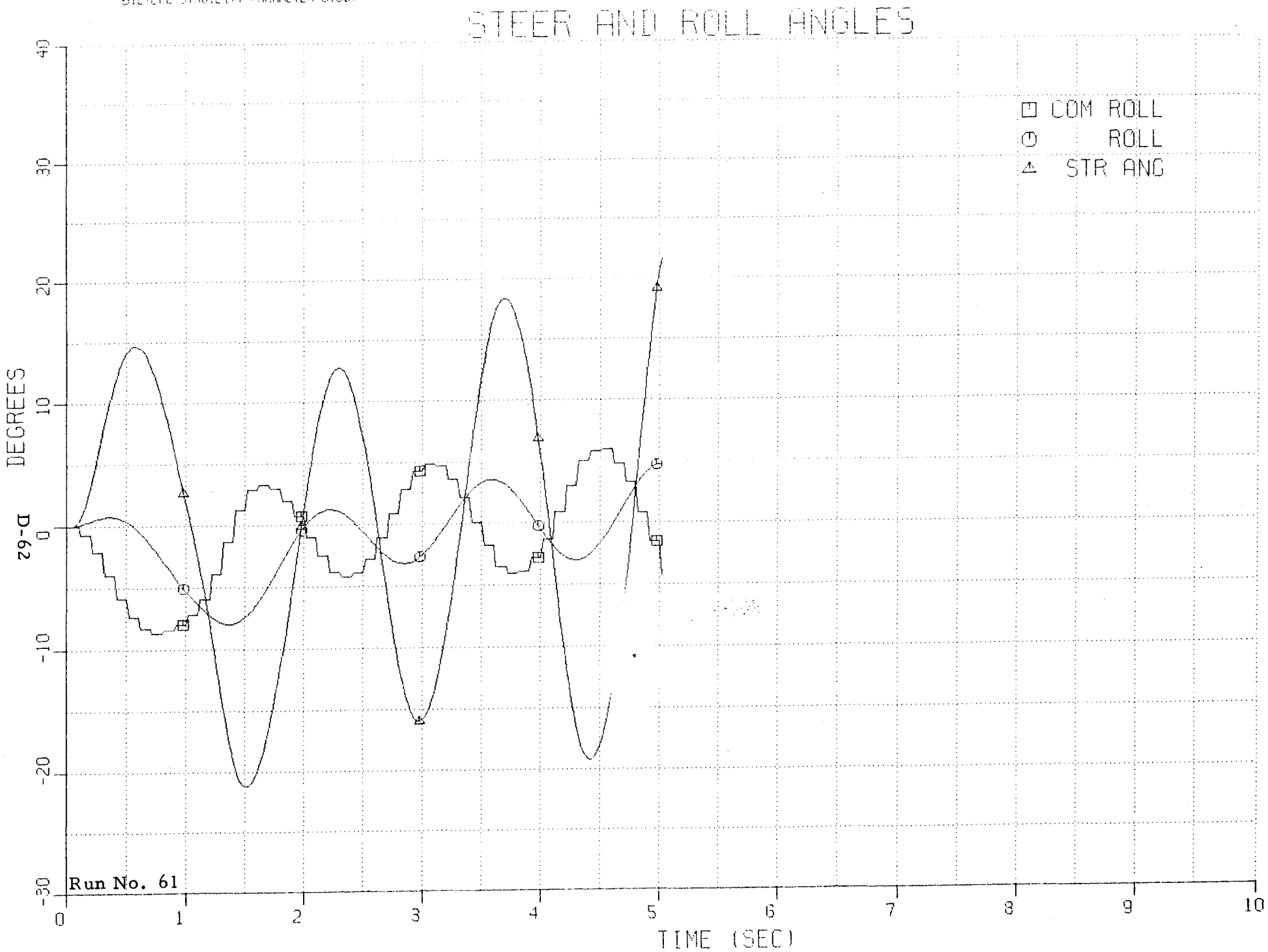

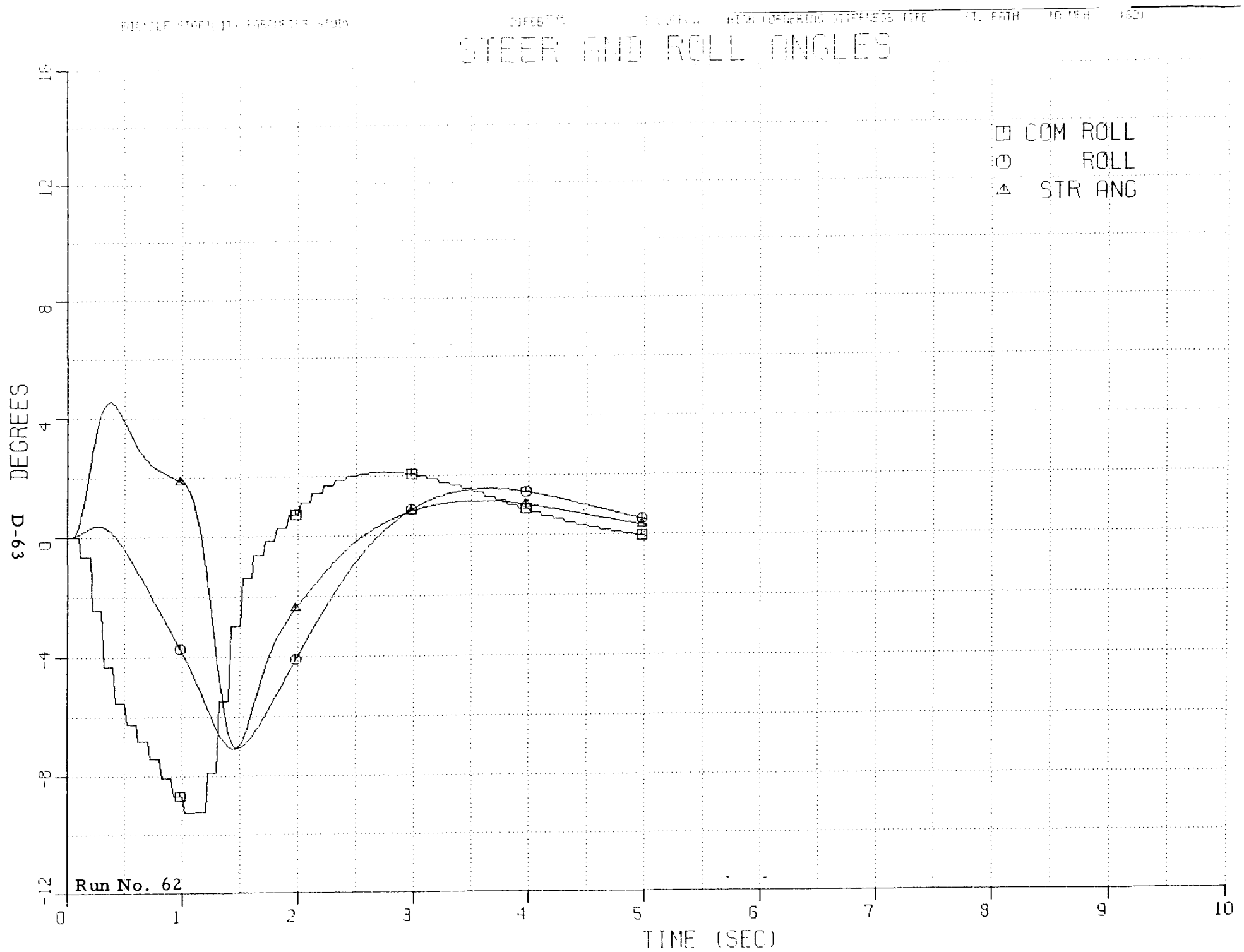
STEER AND ROLL ANGLES
COM ROLL
ROLL
STR ANG
DEGREES
TIME (SEC)
Run No. 62
16
12
8
4
0
-4
-8
-12
0
1
2
3
4
5
6
7
8
9
10

BICYCLE STABILITY [illegible] STUDY SPEED: 20 SUSPENSION HIGH CORNERING STIFFNESS TIRE ST. PATH 15 MPH 1631

STEER AND ROLL ANGLES

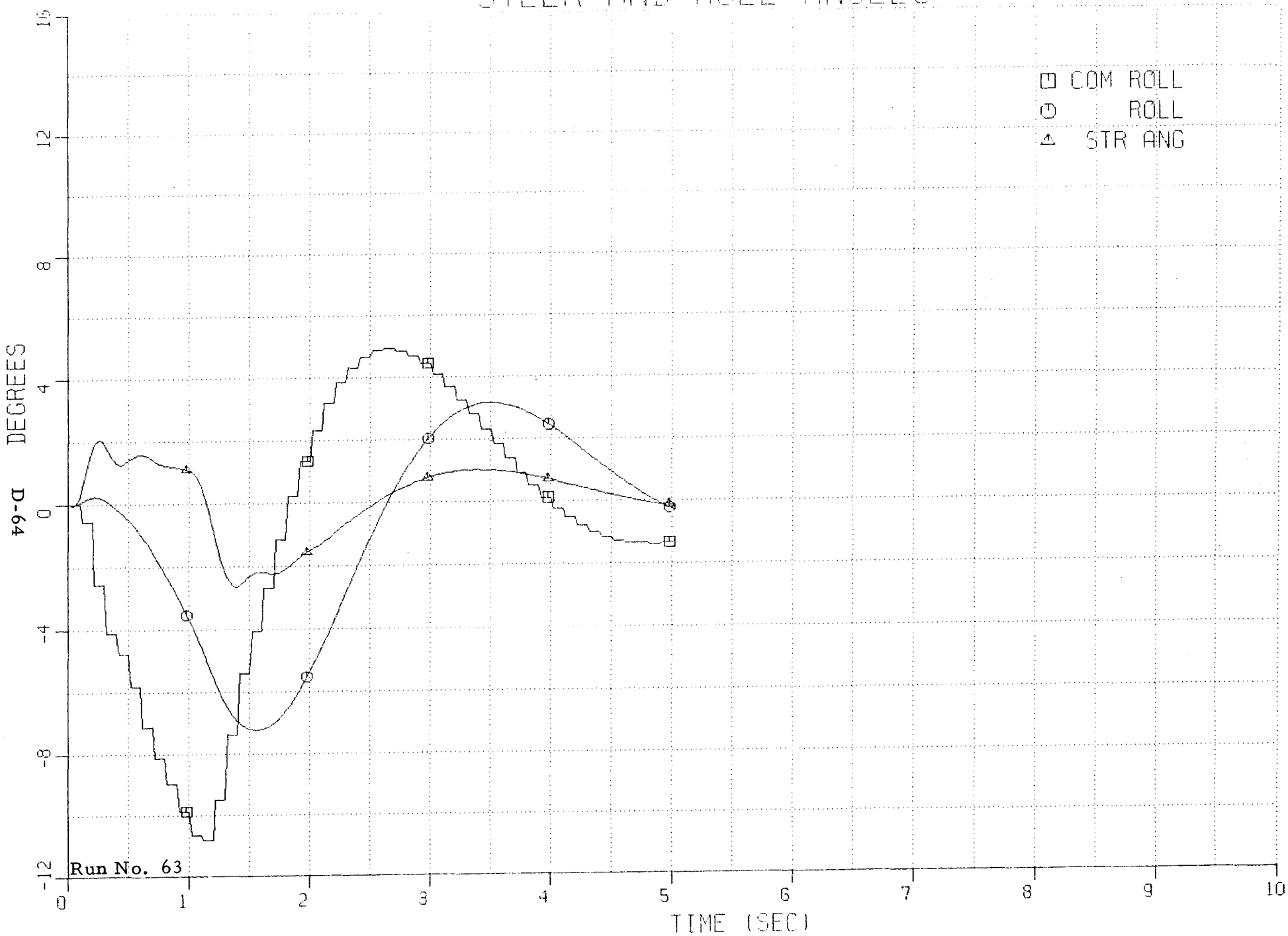

APPENDIX E

Plotted Results of
High Speed Bicycle Stability Study

Run	Speed	Bicycle Configuration
1	30 mph	Standard Paramount
2	40 mph	Standard Paramount
3	50 mph	Standard Paramount
4	30 mph	0.1 in-lb-sec/deg. steering damping
5	30 mph	1.0 in-lb-sec/deg. steering damping
6	30 mph	12.4 deg. caster, std. steering trail (1.71 in)
7	30 mph	22.4 deg. caster, std. steering trail (1.71 in)
8	30 mph	Std. caster (17.4 deg.), 0.71 in. steering trail
9	30 mph	Std. caster (17.4 deg.), 2.71 in. steering trail
10	30 mph	Std. caster (17.4 deg.), zero steering trail
11	30 mph	Std. caster (17.4 deg.), -0.5 in. steering trail

TABLE E-1. Test Configuration and Run Numbers

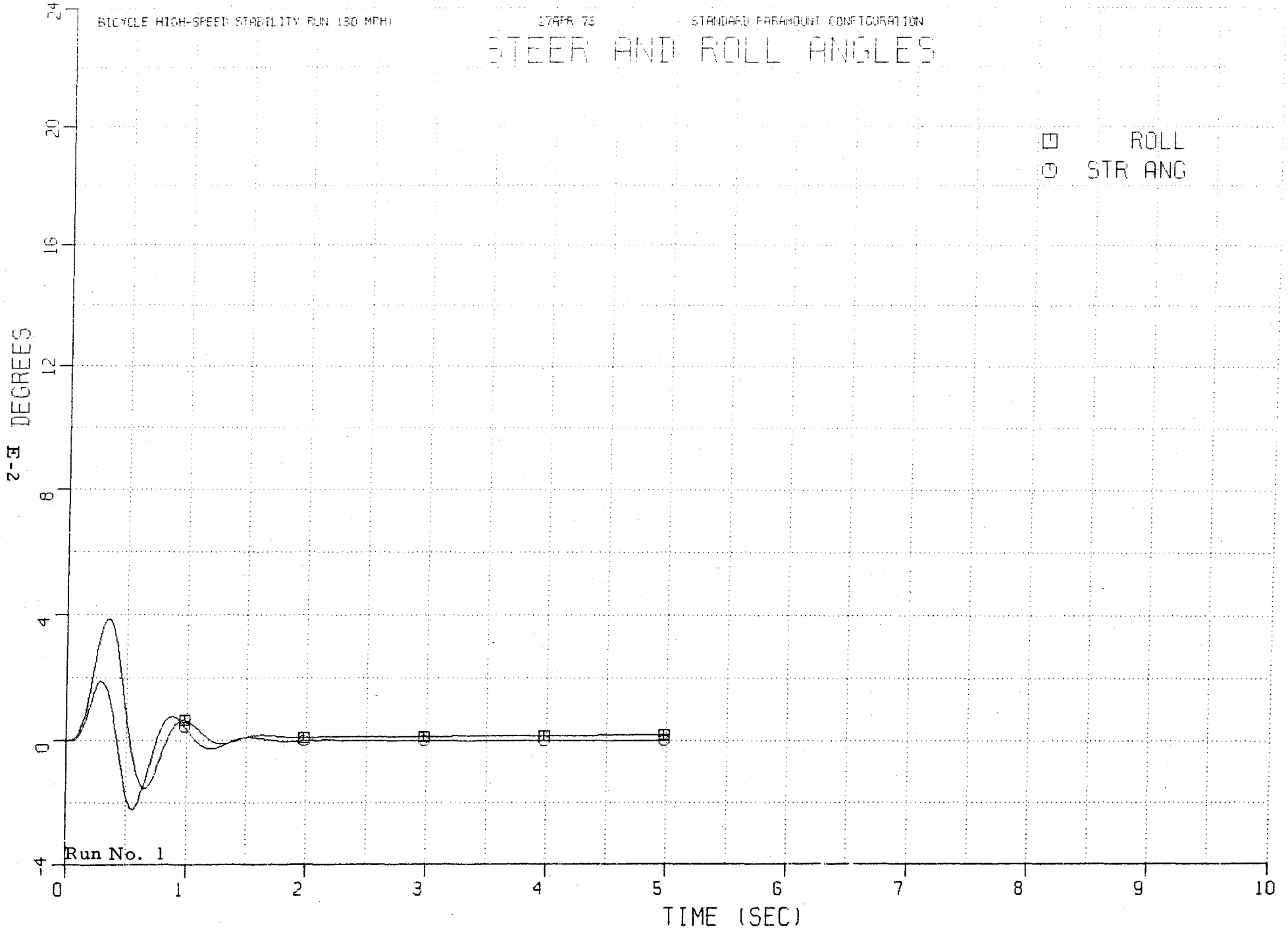
BICYCLE HIGH-SPEED STABILITY RUN (80 MPH)
27APR 73
STANDARD PARAMOUNT CONFIGURATION
STEER AND ROLL ANGLES
ROLL
STR ANG
E-2 DEGREES
24
20
16
12
8
4
0
-4
Run No. 1
0
1
2
3
4
5
6
7
8
9
10
TIME (SEC)

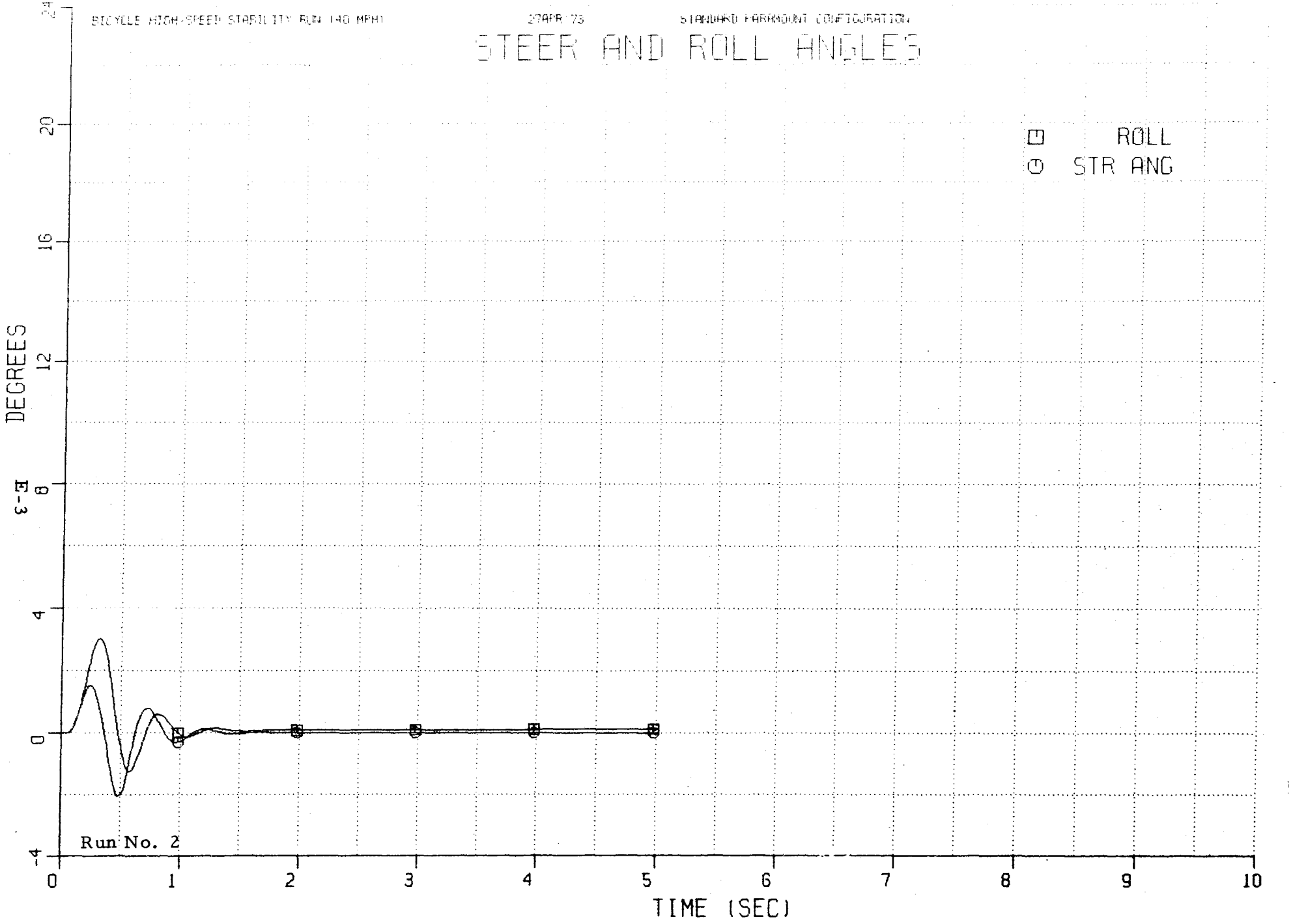
BICYCLE HIGH-SPEED STABILITY RUN 140 MPH1
27APR 73
STANDARD FAIRMOUNT CONFIGURATION
STEER AND ROLL ANGLES
ROLL
STR ANG
DEGREES
E-3
24
20
16
12
8
4
0
-4
0
1
2
3
4
5
6
7
8
9
10
TIME (SEC)
Run No. 2

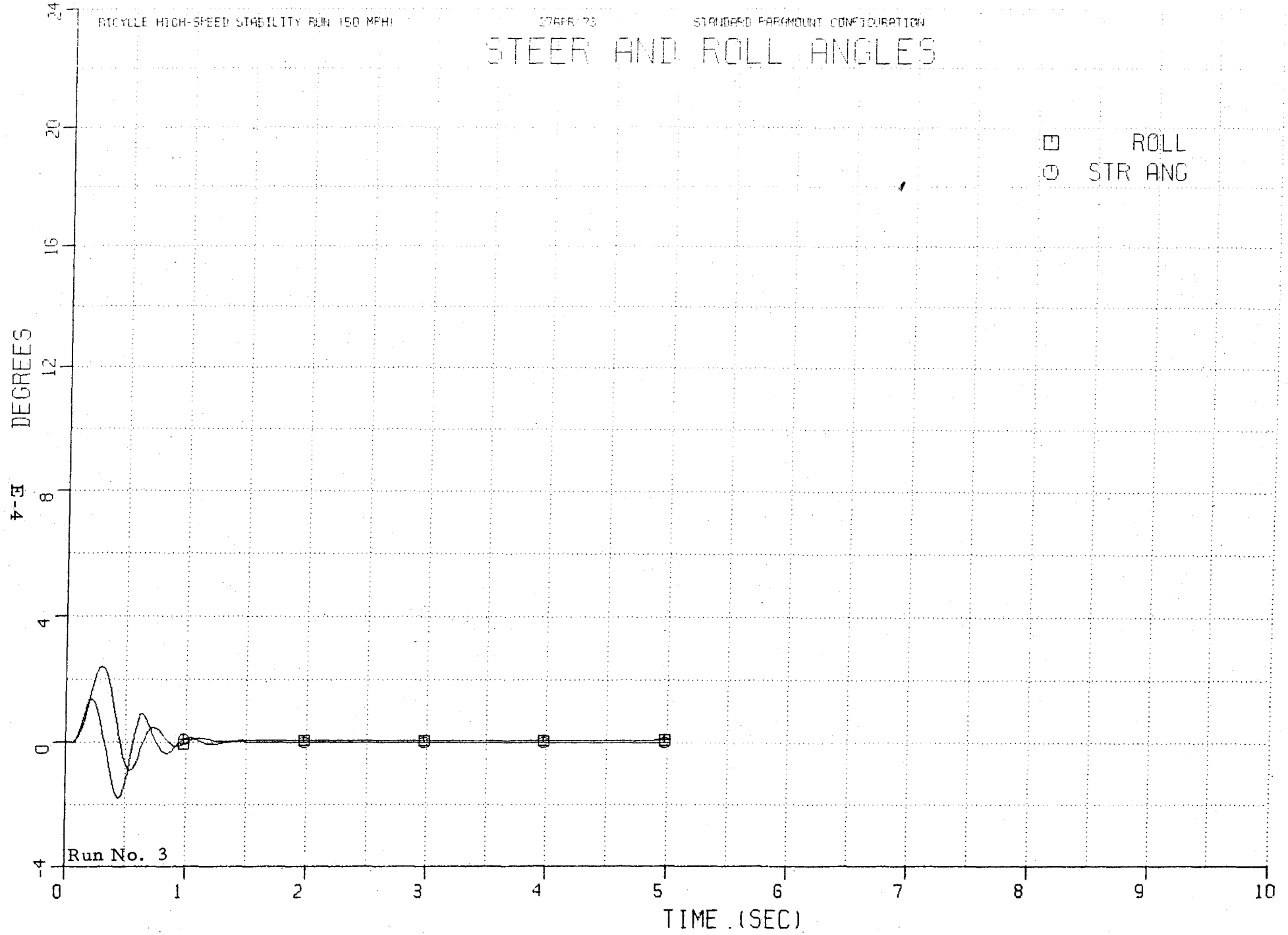
BICYCLE HIGH-SPEED STABILITY RUN 150 MPH
STEER AND ROLL ANGLES
STANDARD PARAMOUNT CONFIGURATION
ROLL
STR ANG
DEGREES
TIME (SEC)
Run No. 3
24
20
16
12
8
4
0
-4
0
1
2
3
4
5
6
7
8
9
10

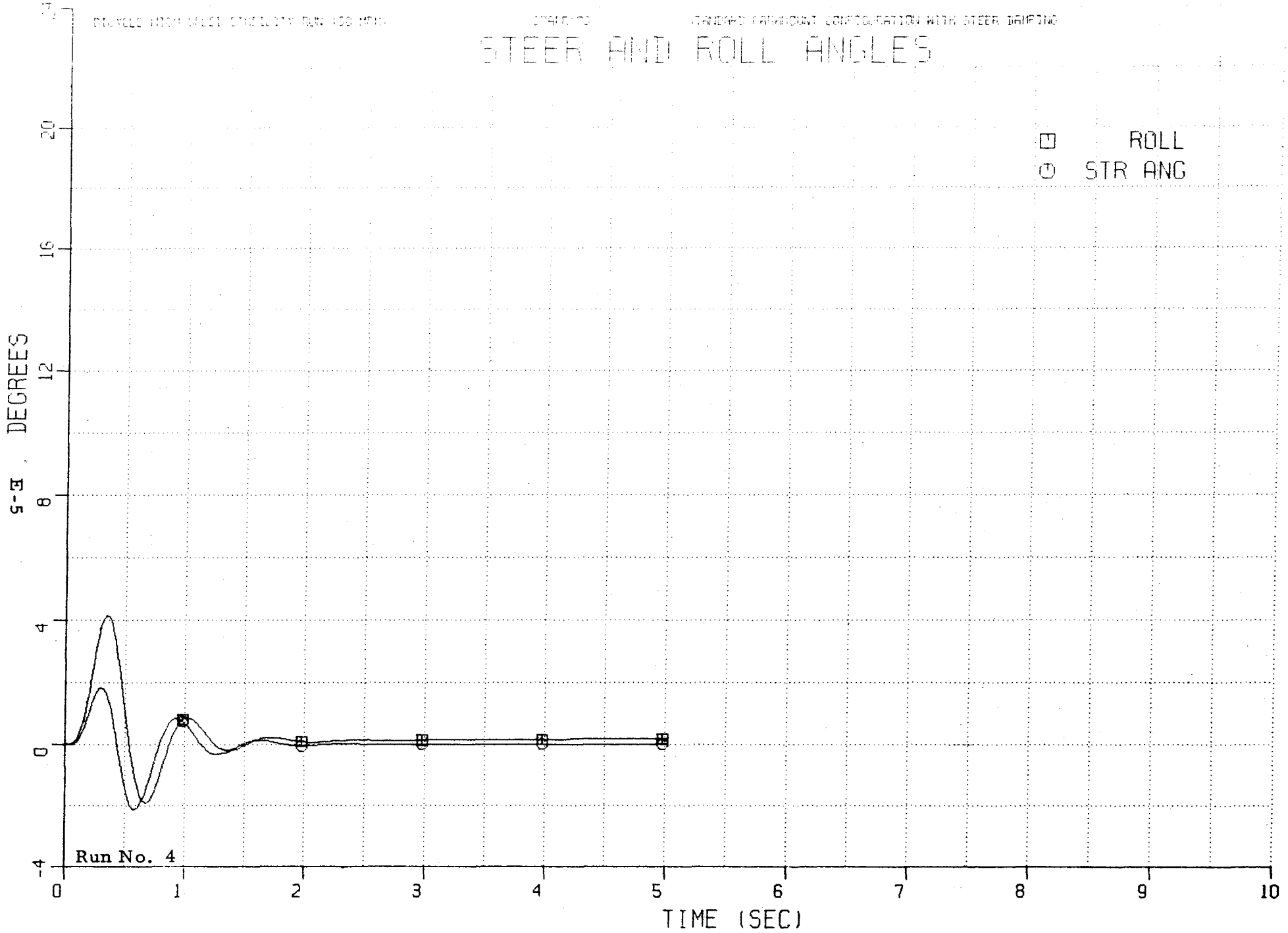
STEER AND ROLL ANGLES
ROLL
STR ANG
DEGREES
E-5
TIME (SEC)
Run No. 4
-4
0
4
8
12
16
20
0
1
2
3
4
5
6
7
8
9
10

1.0 in-lb-sec/deg

BICYCLE HIGH-SPEED STABILITY RUN 130 MPH

STEER AND ROLL ANGLES

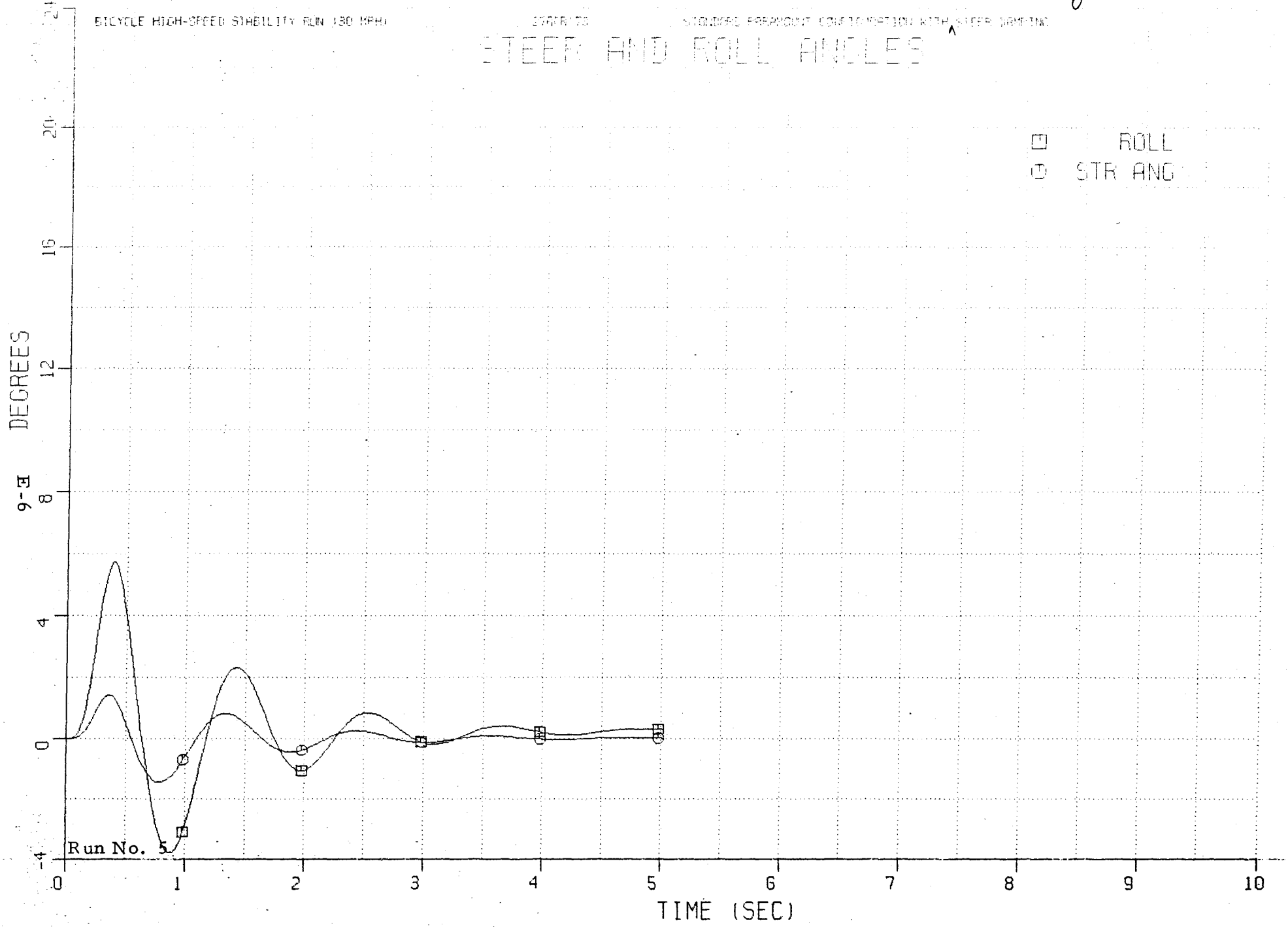

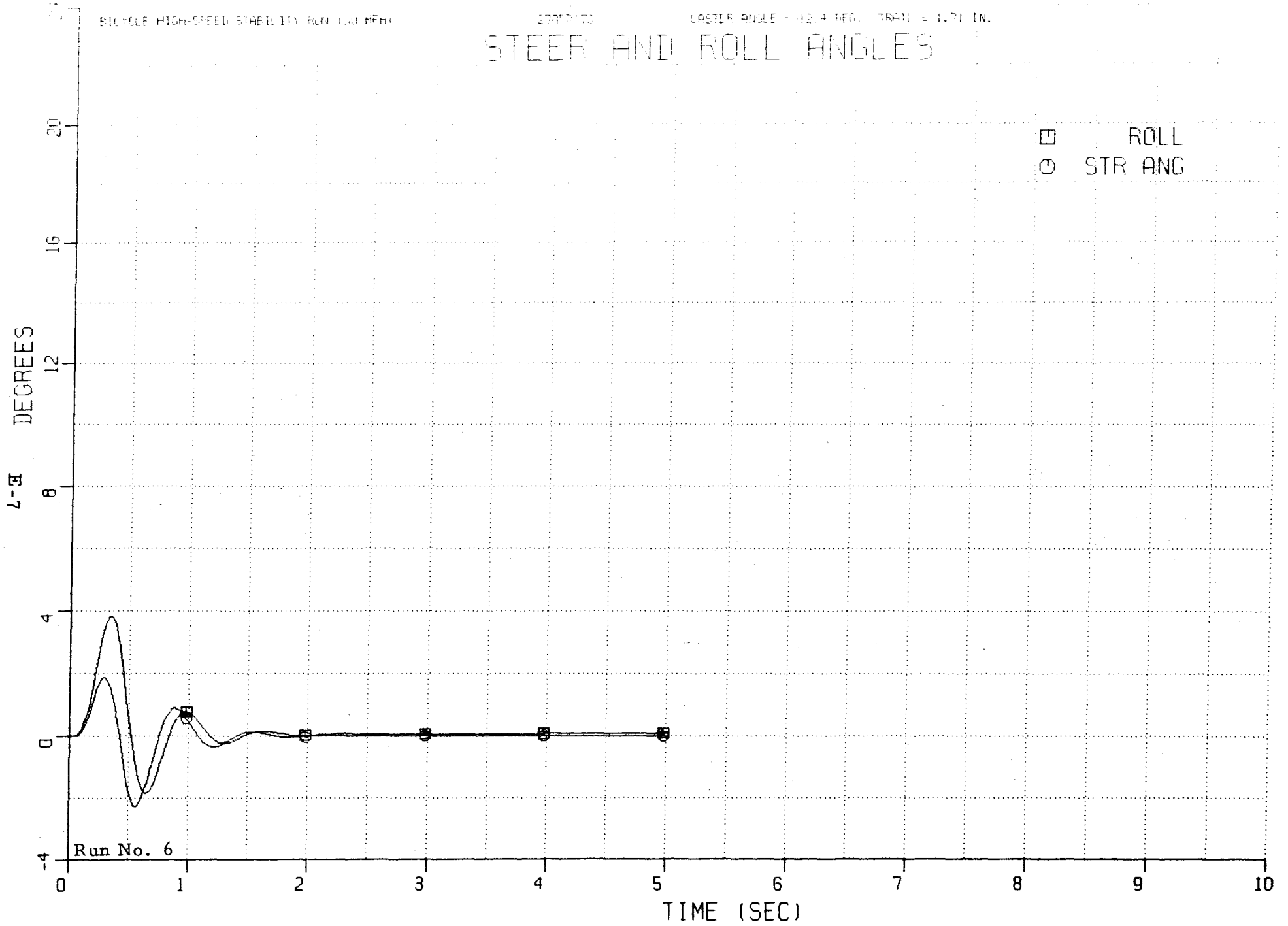
BICYCLE HIGH-SPEED STABILITY RUN [illegible]
CASTER ANGLE = 12.4 DEG. TRAIL = 1.71 IN.
STEER AND ROLL ANGLES
ROLL
STR ANG
DEGREES
20
16
12
8
4
0
-4
Run No. 6
0
1
2
3
4
5
6
7
8
9
10
TIME (SEC)

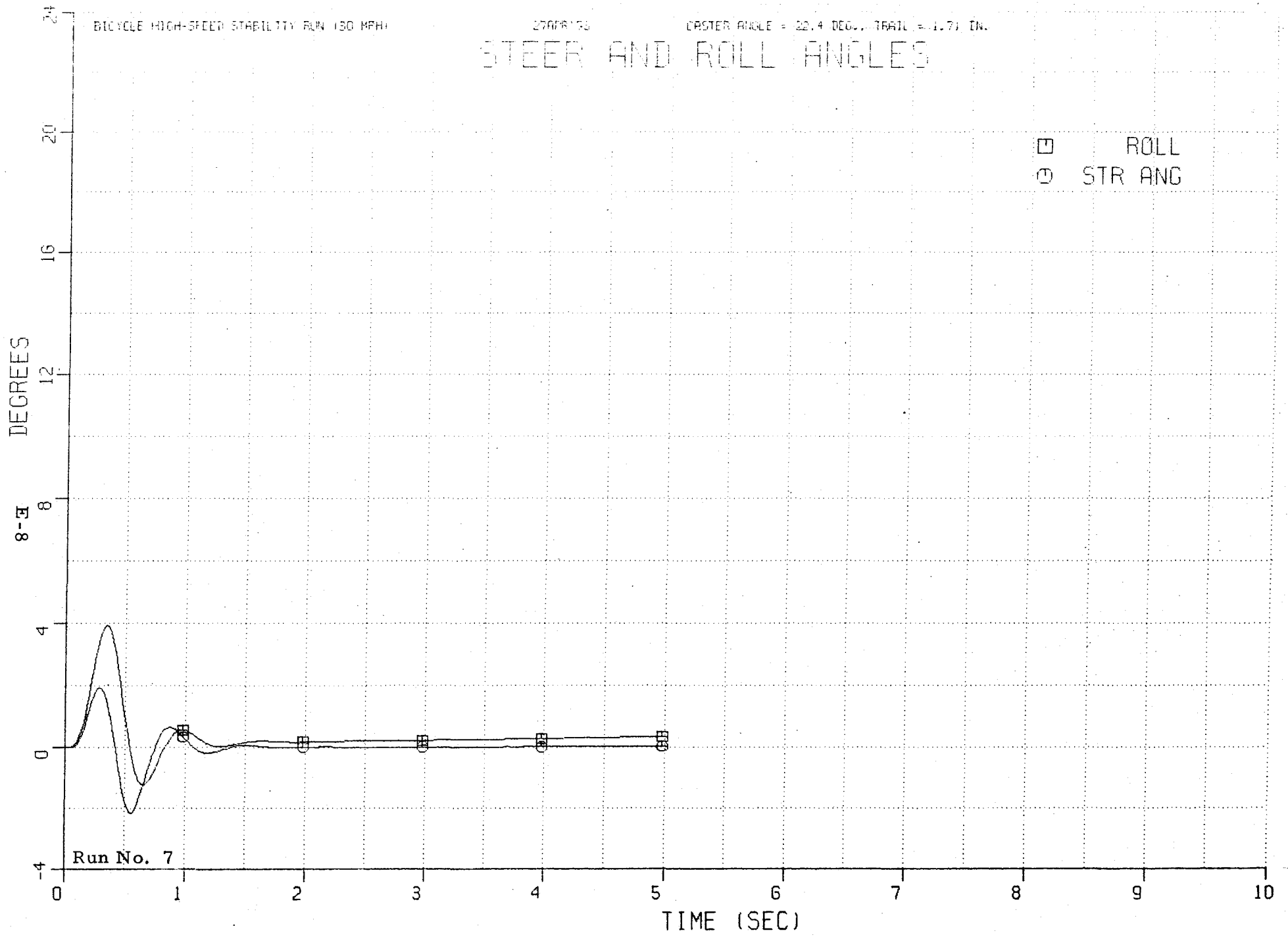
BICYCLE HIGH-SPEED STABILITY RUN (30 MPH)
27APR'75
CASTER ANGLE = 22.4 DEG., TRAIL = 1.7) IN.
STEER AND ROLL ANGLES
ROLL
STR ANG
DEGREES
TIME (SEC)
Run No. 7
24
20
16
12
8
4
0
-4
0
1
2
3
4
5
6
7
8
9
10

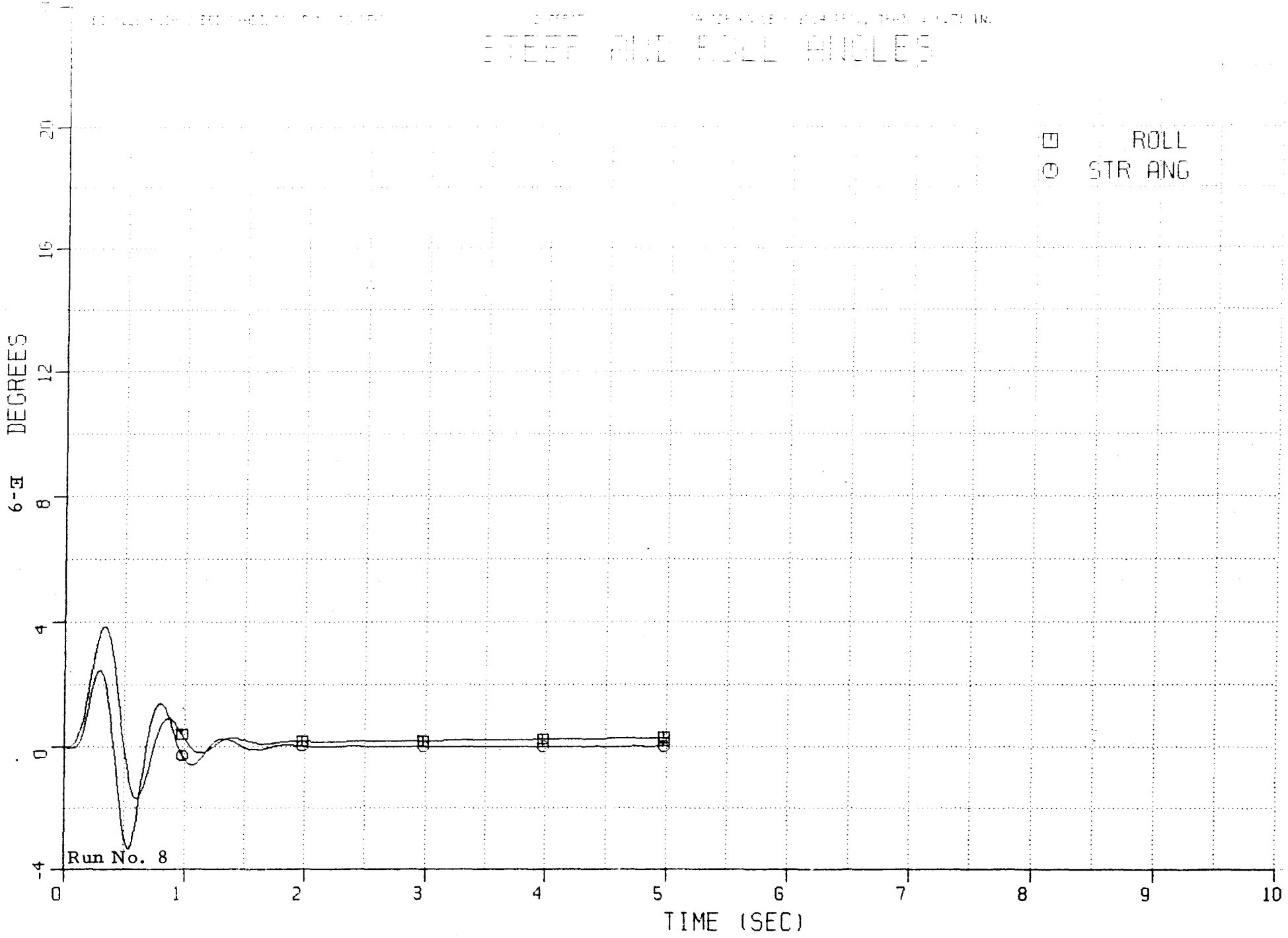
STEER AND ROLL ANGLES
ROLL
STR ANG
DEGREES
20
16
12
8
4
0
-4
Run No. 8
0
1
2
3
4
5
6
7
8
9
10
TIME (SEC)

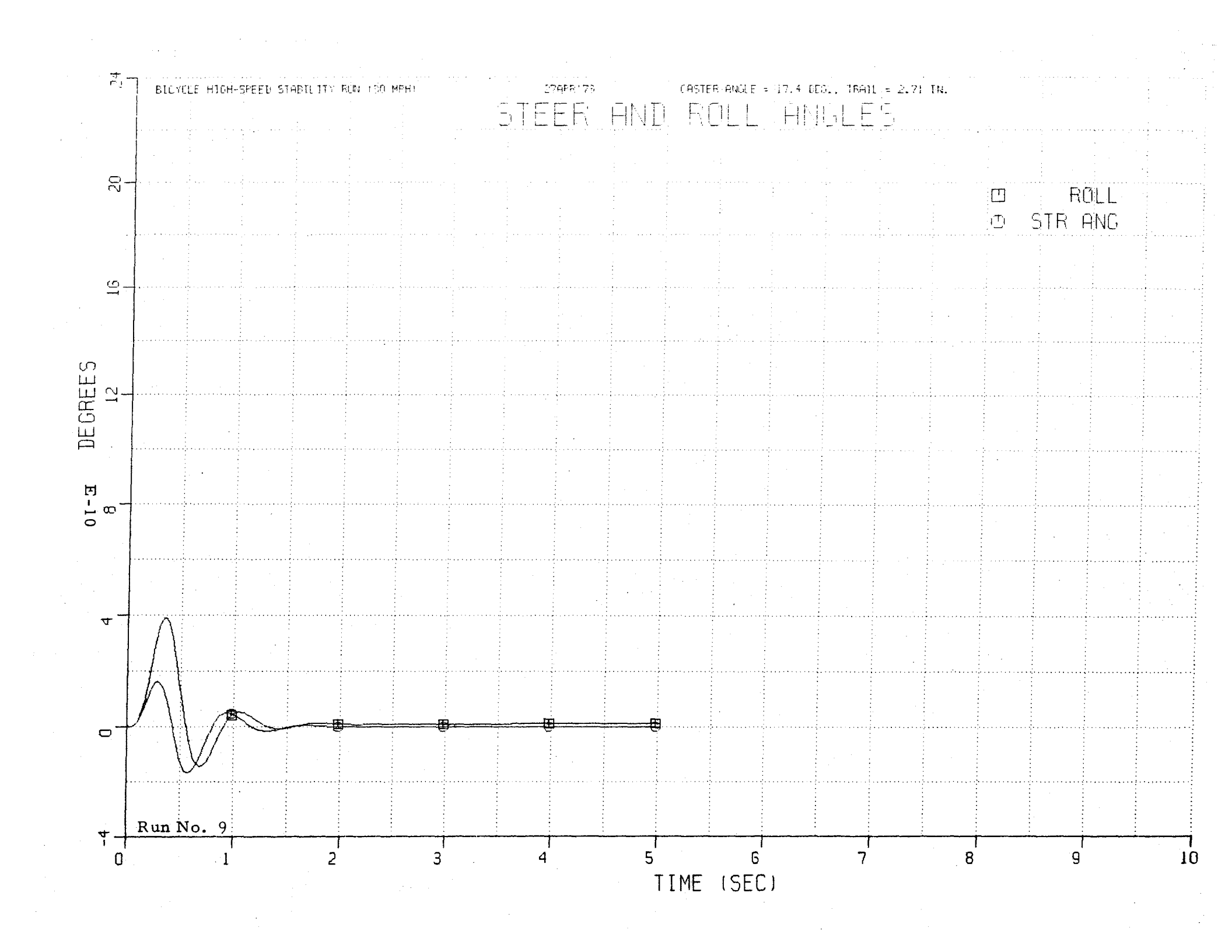
BICYCLE HIGH-SPEED STABILITY RUN (30 MPH)
29APR'78
CASTER ANGLE = 17.4 DEG., TRAIL = 2.71 IN.
STEER AND ROLL ANGLES
ROLL
STR ANG
DEGREES
E-10
24
20
16
12
8
4
0
-4
Run No. 9
0
1
2
3
4
5
6
7
8
9
10
TIME (SEC)

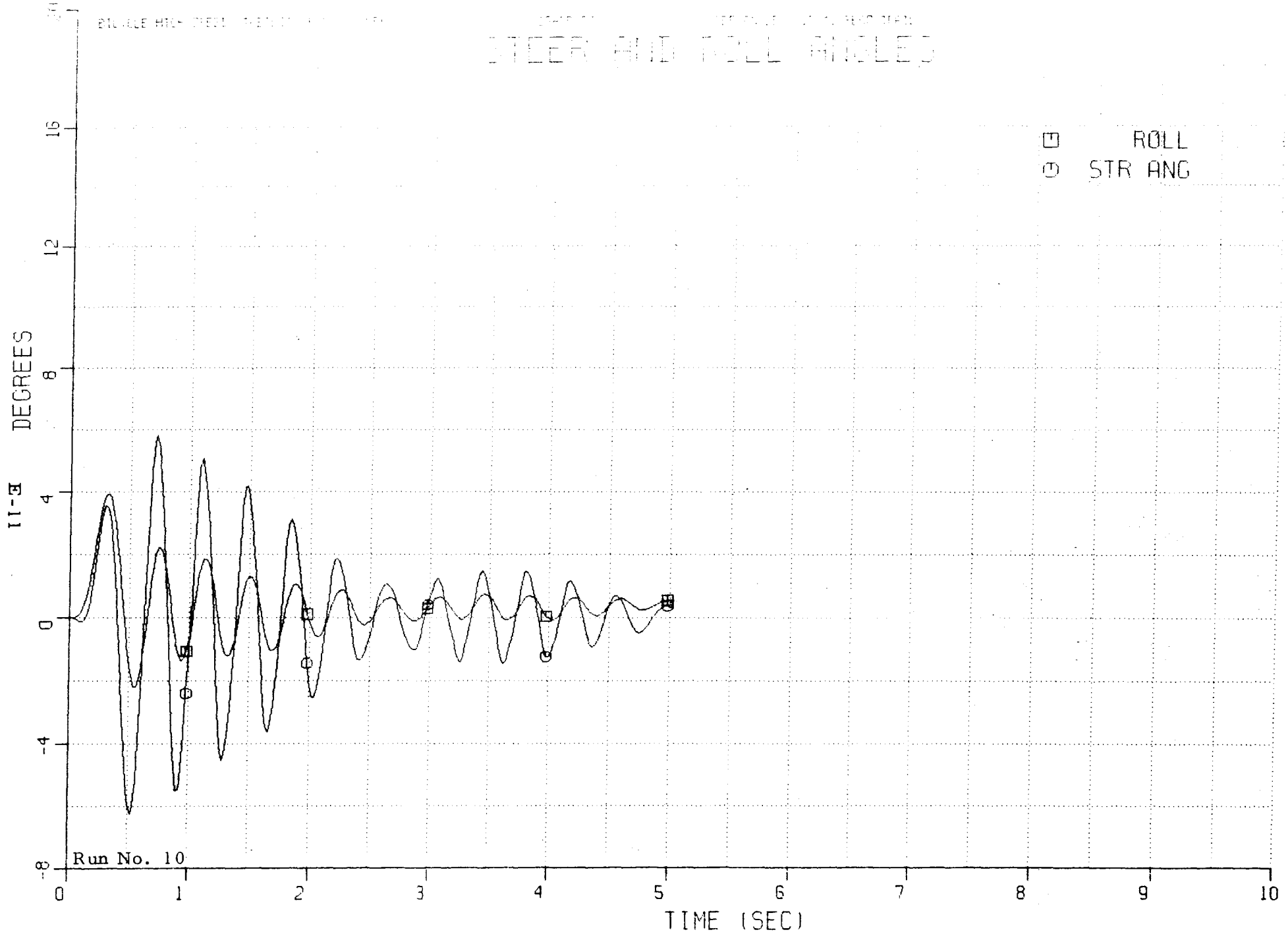
STEER AND ROLL ANGLES
ROLL
STR ANG
DEGREES
E-11
16
12
8
4
0
-4
-8
Run No. 10
0
1
2
3
4
5
6
7
8
9
10
TIME (SEC)

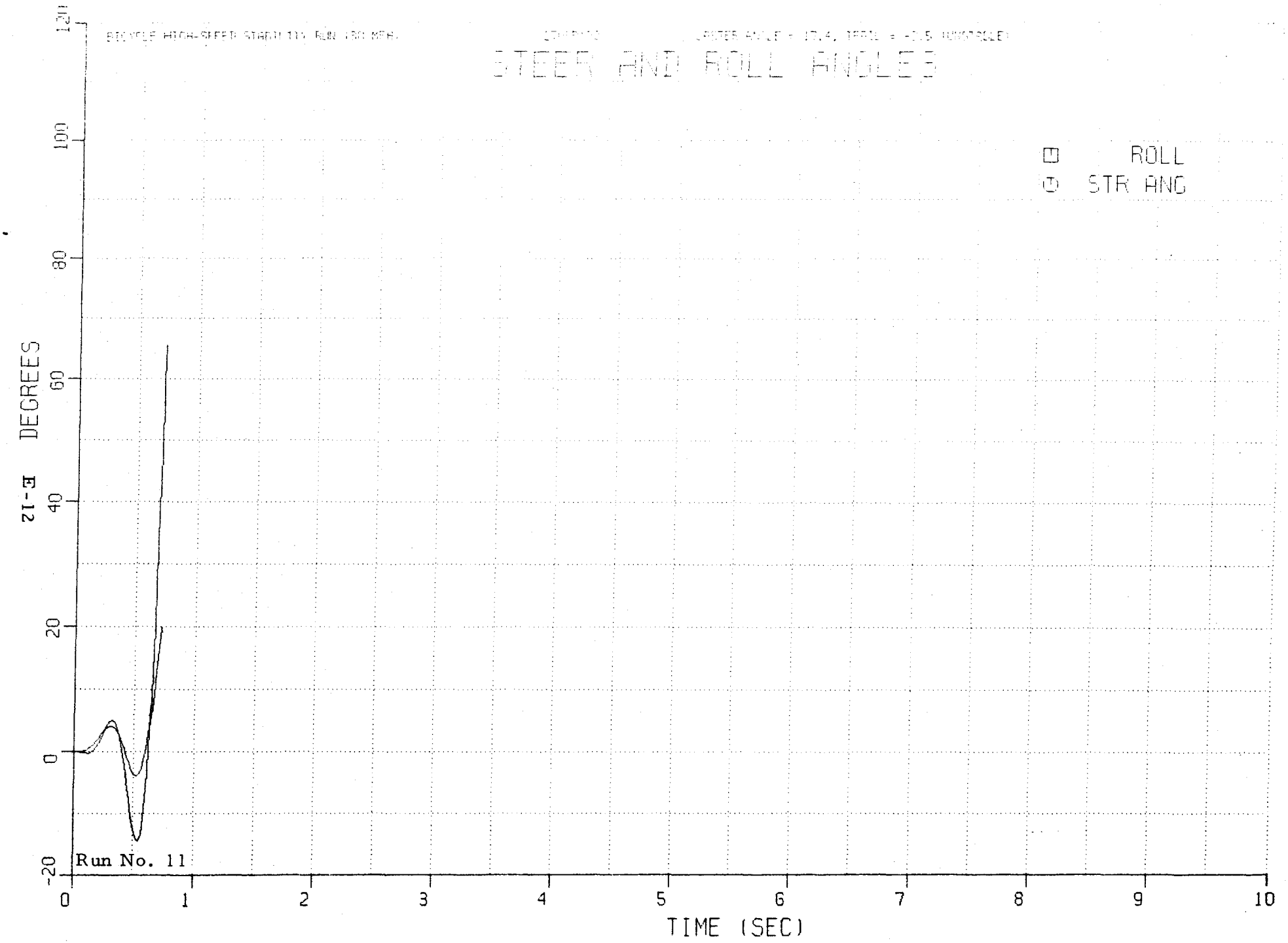
STEER AND ROLL ANGLES
ROLL
STR ANG
DEGREES
TIME (SEC)
Run No. 11
120
100
80
60
40
20
0
-20
0
1
2
3
4
5
6
7
8
9
10

12/3/74

1. Also [illegible] [illegible] [illegible] rider shifting C.G. laterally.

2. Jim believes that the rider may be able to interchange lean and steer control for performing a const. speed const. radius [illegible] but the tendency would be to do much the same thing [illegible].

3. Use the [illegible] response [illegible] [illegible] point [illegible] [illegible] [illegible] [illegible] δ [illegible]. Also question of [illegible] [illegible].

lateral acceleration gains : a_y/δ, a_y/ϕ, a_y/T
(or yaw rate gain) ; also β [illegible]

Const [illegible] : speed [illegible], [illegible]

Const. δ : position control limitations, compatible with simulation ?

Const Throttle : transient, [illegible] [illegible] [illegible] simulation (?)

Careful of any test [illegible] [illegible] constant speed which may be [illegible] [illegible] [illegible] [illegible] or singularity [illegible] transient [illegible]

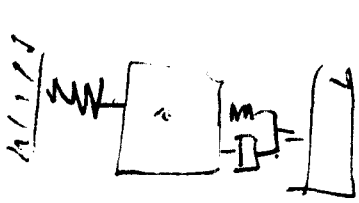

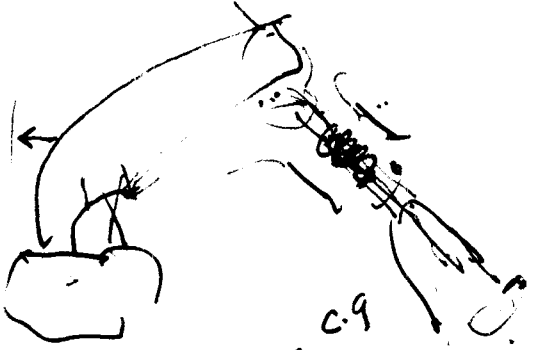

δ+ rh turn
MVr pos for pos. r
−α → pos SF

ΣF pos up.

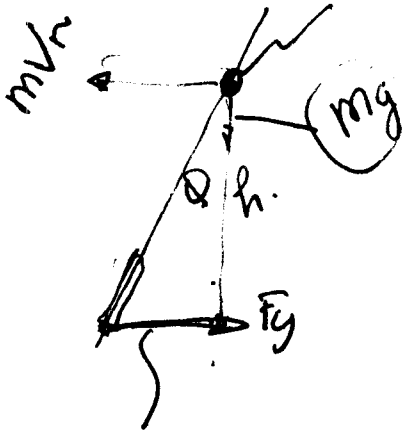

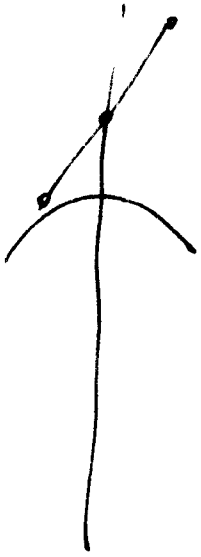

z_F t δ is +
roll mom.
z_F is neg.

$\frac{L_T}{R}$ Vr
is neg.
rolling mom